Molecular Engineering of Group 14 Phthalocyanines and Their Role in Organic Photovoltaic Devices

BY

Trevor Grant

Thesis submitted to the University of Ottawa
in partial fulfilment of the requirements for the
Doctorate of Philosophy degree in Chemical Engineering

Department of Chemical and Biological Engineering
Faculty of Engineering
University of Ottawa

Abstract

Organic photovoltaic (OPV) devices utilizing organic (carbon-based) semiconductors have maintained research interest due to their potential for inexpensive, non-toxic, flexible, and lightweight solar modules. Numerous organic polymers and small molecules have been investigated for OPV applications, however a focus on maximizing the power conversion efficiency (PCE) of lab-scale devices has generated many novel active materials that are too complex to be realistically synthesized on a commercial scale. It has become apparent that developing low-cost, scalable, and stable active materials is crucial for the commercialization of OPV devices. Metal phthalocyanines (MPcs) are a well-known family of molecules with established scale up chemistry from their use as colorants and have demonstrated strong performance as low-cost semiconductors in organic electronic devices. However, their potential in solution-processed OPV devices has not been fully realized. In this thesis, a series of materials based on silicon phthalocyanine (SiPc) and tin phthalocyanine (SnPc) were synthesized and characterized. Novel molecular designs and OPV device architectures were investigated to further establish the use MPcs as low-cost active materials and to probe new applications. Specifically, the chemical and physical differences of structurally analogous soluble SiPc and SnPc derivatives were examined for the first time. The ability of a SiPc derivative to act as a thermal crosslinker to stabilize active layer morphology while simultaneously contributing to photocurrent generation was also proven. SiPc derivatives were then studied as electron acceptors paired with P3HT and PBDB-T donor polymers, achieving a PCE up to 4.3 %. The results herein establish new potential roles for group 14 MPcs in OPV devices while also demonstrating their synthetic simplicity and versatility. This work also serves as a basis for the wealth of chemical functionalization which remains available for continued optimization of these materials.

Abstrait

Les cellules photovoltaïques organiques (OPV), constituées de semi-conducteurs organiques (à base de carbone), ont stimulé l'intérêt des chercheurs en raison de leur potentiel pour l'élaboration de modules solaires peu coûteux, non toxiques, flexibles et légers. De nombreux polymères organiques et petites molécules ont été étudiés pour les applications OPV. Cependant, l'accent étant mis sur la maximisation du rendement de conversion de puissance (PCE) des modules à l'échelle du laboratoire, de nombreux matériaux actifs innovants trop complexes pour être synthétisés de manière réaliste à l'échelle commerciale ont été générés. Il est maintenant devenu évident que le développement de matériaux actifs peu coûteux, stables, et adaptable à grande échelle est crucial pour la commercialisation des dispositifs OPV. Les phtalocyanines métalliques (MPc) sont une famille bien connue de molécules avec une chimie à grande échelle établie grâce à leur utilisation comme colorants, et ont démontré des performances prometteuses en tant que semi-conducteurs à faible coût dans des dispositifs électroniques organiques. Cependant, leur potentiel dans des dispositifs OPV élaborés en solution n'a pas été pleinement évalué. Dans cette thèse, une série de matériaux à base de phtalocyanine de silicium (SiPc) et de phtalocyanine d'étain (SnPc) ont été synthétisés et caractérisés. De nouveaux design moléculaires et de nouvelles architectures de cellules OPV ont été étudiés afin d'évaluer davantage l'utilisation des MPc en tant que matériaux actifs à faible coût et de sonder de nouvelles applications. Plus précisément, les propriétés chimiques et optoélectriques de dérivés de SiPc et SnPc solubles structurellement analogues ont été examinées pour la première fois. La capacité d'un dérivé de SiPc à agir comme un réticulant thermique pour stabiliser la morphologie de la couche active tout en contribuant simultanément à la génération de photocourant a également été prouvée. Enfin, les dérivés de SiPc ont été étudiés en tant qu'accepteurs d'électrons appariés avec des polymères donneurs tels que P3HT et PBDB-T, atteignant un PCE jusqu'à 4,3%. Ces résultats établissent de nouveaux rôles potentiels pour les MPc du groupe 14 dans les dispositifs OPV, tout en démontrant leur simplicité synthétique et leur polyvalence. Ces travaux servent également de base à la richesse de la fonctionnalisation chimique qui reste disponible pour une optimisation continue de ces matériaux.

Acknowledgements

I would like to firstly thank my supervisor Benoit Lessard for first introducing me to research work as an undergraduate student at the University of Toronto and adopting me as the first graduate student in a new lab at the University of Ottawa. Watching the rapid growth in research capabilities for our lab group through my graduate studies has been exceptional, and I am sure it will persist as the group continues to mature.

I would like to thank all group members in the Lessard Group for providing a positive and productive research environment. Special mention to Owen Melville, Alex Peltekoff, and Nicole Rice for their collaborations since the early days of the research group. Also, many thanks to my fellow OPV lab mates Marie Faure, Mario Vebber, and Chloe Dindault for their comradery and support in the lab.

I express my deepest gratitude to the technical staff at uOttawa; James MacDermid, Gerard Nina, and Franco Ziraldo, without whom I would have not been able to implement of countless pieces of hardware and software for the device fabrication and testing capabilities in our new laboratories within the time of my degree.

I would like to thank our many collaborators for their training, input, and contributions throughout my research work. Local collaborators Professor Jacqulin Brusso, Nathan Yutronkie, Professor Karin Hinzer, Trevor Coathup, and Kayden Kaller at the University of Ottawa, and external collaborators Professor Bender, Professor Guillaume Wantz, Therese Goissre, Sufal Swaraj, Luca Muccioli, and Frédéric Castet.

Finally, I thank my family; Dave, Tina and Melanie Grant for their support and encouragement throughout my degree, especially during the COVID lockdowns dealing with laboratory closures and research delays.

Table of Contents

List of Figures

List of Tables

List of Key Abbreviations

α-6T: alpha-sexithiophene

CuPc: Copper phthalocyanine

BABP: 4,4'-bis(azidomethyl)-1,1'-biphenyl

BHJ: Bulk heterojunction

CV: Cyclic voltammetry

DIO: 1,8-diiodooctane

DSC: Differential scanning calorimetry

E_g: Band gap

EQE: External quantum efficiency

ETL: Electron transport layer

FF: Fill factor

HOMO: Highest occupied molecular orbital

HTL: Hole transport layer

$(HxN_3)_2$-SiPc: Bis(6-azohexanoate)silicon phthalocyanine

ITIC: 3,9-bis(2-methylene-(3-(1,1-dicyanomethylene)-indanone))-5,5,11,11-tetrakis(4-hexylphenyl)-dithieno[2,3-d:2',3'-d']-s-indaceno[1,2-b:5,6-b']dithiophene

ITO: Indium tin oxide

J-V: Current density - voltage

J_{SC}: Short circuit current density

LUMO: Lowest unoccupied molecular orbital

MoO_x: Molybdenum oxide

NIR: Near infrared

NMR: Nuclear magnetic resonance

OIDTBR: (5Z,5'Z)-5,5'-((7,7'-(4,4,9,9-tetraoctyl-4,9-dihydro-s-indaceno[1,2-b:5,6-b']dithiophene-2,7-diyl)bis(benzo[c][1,2,5]thiadiazole-7,4-diyl))bis(methanylylidene))bis(3-ethyl-2-thioxothiazolidin-4-one

OLED: Organic light emitting diode

OPV: Organic photovoltaic

OTFT: Organic thin film transistor

Pc: Phthalocyanine

$PC_{61}BM$: Phenyl-C_{61}-butyric acid methyl ester

$PC_{71}BM$: Phenyl-C_{71}-butyric acid methyl ester

PCE: Power conversion efficiency

PBDB-T: Poly[[4,8-bis[5-(2-ethylhexyl)-2-thienyl]benzo[1,2-b:4,5-b']dithiophene-2,6-diyl]-2,5-thiophenediyl[5,7-bis(2-ethylhexyl)-4,8-dioxo-4H,8H-benzo[1,2-c:4,5-c']dithiophene-1,3-diyl]]

PCDTBT: Poly[N-9'-heptadecanyl-2,7-carbazole-alt-5,5-(4',7'-di-2-thienyl-2',1',3'-benzothiadiazole)]

PDI: Perylene diimide

PEDOT:PSS : poly(3,4-ethylenedioxythiophene):poly(styrenesulfonate)

PHJ: Planar heterojunction

PTB7: Poly[[4,8-bis[(2-ethylhexyl)oxy]benzo[1,2-b:4,5-b']dithiophene-2,6-diyl][3-fluoro-2-[(2-ethylhexyl)carbonyl]thieno[3,4-b]thiophenediyl]]

PTQ10: poly[(thiophene)-alt-(6,7-difluoro-2-(2-hexyldecyloxy)quinoxaline)]

P3HT: Poly(3-hexylthiophehne)

SiPc: Silicon phthalocyanine

SnPc: Tin Phthalocyanine

TGA: Thermogravimetric analysis

V_{OC}: Open circuit voltage

XRD: X-ray Diffraction

Y6 (BTP-2F): 2,2'-((2Z,2'Z)-((12,13-bis(2-ethylhexyl)-3,9-diundecyl-12,13-dihydro-[1,2,5]thiadiazolo[3,4-e]thieno[2",3'':4',5']thieno[2',3':4,5]pyrrolo[3,2-g]thieno[2',3':4,5]thieno[3,2-b]indole-2,10-diyl)bis(methanylylidene))bis(5,6-difluoro-3-oxo-2,3-dihydro-1H-indene-2,1-diylidene))dimalononitrile

ZnO: Zinc Oxide

ZnPc: Zinc phthalocyanine

Chapter 1: Introduction

A portion of this chapter was published as a part of a manuscript in *The Chemical Record*:

T. M. Grant, D. S. Josey, K. L. Sampson, T. Mudigonda, T. P. Bender, B. H. Lessard, *Chem. Rec*. **2019**, 19, 1093.

1.1. OPV Devices in the Solar Market

Among renewable energy technologies, solar photovoltaic (PV) devices continue to be one of the most competitive to challenge fossil fuels and reduce global carbon emissions. Solar radiation is an abundant and widespread energy source, providing accessible energy on the order of 5 x 10^4 EJ annually which well surpasses the global energy demand.[1] While PV devices currently make up a small fraction of global energy supply, they are projected the fastest growing energy technology over the next decade.[2] With increasing demand for renewable energy, further development for efficient and low-cost solar energy production is necessary to enable the wide-scale usage of PV devices.

Solar PV technologies are generally divided into three generations. First generation PV technology was defined by crystalline silicon (c-Si) devices, which emerged in 1954 achieving 6% power conversion efficiency (PCE) of solar radiation using a silicon *p-n* junction.[3] Since this discovery, the PCE of c-Si devices has continued to rise to an impressive 26.7 % at present. As the costs of commercial devices has continued to decline, c-Si currently dominates the solar market accounting for over 90 % of total PV production.[4]

Second generation technologies were initially developed to circumvent the initial high production costs of c-Si devices by reducing the active layer thickness and eliminating the energy-intensive process of forming high purity silicon. These included inorganic thin-film cells such as amorphous Si (a-Si), copper indium gallium selenide (CIGS), gallium arsenide (GaAs), and cadmium telluride (CdTe) devices, which currently make up the remainder of the PV market. Inorganic thin-film devices are currently challenged with lower efficiencies compared to c-Si combined with the rarity of tellurium and indium, as well as the toxicity of cadmium preventing them from generating a higher market share.

Third generation or so-called "emerging" technologies share a common aim of providing reduced manufacturing costs compared to c-Si. These technologies include organic photovoltaic (OPV) devices, which utilize organic (carbon-based) semiconductors in their active layer; dye-sensitized solar cells (DSSCs), which utilize porous TiO_2 nanoparticles coated in a molecular dye (often ruthenium-based) immersed in an electrolyte; quantum-dot photovoltaics (QDPVs), which utilize inorganic nanoparticles (often PbS); and perovskite PVs, which utilize a hybrid organic-inorganic tin or lead halide material with the perovskite crystal structure. All of these active materials share the ability to be cast as a thin (< 1 μm) film from solution-based processing. This gives the possibly for modules processed using standard printing techniques onto flexible plastic substrates for low manufacturing costs and extremely short energy payback times (the time for a PV device to generate the energy equivalent to the amount required for its fabrication).

Among emerging technologies, perovskite PV devices have seen and unprecedented rapid rise in research interest and PCE for lab scale devices, surpassing 25 % just over a decade after their first use in PV devices in 2009.[5] Commercial perovskite research is now mainly focused on tandem cells in conjunction with c-Si devices, where they have achieved impressive PCEs above 29 %.[6] Perovskites are currently facing challenges of poor reproducibility, the presence of toxic lead in the active layer, and unproven long term stability for implementation into commercial devices.[7] With the continuing decreasing costs of c-Si devices and the emergence of perovskites, OPV devices are not projected to replace the use of c-Si in the solar market and will instead aim to either work alongside c-Si devices or fit into niche applications where c-Si or perovskites are less suited and the unique advantages of employing organic semiconductors can be utilized (**Figure 1.1**).

Like other third generation technologies, OPV devices have the potential to create lightweight and flexible modules with comparatively lower cost and a shorter energy payback time compared to c-Si. Additionally, organic semiconductors are generally non-toxic unlike the lead-based materials commonly used in QDPV and perovskite devices. They also posses highly tunable absorption spectra allowing for targeted absorption, colour tuning, or fully transparent devices. Suitable applications currently include solar windows[8], agrivoltaics (greenhouse-integrated PV)[9], textile-integrated PV devices[10], and low-light recovery devices[11].

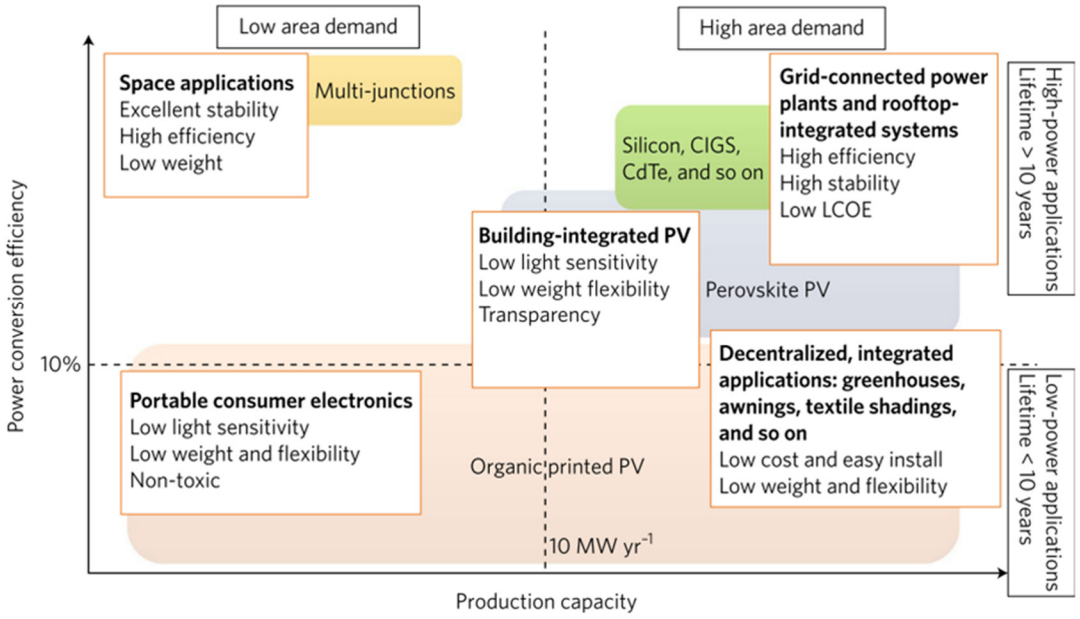

Figure 1.1. Projected solar market for OPV in comparison to other solar technologies.[12]

1.2. OPV Device Structure and Fabrication

OPV devices share the same basic operating principles as inorganic devices, where light is absorbed to generate charge carrier pairs in the form of excited electrons (e^-) and electron holes (h^+) which are separated and collected at opposing electrodes to supply current to an external circuit. The first major breakthrough for OPV devices came in 1986 by C.W. Tang, who approached the 1% efficiency threshold with the first bi-layer planar heterojunction (PHJ) OPV device using an active layer consisting of two organic materials deposited in succession.[13] Tang utilized a high electron affinity perylene diimide (PDI) derivative to act as an electron acceptor, and a low electron affinity copper phthalocyanine (CuPc) to act as an electron donor **(Figure 1.1A)**. The two materials allowed for free electrons and electron holes to be generated at the organic-organic interface and travel to their respective electrodes through the acceptor and donor materials, respectively. This concept of a donor/acceptor pair is critical for efficient charge generation in OPV devices and is currently used in all modern architectures.

The main limitation to a PHJ device configuration is that it provides the minimum possible interfacial surface area between donor and acceptor to facilitate the generation of free charge carriers. In 1995 a second breakthrough was presented by Heeger et. al., reporting the first bulk-

heterojunction (BHJ) device consisting of blended film morphology of a conjugated polymer electron donor poly(2-methoxy-5-(2'-ethyl-hexyloxy)-1,4-phenylene vinylene) (MEH-PPV) paired with the soluble fullerene-based electron acceptor [6,6]-phenyl-C61-butyric acid methyl ester ($PC_{61}BM$).[14] By casting a thin film from a blended solution of the polymer/fullerene pair, an interpenetrating network was formed drastically increasing the interfacial area available for exciton separation (**Figure 1.2 B**). Polymer/small molecule BHJ OPVs have emerged as the popular device configuration and have been utilized for many of the top-performing OPV devices to date.[15–18] These devices will be the focus in the work of this thesis, although it is important to note that all-polymer[19] and all-small molecule[20] BHJ devices, as well as PHJ devices fabricated by PVD methods[21] remain active areas of research with competitive PCEs.

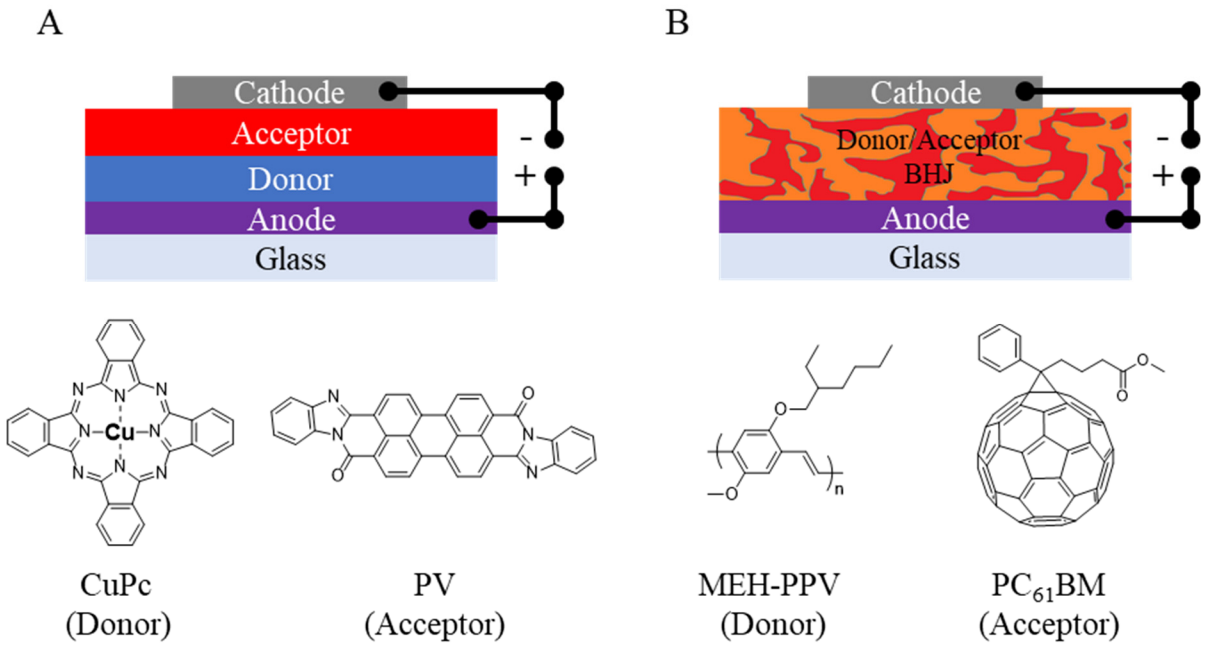

Figure 1.2. Basic (A) planar heterojunction and (B) bulk heterojunction OPV device stacks along with the organic semiconductors used in their conception.

The multiple layers of a BHJ OPV device are deposited in a bottom-up fashion onto a transparent substrate such as plastic or glass with a transparent bottom electrode, commonly indium tin oxide (ITO). Successive layers may be deposited by a combination of techniques, although care must be taken to not destroy existing layers while depositing additional materials. Lab-scale devices are conventionally fabricated on ITO-coated glass, on which the BHJ layer is casted by spin-coating from a blended solution of the active materials. The resulting film

morphology will be determined in part by the chemical structure of the active materials, and may also be significantly influenced by the casting solvent, drying time, solution concentration, donor/acceptor mass ratio, and thermal annealing.[22] The top electrodes are often deposited by PVD, and will ultimately define the device area in regions where the active layer and both electrodes overlap.

OPV devices can be subdivided as direct or inverted based on the direction of charge transport within the device. The direction of charge flow determined by the bias applied by the electrode materials, with electrons being drawn towards the lower work function electrode (cathode) and holes toward the higher work function electrode (anode). Interlayers selective to electron holes (hole transport layer, HTL) and electrons (electron transport layer, ETL) are also deposited between the active layer and the anode and cathode, respectively. These interlayers limit charge recombination at the electrode interface while providing a buffer to stop electrode diffusion into the active layer. Direct device architectures commonly use an aluminum top electrode with a calcium or lithium fluoride electron transport layer, while inverted devices use a silver top electrode with a molybdenum oxide hole transport layer **(Figure 1.3)**.[23] The use of the inverted structure has become increasingly popular as a silver electrode is less prone to oxidation from air, and may also be deposited from an ink at room temperature to eliminate PVD from device fabrication and allow for fully solution processed devices.[24] The bottom electrode must be transparent to allow sufficient light to penetrate the device and strike the active layer. For lab-scale devices, zinc oxide is commonly used as an ETL in the inverted architecture, and poly(3,4-ethylenedioxythiophene):poly(styrenesulfonate) (PEDOT:PSS) is used as a HTL in the direct architecture.

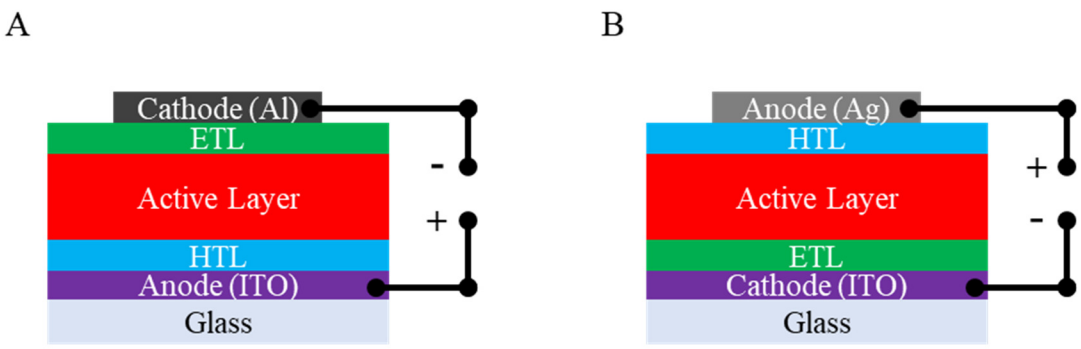

Figure 1.3. Generic OPV devices stacks with a (A) direct and (B) inverted structure.

1.3. Working Principles of OPV Devices

The complete process of charge generation and collection in a donor/acceptor OPV device consists of four steps which must be completed in succession to generate photocurrent (**Figure 1.4**), to be discussed in further detail below. Improving the efficiency of any of these processes can increase the PCE of an OPV device.

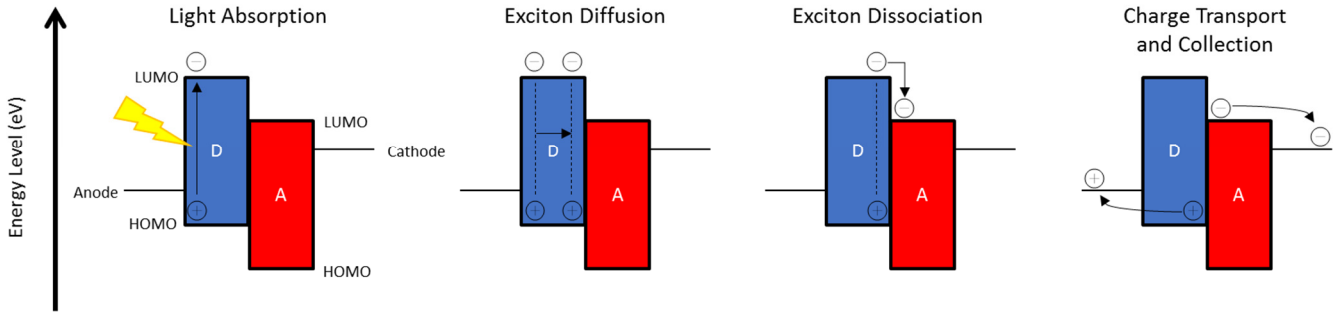

Figure 1.4. Major processes of photocurrent generation in an OPV device, show for light absorbed by the donor material.

Light Absorption

In an organic material, the valence and conductance bands are defined by the highest occupied molecular orbital (HOMO) and the lowest unoccupied molecular orbital (LUMO), with a band gap (E_g) equal to:

$$E_g = |E_{HOMO} - E_{LUMO}|$$

Where E_{HOMO} and E_{LUMO} are the energy levels of the HOMO and LUMO, respectively. Photons with energy greater than the band gap and matching a transition from an occupied molecular orbital to an unoccupied molecular orbital will promote an electron to the higher energy state leaving behind a positive electron hole. The number of photons that are absorbed in the organic active layer is determined by the layer thickness, as well as the absorption spectrum and molar absorptivity of the organic materials in the active layer. Therefore, selecting active materials with absorption spectra that cover a large portion of the solar spectrum is crucial for maximizing light absorption from the device. Alternatively, selecting materials which absorb specific wavelengths allows for colour tuning of the device for aesthetic or practical reasons (e.g., fully transparent devices for solar windows).

Exciton Diffusion

For an exciton to dissociate into free charge carriers, it must first diffuse to the donor/acceptor interface. Excitons have a lifetime on the order of 1-10 ns and can only diffuse a certain distance before recombination occurs, typically 5-20 nm in most organic materials.[25] The result of this limitation is that any exciton that is not generated within approximately 15 nm of the donor/acceptor interface will recombine before it is able to dissociate into a free electron and hole. Therefore, in a BHJ device it is ideal to form donor rich and acceptor rich domains on the order of 15 nm to increase the likelihood that excitons are generated close enough to the donor/acceptor interface to dissociate. The film morphology and the degree of phase separation between donor/acceptor is therefore crucial for efficient exciton diffusion.

Exciton Dissociation

One of the major differences in the operation of OPV devices and conventional c-Si devices is the nature of charge carrier generation in an organic material vs an inorganic material. Within a c-Si solar cell, the electron/hole pairs generated upon light absorption have a low binding energy, on the order of 0.015 eV, due to the high dielectric constant of silicon. Thermal energy at room temperature (300 K = 0.026 eV) is sufficient to immediately separate the electron/hole pairs into free charge carriers which are then transported and collected at their respective electrodes using a doped p/n junction. In an organic material, the absorption of light results in the formation of a Coulombically-bound Frenkel exciton (bound electron/hole pair), with a binding energy on the order of 0.3-1.0 eV.[26] The nature by which this binding energy is overcome to achieve exciton dissociation in OPV devices is not yet fully understood and an ongoing area of research. It was widely believed for a time that a minimum 0.3 eV energetic driving force was required between the HOMO and LUMO energy levels of the donor and acceptor materials to overcome the exciton binding energy and promote dissociation.[27] However, recent examples have shown that donor/acceptor pairs with < 0.3 eV energetic offsets may still produce high PCE devices.[28,29] Multiple factors have been suggested including hot transfer states, charge delocalization, energetic disorder, and entropy.[30–33]

Charge Transport and Collection

Before the free charge carriers can be extracted from the device, they must be transported from the donor/acceptor interface to their respective electrodes. The difference in the work functions of the two electrodes provides a built-in electric field to attract electrons and holes to the cathode and anode, respectively. It is ideal to have balanced electron and hole mobilities for the acceptor and donor materials to avoid the accumulation of charge within the device. Electrons and holes may still recombine while travelling to their respective electrodes or become trapped in isolated regions of donor/acceptor material, therefore an undisrupted path through each of the active materials to the electrodes is ideal. Charge carriers that successfully travel to their respective electrodes are extracted from the device to produce a current that may be applied to an external load.

The efficiency of an OPV device is governed by both the optoelectrical properties of the active materials as well as the nano-scale morphology of the active layer. It is therefore crucial to consider not only the absorption and charge transfer characteristics of new materials, but also their ability to form and maintain an ideal active layer morphology.

1.4. Characterization of OPV Devices

OPV performance is most often characterized by measuring the current-voltage (*I-V*) characteristic of a device, which provides the necessary information to calculate the power conversion efficiency (PCE). Since solar device performance is a function of the incident light intensity and spectrum, both must be specified when reporting calculated efficiencies. The standard for OPV testing uses an intensity of 1000 W/m^2 (100 mW/cm^2) and an air mass 1.5 (AM1.5) spectrum. This corresponds to the solar spectrum when the sun is at an angle of approximately 48° from the horizon, representative of the yearly average solar spectrum experienced at mid-latitude regions to provide a realistic expected efficiency of the device for outdoor use.[34]

In the dark, the *I-V* characteristics of an OPV will behave similar to that of a diode, defined by the equation:

$$I = I_0(e^{\frac{qV}{nkT}} - 1)$$

Where: I is the current flow, I_0 is the reverse bias current, q is the elementary charge, V is the voltage across the device, k is the Boltzmann constant, T is the absolute temperature of the device,

and *n* is an ideality factor typically between 1 and 2. Under illumination the *I-V* curve will shift down as photocurrent is produced and power can be extracted from the device, following the equation:

$$I = I_0\left(e^{\frac{qV}{nkT}} - 1\right) - I_L$$

Where I_L is the photogenerated current. The amount of photocurrent generation is a function of the device area, therefore it is standard to record current density-voltage (*J-V)* curves to allow for more straightforward comparison between devices of different area (**Figure 1.5 A**). It is important to note however that PCE generally decreases with increasing device area due to higher chances for film defects to be present and sheet resistance becoming significant at larger areas. The device area must therefore be considered when directly comparing the PCE between devices.

The PCE of an OPV is determined by the ratio of the maximum power generated by the device to the power of the incident light per unit area, and calculated as:

$$PCE = \frac{P_{max}}{P_{in}} = \frac{J_{SC} \cdot V_{OC} \cdot FF}{P_{in}}$$

Where:

P_{in} – Incident light intensity [mW/cm^2]

Jsc – Short circuit current density [mA/cm^2]. The J_{SC} is the largest amount of current that can be drawn from a device per unit area when it is under short circuit conditions (V = 0), corresponding to the y-intercept of the *J-V* curve. The J_{SC} is representative of the amount of light being absorbed by the device as well as the percentage of excitons which are successfully producing free charge carriers. This percentage is defined as the external quantum efficiency (EQE) which represents the ratio of incident photons to the number of charge carriers generated by the device at a particular wavelength (**Figure 1.5 B)**. The EQE and J_{SC} can be increased by improving the efficiency of any of the four steps of charge generation and collection.

Voc – Open circuit voltage [V]. The V_{OC} is the maximum voltage across the device under open circuit conditions (J = 0), corresponding to the x-intercept of the *J-V* curve. The maximum theoretical V_{OC} is set by the energy level difference of the HOMO of donor material and the LUMO of the acceptor material, therefore energy level matching of the donor and acceptor plays a large role in achieving a high V_{OC}. Numerous factors will affect the measured V_{OC} such as the donor/acceptor interfacial area and recombination losses.[35]

FF – Fill Factor [unitless]. The *FF* is an ideality factor which is defined as the ratio of the theoretical maximum power output of the device (J_{SC} x V_{OC}) to the actual maximum power that can be extracted from the device. The maximum power that can be extracted from a device occurs when the product of current density and voltage is at a maximum, and can be visually represented by the largest area rectangle that can fit within the bounds of the characteristic *J-V* curve under illumination (**Figure 1.5 A**). Therefore, the *FF* essentially describes the "squareness" of the J-V curve, and is defined as:

$$FF = \frac{J_{MPP}V_{MPP}}{J_{SC}V_{OC}}$$

Where J_{MPP} and V_{MPP} are the current and voltage at the maximum power point of the OPV, respectively. The *FF* is a complicated metric with many influences, although it is strongly affected by the amount of charge recombination and resistance losses within the device.[36] Series resistance (R_S) and shunt resistance (R_P) may be measured from the slope of the *J-V* curve at the V_{OC} and J_{SC} points, respectively. R_S describes resistance to current flow from the bulk resistance of each layer as well as all contact resistances at interfaces within the device, and is ideally minimal. R_P describes the resistance to current leakage from the edge of the device, pinholes, and trap states, and is ideally maximized.

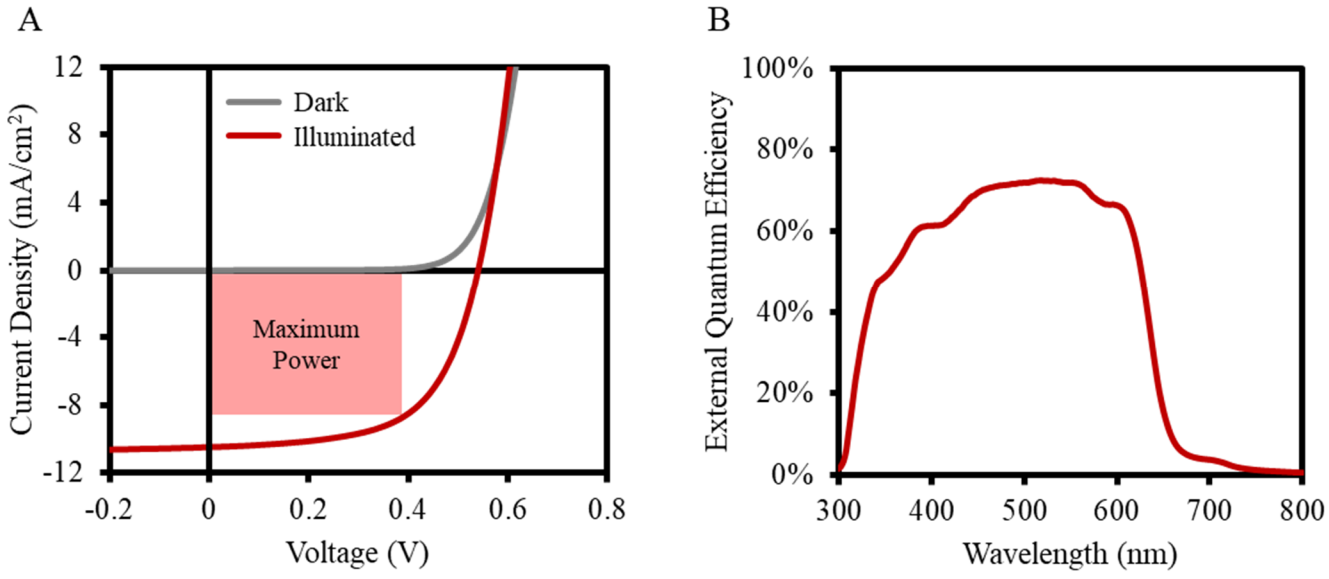

Figure 1.5. Example (A) *J-V* curves measured in the dark (grey) and under illumination (red), and (B) EQE curve for an OPV device.

1.5. State-of-the-art OPV Materials

Since the first BHJ OPV device shown by Heeger et. al., a significant portion of the field has been dedicated to the design and synthesis of novel soluble conjugated polymer donor and small molecular acceptors. The pair of poly(3-hexithiophene) (P3HT) and $PC_{61}BM$ emerged as a popular pair during the 2000s, and has since been by far the most extensively studied.[37] These devices typically achieve a PCE between 3-4 %, and are often used as a baseline for laboratory device fabrication capabilities. More recently however the P3HT/$PC_{61}BM$ pair has made way for higher performing donors and acceptors.

1.5.1. Polymer Donors

The popularity of P3HT stemmed from its relatively straightforward synthesis, a controllable and narrow polydispersity index, and ease of purification. However, its PCE is limited largely due to a relatively high bandgap of 1.9 eV restricting maximum absorption to approximately 660 nm thus missing the NIR region of the solar spectrum. Most novel polymer donors consequently have aimed to provide a reduced bandgap from HOMO and LUMO energy level tuning to push absorption into the NIR range. Side-chain optimization has also been considered to improve active layer morphology in BHJ devices. P3HT along with several common commercially available polymer donors are shown in **Figure 1.6**.

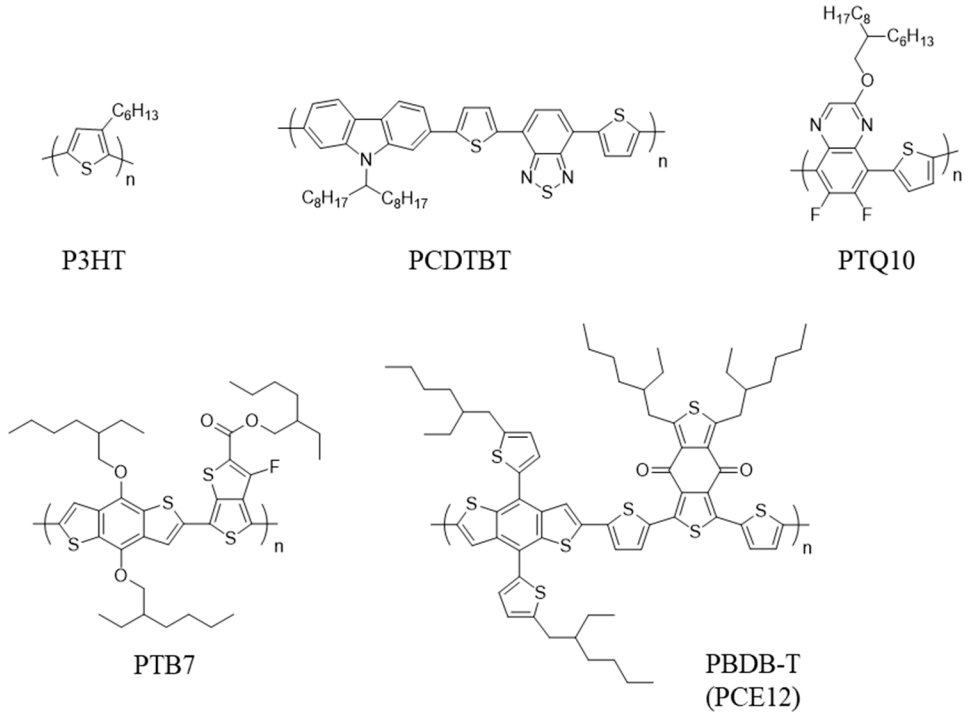

Figure 1.6. Base structures of common commercially available polymer donor materials

Band gap reduction in conjugated polymers has been achieved through the design of so called "push-pull" polymers which contain alternating electron rich and electron deficient moieties in their backbone. Rational selection of the two moieties may tune the HOMO/LUMO energy levels as well as the charge carrier mobilities to maximize device performance. Along with polymers PCDTBT and PTB7, PBDB-T has emerged as one of the top performing commercially available polymer materials, able to achieve PCEs over 17 %.[38]

1.5.2. Small Molecule Acceptors

The fullerene derivative $PC_{61}BM$ has remained an extremely popular electron acceptor after its first use in a BHJ OPV device, although it has slowly made way for a range of high-performance acceptors (**Figure 1.7**). $PC_{61}BM$ benefits from a high electron mobility and the ability to form appropriately sized domains in with polymers in a BHJ morphology for efficient photocurrent generation, however suffers from low molar absorption limiting J_{SC} and a deep LUMO limiting V_{OC}. Alternative fullerene derivatives have been introduced to address these issues, namely [6,6]-Phenyl-C71-butyric acid methyl ester ($PC_{71}BM$) with increased delocalization providing broadened absorption[39], as well as indene-C60 bisadduct (ICBA) with a shallower LUMO energy level to increase V_{OC}[40]. Despite these improvements, the expensive synthesis, low absorption, and poor tunability of fullerene acceptors has led to the investigation of alternative small molecules, so-called non-fullerene acceptors (NFAs).

NFAs are often designed to absorb at high wavelengths outside the absorption window of donor polymers to maximize the spectral coverage in devices. Low bandgaps for red-shifted absorption are also often achieved using a push-pull structure, typically using two electron poor moieties flanking an electron rich core. The material ITIC, consisting of an indacenodithieno[3,2-b]thiophene core flanked by two dicyanovinylindanone groups, was the first NFA to truly challenge fullerene acceptors achieving a PCE of 6.8 % in 2015.[41] With high electron mobility, absorption out to 700 nm, and a LUMO of 3.8 eV, ITIC addressed many of the shortcomings of fullerene acceptors and has remained popular in the literature. ITIC along with its methylated (ITIC-M)[42], chlorinated (ITIC-2Cl)[43], and fluorinated (ITIC-2F)[44] derivatives have all achieved PCEs over 10 %. Other notable commercially available NFAs include O-IDTBR which has been shown to achieve a PCE over 6 % in P3HT-based devices processed by printing techniques[45], and Y6 which currently holds the record PCE for OPV devices at 18 %.[18]

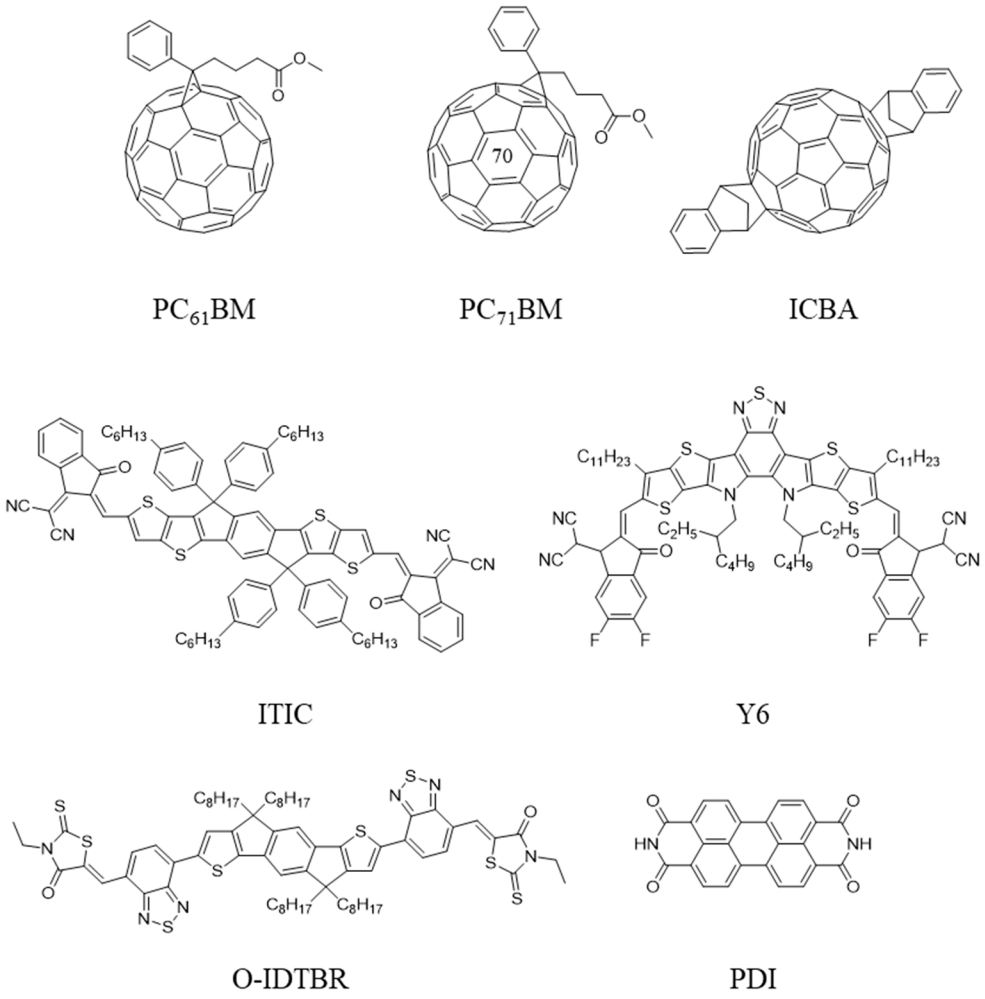

Figure 1.7. Base structures of common commercially available fullerene and non-fullerene acceptor materials.

1.5.3. The Cost of Complexity

In the pursuit of maximizing PCE of lab-scale devices through molecular design, the production cost and scalability of many active materials has been largely overlooked. A large portion of the total cost of OPV modules is modelled to come from the price of producing the active materials,[46] which scale approximately linearly with the number of synthetic steps involved in their synthesis[47]. It has become clear that many novel active materials have become too complex to ever be realized on a commercial scale, such as PCE record-holder Y6 which requires 15 steps to synthesize from commercially available starting materials. This trend of increasing complexity to achieve higher PCEs and the shift in molecular design focus that needs to be undertaken in OPV research has been articulated by a number of prominent OPV researchers in a 2019 paper:[48]

"As we approach 14–15% PCE with organic solar cells, the bottle neck in producing large scale OPV will become factors such as the cost and availability of the materials, compatibility with industrial printing processes and stability, rather than insufficient PCE to compete with rival technologies. Though there is some work currently being carried out on these problems, at present there appears to be less value placed on them in academia than there is on chasing a record PCE, which could relegate the field of OPV to the realms of academic curiosity rather than an achievable renewable energy technology should this imbalance in the research persist."

Several promising active materials with relatively improved scalability have been shown in the literature. For example, the polymer PTQ10 developed by Sun et. al., which employs comparatively simple thiophene and functionalized quinoxaline moieties in its backbone, and is capable of producing PCEs above 10 %.[49] NFAs based on derivatives of perylene diimide (PDI), a common industrial dye, have also shown exceptional PCEs approaching 10 %.[28] However, the cost and scalability of OPV active materials remains a challenge for achieving commercially feasible solution-processed devices, and few examples of low synthetic complexity and scalable donor/acceptor pairs have been demonstrated. In this regard it is also important to not dismiss older more established active materials such as P3HT, which despite comparatively lower PCEs is currently one of the most scalable materials available for BHJ devices.

1.6. Stability of OPV Devices

Along with active material costs, the stability of BHJ OPV devices remains an area of concern for their commercialization. The degradation pathways for OPV devices are numerous and are still an ongoing area of OPV research. Some of the main factors include UV, air, and water sensitivity of the active materials, diffusion of electrodes into the active layer, and phase separation of the active materials.[50] While environmental sensitivity and electrode diffusion can be addressed through the use of interlayers and improved encapsulation techniques, the stability of the active layer must be addressed by the organic materials themselves and will be the degradation pathway addressed in the scope of this thesis.

The interpenetrating network of the donor and acceptor materials in a BHJ device is a metastable morphology and can be lost as the donor and acceptor tend to phase separate and form aggregates that are more thermodynamically favorable. This has been shown to be particularly

problematic for devices using fullerene-based acceptors, where the phase separation of the active layer materials can occur with exposure to heat during operation and has also been shown to occur at room temperature in the dark.[51] Due to the rapid progress of new NFA materials, many high performing polymer/NFA systems have not yet undergone full length ageing studies and expected operational lifetimes are often based on estimations from extrapolation, if reported at all. Therefore, their morphological stability is not as well defined and less consistent across the unique structures of NFA materials.

A commonly studied approach to counteract phase separation of the active layer is to introduce crosslinking groups onto the donor and/or acceptor materials themselves. This can chemically "lock-in" the active layer and prevent rearrangement of the materials. For example, hexylthiophene may be copolymerized with modified monomers containing alkyl chains terminated with an alkene[52], bromine[53] or azide[54] functional groups to produce a cross-linkable P3HT. These P3HT analogues have proven to reduced heat-induced fullerene aggregation in OPV devices using $PC_{61}BM$, however the addition of functional groups to an active material without disrupting the properties of the original material can be challenging and significantly increases the synthetic complexity.

1.7. Ternary Additives in OPV Devices

As an alternative to developing novel donor or acceptor materials to increase efficiency or stability, increased performance has been achieved through the addition of a small amount of a third compound into the donor/acceptor blend, often referred to as a ternary additive. Depending on the nature of the additive, it can interact with the donor and acceptor compounds in several different ways, for example improving film morphology, spectral coverage, charge transfer efficiency, or active layer stability.[55] The term "ternary additive" in the scope of this thesis will be used to describe a material added in low weight percentages to a donor/acceptor blend designed to perform a specific function, and not ternary devices which utilize a pair of traditional donor or acceptor molecules.

Solvent additives for film morphology optimization are the simplest and most common ternary material used in the literature. These are solvating materials added in small amounts (< 3 vol%) which may improve the intermixing of the donor and acceptor materials and increase photocurrent generation. These types of additives are non-conjugated and do not contribute to charge generation

or transfer, only affect the way the active materials interact. The most commonly used example is the additive diiodooctane (DIO) which has been shown to effectively optimize active layer morphology, particularly in fullerene-based devices.[56]

The relative narrow absorption bands of many organic materials make it difficult to cover the entire solar spectrum with two active materials. Therefore, the addition a third compound that has an absorption spectrum complimentary to the donor and acceptor pair can significantly increase light absorption and photocurrent generation. These additives are commonly near-infrared (NIR) absorbing materials designed to absorb light outside the range of the donor polymer, often referred to as dye sensitizers. In addition to light absorption, ternary materials with intermediate HOMO/LUMO energy levels to the donor and acceptor may improve the efficiency of exciton dissociation at the donor/acceptor interface through a cascade charge transfer effect.[57]

Finally, as an alternative to functionalizing the donor or acceptor materials with crosslinking groups to stabilize active layer morphology, a cross-linkable additive can be introduced to perform the same function. These additives have the advantage of working with a range of donor/acceptor pairs and are often much less complex to synthesize than functionalized donor or acceptor materials. Since these additives generally do not work to improve charge generation or transport, care must be taken that the addition of the cross-linkable additive does not significantly reduce the initial device PCE. An example of such an additive was shown by Derue et. al. with the compound 4,4'-bis(azidomethyl)-1,1'-biphenyl (BABP).[58] BABP utilizes the azide (N_3) crosslinking group which undergoes a selective cycloaddition reaction with fullerenes under mild thermal heating. It was shown that by crosslinking only ~20% of fullerenes with the additive prevented active layer aggregation in P3HT/PC_{61}BM devices under thermal ageing tests.

1.8. Phthalocyanines and their use in OPV Devices

1.8.1. Phthalocyanines

In the pursuit of low cost and synthetically simple materials for use as donors, acceptors, or additives, derivatives of organic dyes are an obvious choice. Organic dyes possess many ideal characteristics for OPV device applications including general chemical and thermal stability, high molar absorptivity in the visible range, readily available starting materials, and established capabilities for large-scale production. A number of functionalized organic dyes have shown promising performance in OPV devices including the previously mentioned PDIs, boron-dipyrromethenes (BODIPYs)[59], indigos[60], porphyrins[61,62], and for the interest of this thesis, phthalocyanines (Pcs).

Pcs are a class of molecule closely related to porphyrins and porphyrazines first characterized in the 1930s.[63] The Pc structure consists of four bound isoindoline groups forming a fully conjugated planar heterocycle (**Figure 1.8 A**). The high degree of conjugation of the Pc core gives the material its characteristic deep blue/green colour from strong NIR absorption around 700 nm. Strong absorption combined with exceptional chemical and thermal stability have allowed Pcs to excel as dyes and pigments, for which they are currently produced on the scale of over 50,000 tonnes annualy.[64] However, perhaps the most enticing property of Pcs is their chemical versatility. Pcs can form complexes with over 70 different elements in their center to form metalophthalocyanines (MPcs), and may also be chemically functionalized on the periphery of the Pc ring and/or on the axial positions if the valency of the metal center allows (**Figure 1.8 B**). The high chemical versality of Pcs allow for tuning of their solubility, HOMO/LUMO energy levels, band gap, and solid-state properties which has allowed Pcs to succeed in a variety of disciplines outside of the colourant industry. Aside from their use in conventional OPV devices, MPcs have been studied in molecular photovoltaics[65], organic thin film transistors (OTFTs)[66], and organic light emitting diodes (OLEDs)[67–69]. They have also been investigated in other third generation PV technologies including DSSCs[70] and perovskites[71], and have found applications in other fields such as catalasis[72] and photodynamic therapy[73,74].

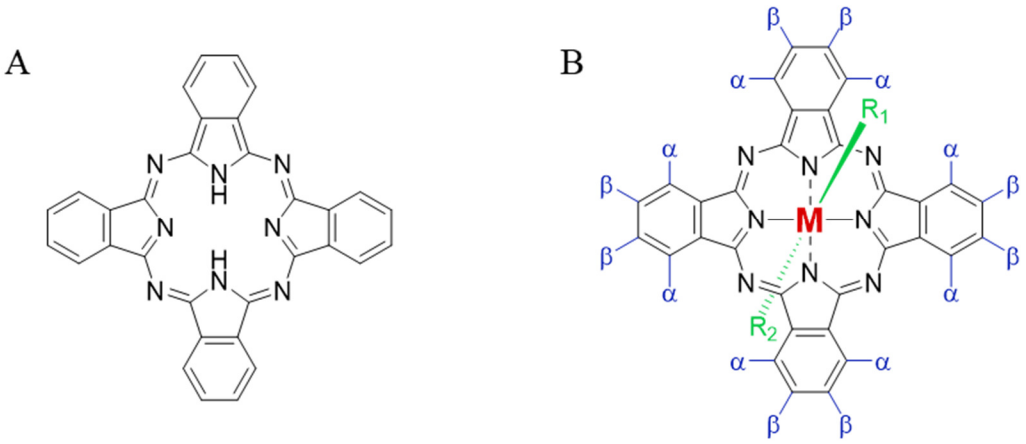

Figure 1.8. (A) Metal-free phthalocyanine, and (B) general structure for substituted phthalocyanines with a variable metal centre (red), peripheral (blue) and axial (green) positions available for chemical tuning.

1.8.2. Group 14 Phthalocyanines in BHJ OPV devices

Phthalocyanines have a long history in PHJ OPV devices, with copper phthalocyanine (CuPc) being employed as the donor in the aforementioned report of the first bilayer device by Tang in 1986.[13] Since this report, CuPc and zinc phthalocyanine (ZnPc) have been by far the most commonly studied derivatives in PHJ OPV devices, typically as an electron donor paired with a PDI derivative or with fullerene (C_{60}). CuPc and ZnPc have since achieved impressive PCEs up to 3.6 %[75] and 4.56 %[76], respectively, when paired with C_{60} in binary devices. Several other MPcs have also been investigated in PHJ devices, including metal-free Pc[77], lead (II) Pc[78], aluminum Pc[79], titanyl Pc[80], and tin Pc[81,82].

The literature of MPc derivatives in solution processed BHJ devices is much less established in comparison to the PHJ architecture. MPcs however have seen recently increased interest in BHJ OPV devices with derivatives of silicon phthalocyanine (SiPc). Pcs have generally poor solubility in most common organic solvents without additional chemical functionalization. Divalent MPcs such as CuPc and ZnPc do not have axial positions available for solubilizing groups and therefore must be functionalized on the peripheral positions, for example with tert-butyl[83] or polyethylene glycol[84] functional groups, to be used in solution-processed BHJ OPV devices. This chemistry is performed before the cyclization of the Pc ring, and products must often be purified by column chromatography techniques due to the poor thermal stability of the peripheral solubilizing chains. Silicon phthalocyanine however may form chemically and thermally stable

derivatives with 2 axial functional groups given the tetravalency of silicon. Axial functionalization gives an simple synthetic handle for chemical tuning as the chemistry can be performed after the formation of the Pc chromophore through straightforward substitution chemistry.

SiPc is relatively unusual in that it can not be readily formed from phthalonitrile, which is one of the standard building blocks for many other MPcs. SiPc is instead most easily formed from a reaction of diiminoisoindoline with silicon tetrachloride in quinoline to form silicon phthalocyanine dichloride (Cl_2-SiPc) **(Scheme 1.1i)**.[85] The axial chlorines of Cl_2-SiPc act as good leaving groups for the substitution of alternative substituents in further reactions.

Most early work with SiPcs in OPV devices utilized the alkylsilane-substituted bis(tri-n-hexylsilyl oxide) silicon phthalocyanine ($(3HS)_2$-SiPc), first synthesized by Wheeler et. al. by converting Cl_2-SiPc to silicon phthalocyanine dihydroxide (OH_2-SiPc) followed by the reaction with tri-n-hexylchlorosilane in refluxing pyridine for 5 h giving yields of approximately 50% (**Scheme 1ii**).[86] More recently, Gessner et. al. showed a 1-step route by reacting Cl_2-SiPc with tri-n-hexylchlorosilane in refluxing chlorobenzene using NaOH and the phase transfer catalyst Aliquat® HTA1 (trioctyl methyl ammonium chloride) (**Scheme 1iii**), achieving yields up to 96%.[87]

Work by Lessard et. al has introduced the use of phenoxy-substituted SiPcs, which may be synthesized in a straightforward reaction combining Cl_2-SiPc with an excess of a phenol in refluxing chlorobenzene overnight (**Scheme 1iv**). This reaction gives the bis(phenoxy) silicon phthalocyanine in yields above 80%.[88,89] More recent studies have explored carboxylate-substituted silicon phthalocyanines, which similarly may be similarly synthesized reacting Cl_2-SiPc with an excess of a carboxylic acid in refluxing diglyme or toluene, depending on the solubility of the reagent (**Scheme 1v,vi**). To date a variety of carboxylate substituents have been reported.[67,90,91] These various synthetic routes allow for exceptionally straightforward functionalization of a diverse range of axial substituents which have not yet been fully investigated.

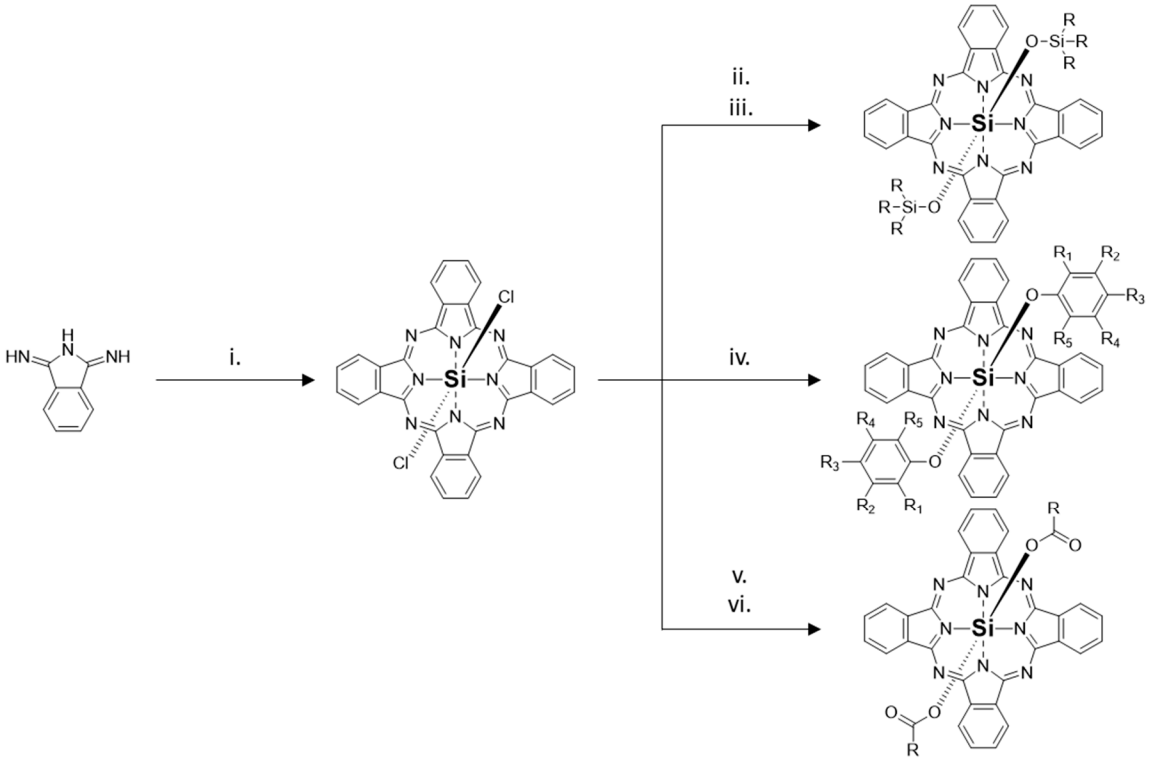

Scheme 1.1. Synthetic pathways for Cl_2-SiPc and commonly utilized SiPc derivatives, Where: (i) $SiCl_4$, quinoline, 219 °C for 2 h. (ii) CsOH, DMF, 120 °C for 4 h. Chlorosilane derivative, pyridine, 130 °C for 4h. (iii) Chlorosilane derivative, Aliquat HTA1, NaOH, chlorobenzene, 132 °C for 6h. (iv) Phenol, chlorobenzene, 132°C for 20 h (v) Carboxylic acid derivative, diglyme, 160°C for 20 h. (v) Carboxylic acid derivative, toluene, 110°C for 20 h

The use of SiPc derivatives in BHJ OPV devices was pioneered by Honda *et. al.* through a series of studies between 2009 and 2012 utilizing $(3HS)_2$-SiPc as a ternary additive in P3HT/PC_{61}BM devices. It was shown that the bulky axial groups of $(3HS)_2$-SiPc reduced the tendency of the material to form aggregate phases which can disrupt the optimal morphology and decrease PCE, a common issue encountered with planar dye molecules such as ZnPc or CuPc.[92,93] The addition of $(3HS)_2$-SiPc in low (< 10%) weight percentages to P3HT/PC_{61}BM devices resulted in a significantly improved J_{SC}, arsing from an increased EQE contribution from the P3HT/PC_{61}BM, as well as contribution from the phthalocyanine absorption in the range of 650-700nm. It was shown that $(3HS)_2$-SiPc tended to selectively migrate to the donor/acceptor interface and, due to its intermediate energy levels to P3HT and PC_{61}BM, was able to facilitate charge transfer to increase J_{SC} while maintaining the optimal BHJ morphology.[94,95]

In 2014, Lessard *et. al.* synthesized a series of phthalocyanine materials chemically similar to $(3HS)_2$-SiPc to determine if they would perform in a similar manner, namely bis(3-pentadecylphenoxy) silicon phthalocyanine ($(PDP)_2$-SiPc) and bis(tri-n-hexylsilyl oxide) germanium phthalocyanine $(3HS)_2$-GePc.[96] This study was the first to use a soluble Group 14 Pc with a center other than silicon in BHJ OPV devices. Despite having high solubility and similar optoelectrical properties to $(3HS)_2$-SiPc, both materials were detrimental to the efficiency of P3HT/PC_{61}BM devices as ternary additives. It was hypothesized that the unique high driving force for $(3HS)_2$-SiPc to crystallize may contribute to its ability to migrate to the donor/acceptor interface and facilitate charge transfer. Dang *et. al.* further explored the effect of alkyl chain length on the properties of bis(tri-n-alkylsilyl oxide) silicon phthalocyanines in a study with bis(tri-n-butylsilyl oxide) silicon phthalocyanine ($(3BS)_2$-SiPc) and bis(tri-n-isopropylsilyl oxide) silicon phthalocyanine ($(3TS)_2$-SiPc).[97] As an additive in P3HT/PC_{61}BM devices, both $(3BS)_2$-SiPc and $(3TS)_2$-SiPc were able to further increase J_{SC} above that of $(3HS)_2$-SiPc. XRD revealed the shorter alkyl chains may allow the derivatives to form smaller crystalline domains and become more dispersed at the donor/acceptor interface.

Honda et. al. demonstrated tri-n-hexylsilyl oxide functionalization of silicon napthalocyanine (SiNc) and its use as a ternary additive, achieving EQE contribution up to 800 nm in P3HT/PC_{61}BM and P3HT/N2200 devices.[93,98,99] Lim et. al. have also shown that tert-butyl functionalization of the peripheral positions of the SiNc can further reduce aggregation effects allowing for higher dye loadings and increased Pc contribution to photocurrent generation achieving an impressive PCE of 4.5 %.[100]

Ke et. al. have recently introduced the use of pyrene-substituted SiPcs, with a focus on the effect of varying the length of the alkyl chain spacer.[90] Surface energy studies showed that the materials should also be present at the P3HT/PC_{61}BM interface to facilitate charge transfer similar to $(3HS)_2$-SiPc. The pyrene-substituted SiPcs were able to increase efficiency up to 51.6% over reference P3HT/PC_{61}BM devices. Similar functional groups were also applied to SiNc and employed in P3HT/PC_{61}BM/SiPc/SiNc quaternary devices.[101]

Only a few preliminary studies have been conducted exploring the use of soluble SiPcs as NFAs in BHJ OPV devices. SiPc interestingly can effectively transport electrons to be used as an NFA, unlike CuPc and ZnPc which are generally *p*-type and therefore used as donor materials.[91] Dang *et. al.* recently explored the use of bis(tri-n-alkylsilyl oxide)-SiPcs as NFAs achieving a PCE up to 1.1 % with P3HT.[97] Zysman-Colman et. al. have also shown the use of soluble carboxylate-substituted SiPcs, achieving an efficiencies as high as 2.7 % when paired with PTB7.[67]

1.9. Scope of Thesis

This chapter has introduced OPV devices as a solar PV technology in context with the solar market. The structures and major working principles of OPV devices have been defined along with commonly employed active materials. The critical challenge of combining efficiency, stability, and scalability for OPV devices to become a commercially viable technology has been outlined. Given the low number of low-cost active materials, the promising preliminary results of soluble MPcs in OPV devices combined with their very straightforward synthetic pathways show the materials merit further investigation. With the small amount of chemical functional groups that have been utilized, the full potential of MPc derivatives in OPV devices has not yet been reached.

The aim of this thesis is to access novel molecular designs and OPV device configurations using Group 14 phthalocyanines to determine what roles they may play in OPV devices, specifically assessing how their performance can be improved as both ternary additives and NFAs. The following chapters will address this by investigating the following questions:

1) How will the chemical and physical properties of structurally analogous soluble SnPcs compare to SiPcs, and is SnPc a viable option to access more complex peripheral chemistry in OPV applications? (Chapter 2)
2) Can the chemical versatility of MPcs be utilized to incorporate crosslinking functionality to address active layer stability as a ternary additive? (Chapter 3)
3) Can the PCE of SiPc derivatives as NFAs be improved, or are they more suited for use as additives in ternary devices? (Chapters 4 & 5)

1.10. References

(1) Kabir, E.; Kumar, P.; Kumar, S.; Adelodun, A. A.; Kim, K. H. Solar Energy: Potential and Future Prospects. *Renew. Sustain. Energy Rev.* **2018**, *82*, 894–900.

(2) IEA (2020). World Energy Outlook 2020, IEA, Paris https://www.iea.org/reports/world-energy-outlook-2020.

(3) Chapin, D. M.; Fuller, C. S.; Pearson, G. L. A New Silicon P-n Junction Photocell for Converting Solar Radiation into Electrical Power. *J. Appl. Phys.* **1954**, *25* (5), 676–677.

(4) Phillips, S. Photovoltaics Report. *Fraunhofer ISE and Werner Warmuth, PSE Projects GmbH*. 2020.

(5) A, K.; K, T.; Y, S.; T, M. Organometal Halide Perovskites as Visible-Light Sensitizers for Photovoltaic Cells. *J. Am. Chem. Soc.* **2009**, *131* (17), 6050–6051.

(6) Al-Ashouri, A.; Köhnen, E.; Li, B.; Magomedov, A.; Hempel, H.; Caprioglio, P.; Márquez, J. A.; Vilches, A. B. M.; Kasparavicius, E.; Smith, J. A.; Phung, N.; Menzel, D.; Grischek, M.; Kegelmann, L.; Skroblin, D.; Gollwitzer, C.; Malinauskas, T.; Jošt, M.; Matič, G.; Rech, B.; Schlatmann, R.; Topič, M.; Korte, L.; Abate, A.; Stannowski, B.; Neher, D.; Stolterfoht, M.; Unold, T.; Getautis, V.; Albrecht, S. Monolithic Perovskite/Silicon Tandem Solar Cell with >29% Efficiency by Enhanced Hole Extraction. *Science.* **2020**, *370* (6522), 1300–1309.

(7) Djurišić, A. B.; Liu, F. Z.; Tam, H. W.; Wong, M. K.; Ng, A.; Surya, C.; Chen, W.; He, Z. B. Perovskite Solar Cells - An Overview of Critical Issues. *Prog. Quantum Electron.* **2017**, *53*, 1–37.

(8) Sun, C.; Xia, R.; Shi, H.; Yao, H.; Liu, X.; Hou, J.; Huang, F.; Yip, H. L.; Cao, Y. Heat-Insulating Multifunctional Semitransparent Polymer Solar Cells. *Joule* **2018**, *2* (9), 1816–1826.

(9) Meitzner, R.; Schubert, U. S.; Hoppe, H. Agrivoltaics—The Perfect Fit for the Future of Organic Photovoltaics. *Adv. Energy Mater.* **2021**, *11* (1), 2002551.

(10) Satharasinghe, A.; Hughes-Riley, T.; Dias, T. A Review of Solar Energy Harvesting Electronic Textiles. *Sensors* **2020**, *20*, 5938.

(11) Ryu, H. S.; Park, S. Y.; Lee, T. H.; Kim, J. Y.; Woo, H. Y. Recent Progress in Indoor Organic Photovoltaics. *Nanoscale*. The Royal Society of Chemistry 2020, pp 5792–5804.

(12) Li, N.; Brabec, C. J. Washing Away Barriers. *Nat. Energy* **2017**, *2* (10), 772–773.

(13) Tang, C. W. Two-Layer Organic Photovoltaic Cell. *Appl. Phys. Lett.* **1986**, *48* (2), 183–185.

(14) Yu, G.; Gao, J.; Hummelen, J. C.; Wudl, F.; Heeger, A. J. Polymer Photovoltaic Cells : Enhanced Efficiencies via a Network of Internal Donor-Acceptor Heterojunctions. *Science.* **1995**, *270*, 1789–1791.

(15) Hong, L.; Yao, H.; Wu, Z.; Cui, Y.; Zhang, T.; Xu, Y.; Yu, R.; Liao, Q.; Gao, B.; Xian, K.; Woo, H. Y.; Ge, Z.; Hou, J. Eco-Compatible Solvent-Processed Organic Photovoltaic Cells with Over 16% Efficiency. *Adv. Mater.* **2019**, *31* (39), 1903441.

(16) Lin, Y.; Adilbekova, B.; Firdaus, Y.; Yengel, E.; Faber, H.; Sajjad, M.; Zheng, X.; Yarali, E.; Seitkhan, A.; Bakr, O. M.; El-Labban, A.; Schwingenschlögl, U.; Tung, V.; McCulloch, I.; Laquai, F.; Anthopoulos, T. D. 17% Efficient Organic Solar Cells Based on Liquid Exfoliated WS2 as a Replacement for PEDOT:PSS. *Adv. Mater.* **2019**, *31*, 1902965.

(17) Cui, Y.; Yao, H.; Zhang, J.; Zhang, T.; Wang, Y.; Hong, L.; Xian, K.; Xu, B.; Zhang, S.; Peng, J.; Wei, Z.; Gao, F.; Hou, J. Over 16% Efficiency Organic Photovoltaic Cells Enabled by a Chlorinated Acceptor with Increased Open-Circuit Voltages. *Nat. Commun.* **2019**, *10* (1), 2515.

(18) Liu, Q.; Jiang, Y.; Jin, K.; Qin, J.; Xu, J.; Li, W.; Xiong, J.; Liu, J.; Xiao, Z.; Sun, K.; Yang, S.; Zhang, X.; Ding, L. 18% Efficiency Organic Solar Cells. *Sci. Bull.* **2020**, *65* (4), 272–275.

(19) Facchetti, A. Polymer Donor-Polymer Acceptor (All-Polymer) Solar Cells. *Mater. Today* **2013**, *16* (4), 123–132.

(20) Collins, S. D.; Ran, N. A.; Heiber, M. C.; Nguyen, T. Small Is Powerful: Recent Progress in Solution-Processed Small Molecule Solar Cells. *Adv. Energy Mater.* **2017**, 1602242.

(21) Venkateswararao, A.; Wong, K.-T. Small Molecules for Vacuum-Processed Organic Photovoltaics: Past, Current Status, and Prospect. *Bull. Chem. Soc. Jpn.* **2021**, *94* (3), 812–838.

(22) Hoppe, H.; Sariciftci, N. S. Morphology of Polymer/Fullerene Bulk Heterojunction Solar Cells. *J. Mater. Chem.* **2006**, *16* (1), 45–61.

(23) Jørgensen, M.; Carlé, J. E.; Søndergaard, R. R.; Lauritzen, M.; Dagnæs-Hansen, N. A.; Byskov, S. L.; Andersen, T. R.; Larsen-Olsen, T. T.; Böttiger, A. P. L.; Andreasen, B.; Fu, L.; Zuo, L.; Liu, Y.; Bundgaard, E.; Zhan, X.; Chen, H.; Krebs, F. C. The State of Organic Solar Cells - A Meta Analysis. *Sol. Energy Mater. Sol. Cells* **2013**, *119*, 84–93.

(24) Yu, J. S.; Kim, I.; Kim, J. S.; Jo, J.; Larsen-Olsen, T. T.; Søndergaard, R. R.; Hösel, M.; Angmo, D.; Jørgensen, M.; Krebs, F. C. Silver Front Electrode Grids for ITO-Free All Printed Polymer Solar Cells with Embedded and Raised Topographies, Prepared by Thermal Imprint, Flexographic and Inkjet Roll-to-Roll Processes. *Nanoscale* **2012**, *4* (19), 6032–6040.

(25) Menke, S. M.; Holmes, R. J. Exciton Diffusion in Organic Photovoltaic Cells. *Energy Environ. Sci.* **2014**, *7* (2), 499–512.

(26) Knupfer, M. Exciton Binding Energies in Organic Semiconductors. *Appl. Phys. A Mater. Sci. Process.* **2003**, *77* (5), 623–626.

(27) Scharber, M. C.; Mühlbacher, D.; Koppe, M.; Denk, P.; Waldauf, C.; Heeger, A. J.; Brabec, C. J. Design Rules for Donors in Bulk-Heterojunction Solar Cells - Towards 10 % Energy-Conversion Efficiency. *Adv. Mater.* **2006**, *18* (6), 789–794.

(28) Liu, J.; Chen, S.; Qian, D.; Gautam, B.; Yang, G.; Zhao, J.; Bergqvist, J.; Zhang, F.; Ma, W.; Ade, H.; Inganäs, O.; Gundogdu, K.; Gao, F.; Yan, H. Fast Charge Separation in a Non-Fullerene Organic Solar Cell with a Small Driving Force. *Nat. Energy* **2016**, *1*, 16089.

(29) Tang, A.; Xiao, B.; Wang, Y.; Gao, F.; Tajima, K.; Bin, H.; Zhang, Z. G.; Li, Y.; Wei, Z.; Zhou, E. Simultaneously Achieved High Open-Circuit Voltage and Efficient Charge Generation by Fine-Tuning Charge-Transfer Driving Force in Nonfullerene Polymer Solar Cells. *Adv. Funct. Mater.* **2018**, *28* (6), 1704507.

(30) Clarke, T. M.; Durrant, J. R. Charge Photogeneration in Organic Solar Cells. *Chem. Rev.* **2010**, *110* (11), 6736–6767.

(31) Tamura, H.; Burghardt, I. Ultrafast Charge Separation in Organic Photovoltaics Enhanced by Charge Delocalization and Vibronically Hot Exciton Dissociation. *J. Am. Chem. Soc.* **2013**, *135* (44), 16364–16367.

(32) Heitzer, H. M.; Savoie, B. M.; Marks, T. J.; Ratner, M. A. Organic Photovoltaics: Elucidating the Ultra-Fast Exciton Dissociation Mechanism in Disordered Materials. *Angew. Chemie - Int. Ed.* **2014**, *53* (29), 7456–7460.

(33) Hood, S. N.; Kassal, I. Entropy and Disorder Enable Charge Separation in Organic Solar Cells. *J. Phys. Chem. Lett.* **2016**, *7* (22), 4495–4500.

(34) Riordan, C.; Hulstrom, R. What Is an Air Mass 1.5 Spectrum? In *Conference Record of the IEEE Photovoltaic Specialists Conference*; 1990; Vol. 2, pp 1085–1088.

(35) Vandewal, K.; Tvingstedt, K.; Gadisa, A.; Inganäs, O.; Manca, J. V. On the Origin of the Open-Circuit Voltage of Polymer-Fullerene Solar Cells. *Nat. Mater.* **2009**, *8* (11), 904–909.

(36) Qi, B.; Wang, J. Fill Factor in Organic Solar Cells. *Phys. Chem. Chem. Phys.* **2013**, *15* (23), 8972.

(37) Dang, M. T.; Hirsch, L.; Wantz, G. P3HT:PCBM, Best Seller in Polymer Photovoltaic Research. *Adv. Mater.* **2011**, *23* (31), 3597–3602.

(38) Zheng, Z.; Yao, H.; Ye, L.; Xu, Y.; Zhang, S.; Hou, J. PBDB-T and Its Derivatives: A Family of Polymer Donors Enables over 17% Efficiency in Organic Photovoltaics. *Mater. Today* **2020**, *35*, 115–130.

(39) Zhang, F.; Zhuo, Z.; Zhang, J.; Wang, X.; Xu, X.; Wang, Z.; Xin, Y.; Wang, J.; Wang, J.; Tang, W.; Xu, Z.; Wang, Y. Influence of PC60BM or PC70BM as Electron Acceptor on the Performance of Polymer Solar Cells. *Sol. Energy Mater. Sol. Cells* **2012**, *97*, 71–77.

(40) He, Y.; Chen, H. Y.; Hou, J.; Li, Y. Indene - C60 Bisadduct: A New Acceptor for High-Performance Polymer Solar Cells. *J. Am. Chem. Soc.* **2010**, *132* (4), 1377–1382.

(41) Lin, Y.; Wang, J.; Zhang, Z. G.; Bai, H.; Li, Y.; Zhu, D.; Zhan, X. An Electron Acceptor Challenging Fullerenes for Efficient Polymer Solar Cells. *Adv. Mater.* **2015**, *27* (7), 1170–1174.

(42) Li, S.; Ye, L.; Zhao, W.; Zhang, S.; Mukherjee, S.; Ade, H.; Hou, J. Energy-Level Modulation of Small-Molecule Electron Acceptors to Achieve over 12% Efficiency in Polymer Solar Cells. *Adv. Mater.* **2016**, *28* (42), 9423–9429.

(43) Zhang, H.; Yao, H.; Hou, J.; Zhu, J.; Zhang, J.; Li, W.; Yu, R.; Gao, B.; Zhang, S.; Hou, J. Over 14% Efficiency in Organic Solar Cells Enabled by Chlorinated Nonfullerene Small-

Molecule Acceptors. *Adv. Mater.* **2018**, *30* (28), 1–7.

(44) Zhao, W.; Li, S.; Yao, H.; Zhang, S.; Zhang, Y.; Yang, B.; Hou, J. Molecular Optimization Enables over 13% Efficiency in Organic Solar Cells. *J. Am. Chem. Soc.* **2017**, *139* (21), 7148–7151.

(45) Gasparini, N.; Salvador, M.; Strohm, S.; Heumueller, T.; Levchuk, I.; Wadsworth, A.; Bannock, J. H.; de Mello, J. C.; Egelhaaf, H. J.; Baran, D.; McCulloch, I.; Brabec, C. J. Burn-in Free Nonfullerene-Based Organic Solar Cells. *Adv. Energy Mater.* **2017**, *7*, 1700770.

(46) Machui, F.; Hösel, M.; Li, N.; Spyropoulos, G. D.; Ameri, T.; Søndergaard, R. R.; Jørgensen, M.; Scheel, A.; Gaiser, D.; Kreul, K.; Lenssen, D.; Legros, M.; Lemaitre, N.; Vilkman, M.; Välimäki, M.; Nordman, S.; Brabec, C. J.; Krebs, F. C. Cost Analysis of Roll-to-Roll Fabricated ITO Free Single and Tandem Organic Solar Modules Based on Data from Manufacture. *Energy Environ. Sci.* **2014**, *7* (9), 2792–2802.

(47) Osedach, T. P.; Andrew, T. L.; Bulović, V. Effect of Synthetic Accessibility on the Commercial Viability of Organic Photovoltaics. *Energy Environ. Sci.* **2013**, *6* (3), 711–718.

(48) Wadsworth, A.; Moser, M.; Marks, A.; Little, M. S.; Gasparini, N.; Brabec, C. J.; Baran, D.; McCulloch, I. Critical Review of the Molecular Design Progress in Non-Fullerene Electron Acceptors towards Commercially Viable Organic Solar Cells. *Chem. Soc. Rev.* **2019**, *48* (6), 1596–1625.

(49) Sun, C.; Pan, F.; Bin, H.; Zhang, J.; Xue, L.; Qiu, B.; Wei, Z.; Zhang, Z. G.; Li, Y. A Low Cost and High Performance Polymer Donor Material for Polymer Solar Cells. *Nat. Commun.* **2018**, *9*, 743.

(50) Jørgensen, M.; Norrman, K.; Krebs, F. C. Stability/Degradation of Polymer Solar Cells. *Sol. Energy Mater. Sol. Cells* **2008**, *92* (7), 686–714.

(51) Li, N.; Perea, J. D.; Kassar, T.; Richter, M.; Heumueller, T.; Matt, G. J.; Hou, Y.; Güldal, N. S.; Chen, H.; Chen, S.; Langner, S.; Berlinghof, M.; Unruh, T.; Brabec, C. J. Abnormal Strong Burn-in Degradation of Highly Efficient Polymer Solar Cells Caused by Spinodal Donor-Acceptor Demixing. *Nat. Commun.* **2017**, *8*, 14541.

(52) Miyanishi, S.; Tajima, K.; Hashimoto, K. Morphological Stabilization of Polymer Photovoltaic Cells by Using Cross-Linkable Poly(3-(5-Hexenyl)Thiophene). *Macromolecules* **2009**, *42* (5), 1610–1618.

(53) Kim, B. J.; Miyamoto, Y.; Ma, B.; Fréchet, J. M. J. Photocrosslinkable Polythiophenes for Efficient, Thermally Stable, Organic Photovoltaics. *Adv. Funct. Mater.* **2009**, *19* (14), 2273–2281.

(54) Kim, H. J.; Han, A. R.; Cho, C. H.; Kang, H.; Cho, H. H.; Lee, M. Y.; Fréchet, J. M. J.; Oh, J. H.; Kim, B. J. Solvent-Resistant Organic Transistors and Thermally Stable Organic Photovoltaics Based on Cross-Linkable Conjugated Polymers. *Chem. Mater.* **2012**, *24* (1), 215–221.

(55) Goubard, F.; Wantz, G. Ternary Blends for Polymer Bulk Heterojunction Solar Cells. *Polym. Int.* **2014**, *63* (8), 1362–1367.

(56) Lou, S. J.; Zhou, N.; Guo, X.; Chang, R. P. H.; Marks, T. J.; Chen, L. X. Effects of 1,8-Diiodooctane on Domain Nanostructure and Charge Separation Dynamics in PC71BM-Based Bulk Heterojunction Solar Cells. *J. Mater. Chem. A* **2018**, *6* (46), 23805–23818.

(57) Lu, L.; Kelly, M. A.; You, W.; Yu, L. Status and Prospects for Ternary Organic Photovoltaics. *Nat. Photonics* **2015**, *9* (8), 491–500.

(58) Derue, L.; Dautel, O.; Tournebize, A.; Drees, M.; Pan, H.; Berthumeyrie, S.; Pavageau, B.; Cloutet, E.; Chambon, S.; Hirsch, L.; Rivaton, A.; Hudhomme, P.; Facchetti, A.; Wantz, G. Thermal Stabilisation of Polymer-Fullerene Bulk Heterojunction Morphology for Efficient Photovoltaic Solar Cells. *Adv. Mater.* **2014**, *26* (33), 5831–5838.

(59) Srinivasa Rao, R.; Bagui, A.; Hanumantha Rao, G.; Gupta, V.; Singh, S. P. Achieving the Highest Efficiency Using a BODIPY Core Decorated with Dithiafulvalene Wings for Small Molecule Based Solution-Processed Organic Solar Cells. *Chem. Commun.* **2017**, *53* (51), 6953–6956.

(60) Brebels, J.; Klider, K. C. C. W. S.; Kelchtermans, M.; Verstappen, P.; Van Landeghem, M.; Van Doorslaer, S.; Goovaerts, E.; Garcia, J. R.; Manca, J.; Lutsen, L.; Vanderzande, D.; Maes, W. Low Bandgap Polymers Based on Bay-Annulated Indigo for Organic Photovoltaics: Enhanced Sustainability in Material Design and Solar Cell Fabrication. *Org. Electron.* **2017**, *50*, 264–272.

(61) Yin, H.; Chen, S.; Cheung, S. H.; Li, H. W.; Xie, Y.; Tsang, S. W.; Zhu, X.; So, S. K. Porphyrin-Based Thick-Film Bulk-Heterojunction Solar Cells for Indoor Light Harvesting. *J. Mater. Chem. C* **2018**, *6* (34), 9111–9118.

(62) Vartanian, M.; Singhal, R.; De La Cruz, P.; Biswas, S.; Sharma, G. D.; Langa, F. Low Energy Loss of 0.57 EV and High Efficiency of 8.80% in Porphyrin-Based BHJ Solar Cells. *ACS Appl. Energy Mater.* **2018**, *1* (3), 1304–1315.

(63) Linstead, R. P. Phthalocyanines. Part I. A New Type of Synthetic Colouring Matters. *J. Chem. Soc.* **1934**, 1016–1017.

(64) Gregory, P. Industrial Applications of Phthalocyanines. *J. Porphyr. Phthalocyanines* **2000**, *4*, 432–437.

(65) Martínez-Díaz, M. V.; De La Torre, G.; Torres, T. Lighting Porphyrins and Phthalocyanines for Molecular Photovoltaics. *Chemical Communications* **2010**, 46, 7090–7108.

(66) Melville, O. A.; Lessard, B. H.; Bender, T. P. Phthalocyanine-Based Organic Thin-Film Transistors: A Review of Recent Advances. *ACS Appl. Mater. Interfaces* **2015**, *7* (24), 13105–13118.

(67) Zysman-Colman, E.; Ghosh, S. S.; Xie, G.; Varghese, S.; Chowdhury, M.; Sharma, N.; Cordes, D. B.; Slawin, A. M. Z.; Samuel, I. D. W. Solution-Processable Silicon Phthalocyanines in Electroluminescent and Photovoltaic Devices. *ACS Appl. Mater. Interfaces* **2016**, *8* (14), 9247–9253.

(68) Pearson, A. J.; Plint, T.; Jones, S. T. E.; Lessard, B. H.; Credgington, D.; Bender, T. P.;

Greenham, N. C. Silicon Phthalocyanines as Dopant Red Emitters for Efficient Solution Processed OLEDs. *J. Mater. Chem. C* **2017**, *5* (48), 12688–12698.

(69) Plint, T.; Lessard, B. H.; Bender, T. P. Assessing the Potential of Group 13 and 14 Metal/Metalloid Phthalocyanines as Hole Transporting Layers in Organic Light Emitting Diodes. *J. Appl. phys.* **2016**, *119* (1), 145502.

(70) Urbani, M.; Ragoussi, M. E.; Nazeeruddin, M. K.; Torres, T. Phthalocyanines for Dye-Sensitized Solar Cells. *Coord. Chem. Rev.* **2019**, *381*, 1–64.

(71) Urbani, M.; De La Torre, G.; Nazeeruddin, M. K.; Torres, T. Phthalocyanines and Porphyrinoid Analogues as Hole-and Electron-Transporting Materials for Perovskite Solar Cells. *Chem. Soc. Rev.* **2019**, *48* (10), 2738–2766.

(72) Sorokin, A. B. Phthalocyanine Metal Complexes in Catalysis. *Chem. Rev.* **2013**, *113*, 8152–8191.

(73) Bonnett, R. Photosensitizers of the Porphyrin and Phthalocyanine Series for Photodynamic Therapy. *Chem. Soc. Rev.* **1995**, *24*, 19–33.

(74) Lo, P. C.; Rodríguez-Morgade, M. S.; Pandey, R. K.; Ng, D. K. P.; Torres, T.; Dumoulin, F. The Unique Features and Promises of Phthalocyanines as Advanced Photosensitisers for Photodynamic Therapy of Cancer. *Chem. Soc. Rev.* **2020**, *49* (4), 1041–1056.

(75) Peumans, P.; Forrest, S. R. Very-High-Efficiency Double-Heterostructure Copper Phthalocyanine/C60 Photovoltaic Cells. *Appl. Phys. Lett.* **2001**, *79* (1), 126–128.

(76) Zhou, Y.; Taima, T.; Miyadera, T.; Yamanari, T.; Kitamura, M.; Nakatsu, K.; Yoshida, Y. Phase Separation of Co-Evaporated ZnPc:C60 Blend Film for Highly Efficient Organic Photovoltaics. *Appl. Phys. Lett.* **2012**, *100* (23), 233302.

(77) Petritsch, K.; Friend, R. H.; Lux, A.; Rozenberg, G.; Moratti, S. C.; Holmes, A. B. Liquid Crystalline Phthalocyanines in Organic Solar Cells. *Synth. Met.* **1999**, *102*, 1776–1777.

(78) Kim, I.; Haverinen, H. M.; Wang, Z.; Madakuni, S.; Kim, Y.; Li, J.; Jabbour, G. E. Efficient Organic Solar Cells Based on Planar Metallophthalocyanines. *Chem. Mater.* **2009**, *21* (18), 4256–4260.

(79) Bailey-Salzman, R. F.; Rand, B. P.; Forrest, S. R. Near-Infrared Sensitive Small Molecule Organic Photovoltaic Cells Based on Chloroaluminum Phthalocyanine. *Appl. Phys. Lett.* **2007**, *91* (1), 2005–2008.

(80) Placencia, D.; Wang, W.; Gantz, J.; Jenkins, J. L.; Armstrong, N. R. Highly Photoactive Titanyl Phthalocyanine Polymorphs as Textured Donor Layers in Organic Solar Cells. *J. Phys. Chem. C* **2011**, *115* (38), 18873–18884.

(81) Pandey, R.; Kerner, R. A.; Menke, S. M.; Holst, J.; Josyula, K. V. B. B.; Holmes, R. J. Tin Naphthalocyanine Complexes for Infrared Absorption in Organic Photovoltaic Cells. *Org. Electron. physics, Mater. Appl.* **2013**, *14* (3), 804–808.

(82) Li, N.; Lassiter, B. E.; Lunt, R. R.; Wei, G.; Forrest, S. R. Open Circuit Voltage Enhancement Due to Reduced Dark Current in Small Molecule Photovoltaic Cells. *Appl. Phys. Lett.* **2009**, *94* (2), 023307.

(83) Bekalé, L.; Barazzouk, S.; Sakai, N.; Murakami, T.; Miyoshi, K.; Miyasaka, T.; Hotchandani, S. Solution-Processed TBu4-ZnPc:C61 Bulk Heterojunction Organic Photovoltaic Cells. *Jpn. J. Appl. Phys.* **2016**, *55* (3), 032301.

(84) Kadem, B.; Kaya, E. N.; Hassan, A.; Durmuş, M.; Basova, T. Composite Materials of P3HT:PCBM with Pyrene Substituted Zinc(II) Phthalocyanines: Characterisation and Application in Organic Solar Cells. *Sol. Energy* **2019**, *189*, 1–7.

(85) Lowery, M. K.; Starshak, A. J.; Esposito, J. N.; Krueger, P. C.; Kenney, M. E. Dichloro(Phthalocyanino)Silicon. *Inorg. Chem* **1965**, 128.

(86) Wheeler, B. L.; Nagasubramanian, G.; Bard, a J.; Schechtman, L. a; Dininny, D. R.; Kenney, M. E. A Silicon Phthalocyanine and a Silicon Naphthalocyanine: Synthesis, Electrochemistry, and Electrogenerated Chemiluminescence. *J. Am. Chem. Soc.* **1984**, *106* (24), 7404–7410.

(87) Gessner, T.; Sens, R.; Ahlers, W.; Vamvakaris, C. Preparation of Silicon Phthalocyanines and Germanium Phthalocyanines and Related Substances. US 2010/0113767 A1, 2010.

(88) Lessard, H.; White, R. T.; Al-amar, M.; Plint, T.; Castrucci, S.; Josey, D. S.; Lu, Z.; Bender, T. P.; Lessard, B. H.; White, R. T.; Al-amar, M.; Plint, T.; Castrucci, S.; Josey, D. S.; Lu, Z.; Bender, T. P. Assessing the Potential Roles of Silicon and Germanium Phthalocyanines in Planar Heterojunction Organic Photovoltaic Devices and How Pentafluoro Phenoxylation Can Enhance $\pi - \pi$ Interactions and Device Performance. *ACS Appl. Mater. Interfaces* **2015**, *7*, 5076–5068.

(89) Lessard, B. H. B. H.; Grant, T. M.; White, R.; Thibau, E.; Lu, Z.-H.; Bender, T. P. The Position and Frequency of Fluorine Atoms Changes the Electron Donor/Acceptor Properties of Fluorophenoxy Silicon Phthalocyanines within Organic Photovoltaic Devices. *J. Mater. Chem. A* **2015**, *3*, 24512–24524.

(90) Ke, L.; Min, J.; Adam, M.; Gasparini, N.; Hou, Y.; Perea, J. D.; Chen, W.; Zhang, H.; Fladischer, S.; Sale, A. C.; Spiecker, E.; Tykwinski, R. R.; Brabec, C. J.; Ameri, T. A Series of Pyrene-Substituted Silicon Phthalocyanines as Near-IR Sensitizers in Organic Ternary Solar Cells. *Adv. Energy Mater.* **2016**, *6* (7), 1502355.

(91) Melville, O. A.; Grant, T. M.; Lessard, B. H. Silicon Phthalocyanines as N-Type Semiconductors in Organic Thin Film Transistors. *J. Mater. Chem. C* **2018**, *6* (20), 5482–5488.

(92) Honda, S.; Nogami, T.; Ohkita, H.; Benten, H.; Ito, S. Improvement of the Light-Harvesting Efficiency in Polymer/Fullerene Bulk Heterojunction Solar Cells by Interfacial Dye Modification. *ACS Appl. Mater. Interfaces* **2009**, *1* (4), 804–810.

(93) Honda, S.; Ohkita, H.; Benten, H.; Ito, S. Multi-Colored Dye Sensitization of Polymer/Fullerene Bulk Heterojunction Solar Cells. *Chem. Commun.* **2010**, *46* (35), 6596–6598.

(94) Honda, S.; Yokoya, S.; Ohkita, H.; Benten, H.; Ito, S. Light-Harvesting Mechanism in Polymer/Fullerene/Dye Ternary Blends Studied by Transient Absorption Spectroscopy. *J. Phys. Chem. C* **2011**, *115* (22), 11306–11317.

(95) Honda, S.; Ohkita, H.; Benten, H.; Ito, S. Selective Dye Loading at the Heterojunction in Polymer/Fullerene Solar Cells. *Adv. Energy Mater.* **2011**, *1* (4), 588–598.

(96) Lessard, B. H.; Dang, J. D.; Grant, T. M.; Gao, D.; Seferos, D. S.; Bender, T. P. Bis(Tri-n-Hexylsilyl Oxide) Silicon Phthalocyanine: A Unique Additive in Ternary Bulk Heterojunction Organic Photovoltaic Devices. *ACS Appl. Mater. Interfaces* **2014**, *6*, 15040–15051.

(97) Dang, M. T.; Grant, T. M.; Yan, H.; Seferos, D. S.; Lessard, B. H.; Bender, T. P. Bis(Tri-n-Alkylsilyl Oxide) Silicon Phthalocyanines: A Start to Establishing a Structure Property Relationship as Both Ternary Additives and Non-Fullerene Electron Acceptors in Bulk Heterojunction Organic Photovoltaic Devices. *J. Mater. Chem. A* **2017**, *5* (24), 12168–12182.

(98) Ito, S.; Hirata, T.; Mori, D.; Benten, H.; Ohkita, H.; Honda, S. Near-Infrared Dye Sensitization of Polymer/Polymer Thin-Film Solar Cells. *Mol. Cryst. Liq. Cryst.* **2013**, *578*, 19–25.

(99) Xu, H.; Ohkita, H.; Hirata, T.; Benten, H.; Ito, S. Near-IR Dye Sensitization of Polymer Blend Solar Cells. *Polymer.* **2014**, *55* (12), 2856–2860.

(100) Lim, B.; Bloking, J. T.; Ponec, A.; Mcgehee, M. D.; Sellinger, A. Ternary Bulk Heterojunction Solar Cells: Addition of Soluble NIR Dyes for Photocurrent Generation beyond 800 Nm. *ACS Appl. Mater. Interfaces* **2014**, *6*, 6905–6913.

(101) Ke, L.; Gasparini, N.; Min, J.; Zhang, H.; Adam, M.; Rechberger, S.; Forberich, K.; Zhang, C.; Spiecker, E.; Tykwinski, R. R.; Brabec, C. J.; Ameri, T. Panchromatic Ternary/Quaternary Polymer/Fullerene BHJ Solar Cells Based on Novel Silicon Naphthalocyanine and Silicon Phthalocyanine Dye Sensitizers. *J. Mater. Chem. A* **2017**, *5* (6), 2550–2562.

Chapter 2: Soluble Tin Phthalocyanines in OPV Devices and OTFTs

This chapter contains work published in *ACS Applied Electronic Materials:*

T. M. Grant, N. A. Rice, L. Muccioli, F. Castet, and B. H. Lessard., *ACS Appl. Electron. Mater.* **2019**, 1, 4, 494-504.

2.1. Context

As outlined in **Chapter 1**, the use of group 14 phthalocyanines in solution-processed BHJ OPV devices is generally limited to derivatives of SiPc. During the first part of my thesis, I was interested in considering alternative metal centers to silicon to circumvent the requirement of a diiminoisoindoline starting material in place of a simpler Pc building block such as phthalonitrile. Tin phthalocyanine was chosen as an alternative due to its previous success in PHJ OPV devices and OTFTs, and ability to be synthesized directly from phthalonitrile. I aimed to establish if the same conventional alkylsiloxy axial chemistry could be applied to SnPc and study how changing the metal center would affect the physical and optoelectrical properties of the materials. If the tin center was comparable or superior in performance than silicon, SnPc would have a much simpler synthetic handle to explore the peripheral functionalization of Group IV phthalocyanines.

2.2. Contribution of Authors

I performed all chemical synthesis and characterization of the reported phthalocyanines compounds, as well as the fabrication and characterization of all OPV devices. NAR performed the fabrication and characterization of OTFT devices as well as AFM measurements, while LM and FC performed the DFT modelling. This work was supervised by BHL. I wrote the first draft of the manuscript with written contributions for the OTFT and DFT sections by NAR and LM/FC, respectively. All authors assisted with editing the manuscript.

2.3. Abstract

Tin phthalocyanines have shown promise in both organic thin film transistors (OTFTs) and organic photovoltaic (OPV) devices, however no examples of solution processable axial derivatives have been reported. We synthesized and characterized tin phthalocyanines (SnPcs) with tributyl silane and trihexyl silane axial functional groups and examined their performance in OTFTs and in poly(3-hexylthiophene) : phenyl-C61-butyric acid methyl ester (P3HT:$PC_{61}BM$) OPV devices as ternary additives. We also report the OTFT performance of the previously studied trialkyl silane silicon phthalocyanines for comparison. In polycrystalline OTFTs the tin derivatives show higher electron mobilities than their silicon counterparts due to increased molecular interactions. As a ternary additive in OPV devices, similar to the SiPc analogues, both SnPc derivatives show an EQE contribution > 20 % in the range of 650 – 750 nm. These results suggest soluble SnPcs show potential as active materials in OTFTs and OPV devices, justifying further investigation into additional derivatives of SnPcs.

2.4. Introduction

Metal phthalocyanines (MPcs) are a versatile family of molecules that have seen considerable interest as active materials in organic electronic devices due to their chemical and thermal stability, favourable optoelectrical properties, and chemical versatility. Recently, group 14 metal/metalloid phthalocyanines such as silicon phthalocyanine (SiPc) have seen interest in organic light emitting diodes (OLEDs),[1–3] organic photovoltaic (OPV) devices,[1,4,5] and more recently organic thin film transistors (OTFTs)[6] due to their ability to form derivatives with two axial substituents, one above and one below the planar phthalocyanine chromophore, unlike the commonly studied copper and zinc phthalocyanines. These axial substituents facilitate modification of material properties such as solubility and solid-state arrangement to tune their performance in organic electronic devices without compromising the extremely low reorganization energies characteristic of unsubstituted metal phthalocyanines,[7,8] a fundamental requirement for achieving optimal charge transport.

SiPcs have most extensively been studied as additives in ternary bulk heterojunction (BHJ) OPV devices, where a third compound is introduced into the conventional donor/acceptor blend which may work to provide additional light absorption, improve active layer morphology, increase charge transfer efficiency, or extend device lifetime.[9–11] Honda et. al. first established the use of bis(tri-n-hexylsilyl oxide) silicon phthalocyanine ($(3HS)_2$-SiPc) as an additive in poly(3-hexylthiophene) (P3HT) and phenyl-C61-butyric acid methyl ester ($PC_{61}BM$) OPV devices through a series of studies.[12–15] Addition of $(3HS)_2$-SiPc below 10 weight percent resulted in an increased J_{SC} due to NIR absorption from the phthalocyanine chromophore in conjunction with improved charge transfer between the P3HT and $PC_{61}BM$ due to a cascade energy transfer effect. Similar results have since been achieved with SiPcs functionalized with other trialkylsilanes,[16] pyrenes,[17] carboxylic acids,[18] as well as trialkylsilane-functionalized silicon naphthalocyanines (SiNcs)[13,19] This cascade energy transfer with an IR sensitizer has also been shown in P3HT devices using metal-free phthalocyanine,[20] other small molecule additives,[21,22] as well as the low band-gap polymer poly[(4,40-bis(2-ethylhexyl)dithieno[3,2-b:2′,3′-d]-silole)-2,6-diyl-alt-(4,7-bis(2-thienyl)-2,1,3-benzothiadiazole)-5,5′-diyl] (Si-PCPDTBT) in both P3HT/$PC_{61}BM$[23,24] and P3HT/indene-C60-bisadduct (ICBA)[25,26] devices.

In order to further explore the use of group 14 MPcs in organic electronic devices, we are interested in looking down the periodic table to study alternative metal/metalloid centres in place of silicon. Germanium phthalocyanine has previously been used as an additive in ternary P3HT/$PC_{61}BM$ BHJ OPV devices, however addition as low as 3.7 weight percent resulted in efficiencies below 0.05 %.[27] Alternatively, tin phthalocyanine (SnPc) has shown positive results in vapor deposited organic electronic devices. Dichloro tin phthalocyanine (Cl_2-SnPc)[28] and tin phthalocyanine oxide (SnOPc)[29] have been investigated in OTFTs with reported electron mobilities as high as 0.30 and 0.44 cm^2/Vs, respectively. Tin (II) phthalocyanine has been studied in OPV devices due to its redshifted absorption resulting from dimer formation effectively lowering the band gap of the material.[30–33] Additionally, unlike SiPc, SnPc may be synthesized directly from phthalonitrile and does not require the formation of a diiminoisoindoline intermediate.[34] This lowers the complexity of the synthesis and facilitates the incorporation of functional groups onto the peripheral positions of the phthalocyanine which is often used to extended conjugation of the chromophore to redshift the peak absorption wavelength into the infrared.[31] Currently the literature of axially-substituted SnPcs is not well established,[35] and to the best of our knowledge, no examples exist of solution-processable SnPcs incorporated in organic electronic devices.

Here, we report the synthesis and characterization of two novel soluble axially-substituted SnPcs: bis(tri-n-hexylsily oxide) tin phthalocyanine ($(3HS)_2$-SnPc) and bis(tri-n-butylsily oxide) tin phthalocyanine ($(3BS)_2$-SnPc). The materials properties of these new phthalocyanines were compared to structurally analogous SiPcs through UV-Vis absorbance spectroscopy, thermogravimetric analysis (TGA), differential scanning calorimetry (DSC), cyclic voltammetry (CV), X-ray crystallography and density functional theory (DFT) calculations. Additionally, the four phthalocyanine derivatives were incorporated as active layers in OTFTs and as ternary additives in OPV devices (**Figure 2.1**), allowing for a comparison of the performance of the two new SnPcs in two types of organic electronic devices.

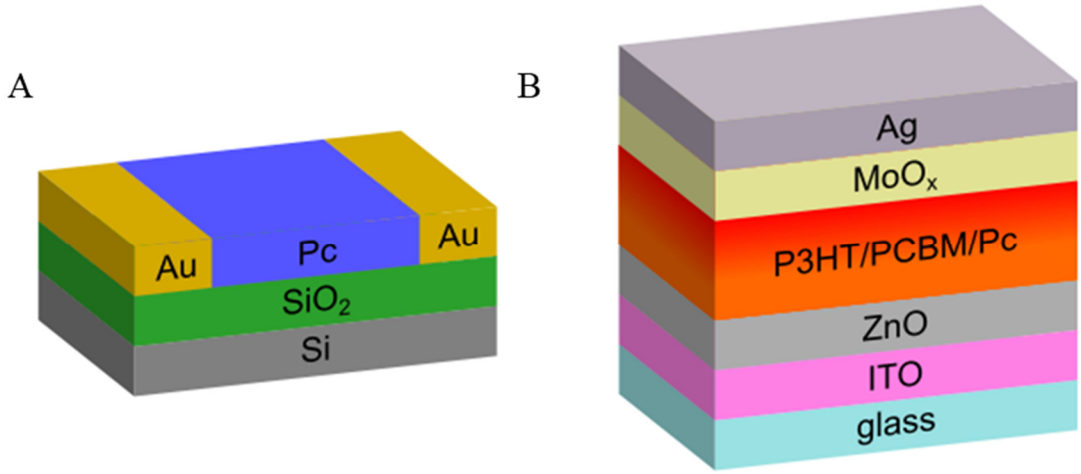

Figure 2.1. Schematic of (A) OTFT and (B) OPV architectures used in this study.

2.5. Results and Discussion

Synthesis and Characterization of SnPcs

$(3BS)_2$-SnPc and $(3HS)_2$-SnPc were prepared by applying the synthetic procedure for bis(tri-*n*-alkylsilyl) silicon phthalocyanines developed by Gressner et al. to Cl_2-SnPc (Scheme 2.1).[36] Both products were purified by train sublimation and isolated as blue powders soluble above 20 mg/mL in common OPV processing solvents (including chloroform, chlorobenzene and dichlorobenzene), forming teal/blue-coloured solutions. The phthalocyanines were also soluble in toluene, THF, diethyl ether, and acetone, while insoluble in methanol and isopropanol.

Scheme 2.1. Synthetic route for preparing $(3HS)_2$-SnPc and $(3BS)_2$-SnPc, where (i) $SnCl_4$, quinoline, 219 °C, 2 h; (ii) tri-n-alkylchlorosilane, Aliquat® HTA1, sodium hydroxide, chlorobenzene, 132 °C, 6 h.

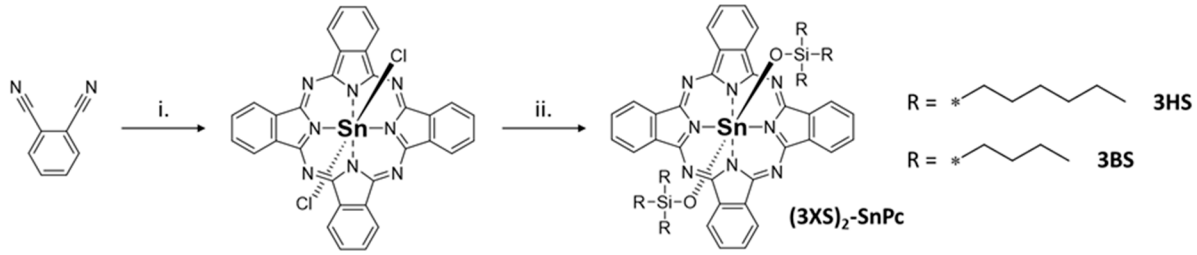

The novel SnPcs were characterized by solution-state UV-Vis absorbance spectroscopy, CV, TGA and DSC for comparison with their SiPc analogues which have been previously reported.[16,33] A summary of these results can be found in **Table 2.1**. UV-Vis spectra in toluene for $(3HS)_2$-SnPc and $(3BS)_2$-SnPc showed identical characteristic phthalocyanine absorption in the NIR region, with a maximum absorption peak of 682 nm; this is slightly red-shifted from 669 nm reported for the SiPc analogues (**Figure 2.2 A**).[16] An optical band gap ($E_{gap,opt}$) of 1.78 eV was estimated from the onset of the absorption spectra, and is similar to previously reported values for axial substituted phthalocyanines.[5,6,16,17]

Highest occupied molecular orbital (HOMO) energy levels were estimated from cyclic voltammetry using empirical correlations.[37,38] Characteristic cyclic voltammograms can be found in the Supporting Information. Lowest unoccupied molecular orbitals (LUMOs) were estimated using $E_{gap,opt}$ in dichloromethane. $(3HS)_2$-SnPc and $(3BS)_2$-SnPc were found to have identical HOMO and LUMO energy levels of -5.52 and -3.74 eV, respectively. These values are approximately 0.2 eV deeper than the reported values for $(3HS)_2$-SiPc and $(3BS)_2$-SiPc but remain intermediate to P3HT and $PC_{61}BM$ (**Figure 2.2 B**). These trends correlate well with DFT calculations, which predict a downshift of the HOMO (LUMO) energy levels of 0.25 (0.31) eV, as well as a slight redshift of ~0.04 eV (~10 nm) of the first absorption band, when going from $(3XS)_2$-SiPc to $(3XS)_2$-SnPc (**Table 2.2**).

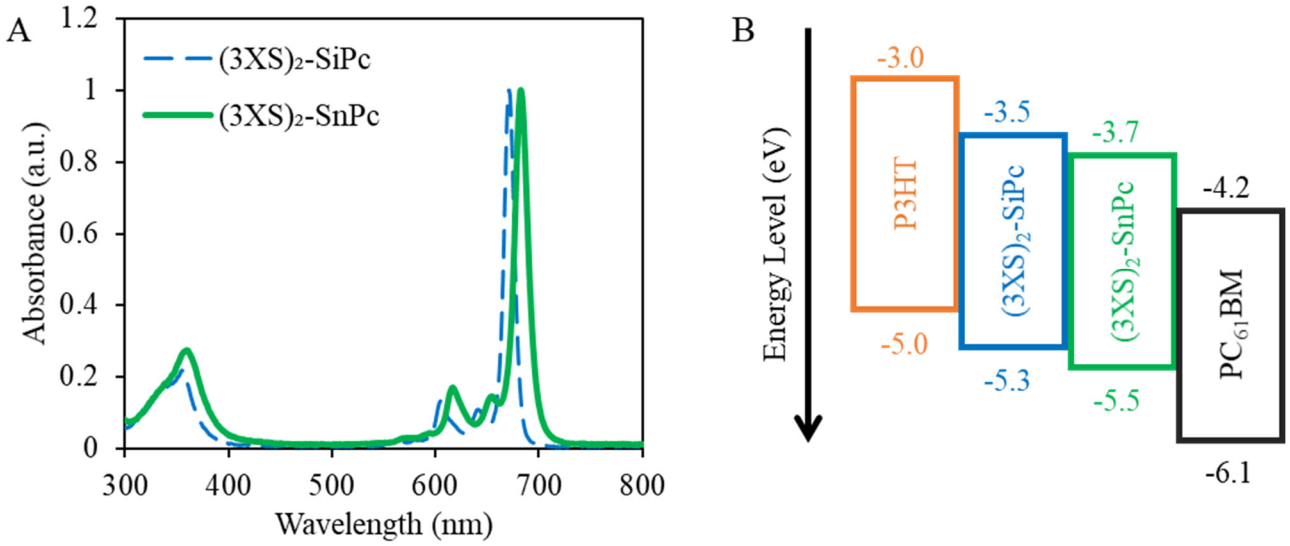

Figure 2.2. (A) UV-Vis absorption spectra of $(3XS)_2$-SiPc (blue) and $(3XS)_2$-SnPc (green) in toluene solution. (B) Energy level diagram for P3HT, $(3XS)_2$-SiPc, $(3XS)_2$-SnPc, and $PC_{61}BM$. Where X is H (hexyl) or B (butyl).

Table 2.1. Summary of UV-Vis in toluene, electrochemical and thermal characterization of $(3HS)_2$-SnPc and $(3BS)_2$-SnPc. Previously reported values for $(3HS)_2$-SiPc and $(3BS)_2$-SiPc are included for comparison.[16,27]

	E_{HOMO} (eV)	E_{LUMO} (eV)	$E_{gap,opt}$ (eV)	λ_{max} (nm)	T_d (°C)	T_m (°C)	T_c (°C)	Ref.
$(3HS)_2$-SiPc	-5.31	-3.49	1.82	669	342	173	110	[16,27]
$(3BS)_2$-SiPc	-5.31	-3.49	1.82	669	318	231/61	219/63	[16]
$(3HS)_2$-SnPc	-5.52	-3.74	1.78	682	199	/	/	This work
$(3BS)_2$-SnPc	-5.52	-3.74	1.78	682	227	45	46	This work

Table 2.2. DFT energy values of the HOMO, LUMO, LUMO+1, electron affinity (obtained from differences in the total energies of the charged and neutral molecules in their optimized geometries), internal reorganization energies (λ_i) and transition energies towards the two nearly-degenerate singlet states S_1 and S_2 (ΔE_{01} and ΔE_{02}, in both eV and nm), calculated at the B3LYP/6-31G(d) level (using the DZVP basis set for Sn).

	E_{HOMO} (eV)	E_{LUMO} (eV)	E_{LUMO+1} (eV)	EA (eV)	ΔE_{01} (eV (nm))	ΔE_{02} (eV (nm))	λ_i (meV)
$(3HS)_2$-SiPc	-5.14	-2.95	-2.94	2.07	2.05 (605)	2.06 (602)	266
$(3BS)_2$-SiPc	-5.12	-2.93	-2.92	2.03	2.05 (604)	2.06 (602)	241
$(3HS)_2$-SnPc	-5.39	-3.26	-3.24	2.39	2.01 (616)	2.03 (610)	259
$(3BS)_2$-SnPc	-5.37	-3.23	-3.22	2.34	2.02 (614)	2.03 (610)	234

From TGA, the thermal decomposition temperature (T_d) for $(3HS)_2$-SnPc and $(3BS)_2$-SnPc were found to be 199 °C and 227 °C, respectively. These values are significantly lower than the previously reported values for $(3HS)_2$-SiPc (342 °C) and $(3BS)_2$-SiPc (318 °C), not surprising given the weaker Sn-O bond. DSC was used to identify the melting temperature (T_m) and crystallization temperature (T_c) of the SnPc analogues. Characteristic heat flow versus temperature plots can be found in the Supporting Information. $(3HS)_2$-SiPc showed no discernable transitions below 199 °C, while $(3BS)_2$-SnPc showed a single transition with a T_m of 45 °C and T_c of 46 °C.

Crystal structure

Variations in solid state packing can drastically affect the performance of a material in organic electronic devices, therefore it is essential to determine if the tin metal centre will alter the molecular packing compared to the silane-substituted silicon phthalocyanines. Single crystals of $(3HS)_2$-SnPc (CCDC# 1884805) and $(3BS)_2$-SnPc (CCDC# 1884804) were grown by evaporation from DCM solution and analysed by single crystal X-ray diffraction. The resulting packing motifs are shown in **Figure 2.3**. $(3HS)_2$-SnPc shows no significant π-π stacking between phthalocyanine rings, and the hexyl chains are oriented either parallel to the phthalocyanine plane or at an angle of 45°. However, $(3BS)_2$-SnPc shows significant π-π stacking, with dual overlap between phthalocyanines with a centroid-centroid distance of 3.635 Å. The closer stacking is a result of the perpendicular orientation of two butyl chains on each $(3BS)_2$-SnPc molecule, allowing neighbouring phthalocyanine chromophores to overlap. These motifs are significantly different than those reported for $(3HS)_2$-SiPc (CCDC #988974)[27] and $(3BS)_2$-SiPc (CCDC #1522758)[16] which show no π- π overlap between adjacent phthalocyanine rings, and alkyl chains oriented parallel to the phthalocyanine plans (**Figure 2.3**). The different crystal structure indicate that SnPcs may show significantly different solid-state packing compared to SiPcs even for the same axial substituents.

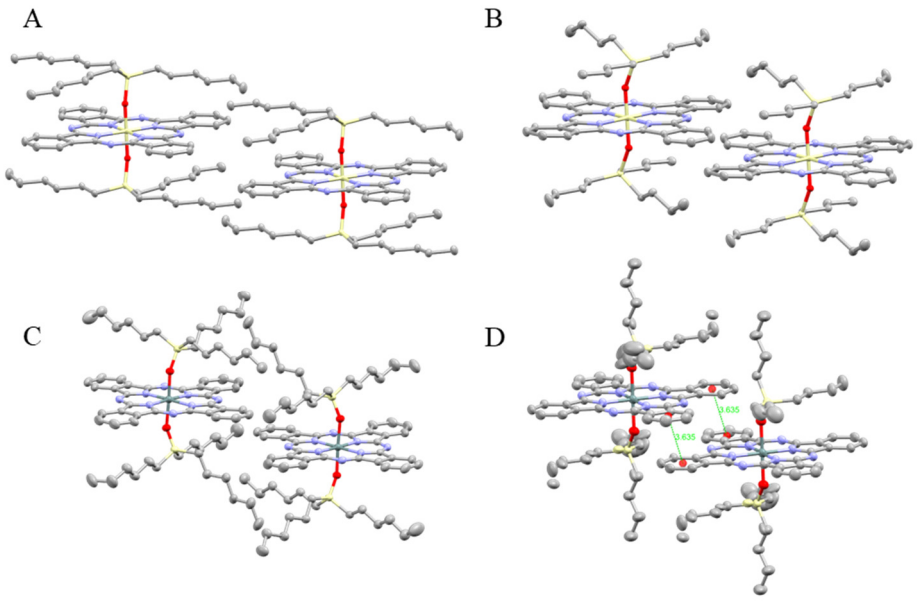

Figure 2.3. Crystal structures for (A) $(3HS)_2$-SiPc and (B) $(3BS)_2$-SiPc (C) $(3HS)_2$-SnPc and (D) $(3BS)_2$-SnPc determined by single crystal X-ray diffraction.

Charge Mobility Calculations

Although mobilities calculated for perfectly ordered single crystals cannot be directly compared to device performances measured on polycrystalline and partially amorphous film morphologies (see below), DFT calculations enable a reliable prediction of these intrinsic material properties and possibly a useful rationalization of the measured mobility trends. Intramolecular reorganization energies ($\boldsymbol{\lambda_i}$, **Table 2.2**) and transfer integrals ($\boldsymbol{J_\kappa}$) characterizing the electron coupling between molecular pairs (**Table S 2.1**) were first calculated at the B3LYP/6-31G(d) level. Then, relative electron mobilities along the crystal axes (see the computational section for details), along with the expected dimensionality of the transport properties, were evaluated for the four compounds (**Table 2.3**).

$(3HS)_2$-SiPc exhibits the lowest electron mobility within the four investigated crystals, due to the slightly larger value of $\boldsymbol{\lambda_i}$ and, more importantly, to the weaker intermolecular couplings arising from the absence of π-π stacking between adjacent phthalocyanine rings (**Figure S2.7**). Replacing the axial trihexyl silane by a tributyl silane group induces a lowering of the internal reorganisation energy by 25 meV, combined with an increase by a factor 3 of the largest transfer integral. As a consequence, the average mobility is enhanced by a factor ~6. DFT calculations also predict a significant enhancement of the electron mobility upon changing the core atom from $(3XS)_2$-SiPc to $(3XS)_2$-SnPc, owing to the higher spatial overlap between molecular neighbours, which heightens the electronic couplings. The enhancement factor depends on the nature of the axial functional group (4.1 with HS, 1.5 with BS). Furthermore, in both Si- and Sn-based phthalocyanine crystals, shortening the axial alkyl chains reduces the dimensionality of the charge transport from 2D to 1D. The calculated mobilities evolve in the order $(3HS)_2$-SiPc < $(3HS)_2$-SnPc < $(3BS)_2$-SiPc < $(3BS)_2$-SnPc, with all the investigated compounds showing adequate electron transport characteristics; however the predominant one dimensional character of the transport could limit the performance in devices in which perfectly aligned domains could not be achieved.[39]

Table 2.3. Computed electron mobilities along the crystal axes (μ_i with i = a, b, c; see Equation 4) in the four phthalocyanine crystals, average mobility ($\mu_{avg} = (\mu_a + \mu_b + \mu_c)/3$), and dimensionality (D) of the electron transport (as defined as in [8]).

	μ_a (cm²/Vs)	μ_b (cm²/Vs)	μ_c (cm²/Vs)	μ_{avg} (cm²/Vs)	D
(3HS)$_2$-SiPc	0.012	0.092	0.054	0.053	2D
(3BS)$_2$-SiPc	0.051	0.811	0.100	0.321	1D
(3HS)$_2$-SnPc	0.270	0.071	0.307	0.216	2D
(3BS)$_2$-SnPc	1.099	0.296	0.003	0.466	1D

Organic Thin Film Transistors

Due to the significant change in solid-state packing arising from altering the phthalocyanine metal centre and the axial substituent, we first characterized the four derivatives, (3HS)$_2$-SnPc, (3BS)$_2$-SnPc, (3HS)$_2$-SiPc, and (3BS)$_2$-SiPc, in solution-processed bottom-gate bottom-contact (BGBC) OTFTs to determine their charge transport characteristics. OTFTs were fabricated by drop-casting chloroform solutions of each phthalocyanine onto Si/SiO_2 substrates with pre-patterned gold electrodes having channel lengths (L) of 2.5, 5, 10, and 20 μm. After drop-casting, devices were dried at 100 °C (under vacuum for 1 h) and characterized under vacuum (P < 0.1 Pa) to measure the saturation-regime electron field-effect mobility (μ_e), threshold voltage (V_T) and on/off current ratio ($I_{on/off}$). After initial characterization, the devices were annealed at 150 °C (in vacuum) then re-characterized under vacuum. Both the SiPc and SnPc materials displayed higher μ_e at lower channel lengths, which could be a result of incomplete or inhomogeneous thin film formation at the higher channel lengths. Characteristic output and transfer curves for L = 5 μm for each material are shown in **Figure 2.4**, and a summary of the OTFT characterization is shown in **Table 2.4**.

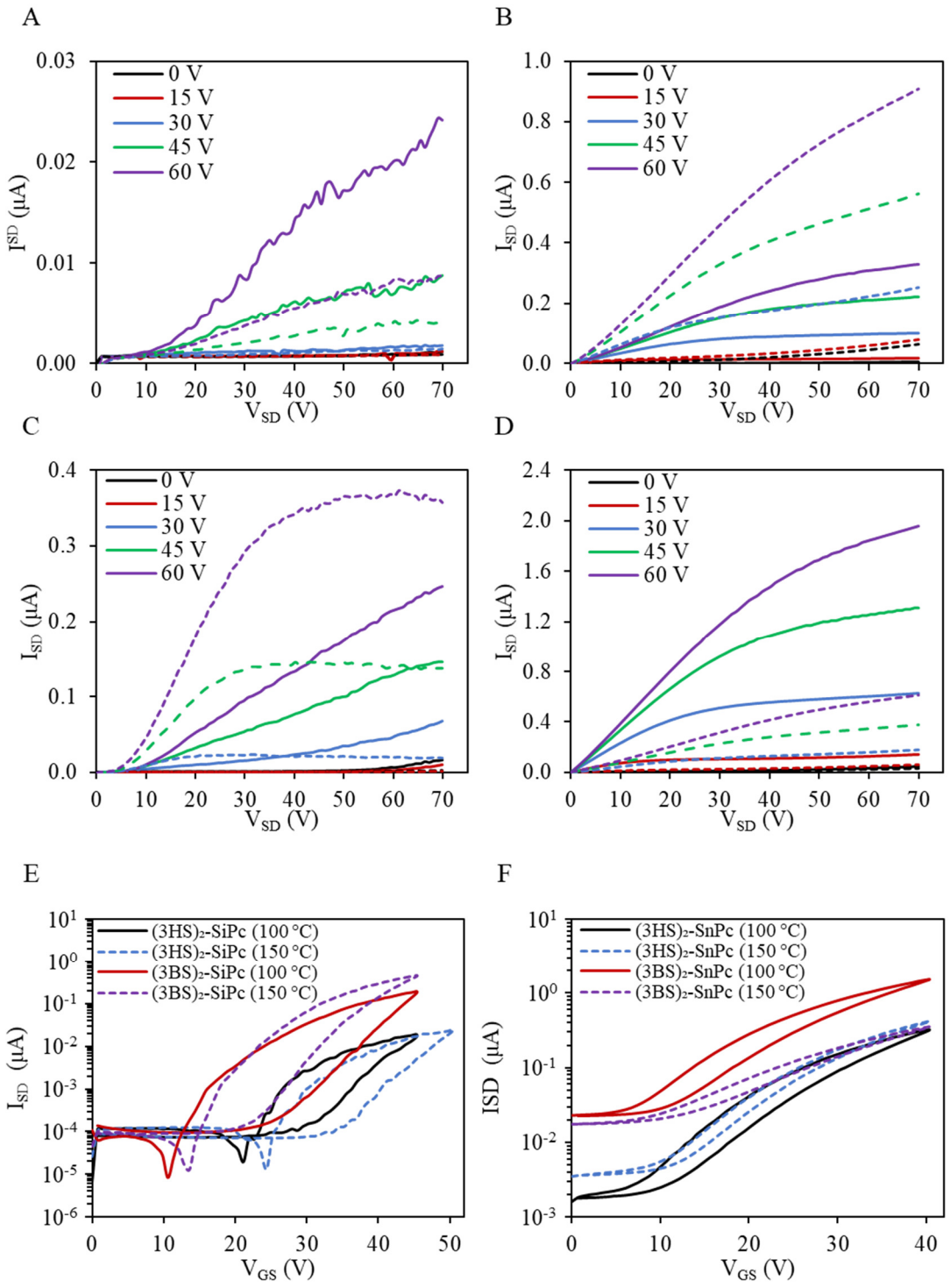

Figure 2.4. Characteristic output curves for devices with L = 5 µm for (A) $(3HS)_2$-SiPc, (B) $(3HS)_2$-SnPc, (C) $(3BS)_2$-SiPc and (D) $(3BS)_2$-SnPc; characteristic transfer curves for (E) $(3HS)_2$-SiPc and $(3BS)_2$-SiPc and (F) $(3HS)_2$-SnPc and $(3BS)_2$-SnPc, tested under vacuum after annealing for 1 hour at 100 °C (solid lines) and 150 °C (dashed lines).

Of the four compounds investigated, OTFTs prepared from $(3HS)_2$-SiPc had the worst average μ_e of 7.3 x 10^{-6} cm^2/Vs, which decreased slightly to 5.1 x 10^{-6} cm^2/Vs after annealing. Consistent with DFT calculations, devices prepared from $(3BS)_2$-SiPc showed better performance, with an average mobility of 5.6 x 10^{-5} cm^2/Vs before annealing, increasing to 1.64 x 10^{-4} cm^2/Vs after annealing. Threshold voltages for both $(3HS)_2$-SiPc and $(3BS)_2$-SiPc were relatively high, with all values above 20 V before and after annealing. Output curves from both SiPc materials also indicate significant contact resistance at the source and drain electrodes. The LUMO levels of the SiPc and SnPc molecules do not align well with the work function of gold. Additionally, BGBC OTFTs often have significant contact resistance, a phenomenon we have observed previously in devices with thermally evaporated SiPc films.[6] In general, OTFTs prepared with $(3HS)_2$-SnPc displayed lower mobilities compared to $(3BS)_2$-SnPc, with an average μ_e = 5.4 x 10^{-5} cm^2/Vs, with only an insignificant increase to 9.6 x 10^{-5} cm^2/Vs after annealing at 150 °C. The average mobility for $(3BS)_2$-SnPc was almost an order of magnitude higher (1.2 x 10^{-4} cm^2/Vs) compared to $(3HS)_2$-SnPc before annealing; this was expected given the π-π overlap observed in the solid-state structure, and predicted by DFT calculations. However, the average mobility for $(3BS)_2$-SnPc decreased after annealing at 150 °C, dropping an order of magnitude to 2.7 x 10^{-5} cm^2/Vs. Transistors prepared from the SnPcs had relatively lower V_T, with $(3HS)_2$-SnPc and $(3BS)_2$-SnPc turning on at 6.8 V and 0.2 V, respectively.

Table 2.4. Summary of the saturation-regime electron field-effect mobility (μ_e), threshold voltage (V_T), and on/off current ratio ($I_{on/off}$) for bottom-gate bottom-contact transistors with L = 5 μm and W = 2000 μm, tested in vacuum (P < 0.1 Pa).

	Annealing Temp (°C)	**$\mu_{e,max}$ (x10^{-5} cm^2/Vs)**	**$\mu_{e,avg}$ (x10^{-5} cm^2/Vs)**	**V_T (V)**	**$I_{on/off}$**
$(3HS)_2$-SiPc	100	2.66	0.731 ± 0.079	22.4 ± 1.0	$10-10^4$
	150	1.62	0.509 ± 0.072	25.4 ± 1.1	$10-10^3$
$(3BS)_2$-SiPc	100	14.4	5.63 ± 1.0	21.8 ± 1.8	10^2-10^3
	150	159	16.4 ± 4.7	21.8 ± 0.69	10^2-10^3
$(3HS)_2$-SnPc	100	12.6	5.42 ± 0.44	9.26 ± 1.1	$10-10^2$
	150	17.6	9.58 ± 1.3	6.79 ± 0.97	$10-10^2$
$(3BS)_2$-SnPc	100	44.0	12.0 ± 2.0	0.21 ± 0.68	10
	150	9.16	2.72 ± 0.47	-2.90 ± 1.2	1-10

The several order of magnitude difference between calculated mobilities and the ones registered in OFETs strongly points towards amorphous or polycrystalline molecular organization in the devices. The improved performance for $(3BS)_2$-SiPc and $(3HS)_2$-SnPc can then possibly be attributed to the formation of more homogenous films through the healing of grain boundaries due to the low T_m of the two compounds (61 °C and 45 °C, respectively). $(3HS)_2$-SiPc and $(3BS)_2$-SnPc do not have such transitions below 150 °C, so a secondary annealing step does not result in improved performance. AFM measurements performed on drop-cast films of $(3BS)_2$-SiPc and $(3BS)_2$-SnPc on OTS treated SiO_2 substrates (**Figure S2.6**) seem to support this theory, as increased grain size was observed in the $(3BS)_2$-SiPc films after annealing at 150 °C. However, as all the films were relatively amorphous with large features, it is difficult to draw definitive conclusions. Work to better understand the effects of processing conditions on the film microstructure and transistor performance are underway. Regardless, these results indicate that the simple change from Si to Sn core has a significant effect on device performance, even when the same functional substituents are employed.

Organic Photovoltaic Devices

Following OTFT characterization, $(3HS)_2$-SnPc and $(3BS)_2$-SnPc were also characterized as ternary additives in P3HT/PC_{61}BM BHJ OPV devices to determine if they could increase J_{SC} through increased light absorption in the NIR and improved donor/acceptor electron transport similarly to their SiPc analogues.[16,27] Inverted OPV devices with the structure Glass/ITO/ZnO/P3HT:$(3XS)_2$-SnPc:PC_{61}BM/MoO_3/Ag (**Figure 2.1 B**) with a range of SnPc loadings were fabricated and characterized. The current density-voltage (*J*-*V*) characteristics of the devices are shown in **Figure 2.5** and summarized in **Table 2.5**. Baseline P3HT/PC_{61}BM devices showed an average efficiency of 2.8 %, consistent with average baseline results found in the literature.[40]

All loadings of the SnPc compounds resulted in a net decrease in device efficiency. The V_{OC} and fill factor (*FF*) of devices dropped consistently with increased loading. Measured J_{SC} values for devices with $(3HS)_2$-SnPc or $(3BS)_2$-SiPc were inconsistent for different devices tested on the same substrate, leading to high standard deviations. Upon further investigation, it was observed that the J_{SC} for devices containing either $(3HS)_2$-SnPc or $(3BS)_2$-SiPc decreased over time with exposure to simulated sunlight (**Figure S2.8**). Due to this variation, it is difficult to compare the J_{SC} and efficiency trends for different additive loadings. This could possibly be caused

by a thermally induced rearrangement of the SnPcs causing disruption of the BHJ morphology. Work to better understand the stability of these materials is underway.

Previous work from our group has shown that increasing the loading of SiPc derivatives as ternary additives above 10 % induces a significant drop in the J_{SC}. This is due to disruption of the desired BHJ morphology from the aggregation of the ternary additive into a third discrete phase.[16,27] Lim et al. showed that incorporating peripheral tert-butyl groups to silicon naphthalocyanine reduced aggregation of the material by weakening intermolecular interactions between neighbouring molecules, allowing for higher loadings as an additive.[19] The negative impact of the SnPc compounds on the J_{SC} both initially and over time suggest these materials may be aggregating and disrupting the optimal P3HT/PC_{61}BM morphology. These results would be consistent with the solid-state single crystal x-ray diffraction data which illustrates that greater interaction between the SnPcs was observed compared to the SiPc derivatives, suggesting a stronger affinity for aggregation.

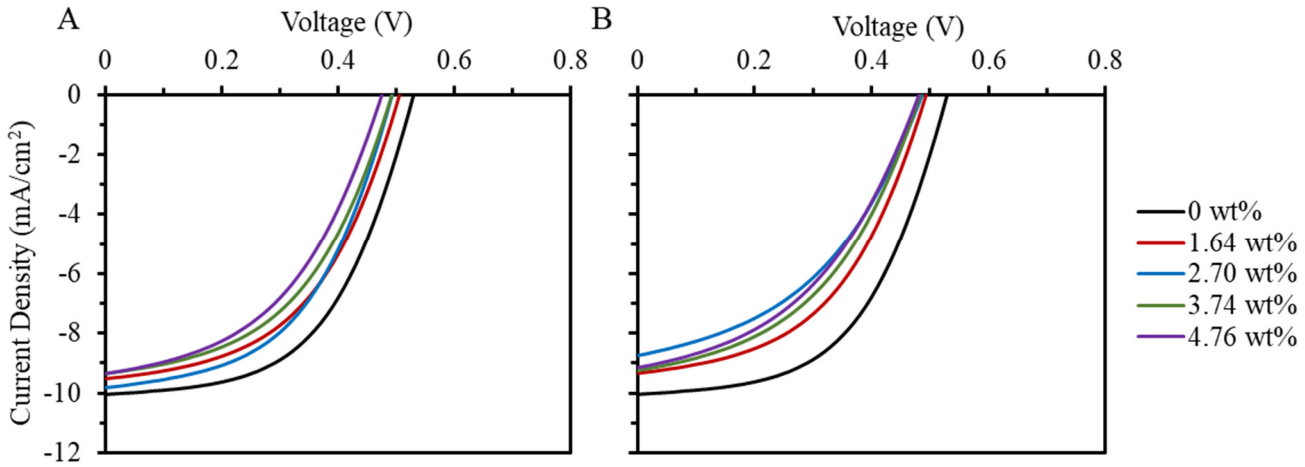

Figure 2.5. Characteristic current density-voltage (J-V) curves for (A) P3HT/PC_{61}BM/ $(3HS)_2$-SnPc and (B) P3HT/PC_{61}BM/$(3BS)_2$-SnPc. Reference P3HT/PC_{61}BM devices are shown in black, legend is the same for (A) and (B).

Table 2.5. Summary of the OPV performance of P3HT/$PC_{61}BM$ devices incorporating $(3HS)_2$-SnPc and $(3BS)_2$-SnPc as ternary additives for different weight ratios.

	P3HT:PCBM:Pc (wt% Pc)	V_{OC} (V)	J_{sc} (mA/cm^2)	FF	PCE (%)
	1:0.8:0 (0 %)	0.53 ± 0.01	10.06 ± 0.15	0.53 ± 0.01	2.84 ± 0.07
$(3HS)_2$-SnPc	1:0.8:0.03 (1.64 %)	0.50 ± 0.01	9.51 ± 0.13	0.50 ± 0.01	2.38 ± 0.10
	1:0.8:0.05 (2.70 %)	0.49 ± 0.01	9.82 ± 0.43	0.50 ± 0.02	2.43 ± 0.23
	1:0.8:0.07 (3.74 %)	0.49 ± 0.01	9.35 ± 0.27	0.48 ± 0.02	2.20 ± 0.15
	1:0.8:0.09 (4.74 %)	0.47 ± 0.01	9.34 ± 0.32	0.46 ± 0.01	2.04 ± 0.14
$(3BS)_2$-SnPc	1:0.8:0.03 (1.64 %)	0.49 ± 0.04	9.33 ± 0.18	0.49 ± 0.01	2.24 ± 0.08
	1:0.8:0.05 (2.70 %)	0.48 ± 0.01	8.75 ± 0.21	0.43 ± 0.01	1.85 ± 0.04
	1:0.8:0.07 (3.74 %)	0.48 ± 0.01	9.25 ± 0.19	0.45 ± 0.02	2.03 ± 0.16
	1:0.8:0.09 (4.74 %)	0.48 ± 0.01	9.13 ± 0.38	0.43 ± 0.01	1.91 ± 0.14

Although the overall J_{SC} of the P3HT/$PC_{61}BM$ devices was lowered upon addition of the SnPc compounds, external quantum efficiency (EQE) measurements demonstrated photocurrent contribution corresponding to the SnPc absorption (680 – 710 nm). The EQE plots for different loadings of the SnPc compounds are shown in **Figure 2.6**. The SnPc compounds decreased the P3HT/$PC_{61}BM$ contribution from 300 – 650 nm, as expected given the reduced overall J_{SC}. This is in contrast to $(3HS)_2$-SiPc and $(3HS)_2$-SiPc, which both increase the EQE in the region of 300 – 650 nm.[16] However, at all loadings, a significant contribution from 650 – 750 nm was seen, increasing with higher additive loadings up to 27 % for $(3HS)_2$-SnPc and 21 % for $(3BS)_2$-SnPc. At a loading of 4.76 %, $(3BS)_2$-SnPc exhibited a shoulder in the EQE (750 nm), suggesting that SnPc has a tendency to self-aggregate which is detrimental to the overall performance of the OPV. The significant EQE contribution in the 680 – 750 nm region show that the SnPcs, similarly to the SiPc analogues, very effectively absorb light and generate photocurrent. These results suggest that other SnPcs derivatives with different axial or peripheral substituents may prove to be effective ternary additives for capturing low-energy photons in BHJ OPV devices, provided that their self-aggregation could be avoided.

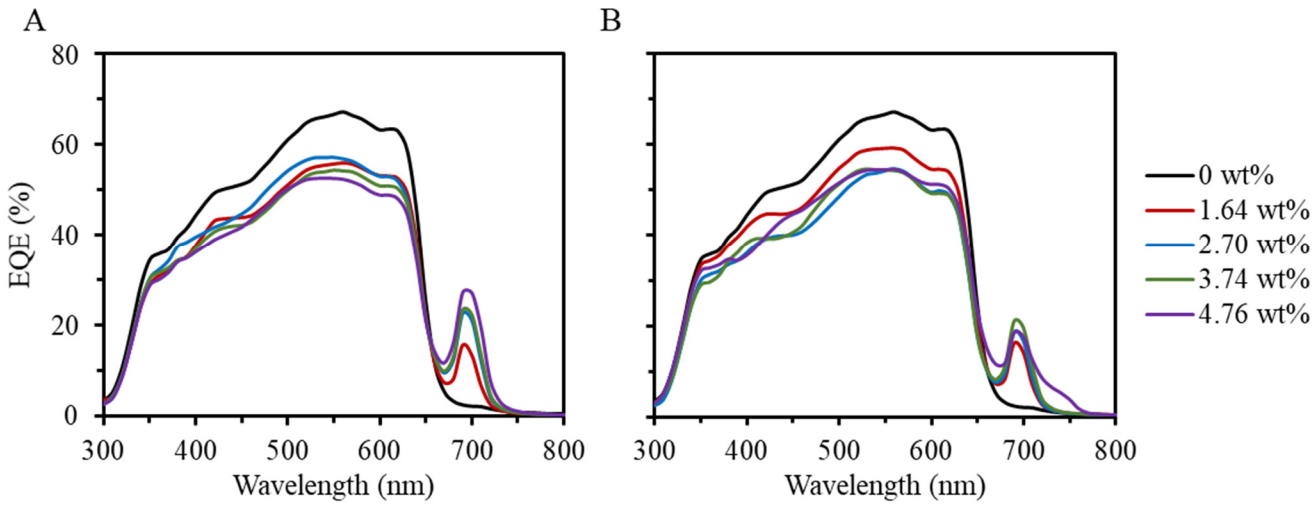

Figure 2.6. Characteristic external quantum efficiency (EQE) curves for (A) P3HT/$PC_{61}BM$/$(3HS)_2$-SnPc and (B) P3HT/$PC_{61}BM$/$(3BS)_2$-SnPc OPV devices. Reference P3HT/$PC_{61}BM$ devices are shown in black, legend is the same for (A) and (B).

Contact Angle

To gain more insight into the reduction in OPV performance from the SnPc compounds, we measured the contact angles of neat films of the four phthalocyanine materials to determine if the metal centre had any effect on the surface energy of the materials. Previous studies have shown that the surface energy can give insight into the segregation behaviour of the ternary additive in a BHJ morphology.[14,17,26] It was shown that the intermediate surface energy of $(3HS)_2$-SiPc to P3HT and $PC_{61}BM$ caused it to migrate to the interface of the two materials in a BHJ morphology and therefore facilitated the cascade of charge transfer.[14] Xu et al have demonstrated that changes to both axial and peripheral substituents of SiPc can alter the surface energy of the material and control where it will migrate to in a P3HT/$PC_{61}BM$ BHJ.[41]

Contact angle measurements on pristine films of the four phthalocyanines are summarized in **Table 2.6**. The contact angle of $(3HS)_2$-SiPc was measured to be approximately 100°, consistent with previous reports.[14,41] No changes in the contact angle were observed for $(3BS)_2$-SiPc, which was expected given the similarity of the two materials. $(3HS)_2$-SnPc and $(3BS)_2$-SnPc showed marginally higher contact angles, however the increase was not statistically significant. These results suggest that changing the metal centre of the phthalocyanine does not have a marked effect on the surface energy of the material, and that SnPcs should also be present at the interface of P3HT and $PC_{61}BM$.

Table 2.6. Summary of H_2O contact angle measurements on neat phthalocyanine films. Average and standard deviation for 10 measurements on each film is shown.

Phthalocyanine	Contact Angle (°)
$(3HS)_2$-SiPc	99.6 ± 0.6
$(3BS)_2$-SiPc	99.6 ± 0.7
$(3HS)_2$-SnPc	100.2 ± 0.6
$(3BS)_2$-SnPc	100.6 ± 0.6

Atomic Force Microscopy

We performed AFM measurements on films of P3HT/$PC_{61}BM$ incorporating $(3HS)_2$-SnPc and $(3BS)_2$-SnPc (**Figure 2.7**). P3HT/$PC_{61}BM$ binary films showed a root-mean-square roughness (R_{RMS}) value of 13.24 nm, with characteristic worm-like features. Films incorporating 4.76 % of $(3HS)_2$-SnPc had a similar R_{RMS} value of 12.41 nm with similar topography. Films with 4.76 % $(3BS)_2$-SnPc showed slightly increased R_{RMS} of 13.97. This increase in roughness, combined with an increased number of surface features, could be due to the aggregation of $(3BS)_2$-SnPc into a third domain, consistent with the EQE shoulder at 750 nm discussed above.

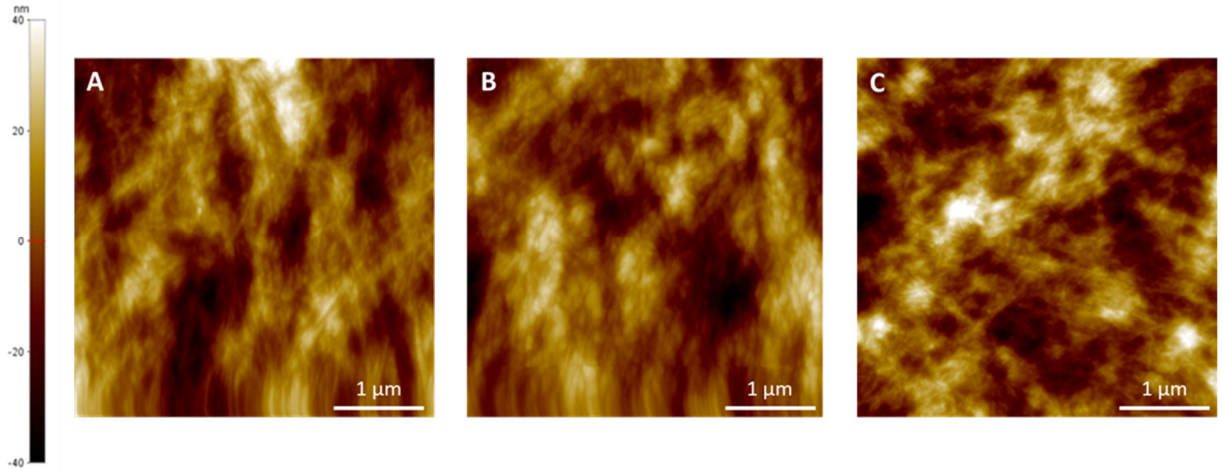

Figure 2.7. AFM images of the photoactive layer of devices with (A) P3HT/$PC_{61}BM$ R_{RMS} = 13.24 nm (B) P3HT/$PC_{61}BM$/$(3HS)_2$-SnPc (4.76 %) R_{RMS} = 12.41 nm and (C) P3HT/ $PC_{61}BM$ /$(3BS)_2$-SnPc (4.76 %) R_{RMS} = 13.97 nm

2.6. Experimental

Materials

Tri-*n*-hexylchlorosilane and tri-*n*-butylchlorosilane were purchased from Gelest and used as received. All solvents were purchased from commercial suppliers and used as received, unless otherwise specified. Dichloro silicon phthalocyanine (Cl_2-SiPc)[43] and dichloro tin phthalocyanine (Cl_2-SnPc) were synthesized according to the literature procedure for dichloro germanium phthalocyanine[44] (Cl_2-GePc), substituting $GeCl_4$ with $SnCl_4$. Bis(tri-*n*-hexylsily oxide) silicon phthalocyanine ($(3HS)_2$-SiPc), and bis(tri-*n*-butylsily oxide) silicon phthalocyanine ($(3BS)_2$-SnPc) were synthesized as described in the literature.[36]

Synthesis of Bis(tri-n-hexylsily oxide) tin phthalocyanine ($(3HS)_2$-SnPc):[36]

A 100 mL reaction flask was charged with Cl_2-SnPc (1.00 g, 1.4 mmol), sodium hydroxide (0.30 g, 7.6 mmol), tri-*n*-hexylchlorosilane (1.49 g, 4.5 mmol), Aliquat HTA-1 (0.015 g) and chlorobenzene (10 mL). The reaction mixture was stirred under reflux (132 °C) for 1 hour before adding additional tri-*n*-hexylchlorosilane (0.50 g, 1.5 mmol). After a further hour of reflux, sodium hydroxide (0.12 g, 3.0 mmol) and tri-*n*-hexylchlorosilane (0.50 g, 1.5 mmol) were added. The reaction mixture was refluxed for a further 4 hours before being allowed to cool to room temperature. The solution was filtered, leaving a blue/purple residue. The filtrate was concentrated to dryness then admixed with methanol. The solids were filtered under vacuum, washed with methanol and water, and dried under vacuum (1.03 g, yield = 63%). The product was purified by train sublimation before use in devices (sublimation yield = 71%). ^{1}H NMR (400 MHz, CDCl3): δ = 9.66 – 9.56 (m, 8H), 8.37 – 8.30 (m, 8H), 0.89 – 0.75 (m, 12H), 0.72 – 0.65 (m, 18H), 0.40 – 0.30 (m, 12H), 0.02 – -0.09 (m, 12H), -1.12 – -1.22 (m, 12H). MS [EI] calculated mass: 1230.61, obtained mass 1230.6.

Synthesis of Bis(tri-n-butylsily oxide) tin phthalocyanine ($(3BS)_2$-SnPc)[36]

A 100 mL reaction flask was charged with Cl_2-SnPc (1.00 g, 1.4 mmol), sodium hydroxide (0.30 g, 7.6 mmol), tri-*n*-butylchlorosilane (1.07 g, 4.5 mmol), Aliquat HTA-1 (0.015 g) and chlorobenzene (10 mL). The reaction mixture was stirred under reflux (132 °C) for 1 hour before adding additional tri-*n*-butylchlorosilane (0.36 g, 1.5 mmol). After a further hour of reflux, sodium hydroxide (0.12 g, 3.0 mmol) and tri-*n*-butylchlorosilane (0.36 g, 1.5 mmol) were added.

The reaction mixture was heated at reflux for a further 4 hours before being allowed to cool to room temperature. The solution was filtered, leaving a blue/purple residue. The filtrate was concentrated to dryness then admixed with methanol. The solids were filtered under vacuum, washed with methanol and water, and dried under vacuum (0.58 g, yield = 42%). The product was purified by train sublimation before use in devices (sublimation yield = 73%). ^{1}H NMR (400 MHz, $CDCl_3$): δ = 9.66 – 9.57 ppm (8H, m), 8.38 – 8.31 ppm (8H, m), 0.08 – 0.12 ppm (30H, m), -1.10 – -1.26 ppm (12H, m). MS [EI] calculated mass: 1062.42, obtained mass 1062.4.

Material Characterization

Nuclear magnetic resonance (NMR) spectra were recorded on a Bruker Avance II spectrometer at room temperature in $CDCl_3$ operating at 400 MHz. Chemical shifts are reported in parts per million (ppm) referenced to tetramethylsilane (0 ppm). Ultravoilet-visible (UV-Vis) absorption spectra were collected from an Ocean Optics Flame spectrophotometer and DH-2000 light source, with a 10 mm path length quartz cuvette. Cyclic voltammograms were obtained using a VersaSTAT 3 potentiostat, with a platinum disk working electrode, platinum wire counter electrode, and an Ag/AgCl reference electrode. Four cycles from -1.2 V to 1.6 V at a scan rate of 0.1 V/s were obtained. Measurements were conducted in N_2 purged DCM with tetrabutylammonium perchlorate as the supporting electrolyte and ferrocene as an internal reference. HOMO energy levels were estimated from the correlation: E_{HOMO} (eV) = -($E_{ox,onset}$ - $E_{ox\ Fc/Fc+,onset}$) - 4.80 eV, where $E_{ox,onset}$ and $E_{oxFc/Fc+,onset}$ are the onset oxidation potentials for the phthalocyanine and the ferrocene reference, respectively, against the Ag/AgCl reference. Atomic force microscopy was obtained using a Bruker Dimension Icon AFM equipped with ScanAsyst-Air tips, set to tapping mode. Scans were performed at a scan rate of 1 Hz, and images were processed using NanoScope Analysis v.1.8.

Solution Processed Bottom Gate Bottom Contact OTFTs

Bottom-gate bottom-contact (BGBC) devices were constructed using pre-fabricated OTFT chips (Generation 5) purchased from Fraunhofer Institute for Photonic Microsystems (IPMS). The gate was n-doped Si, with a 230 nm SiO_2 dielectric; the drain and source electrodes were 30 nm Au (with a 10 nm ITO adhesion layer). Each chip contained 16 transistors, four each of four different channel lengths: 2.5, 5, 10 and 20 µm; the width of all the devices was 2000 µm. All device preparation was performed in air. The Fraunhofer chips were rinsed well with acetone to

remove the resist, plasma treated (Harrick Plasma Cleaner - PDC-32G) for 15 min, and rinsed with water and isopropanol before being dried with N_2. The chips were immediately submerged in a 1 % solution of octyltrichlorosilane (OTS) in toluene for 1 h at 70 °C, rinsed well with toluene, and dried in a vacuum oven at 70 °C for 1h. Solutions with a concentration of 1 mg/mL were prepared for each of the four phthalocyanines in $CHCl_3$. The solutions were heated to 60 °C for 20 min to ensure that all the material dissolved, then cooled to room temperature and filtered through PTFE membranes (0.2 μm pore size). The semiconducting layer was prepared by solution drop-cast of 1 μL into each of the channels. The solvent was allowed to evaporate off under ambient conditions, and the chips were further dried in a vacuum oven at 100 °C for 1 h. After testing, the chips were placed back in the vacuum oven and heated to 150 °C for 1 h for the annealing study.

Electrical measurements were performed on a custom electrical probe station with environmental chamber with controlled atmosphere, oesProbe A10000-P290 (Element Instrumentation Inc. & Kreus Design Inc.) using a Keithley 2614B to set V_{DS} and V_{GS} and to measure I_{DS}. Voltages were increased in a step-wise manner, rather than pulsed, with a delay of 100 ms between measurements. Each device was tested four times and values averaged. Transfer curves were measured in the saturation regime and were modelled using the following equation:

$$I_{DS} = \frac{\mu C_i W}{2L}(V_{GS} - V_T)^2 \qquad \text{Equation 1}$$

where L and W are the channel length and width, respectively; C_i is the capacitance density of the gate dielectric, calculated using $C_i = (\varepsilon_0 \varepsilon_r)/t$, where t is the thickness of the dielectric (230 nm) and ε_r is the relative dielectric constant of SiO_2 (3.9). μ is the field-effect mobility and is calculated from the slope of best fit though the most linear region of $\sqrt{I_{DS}}$ plotted against V_{GS}. The threshold voltage V_T is calculated as the x-intercept of the same line fitting. All measurements were performed in vacuum (pressure less than 0.1 Pa). The devices were tested within 48 h of being prepared and were allowed to acclimatize for 30 min in the probe station before beginning characterization.

Inverted Ternary BHJ OPV Devices

1" x 1" ITO coated glass slides were cleaned in a sonication bath by successive washes (10 min each) of soap-water, water, acetone, and methanol before being exposed to air plasma for 10 minutes. The zinc oxide solution was prepared by combining zinc acetate dihydrate (0.1956 g, 1.066 mmol) and ethanolamine (0.0544 mL, 0.9 mmol) in ethanol (6 mL), which was stirred at 50 °C for 2 h then stored at room temperature before spin coating onto the UV-ozone treated substrates at 2000 rpm for 60 s. The substrates were annealed on a hotplate for 1 h at 180 °C before being moved into a nitrogen glove box for the remainder of fabrication.

P3HT and $PC_{61}BM$ were weighed in a 1:0.8 ratio and dissolved in *o*-dichlorobenzene to form a P3HT concentration of 22 mg/mL, while the SnPc derivatives were dissolved in 30 mg/mL solutions. For each additive loading, the SnPc and P3HT/$PC_{61}BM$ solutions were mixed at appropriate ratios, adding additional *o*-DCB as necessary, to form a final P3HT concentration of 20 mg/mL. The mixed solutions were stirred at 50 °C for at least 1 h before spin coating. The still warm solutions were spin coated at 1000 rpm for 35 s then allowed to dry in closed petri dishes. Molybdenum trioxide (MoO_3, 7 nm) and silver (70 nm) were deposited using a thermal evaporator at $< 2 \times 10^{-6}$ Torr for device areas of 0.325 cm^2 as defined by a shadow mask. Current density vs voltage curves were measured under nitrogen using a Kiethley 2400 under illumination from an AM1.5 solar simulator with a xenon lamp, calibrated with a silicon reference cell (Abet 15150) to 1000 W/m^2. Devices were encapsulated using an optical adhesive (Norland NOA61) and a glass coverslip before EQE measurements in air.

Computational

Molecular geometries were optimized using the density functional theory (DFT) with the B3LYP exchange-correlation functional. The 6-31G(d) basis set was used for all atoms except Sn, for which the double-ζ-split-valence + polarization (DZVP) basis set was employed.[39] Each structure was characterized as a minimum of the potential energy surface on the basis of its real harmonic vibrational frequencies. Transition energies towards the first optically allowed excited states were computed by means of time-dependent DFT using the same level of approximation. Internal reorganization energies (λ_i) were also calculated at the B3LYP/6-31G(d) level, using the expression derived from the four point adiabatic potential approach:

$$\lambda_i = E^{(-)}(M) - E^{(0)}(M) + E^{(-)}(M^-) - E^{(0)}(M^-) \quad \text{Equation 2}$$

where $E^{(0)}(M)$ and $E^{(-)}(M^-)$ denote the ground-state energy of the neutral state and of the negatively charged state, respectively; $E^{(-)}(M)$ is the energy of the neutral molecule in the optimized geometry of the anion and $E^{(0)}(M^-)$, the energy of the anion in the optimized geometry of the neutral molecule.

Transfer integrals J_k characterizing the electron coupling between molecular pairs *k* were obtained by employing the projection method involving the LUMOs of monomers.[45] Since all molecules possess degenerate or nearly degenerate LUMO (L) and LUMO+1 (L+1) levels, the effective squared transfer integrals for electron transport were computed as:

$$J_k = \frac{1}{\sqrt{2}}\left\{J_{L,L}^2 + J_{L+1,L}^2 + J_{L,L+1}^2 + J_{L+1,L+1}^2\right\}^{1/2} \quad \text{Equation 3}$$

in line with previous works.[8] The relative electron mobilities along the crystal axis *i = a, b, c* were evaluated at zero field neglecting energetic disorder in the transport level energies, using the expression:[39,46]

$$\mu_i = \frac{q}{h}\left(\frac{\pi}{kT}\right)^{3/2}\frac{1}{\sqrt{\lambda_i}}\exp\left(-\frac{\lambda_i}{4kT}\right)\sum_k J_k^2\,(\vec{r}_k \cdot \vec{e}_i)^2 \quad \text{Equation 4}$$

where the sum runs over all pairs of molecular neighbours separated by the distance vector $\vec{r}_k$, $\vec{e}_i$ is a cell axis unit vector. *q*, *h* and *k* are respectively the elementary charge, the Planck and Boltzmann constants, and T = 300 K. Equation 4 combines i) Marcus formula for the hopping rate ν_k between two neighbouring sites in absence of energetic disorder, with ii) the equation for the diffusion coefficient in one dimension, $D = \frac{1}{2}\sum_k \nu_k\,(\vec{r}_k \cdot \vec{e}_i)^2$, and iii) Einstein's equation relating mobility with diffusion, $\mu = \frac{qD}{k_B T}$ see reference for further details.[39] Quantum chemical calculations were performed with the ORCA[47] and Gaussian[48] programs.

2.7. Conclusion

We have synthesized two novel soluble tin phthalocyanines, $(3HS)_2$-SnPc and $(3BS)_2$-SnPc, and compared them to previously reported silicon phthalocyanines $(3HS)_2$-SiPc and $(3BS)_2$-SiPc in OTFTs and OPV devices. We show that the SiPc and SnPc materials display similar optical and electrochemical characteristics with a 0.2 eV drop in HOMO/LUMO energy levels. Single crystal X-ray diffraction revealed the SnPc compounds show significantly increased interaction between neighbouring phthalocyanines compared to their SiPc counterparts and demonstrate that despite relatively bulky axial substituents, the metal center plays a large role in the solid-sate arrangement of the materials. In OTFTs, the materials showed an electron mobility trend of $(3HS)_2$-SiPc < $(3HS)_2$-SnPc < $(3BS)_2$-SiPc < $(3BS)_2$-SnPc, which was consistent with the trends obtained from DFT calculations. As ternary additives in P3HT/PC_{61}BM OPV devices, both SnPc materials showed a significant EQE contribution from 650 – 750 nm, however decreased P3HT/PC_{61}BM contribution, resulting in a net loss in J_{SC} at all loadings. These initial results suggest soluble SnPc derivatives may be more suited from OTFT applications, however the strong photocurrent contribution suggests that SnPc derivatives with more stable axial or peripheral substituents may prove to be effective ternary additives.

2.8. References

(1) Zysman-Colman, E.; Ghosh, S. S.; Xie, G.; Varghese, S.; Chowdhury, M.; Sharma, N.; Cordes, D. B.; Slawin, A. M. Z.; Samuel, I. D. W. Solution-Processable Silicon Phthalocyanines in Electroluminescent and Photovoltaic Devices. *ACS Appl. Mater. Interfaces* **2016**, *8* (14), 9247–9253.

(2) Plint, T.; Lessard, B. H.; Bender, T. P. Assessing the Potential of Group 13 and 14 Metal/Metalloid Phthalocyanines as Hole Transporting Layers in Organic Light Emitting Diodes. *J. Appl. phys.* **2016**, *119* (1), 145502.

(3) Pearson, A. J.; Plint, T.; Jones, S. T. E.; Lessard, B. H.; Credgington, D.; Bender, T. P.; Greenham, N. C. Silicon Phthalocyanines as Dopant Red Emitters for Efficient Solution Processed OLEDs. *J. Mater. Chem. C* **2017**, *5* (48), 12688–12698.

(4) Lessard, B. H.; White, R. T.; Al-amar, M.; Plint, T.; Castrucci, S.; Josey, D. S.; Lu, Z.; Bender, T. P. Assessing the Potential Roles of Silicon and Germanium Phthalocyanines in Planar Heterojunction Organic Photovoltaic Devices and How Pentafluoro Phenoxylation Can Enhance $\pi - \pi$ Interactions and Device Performance. *ACS Appl. Mater. Interfaces* **2015**, *7*, 5076–5068.

(5) Lessard, B. H. B. H.; Grant, T. M.; White, R.; Thibau, E.; Lu, Z.-H.; Bender, T. P. The Position and Frequency of Fluorine Atoms Changes the Electron Donor/Acceptor Properties of Fluorophenoxy Silicon Phthalocyanines within Organic Photovoltaic Devices. *J. Mater. Chem. A* **2015**, *3*, 24512–24524.

(6) Melville, O. A.; Grant, T. M.; Lessard, B. H. Silicon Phthalocyanines as N-Type Semiconductors in Organic Thin Film Transistors. *J. Mater. Chem. C* **2018**, *6* (20), 5482–5488.

(7) da Silva Filho, D. A.; Coropceanu, V.; Gruhn, N. E.; de Oliveira Neto, P. H.; Brédas, J.-L. Intramolecular Reorganization Energy in Zinc Phthalocyanine and Its Fluorinated Derivatives: A Joint Experimental and Theoretical Study. *Chem. Commun.* **2013**, *49* (54), 6069.

(8) Gali, S. M.; Matta, M.; Lessard, B. H.; Castet, F.; Muccioli, L. Ambipolarity and Dimensionality of Charge Transport in Crystalline Group 14 Phthalocyanines: A Computational Study. *J. Phys. Chem. C* **2018**, *122* (5), 2554–2563.

(9) Goubard, F.; Wantz, G. Ternary Blends for Polymer Bulk Heterojunction Solar Cells. *Polym. Int.* **2014**, *63* (8), 1362–1367.

(10) Lu, L.; Kelly, M. A.; You, W.; Yu, L. Status and Prospects for Ternary Organic Photovoltaics. *Nat. Photonics* **2015**, *9* (8), 491–500.

(11) Chen, Y. C.; Hsu, C. Y.; Lin, R. Y. Y.; Ho, K. C.; Lin, J. T. Materials for the Active Layer of Organic Photovoltaics: Ternary Solar Cell Approach. *ChemSusChem* **2013**, *6* (1), 20–35.

(12) Honda, S.; Nogami, T.; Ohkita, H.; Benten, H.; Ito, S. Improvement of the Light-Harvesting Efficiency in Polymer/Fullerene Bulk Heterojunction Solar Cells by Interfacial Dye Modification. *ACS Appl. Mater. Interfaces* **2009**, *1* (4), 804–810.

(13) Honda, S.; Ohkita, H.; Benten, H.; Ito, S. Multi-Colored Dye Sensitization of Polymer/Fullerene Bulk Heterojunction Solar Cells. *Chem. Commun.* **2010**, *46* (35), 6596–6598.

(14) Honda, S.; Ohkita, H.; Benten, H.; Ito, S. Selective Dye Loading at the Heterojunction in Polymer/Fullerene Solar Cells. *Adv. Energy Mater.* **2011**, *1* (4), 588–598.

(15) Honda, S.; Yokoya, S.; Ohkita, H.; Benten, H.; Ito, S. Light-Harvesting Mechanism in Polymer/Fullerene/Dye Ternary Blends Studied by Transient Absorption Spectroscopy. *J. Phys. Chem. C* **2011**, *115* (22), 11306–11317.

(16) Dang, M. T.; Grant, T. M.; Yan, H.; Seferos, D. S.; Lessard, B. H.; Bender, T. P. Bis(Tri-n-Alkylsilyl Oxide) Silicon Phthalocyanines: A Start to Establishing a Structure Property Relationship as Both Ternary Additives and Non-Fullerene Electron Acceptors in Bulk Heterojunction Organic Photovoltaic Devices. *J. Mater. Chem. A* **2017**, *5* (24), 12168–12182.

(17) Ke, L.; Min, J.; Adam, M.; Gasparini, N.; Hou, Y.; Perea, J. D.; Chen, W.; Zhang, H.; Fladischer, S.; Sale, A. C.; Spiecker, E.; Tykwinski, R. R.; Brabec, C. J.; Ameri, T. A Series of Pyrene-Substituted Silicon Phthalocyanines as Near-IR Sensitizers in Organic Ternary Solar Cells. *Adv. Energy Mater.* **2016**, *6* (7), 1502355.

(18) Grant, T. M.; Gorisse, T.; Dautel, O.; Wantz, G.; Lessard, B. H. Multifunctional Ternary Additive in Bulk Heterojunction OPV: Increased Device Performance and Stability. *J. Mater. Chem. A* **2017**, *5* (4), 1581–1587.

(19) Lim, B.; Bloking, J. T.; Ponec, A.; Mcgehee, M. D.; Sellinger, A. Ternary Bulk Heterojunction Solar Cells: Addition of Soluble NIR Dyes for Photocurrent Generation beyond 800 Nm. *ACS Appl. Mater. Interfaces* **2014**, *6*, 6905–6913.

(20) Hori, T.; Masuda, T.; Fukuoka, N.; Hayashi, T.; Miyake, Y.; Kamikado, T.; Yoshida, H.; Fujii, A.; Shimizu, Y.; Ozaki, M. Non-Peripheral Octahexylphthalocyanine Doping Effects in Bulk Heterojunction Polymer Solar Cells. *Org. Electron.* **2012**, *13* (2), 335–340.

(21) Sharma, S. S.; Sharma, G. D.; Mikroyannidis, J. A. Improved Power Conversion Efficiency of Bulk Heterojunction Poly(3-Hexylthiophene):PCBM Photovoltaic Devices Using Small Molecule Additive. *Sol. Energy Mater. Sol. Cells* **2011**, *95* (4), 1219–1223.

(22) Sharma, G. D.; Singh, S. P.; Roy, M. S.; Mikroyannidis, J. A. Solution Processed Bulk Heterojunction Polymer Solar Cells with Low Band Gap DPP-CN Small Molecule Sensitizer. *Org. Electron. physics, Mater. Appl.* **2012**, *13* (9), 1756–1762.

(23) Ameri, T.; Min, J.; Li, N.; Machui, F.; Baran, D.; Forster, M.; Schottler, K. J.; Dolfen, D.; Scherf, U.; Brabec, C. J. Performance Enhancement of the P3HT/PCBM Solar Cells through NIR Sensitization Using a Small-Bandgap Polymer. *Adv. Energy Mater.* **2012**, *2* (10), 1198–1202.

(24) Koppe, M.; Egelhaaf, H. J.; Clodic, E.; Morana, M.; Lüer, L.; Troeger, A.; Sgobba, V.; Guldi, D. M.; Ameri, T.; Brabec, C. J. Charge Carrier Dynamics in a Ternary Bulk Heterojunction System Consisting of P3HT, Fullerene, and a Low Bandgap Polymer. *Adv. Energy Mater.* **2013**, *3* (7), 949–958.

(25) Ameri, T.; Heumüller, T.; Min, J.; Li, N.; Matt, G.; Scherf, U.; Brabec, C. J. IR Sensitization of an Indene-C60 Bisadduct (ICBA) in Ternary Organic Solar Cells. *Energy Environ. Sci.* **2013**, *6* (6), 1796.

(26) Ameri, T.; Khoram, P.; Heumueller, T.; Baran, D.; Machui, F.; Troeger, A.; Sgobba, V.; Guldi, D. M.; Halik, M.; Rathgeber, S.; Brabec, C. J.; Heumüller, T.; Baran, D.; Machui, F.; Troeger, A.; Sgobba, V.; Guldi, D. M.; Halik, M.; Rathgeber, S.; Scherf, U.; Brabec, C. J. Morphology Analysis of near IR Sensitized Polymer/Fullerene Organic Solar Cells by Implementing Low Bandgap Heteroanalogue C-/Si-PCPDTBT. *J. Mater. Chem. A* **2014**, *2* (45), 19461–19472.

(27) Lessard, B. H.; Dang, J. D.; Grant, T. M.; Gao, D.; Seferos, D. S.; Bender, T. P. Bis(Tri-n-Hexylsilyl Oxide) Silicon Phthalocyanine: A Unique Additive in Ternary Bulk Heterojunction Organic Photovoltaic Devices. *ACS Appl. Mater. Interfaces* **2014**, *6*, 15040–15051.

(28) Song, D.; Wang, H.; Zhu, F.; Yang, J.; Tian, H.; Geng, Y.; Yan, D. Phthalocyanato Tin(IV) Dichloride: An Air-Stable, High-Performance, n-Type Organic Semiconductor with a High Field-Effect Electron Mobility. *Adv. Mater.* **2008**, *20*, 2142–2144.

(29) Song, D.; Zhu, F.; Yu, B.; Huang, L.; Geng, Y.; Yan, D.; Song, D.; Zhu, F.; Yu, B.; Huang, L.; Geng, Y.; Yan, D. Tin (IV) Phthalocyanine Oxide : An Air-Stable Semiconductor with High Electron Mobility. *Appl. Phys. Lett.* **2008**, *92*, 143303.

(30) Yang, F.; Lunt, R. R.; Forrest, S. R. Simultaneous Heterojunction Organic Solar Cells with Broad Spectral Sensitivity. *Appl. Phys. Lett.* **2008**, *92* (5), 10–13.

(31) Pandey, R.; Kerner, R. A.; Menke, S. M.; Holst, J.; Josyula, K. V. B. B.; Holmes, R. J. Tin Naphthalocyanine Complexes for Infrared Absorption in Organic Photovoltaic Cells. *Org. Electron. physics, Mater. Appl.* **2013**, *14* (3), 804–808.

(32) Rand, B. P.; Xue, J.; Yang, F.; Forrest, S. R.; Rand, B. P.; Xue, J.; Yang, F.; Forrest, S. R. Organic Solar Cells with Sensitivity Extending into the near Infrared. *Appl. Phys. Lett.* **2005**, *87* (23), 1–3.

(33) Kim, D. Y.; Sarasqueta, G.; So, F. SnPc:C60 Bulk Heterojunction Organic Photovoltaic Cells with MoO3 Interlayer. *Sol. Energy Mater. Sol. Cells* **2009**, *93* (8), 1452–1456.

(34) Dirk, C. W.; Inabe, T.; Schoch, K. F.; Marks, T. J. Cofacial Assembly of Partially Oxidized Metallomacrocycles as an Approach to Controlling Lattice Architecture in Low-Dimensional Molecular Solids. Chemical and Architectural Properties of the "Face-to-Face" Polymers [M(Phthalocyaninato)O]n Where M = Si,. *J. Am. Chem. Soc.* **1983**, *105* (6), 1539–1550.

(35) Ford, W. E.; Rodgers, M. a J.; Schechtman, L. a; Sounik, J. R.; Rihter, B. D.; Kenney, M. E. Synthesis and Photochemical Properties of Aluminum, Gallium, Silicon, and Tin Naphthalocyanines. *Inorg. Chem.* **1992**, *31* (16), 3371–3377.

(36) Gessner, T.; Sens, R.; Ahlers, W.; Vamvakaris, C. Preparation of Silicon Phthalocyanines and Germanium Phthalocyanines and Related Substances. US 2010/0113767 A1, 2010.

(37) Li, Y.; Cao, Y.; Gao, J.; Wang, D.; Yu, G.; Heeger, A. J. Electrochemical Properties of Luminescent Polymers and Polymer Light-Emitting Electrochemical Cells. *Synth. Met.* **1999**, *99* (3), 243–248.

(38) Li, S. G.; Yuan, Z. C.; Yuan, J. Y.; Deng, P.; Zhang, Q.; Sun, B. Q. An Expanded Isoindigo Unit as a New Building Block for a Conjugated Polymer Leading to High-Performance Solar Cells. *J. Mater. Chem. A* **2014**, *2* (15), 5427–5433.

(39) Skabara, P. J.; Arlin, J.-B.; Geerts, Y. H. Close Encounters of the 3D Kind - Exploiting High Dimensionality in Molecular Semiconductors. *Adv. Mater.* **2013**, *25* (13), 1948–1954.

(40) Dang, M. T.; Hirsch, L.; Wantz, G. P3HT:PCBM, Best Seller in Polymer Photovoltaic Research. *Adv. Mater.* **2011**, *23* (31), 3597–3602.

(41) Xu, H.; Wada, T.; Ohkita, H.; Benten, H.; Ito, S. Molecular Design of Near-IR Dyes with Different Surface Energy for Selective Loading to the Heterojunction in Blend. *Sci. Rep.* **2015**, *5*, 9321.

(42) Lowery, M. K.; Starshak, A. J.; Esposito, J. N.; Krueger, P. C.; Kenney, M. E. Dichloro(Phthalocyanino)Silicon. *Inorg. Chem* **1965**, 128.

(43) Joyner, R. D.; Kenney, M. E. *Germanium Phthalocyanines*; UTC, 1960; Vol. 82.

(44) Godbout, N.; Salahub, D. R.; Andzelm, J.; Wimmer, E. Optimization of Gaussian-Type Basis Sets for Local Spin Density Functional Calculations. Part I. Boron through Neon, Optimization Technique and Validation. *Can. J. Chem.* **1992**, *70* (2), 560–571.

(45) Valeev, E. F.; Coropceanu, V.; da Silva Filho, D. A.; Salman, S.; Brédas, J.-L. Effect of Electronic Polarization on Charge-Transport Parameters in Molecular Organic Semiconductors. *J. Am. Chem. Soc.* **2006**, *128* (30), 9882–9886.

(46) Matta, M.; Pereira, M. J.; Gali, S. M.; Thuau, D.; Olivier, Y.; Briseno, A.; Dufour, I.; Ayela, C.; Wantz, G.; Muccioli, L. Unusual Electromechanical Response in Rubrene Single Crystals. *Mater. Horizons* **2018**, *5* (1), 41–50.

(47) Stehr, V.; Pfister, J.; Fink, R. F.; Engels, B.; Deibel, C. First-Principles Calculations of Anisotropic Charge-Carrier Mobilities in Organic Semiconductor Crystals. *Phys. Rev. B* **2011**, *83* (15), 155208.

(48) Neese, F. The ORCA Program System. *Wiley Interdiscip. Rev. Comput. Mol. Sci.* **2012**, *2* (1), 73–78.

(49) Frisch, M. J.; Trucks, G. W.; Schlegel, H. B.; Scuseria, G. E.; Robb, M. A.; Cheeseman, J. R.; Scalmani, G.; Barone, V.; Petersson, G. A.; Nakatsuji, H.; Li, X.; Caricato, M.; Marenich, A. V.; Bloino, J.; Janesko, B. G.; Gomperts, R.; Mennucci, B.; Hratchian, H. P.; Ortiz, J. V.; Izmaylov, A. F.; Sonnenberg, J. L.; Williams-Young, D.; Ding, F.; Lipparini, F.; Egidi, F.; Goings, J.; Peng, B.; Petrone, A.; Henderson, T.; Ranasinghe, D.; Zakrzewski, V. G.; Gao, J.; Rega, N.; Zheng, G.; Liang, W.; Hada, M.; Ehara, M.; Toyota, K.; Fukuda, R.; Hasegawa, J.; Ishida, M.; Nakajima, T.; Honda, Y.; Kitao, O.; Nakai, H.; Vreven, T.; Throssell, K.; Montgomery, J. A. J.; Peralta, J. E.; Ogliaro, F.; Bearpark, M. J.; Heyd, J. J.; Brothers, E. N.; Kudin, K. N.; Staroverov, V. N.; Keith, T. A.; Kobayashi, R.; Normand, J.; Raghavachari, K.; Rendell, A. P.; Burant, J. C.; Iyengar, S. S.; Tomasi, J.; Cossi, M.; Millam, J. M.; Klene, M.; Adamo, C.; Cammi, R.; Ochterski, J. W.; Martin, R. L.; Morokuma, K.; Farkas, O.; Foresman, J. B.; Fox, D. J. Gaussian 16, Revision A.03. Gaussian, Inc.: Wallingford, CT 2016.

Chapter 3: Multifunctional SiPc Additive Combining Crosslinking and Increased Spectral Coverage

This chapter contains work published in *Journal of Materials Chemistry A:*

T. M. Grant, T. Gorisse, O. Dautel, G. Wantz, and B. H. Lessard., *J. Mater. Chem. A*, **2017**, 5, 1581–1587.

3.1. Context

The use of ternary additives to increase efficiency or improve active layer stability is well documented in the literature as outlined in **Chapter 1**, however additives are most often designed to perform one of these functions. To highlight the chemical versality of the axial functional groups available for SiPcs, I aimed to synthesise a soluble SiPc derivative containing azide groups to allow for crosslinking and stabilizing a P3HT/$PC_{61}BM$ active layer morphology, while simultaneously expanding spectral coverage of the device. A series of SiPc derivatives containing soluble, chlorine-terminated axial functional groups were synthesized. The highest solubility was observed for 6-chlorohexanoate pendants, which was selected for use in the associated publication.

3.2. Contribution of Authors

I performed all the chemical synthesis and characterization of the novel phthalocyanine compounds used in this study. I fabricated and characterized the OPV devices under the supervision of TG in Bordeaux, France. I solely wrote the first drat of the manuscript and received editing contributions from all other authors.

3.3. Abstract

Great improvements in the development of organic photovoltaic (OPV) devices have been reported over the years; however, the overall efficiency and operational lifetimes of the devices must be improved. Maintaining a stable power conversion efficiency (PCE) in bulk heterojunction OPV devices can be achieved by utilizing cross-linkable ternary additives that freeze the optimal morphology. However, these additives currently do not contribute to improving the PCE of the device therefore limiting their overall effectiveness. In this study we present a dual functional bis(6-azidohexanoate) silicon phthalocyanine ($(HxN_3)_2$-SiPc) with cross-linking groups and near IR absorption as a ternary additive in poly-(3-hexylthiophene) (P3HT) and phenyl-C61-butyric acid methyl ester ($PC_{61}BM$) devices. As an additive at 10 wt% with respect to $PC_{61}BM$, $(HxN_3)_2$-SiPc increased the short circuit current density (Jsc) by 9 % due to increased photocurrent generation in the near IR region. In addition, devices utilizing $(HxN_3)_2$- SiPc exhibited a 97 % PCE retention after thermal ageing at 150 C for 23 h (compared to 47 % retention for baseline devices) showing the compound is an effective cross-linker. These findings represent the first example of a multifunctional dye additive in an OPV device that simultaneously broadens the spectral coverage, resulting in added photogeneration, and stabilizes the active layer morphology, resulting in increased PCE retention.

3.4. Introduction

In the past decade, advancements in OPVs have shown promise for the technology to reach a commercially viable state with new materials and techniques allowing for devices with power conversion efficiencies (PCE's) above 10 % on a laboratory scale,[1] however the low operational lifetime of devices remains an active area of research. Standard bulk hetero junction (BHJ) OPVs consist of a thin film cast from a pair of blended photoactive materials: an electron donor and electron acceptor, positioned between two electrodes. In the past decade poly(3-hexithiophene) (P3HT), a conjugated polymer donor, and phenyl-C_{60}-butyric acid methyl ester ($PC_{61}BM$), fullerene derivative acceptor, have been the most extensively studied pair. Among the different degradation mechanisms responsible for the short lifetime of OPV devices,[2,3] the unfavorable phase separation of the donor/acceptor network over time and with exposure to heat remains a current concern. A key feature to obtaining high performing OPVs is to create and maintain the appropriate nanoscale blend morphology of intermixing donor and acceptor domains to maximize the donor/acceptor interfacial area that will facilitate efficient charge separation.[4–6] Fullerenes in particular are susceptible to forming clusters over time and with exposure of heat that disrupt this morphology and severely inhibit device performance.[7] In order to achieve highly efficient and stable OPVs, it is therefore important to minimize these forms of degradation.

A commonly studied approach to mitigate the phase separation of the OPV active layer is through the chemical modification of the donor or acceptor molecules themselves. Positive results have been shown by introducing functional side chains to donor polymers that can alter their glass transition temperature to slow thermal degradation.[8,9] Alternatively, crosslinking of the donor and/or acceptor remains a promising method to maintaining a desirable film morphology.[10,11] First examples of this approach utilized novel cross-linkable polymers[12,13] or fullerene derivatives,[14–16] however these materials require numerous synthetic steps and must be carefully designed as to obtain the desired original morphology resulting from the blend of the respective unfunctionalized derivatives. As an alternative method, ternary additives with crosslinking functionality have shown promise due to their more straightforward synthesis and ability to be used across a variety of donor/acceptor pairs. Derue et al. used a di-azo additive 4,4′-bis(azidomethyl)-1,1′-biphenyl (BABP) to effectively stabilize OPVs with P3HT, poly({4,8-bis[(2-ethylhexyl)oxy]benzo[1,2-b:4,5-b′]dithiophene-2,6-diyl}{3-fluoro-2-[(2-ethylhexyl)carbonyl]thieno[3,4-b]thiophenediyl}) (PTB7), and poly[[9-(1-octylnonyl)-9H-carbazole-2,7-diyl]-2,5-thiophenediyl-2,1,3-

benzothiadiazole-4,7-diyl-2,5-thiophenediyl] (PCDTBT) as the donor polymers.[17] A mild thermal treatment (≈ 80 °C) activates the cycloaddition reaction of the azo groups between the additive and the fullerene, which suppresses the fullerene crystallization. More recently Chao et al. demonstrated another additive for fullerene crosslinking with a triphenylamine dithiophene (TBT) derivative containing azide functional groups that successfully stabilized both P3HT and PTB7 devices.[18]

Currently OPV devices utilizing ternary additives designed exclusively for stabilizing the film morphology exhibit an inevitable small drop in PCE due to the presence of the cross-linker, especially at higher loadings.[17-18] For maximum effectiveness it is desirable to create a multifunctional additive that not only provides high PCE retention over time, but can also simultaneously improve the initial PCE when compared to a reference device through additional functionality. Numerous ternary additives specifically designed for increased PCE in OPV's have been reported,[19-20] with functionalities such as broadening spectral coverage, increasing charge transport, and improving the film morphology. Recently Gasparini et al. achieved a record high fill factor of 0.77 in PTB7:$PC_{71}BM$ devices by utilizing the additive poly[(4,4'-bis(2-ethyl h-exyl)dithieno[3,2-b:2',3'-d]silole)-2,6-diyl-alt-(4,7-bis(2-thienyl)-2,1,3-benzothiadiazole)-5,5'-diyl] (Si-PCPDTBT) that minimizes charge recombination within the device, showing the potential of ternary additives as a method to achieving highly efficient OPV's.[21] Designing a multifunctional additive requires both a structure for increasing PCE as well as stabilizing the film morphology. Derue et al. have demonstrated this concept with the additive 1,10-diazidodecane which can work as both a solvent additive to improve the active layer morphology and also act as a crosslinker.[22] However, to the best of our knowledge a dye-based ternary additive that can itself generate photocurrent and simultaneously crosslink the film morphology has not yet been reported.

Recently researchers have shown silicon phthalocyanine (SiPc) derivatives as promising candidates for ternary additives to increase OPV efficiency in P3HT:$PC_{61}BM$ devices.[2324252627] SiPcs absorb in the near IR range and are able to provide photocurrent generation outside the absorption range of P3HT and $PC_{61}BM$, while also being able to provide cascade energy transfer due to their intermediate energy levels. Use of the highly soluble compound bis(tri-n-hexylsilyl oxide) silicon phthalocyanine ($(3HS)_2$-SiPc) was shown to cause an increase in PCE of 20 % in P3HT:$PC_{61}BM$ devices due to a highly improved *Jsc*.[28] Researchers have also introduced SiPc derivatives in organic light emitting diodes [29] and planar heterojunction OPVs as both acceptor

layers and donor layers,[30] suggesting these compounds can transport electrons and holes effectively. In this study we looked to combine the optoelectronic properties of SiPc with the functionality of a crosslinkable additive in the compound bis(6-azidohexanoate) silicon phthalocyanine ($(HxN_3)_2$-SiPc). In the following study, we present the synthesis of $(HxN_3)_2$-SiPc and its use as a dual functional ternary additive in P3HT:$PC_{61}BM$ BHJ OPVs.

3.5. Results and Discussion

The azide functional silicon phthalocyanine $(HxN_3)_2$-SiPc (**Figure 3.1A**) was synthesized by reacting dichloro SiPc (Cl_2-SiPc) with 6-chlorohexanoic acid followed by a halide substitution with sodium azide forming a blue powder soluble up to 15 mg/mL in chlorobenzene (see experimental section for more details). An absorbance spectrum was obtained for $(HxN_3)_2$-SiPc with a peak absorbance of 685 nm in solution and a red-shifted peak of 720 nm in the solid state, outside the absorption of P3HT (**Figure 3.1B**). Electrochemical characterization yielded an estimate for E_{HOMO} of 5.4 eV using an empirical correlation,[31,32] and an E_{LUMO} of 3.6 eV was estimated using the optical band gap. Characteristic cyclic voltammogram can be found in the supporting information (Figure S3.1). These values are characteristic of SiPc derivatives[28] confirming that the absorbance and electrochemical properties remained unchanged by the addition of the azide functional groups.

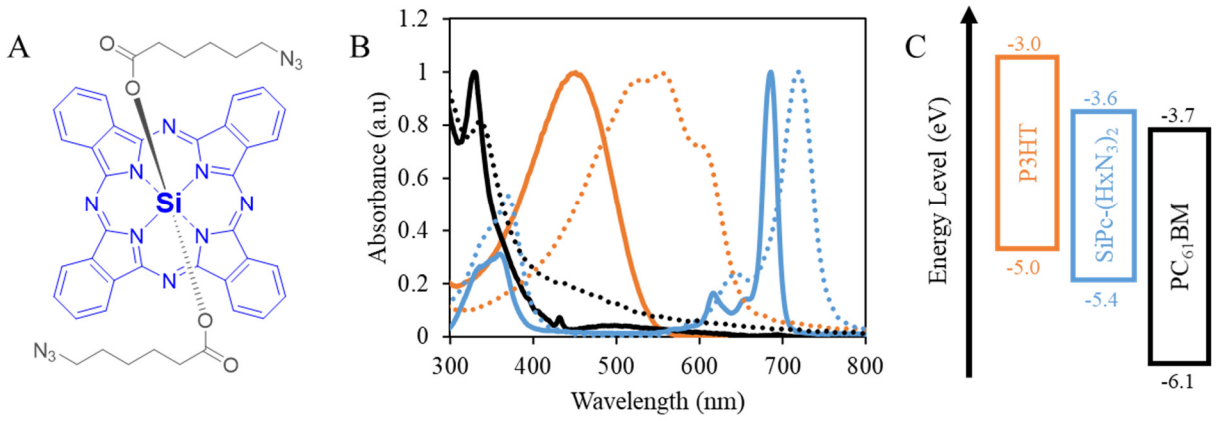

Figure 3.1. (A) Structure of silicon phthalocyanine (blue), with cross-linkable carboxylic acid functional groups (Grey). (B) Normalized UV-Vis absorption in chloroform (solid lines) and solid state (dashed lines) of PCBM (black), P3HT (orange) and (HxN3)2-SiPc (blue). (C) Molecular energy level diagram for P3HT/$(HxN_3)_2$-SiPc/$PC_{61}BM$.

It was observed that $(HxN_3)_2$-SiPc had a strong tendency to crystalize from solution, similar to $(3HS)_2$-SiPc,[28] with large needle like crystals easily grown by slow evaporation from dichloromethane. We performed single-crystal x-ray diffraction on the needles and the resulting packing motif can be found in **Figure 3.2 A** (CCDC number 1507656). The crystal structure displayed a relatively tight packing of the conjugated phthalocyanine rings, where a shortest distance of 3.579 Å was measured between benzene groups (**Figure 3.2 B**). This is in contrast to $(3HS)_2$-SiPc which does not exhibit any significant π-π staking in its crystal structure due to intermolecular spacing caused by the large tri-hexyl groups.[28] It has been established that significant π-π stacking (< 4 Å) increases device performance when using SiPc derivatives as both acceptor or donor layers in planar OPVs,[30] however it is currently unclear if π-π stacking is favorable or detrimental to the ability of a SiPc to act as a ternary additive in BHJ OPVs.

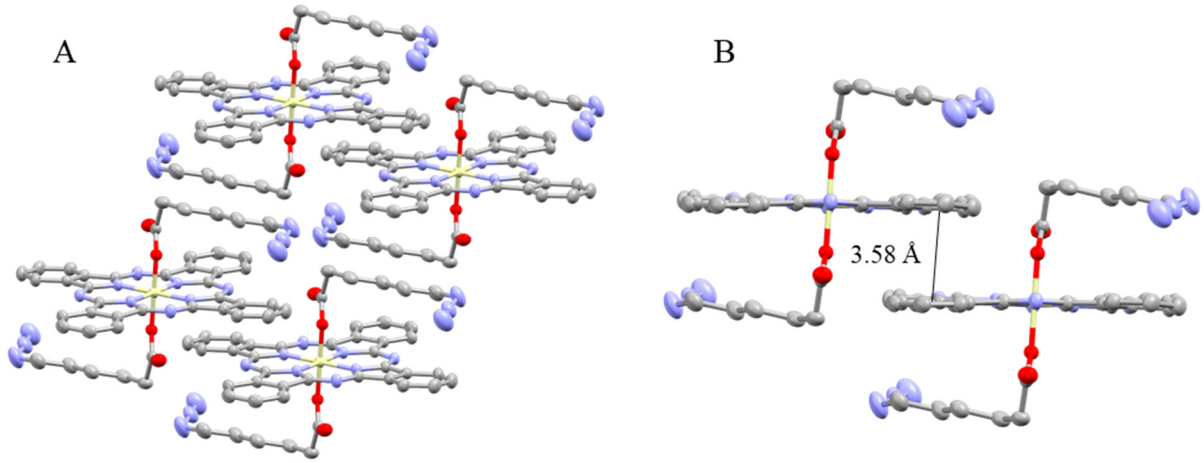

Figure 3.2. (A) Crystal structure arrangement of multiple $(HxN_3)_2$-SiPc molecules. (B) Centroid-centroid distance of the conjugated benzene groups within $(HxN_3)_2$-SiPc.

We characterized the multi functionality of $(HxN_3)_2$-SiPc as a ternary additive was studied through the fabrication and characterization of inverted BHJ OPV devices with the structure Glass/ITO/ZnO/P3HT:$PC_{61}BM$:$(HxN_3)_2$-SiPc/MoO_3/Ag, while varying the $(HxN_3)_2$-SiPc weight percent with respect to $PC_{61}BM$ at 0 %, 6 %, 8 % and 10 % (see experimental for more info). For each additive loading the photovoltaic properties of three heating profiles were characterized: 1) no heat treatment (as cast); 2) 80 °C for 10 minutes (curing of the film to perform the crosslinking reaction on fullerene derivatives); and 3) 80 °C for 10 minutes followed by 150 °C for 23h (thermal ageing). The heat treatments were carried out before thermal deposition of the metal electrode

under nitrogen atmosphere. A summary of the photovoltaic parameters can be found in **Table 3.1**, EQE and *J-V* curves in **Figure 3.3**. P3HT:$PC_{61}BM$ baseline devices without additive performed according to literature[33] with short circuit current (*Jsc*) = 10.52 ± 0.03 mA/cm^{-2}, open circuit voltage (*Voc*) = 0.54 ± 0.00 V, and fill factor (*FF*) = 0.60 ± 0.01 resulting in an average PCE of 3.41 ± 0.01%. P3HT:$PC_{61}BM$ devices subject to the curing treatment of 80 °C for 10 minutes performed marginally better than untreated devices and were used as the baseline comparison. It was found that the device active layer thickness increases linearly with increasing weight percent of $(HxN_3)_2$-SiPc, reaching a maximum of a 13 % thickness increase for 10 % $(HxN_3)_2$-SiPc relative to the reference devices. These results suggest that further device performance could result from optimization the film thickness.

For non-thermally treated devices, a loading of 6 % $(HxN_3)_2$-SiPc resulted in the largest PCE increase to 3.58 % (5 % increase from baseline) resulting from a *Jsc* increase to 11.42 mA/cm^{-2} while maintaining a *Voc* = 0.52 V and *FF* = 0.60 (**Figure 3.3A**). Devices at 8 % and 10 % loadings also exhibit an increase in *Jsc*, however a decrease in *FF* resulted in no net PCE gain.

Table 3.3. Summary of photovoltaic parameters for P3HT/$PC_{61}BM$/$(HxN_3)_2$-SiPc devices[a]

Active Layer (P3HT:$PC_{61}BM$:SiPc)	Annealing Conditions	Jsc (mA/cm^2)	Voc (V)	FF	PCE (%)
1:1:0	/	11.19 ± 0.01	0.51 ± 0.00	0.58 ± 0.00	3.28 ± 0.02
1:1:0	10 min 80 °C	10.52 ± 0.03	0.54 ± 0.00	0.60 ± 0.00	3.41 ± 0.01
1:1:0	23 h 150 °C	5.72 ± 0.07	0.50 ± 0.00	0.52 ± 0.00	1.48 ± 0.02
1:1:0.06	/	11.42 ± 0.09	0.52 ± 0.00	0.60 ± 0.00	3.58 ± 0.02
1:1:0.06	10 min 80 °C	10.93 ± 0.04	0.53 ± 0.00	0.57 ± 0.01	3.31 ± 0.08
1:1:0.06	23 h 150 °C	9.74 ± 0.04	0.55 ± 0.00	0.58 ± 0.01	3.08 ± 0.05
1:1:0.08	/	11.94 ± 0.07	0.52 ± 0.00	0.57 ± 0.00	3.54 ± 0.04
1:1:0.08	10 min 80 °C	10.89 ± 0.14	0.53 ± 0.01	0.58 ± 0.01	3.31 ± 0.05
1:1:0.08	23 h 150 °C	10.13 ± 0.09	0.54 ± 0.00	0.57 ± 0.01	3.07 ± 0.05
1:1:0.1	/	11.51 ± 0.12	0.52 ± 0.00	0.57 ± 0.00	3.39 ± 0.02
1:1:0.1	10 min 80 °C	10.53 ± 0.05	0.54 ± 0.00	0.58 ± 0.00	3.27 ± 0.02
1:1:0.1	23 h 150 °C	9.98 ± 0.05	0.54 ± 0.00	0.61 ± 0.00	3.28 ± 0.03

[a] Results were averaged for a minimum of 4 devices, errors shown are standard deviation.

This is consistent with previous work with the additive $(3HS)_2$-SiPc, that exhibited a decreasing *FF* from 0.59 to 0.51 with increased additive loadings from 3.7 % to 10.6 % (total weight percent) due to the disruption of the P3HT:PC_{61}BM morphology.[28]Regardless of the $(HxN_3)_2$-SiPc loading amount, the *Jsc* increase was a result of only increased photogeneration in the EQE from the near-IR absorption of $(HxN_3)_2$-SiPc (≈ 690 nm) and not from an increased P3HT:PC_{61}BM contribution (300-600 nm) (**Figure 3.3B,D**). This observation is not consistent with the use of $(3HS)_2$-SiPc which observed an improvement in photogeneration through 300-690 nm.[28] It is interesting to observe that the addition of $(HxN_3)_2$-SiPc appears to result in disruption in the favourable P3HT:PC_{61}BM morphology as evidenced by the microscopy images of the untreated devices (**Figure 3.4C,F,I**).

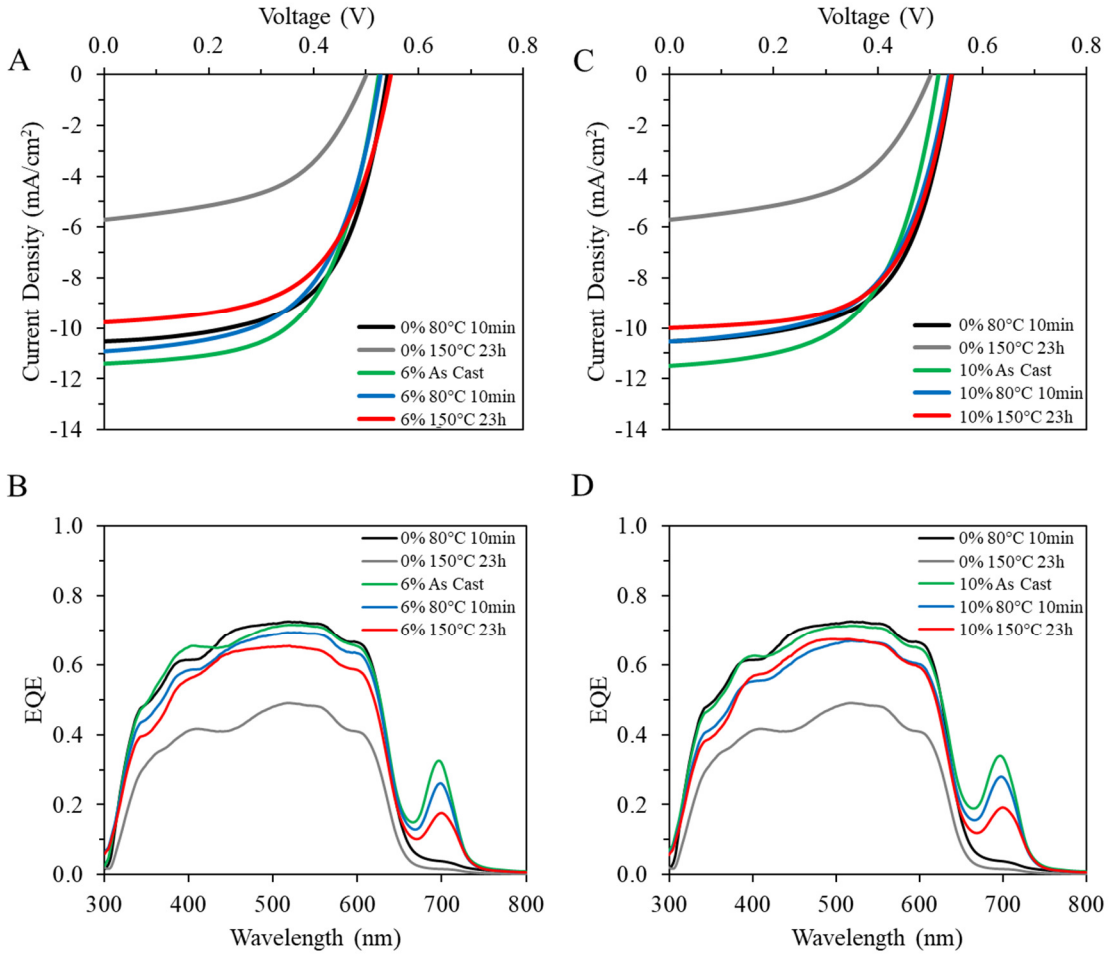

Figure 3.3. Characteristic current density vs voltage (*J-V*) and external quantum efficiency (EQE) plots for P3HT:PC_{61}BM:$(HxN_3)_2$-SiPc devices at loadings of (A, B) 6 % and (C, D) 10 % with no heat treatment (green), cured at 80°C for 10 minutes (blue), and thermally aged at 150 °C for 23 h (red). Data for P3HT:PC_{61}BM devices after curing (black) and ageing (grey) is included for reference.

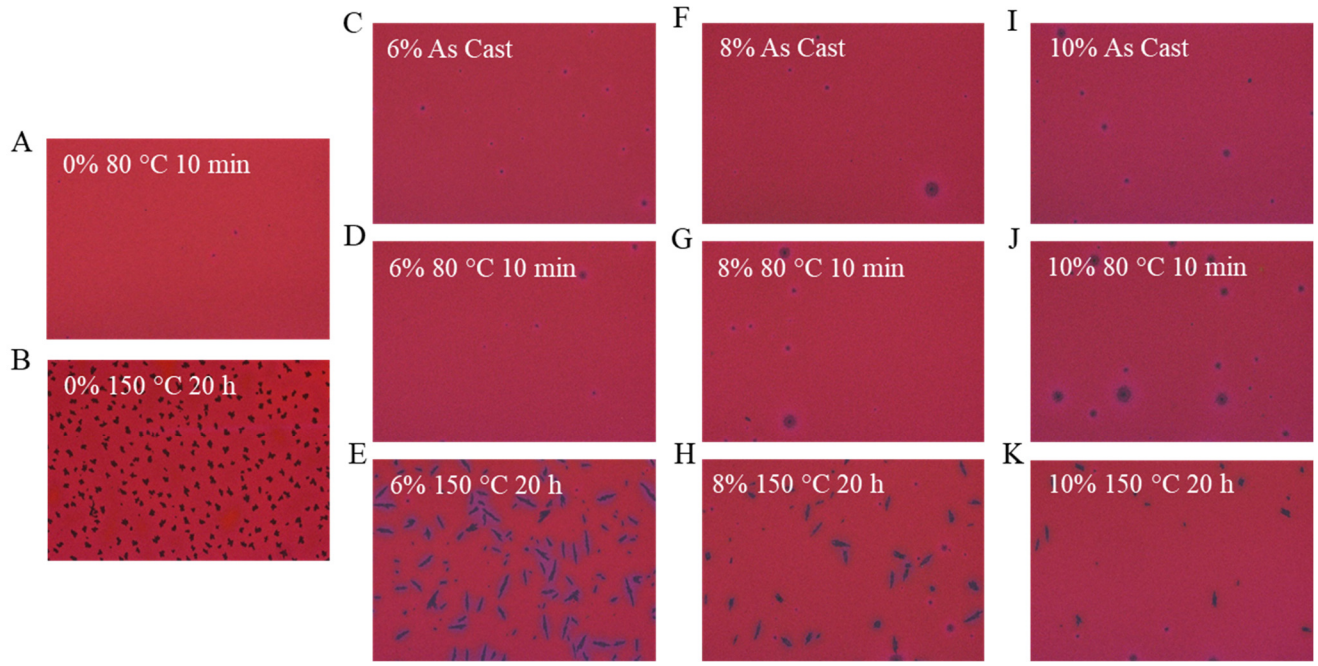

Figure 3.4. Microscopic images (20x magnification) with varying weight % of $(HxN_3)_2$-SiPc and for as cast, cured, and aged films.

When exposing the ternary devices to a thermal treatment of 80 °C for 10 minutes to activate the crosslinking reaction, all devices experienced a slight drop in PCE. This drop in PCE was a result of decreased *Jsc* which corresponded to a drop in EQE between the P3HT:PC_{61}BM contribution (350 – 600 nm) and the $(HxN_3)_2$-SiPc contribution (700 nm) (**Figure 3.3B,D**). We surmise this decrease in PCE could be due to an increased content of $(HxN_3)_2$-SiPc which results in visible aggregates within the film blend, which are noticeably visible in microscope images for the cured devices at the 10 % loading (**Figure 3.4J**), and this growth of a separate phase further disrupts the P3HT:PC_{61}BM morphology to decrease the overall *Jsc*.

When exposing the devices to a thermal ageing of 150 °C for 23h, it was found that the baseline P3HT:PC_{61}BM devices significantly degraded, resulting in a drop in *Jsc* = 5.7 mA/cm^2 and PCE = 1.48 %. As expected, significant PC_{61}BM crystallization is visible in the microscope images of the films because of the heat treatment (**Figure 3.4B**), suggesting the loss in device performance is a result of phase separation and crystallization of the PC_{61}BM. Device images after ageing clearly show a decrease in PC_{61}BM crystallization with higher loadings of the additive, with 10 % showing minimal crystals (**Figure 3.4K**). This trend is also displayed in the PCEs for

the aged devices, with the 6 %, 8 % and 10 % loadings achieving approximately 93 %, 93 % and 100 % PCE retention respectively vs the cured devices, and approximately 90 %, 90 % and 97 % PCE retention respectively vs the neat devices. While the addition of 6 % $(HxN_3)_2$-SiPc was the most effective loading ratio in terms of increasing the initial PCE, it was determined that an addition of 10 % $(HxN_3)_2$-SiPc resulted in the most significant PCE retention after ageing process. As a comparison, the use of $(HxN_3)_2$-SiPc as a ternary additive was compared to literature values of other ternary additives to assess the PCE retention when used in P3HT:$PC_{61}BM$ BHJ OPVs (**Table 3.2**). It becomes apparent that under similar loadings, the $(HxN_3)_2$-SiPc can obtain comparable if not superior PCE retention compared to previously report ternary additives. These results are evidence that $(HxN_3)_2$-SiPc is effective at both increasing the overall device performance as well cross-linking the active layer resulting in improved PCE retention.

Table 3.7. Comparison of the effectiveness of azide-functional crosslinking ternary additives in P3HT/$PC_{61}BM$ devices.

Crosslinker (wt%)[1]	Ageing Conditions	Reference PCE	Initial PCE	Aged PCE	Initial PCE Retention	Aged PCE Retention	Reference
$(HxN_3)_2$-SiPc (6%)	23h 150°C	3.41	3.58	3.08	105%	86%	This work
$(HxN_3)_2$-SiPc (10%)	23h 150°C	3.41	3.39	3.28	99%	97%	This work
BABP (2%)	24h 150°C	3.40	3.40	3.13	100%	92%	[173]
TBT-N_3 (5%)	24h 150°C	3.44[2]	3.36[2]	2.69	98%	80%	[18]

1) Crosslinker (wt%) is the chemical structure of the additive itself and the wt% relative to $PC_{61}BM$.
2) Annealed at 150°C for 20min
3) Data from a larger subset then what was presented in the reference

3.6. Experimental

Materials

6-chlorohexanoic acid was purchased from TCI Chemicals and used as received. Sodium azide was purchased from Oakwood chemicals and used as received. o-Dichlorobenzene (> 99 %) was purchased from Sigma-Aldrich and used as received. Dimethylformamide (DMF) and dichloromethane (DCM) were purchased from Fischer Scientific and used as received unless otherwise specified. Deuterated chloroform ($CDCl_3$) was purchased from Cambridge Isotope Laboratories and used as received. Dichlorosilicon phthalocyanine (Cl_2-SiPc) was synthesized as described in the literature[34] and was purified by sublimation before further use.

Synthesis of bis(6-chlorohexylacrylate) silicon phthalocyanine ($(HxCl)_2$-SiPc):

To a three-neck round-bottom flask was added Cl_2-SiPc (1.00 g, 1.64 mmol), toluene (60 mL), and 6-chlorohexyl carboxylic acid (2.47 g, 16.4 mmol) under nitrogen. We heated the reaction mixture to 120 °C overnight before cooling it to room temperature. The product was precipitated in methanol and filtered by gravity. The resulting solid was dissolved in DCM and washed exhaustively with 2M NaCl followed by water, then recovered by rotary evaporation and dried under vacuum yielding a blue powder (0.95 g, yield = 69 %). HRMS (Ion Spray) calcd. for $C_{44}H_{36}Cl_2N_8O_4Si$ 839.7993, found 839.1850. ^{1}H NMR (400 MHz, $CDCl_3$) 9.64–9.72 (m, 8H), 8.42–8.34 (m, 8H), 2.82-2.76 (t, 4H), 0.60-0.50 (m, 4H), (-0.58) - (-0.62) (m, 8H), (-0.84) - (-0.88) (m, 4H).

Synthesis of bis(6-azidohexanoate) silicon phthalocyanine ($(HxN_3)_2$-SiPc):

To a three-neck round-bottom flask was added $(HxCl)_2$-SiPc (0.5 g, 0.60 mmol), dimethylformamide (50 mL), and sodium azide (0.117 g, 1.8 mmol) under nitrogen. We heated the reaction mixture to 90 °C for 24h before cooling it to room temperature and precipitating it in water and filtering under vacuum. The extracted solid was dissolved in DCM and washed exhaustively with water, then recovered by rotary evaporation and dried under vacuum yielding a blue powder (0.36 g, yield = 71 %). HRMS (Ion Spray) calcd. for $C_{44}H_{36}N_{14}O_4Si$ 852.9335, found 852.2672. ^{1}H NMR (400 MHz, $CDCl_3$) 9.64–9.72 (m, 8H), 8.42–8.34 (m, 8H), 2.52-2.44 (t, 4H), 0.42-0.32 (m, 4H), (-0.60) - (-0.68) (m, 8H), (-0.84) - (-0.88) (m, 4H).

Equipment

Nuclear magnetic resonance (NMR) spectra were recorded on a Bruker Avance II spectrometer at room temperature in $CDCl_3$ operating at 400 MHz. Chemical shifts are reported in parts per million (ppm) referenced to tetramethylsilane (0 ppm). Spin multiplicities are designated by the following abbreviations: s (singlet), d (doublet), t (triplet), q (quartet), m (multiplet), and br (broad). We collected UV-vis absorption spectra from an Ocean Optics Flame spectrophotometer and DH-2000 light source, with a 10mm path-length quartz cuvette. Cyclic voltammetry was carried out using a VersaSTAT 3 potentiostat, with a platinum disk working electrode, platinum wire counter electrode, and a $Ag/AgCl_2$ reference electrode. Four cycles from -1.2 V to 1.6 V at a scan rate of 0.1 V/s were obtained. Measurements were conducted in N_2 purged dichloromethane with tetraburylammonium perchlorate as the supporting electrolyte, and ferrocene was used as an internal reference. The HOMO levels were estimated from the correlation: E_{HOMO} (eV) = - ($E_{ox,\ onset} - E_{ox\ Fc/Fc+,\ onset}$) – 4.80 eV, where $E_{ox,\ onset}$ and $E_{ox\ Fc/Fc+,\ onset}$ are the onset oxidation potentials for the dye and the ferrocene refence respectively against the Ag/AgCl reference.

BHJ OPV Devices

Inverted cells were fabricated with the structure Glass / ITO / ZnO / P3HT:$PC_{61}BM$: $(HxN_3)_2$-SiPc / MoO_3 / Ag. ITO coated glass slides we cleaned in a sonication bath for 10 minutes successively in soap-water, water, acetone, and isopropanol then exposed to UV-ozone for 10 minutes. The zinc oxide solution was prepared by combining zinc acetate dihydrate (0.1956 g, 1.066 mmol), ethanolamine (0.0544 mL, 0.9 mmol) in absolute ethanol (6 mL), and stirred at 50°C for 2 h before spin coating. The solution was spin coated onto the UV-ozone treated substrates at 2000 rpm for 60 s and dried on a hotplate for 1 h at 180 °C before being moved into a glove box for the remainder of fabrication. P3HT:$PC_{61}BM$:$(HxN_3)_2$-SiPc solutions were prepared in o-dichlorobenzene with final P3HT and PCBM concentrations of 20 mg/mL respectively (1:1 ratio) after the addition of $(HxN_3)_2$-SiPc from a 15 mg/mL solution. Solutions were prepared for 0 %, 6 %, 8 %, and 10 % $(HxN_3)_2$-SiPc content by weight with respect to PCBM. Before the addition of $(HxN_3)_2$-SiPc, the P3HT:$PC_{61}BM$ solution was stirred for 10 min at 90 °C for 10 min then 50 °C for 24 h, and the $(HxN_3)_2$-SiPc solution was stirred at room temperature for 24 h. P3HT:$PC_{61}BM$:$(HxN_3)_2$-SiPc solutions stirred for at least 10 min at 50 °C before spin coating. The BHJ layers were spin coated under a nitrogen atmosphere at 1000 rpm for 35 seconds and dried them in a closed petri dish (solvent annealing). We then cured and aged the devices before

depositing the electrodes under nitrogen atmosphere. Curing was carried out on a hotplate at 80 °C for 10 min, and ageing at 150 °C for 23 h. Molybdenum trioxide (MoO_3, 7 nm) and silver (70 nm) were deposited on the devices using a thermal evaporator at 4 x 10^{-6} torr for a device area of 10 mm² as defined by a shadow mask. Finished devices were encapsulated using a glass slide adhered with a UV curable glue (NOA61 glue, Epotecny) before testing outside the fume hood. Current density vs voltage (*J-V*) curves were measured with a Keithley 4200 under an AM1.5 sun-simulator with a Xenon lamp calibrated with a radiometer (IM1400) at 100 mA/cm². External Quantum Efficiency (EQE) was performed with a home-made set-up consisting of a Xenon lamp connected to a Horiba monochromator. Optical images were taken with a Zeiss microscope.

3.7. Conclusions

We have presented a relatively easy to synthesize multifunctional ternary additive that can both increase the PCE due to increased photo-generation in the near-IR and retain the PCE during aging experiments due to crosslinking of the P3HT:PC_{61}BM BHJ morphology. The ageing studies also suggest that $(HxN_3)_2$-SiPc is a more effective crosslinking additive compared to previously published molecules. These findings show promise for the use of multifunctional ternary additives in attempts to increase OPV performance and stability. It is possible a SiPc derivative with improved solubility would allow for higher loadings to maintain a more optimal morphology and improve both the initial and aged PCEs. Future work will look at increasing both the photogeneration efficiency and stability enhancement of these ternary additives in conjugation with additional polymer-fullerene BHJ OPV systems.

3.8. References

(1) You, J.; Dou, L.; Yoshimura, K.; Kato, T.; Ohya, K.; Moriarty, T.; Emery, K.; Chen, C.-C.; Gao, J.; Li, G.; Yang, Y. A Polymer Tandem Solar Cell with 10.6% Power Conversion Efficiency. *Nat. Commun.* **2013**, *4*, 1446.

(2) Jørgensen, M.; Norrman, K.; Gevorgyan, S. A.; Tromholt, T.; Andreasen, B.; Krebs, F. C. Stability of Polymer Solar Cells. *Adv. Mater.* **2012**, *24* (5), 580–612.

(3) Grossiord, N.; Kroon, J. M.; Andriessen, R.; Blom, P. W. M. Degradation Mechanisms in Organic Photovoltaic Devices. *Org. Electron.* **2012**, *13* (3), 432–456.

(4) Campoy-Quiles, M.; Ferenczi, T.; Agostinelli, T.; Etchegoin, P. G.; Kim, Y.; Anthopoulos, T. D.; Stavrinou, P. N.; Bradley, D. D. C.; Nelson, J. Morphology Evolution via Self-Organization and Lateral and Vertical Diffusion in Polymer:Fullerene Solar Cell Blends. *Nat. Mater.* **2008**, *7* (2), 158–164.

(5) Liu, F.; Gu, Y.; Jung, J. W.; Jo, W. H.; Russell, T. P. On the Morphology of Polymer-Based Photovoltaics. *J. Polym. Sci. Part B Polym. Phys.* **2012**, *50* (15), 1018–1044.

(6) Defour, M.; Van den Brande, N.; Van Lokeren, L.; Van Assche, G.; Maes, W.; Vanderzande, D.; Van Mele, B. Eutectic Composition and Temperature in the State Diagram of P3HT:PC61BM Determined by Rapid Heat-Cool Calorimetry. *J. Mater. Chem. A* **2016**, *Submitted*, 92981–92988.

(7) Schaffer, C. J.; Palumbiny, C. M.; Niedermeier, M. A.; Jendrzejewski, C.; Santoro, G.; Roth, S. V; Müller-Buschbaum, P. A Direct Evidence of Morphological Degradation on a Nanometer Scale in Polymer Solar Cells. *Adv. Mater.* **2013**, *25* (46), 6760–6764.

(8) Kesters, J.; Kudret, S.; Bertho, S.; Van Den Brande, N.; Defour, M.; Van Mele, B.; Penxten, H.; Lutsen, L.; Manca, J.; Vanderzande, D.; Maes, W. Enhanced Intrinsic Stability of the Bulk Heterojunction Active Layer Blend of Polymer Solar Cells by Varying the Polymer Side Chain Pattern. *Org. Electron. physics, Mater. Appl.* **2014**, *15* (2), 549–562.

(9) Kesters, J.; Verstappen, P.; Raymakers, J.; Vanormelingen, W.; Drijkoningen, J.; D'Haen, J.; Manca, J.; Lutsen, L.; Vanderzande, D.; Maes, W. Enhanced Organic Solar Cell Stability by Polymer (PCPDTBT) Side Chain Functionalization. *Chem. Mater.* **2015**, *27* (4), 1332–1341.

(10) Wantz, G.; Derue, L.; Dautel, O.; Rivaton, A.; Hudhomme, P.; Dagron-Lartigau, C. Stabilizing Polymer-Based Bulk Heterojunction Solar Cells via Crosslinking. *Polym. Int.* **2014**, *63* (8), 1346–1361.

(11) Rumer, J. W.; McCulloch, I. Organic Photovoltaics: Crosslinking for Optimal Morphology and Stability. *Mater. Today* **2015**, *18* (8), 425–435.

(12) Kim, B. J.; Miyamoto, Y.; Ma, B.; Fréchet, J. M. J. Photocrosslinkable Polythiophenes for Efficient, Thermally Stable, Organic Photovoltaics. *Adv. Funct. Mater.* **2009**, *19* (14), 2273–2281.

(13) Nam, C.-Y.; Qin, Y.; Park, Y. S.; Hlaing, H.; Lu, X.; Ocko, B. M.; Black, C. T.; Grubbs, R. B. Photo-Cross-Linkable Azide-Functionalized Polythiophene for Thermally Stable Bulk

Heterojunction Solar Cells. *Macromolecules* **2012**, *45* (5), 2338–2347.

(14) Diacon, A.; Derue, L.; Lecourtier, C.; Dautel, O.; Wantz, G.; Hudhomme, P. Cross-Linkable Azido C 60 -Fullerene Derivatives for Efficient Thermal Stabilization of Polymer Bulk-Heterojunction Solar Cells. *J. Mater. Chem. C* **2014**, *2* (35), 7163.

(15) Drees, M.; Hoppe, H.; Winder, C.; Neugebauer, H.; Sariciftci, N. S.; Schwinger, W.; Schäffler, F.; Topf, C.; Scharber, M. C.; Zhu, Z.; Gaudiana, R. Stabilization of the Nanomorphology of Polymer–Fullerene "Bulk Heterojunction" Blends Using a Novel Polymerizable Fullerene Derivative. *J. Mater. Chem.* **2005**, *15* (48), 5158.

(16) Cheng, Y. J.; Hsieh, C. H.; Li, P. J.; Hsu, C. S. Morphological Stabilization by in Situ Polymerization of Fullerene Derivatives Leading to Efficient, Thermally Stable Organic Photovoltaics. *Adv. Funct. Mater.* **2011**, *21* (9), 1723–1732.

(17) Derue, L.; Dautel, O.; Tournebize, A.; Drees, M.; Pan, H.; Berthumeyrie, S.; Pavageau, B.; Cloutet, E.; Chambon, S.; Hirsch, L.; Rivaton, A.; Hudhomme, P.; Facchetti, A.; Wantz, G. Thermal Stabilisation of Polymer-Fullerene Bulk Heterojunction Morphology for Efficient Photovoltaic Solar Cells. *Adv. Mater.* **2014**, *26* (33), 5831–5838.

(18) Chao, Y.-C.; Chuang, C.-H.; Hsu, H.-L.; Wang, H.-J.; Hsu, Y.-C.; Chen, C.-P.; Jeng, R.-J. Enhanced Thermal Stability of Organic Photovoltaics via Incorporating Triphenylamine Derivatives as Additives. *Sol. Energy Mater. Sol. Cells* **2016**, *157*, 666–675.

(19) Chen, Y. C.; Hsu, C. Y.; Lin, R. Y. Y.; Ho, K. C.; Lin, J. T. Materials for the Active Layer of Organic Photovoltaics: Ternary Solar Cell Approach. *ChemSusChem* **2013**, *6* (1), 20–35.

(20) Goubard, F.; Wantz, G. Ternary Blends for Polymer Bulk Heterojunction Solar Cells. *Polym. Int.* **2014**, *63* (8), 1362–1367.

(21) Fladischer, S.; Gasparini, N.; Spiecker, E.; Jiao, X.; Brabec, C. J.; Baran, D.; Matt, G. J.; Heumueller, T.; Ade, H.; Ameri, T. Designing Ternary Blend Bulk Heterojunction Solar Cells with Reduced Carrier Recombination and a Fill Factor of 77%. *Nat. Energy* **2016**, *1* (9), 1–9.

(22) Derue, L.; Lecourtier, C.; Gorisse, T.; Hirsch, L.; Dautel, O.; Wantz, G. A Solvent Additive to Enhance the Efficiency and the Thermal Stability of Polymer:Fullerene Solar Cells. *RSC Adv.* **2015**, *5* (5), 3840–3843.

(23) Honda, S.; Ohkita, H.; Benten, H.; Ito, S. Selective Dye Loading at the Heterojunction in Polymer/Fullerene Solar Cells. *Adv. Energy Mater.* **2011**, *1* (4), 588–598.

(24) Honda, S.; Nogami, T.; Ohkita, H.; Benten, H.; Ito, S. Improvement of the Light-Harvesting Efficiency in Polymer/Fullerene Bulk Heterojunction Solar Cells by Interfacial Dye Modification. *ACS Appl. Mater. Interfaces* **2009**, *1* (4), 804–810.

(25) Honda, S.; Yokoya, S.; Ohkita, H.; Benten, H.; Ito, S. Light-Harvesting Mechanism in Polymer/Fullerene/Dye Ternary Blends Studied by Transient Absorption Spectroscopy. *J. Phys. Chem. C* **2011**, *115* (22), 11306–11317.

(26) Honda, S.; Ohkita, H.; Benten, H.; Ito, S. Multi-Colored Dye Sensitization of Polymer/Fullerene Bulk Heterojunction Solar Cells. *Chem. Commun.* **2010**, *46* (35), 6596–

6598.

(27) Ito, S.; Ohkita, H.; Benten, H.; Honda, S. Spectroscopic Analysis of NIR-Dye Sensitization in Bulk Heterojunction Polymer Solar Cells. *Ambio* **2012**, *41*, 132–134.

(28) Lessard, B. H.; Dang, J. D.; Grant, T. M.; Gao, D.; Seferos, D. S.; Bender, T. P. Bis(Tri-n-Hexylsilyl Oxide) Silicon Phthalocyanine: A Unique Additive in Ternary Bulk Heterojunction Organic Photovoltaic Devices. *ACS Appl. Mater. Interfaces* **2014**, *6*, 15040–15051.

(29) Plint, T.; Lessard, B. H.; Bender, T. P. Assessing the Potential of Group 13 and 14 Metal/Metalloid Phthalocyanines as Hole Transporting Layers in Organic Light Emitting Diodes. *J. Appl. phys.* **2016**, *119* (1), 145502.

(30) Lessard, B. H. B. H.; Grant, T. M.; White, R.; Thibau, E.; Lu, Z.-H.; Bender, T. P. The Position and Frequency of Fluorine Atoms Changes the Electron Donor/Acceptor Properties of Fluorophenoxy Silicon Phthalocyanines within Organic Photovoltaic Devices. *J. Mater. Chem. A* **2015**, *3*, 24512–24524.

(31) Li, Y.; Cao, Y.; Gao, J.; Wang, D.; Yu, G.; Heeger, A. J. Electrochemical Properties of Luminescent Polymers and Polymer Light-Emitting Electrochemical Cells. *Synth. Met.* **1999**, *99* (3), 243–248.

(32) Li, S. G.; Yuan, Z. C.; Yuan, J. Y.; Deng, P.; Zhang, Q.; Sun, B. Q. An Expanded Isoindigo Unit as a New Building Block for a Conjugated Polymer Leading to High-Performance Solar Cells. *J. Mater. Chem. A* **2014**, *2* (15), 5427–5433.

(33) Dang, M. T.; Hirsch, L.; Wantz, G. P3HT:PCBM, Best Seller in Polymer Photovoltaic Research. *Adv. Mater.* **2011**, *23* (31), 3597–3602.

(34) Lowery, M. K.; Starshak, A. J.; Esposito, J. N.; Krueger, P. C.; Kenney, M. E. Dichloro(Phthalocyanino)Silicon. *Inorg. Chem* **1965**, 128.

Chapter 4: High V_{OC} OPV Devices Using SiPc as an NFA

This chapter contains work published in *Organic Electronics*:

T. M. Grant, K. L.C. Kaller, T. J. Coathup, N. A. Rice, K. Hinzer, and B. H. Lessard., *Organic Electronics*, **2020**, 87, 105976.

4.1. Context

As outlined in **Chapter 1**, SiPc derivatives have been used as NFAs in only two instances in the literature with moderate results. During my preliminary device work at uOttawa, I began optimizing P3HT/SiPc binary devices, and was able to achieve a significantly improved PCE using bis(tri-n-butylsilyl oxide) SiPc ($(3BS)_2$-SiPc) as an NFA with P3HT, surpassing 3 %. The devices were characterized by a relatively high V_{OC}, a result of the relatively shallow LUMO level of $(3BS)_2$-SiPc consistent with previously reported devices. We were also interested in further characterizing the devices under reduced light intensity and variable angles to observe the effects on FF and absorption in comparison to $PC_{61}BM$. I also paired $(3BS)_2$-SiPc with higher performing polymer, PBDB-T, in an attempt to produce an even high V_{OC} due to the large $HOMO_{donor}$ – $LUMO_{acceptor}$ overlap between PBDB-T and $(3BS)_2$-SiPc.

4.2. Contribution of Authors

I performed the chemical synthesis and purification of the phthalocyanine compound, as well as the fabrication, optimization, and initial characterization of all OPV devices. KK and TC performed the reduced light intensity, incident angle, and ellipsometry measurements. NAR performed the AFM measurements. I solely wrote the first draft of the manuscript and received editing contributions from all other authors.

4.3. Abstract

Silicon phthalocyanines (SiPcs) have been identified as a candidate material for synthetically facile non-fullerene electron acceptors (NFAs) in solution processed organic photovoltaic (OPV) devices. Here we continue to investigate the use of bis(tri-n-butylsilyl oxide) SiPc ($(3BS)_2$-SiPc) as a NFA paired with poly(3-hexylthiophene) (P3HT) and for the first time with poly[(2,6-(4,8-bis(5-(2-ethylhexyl)thiophen-2-yl)-benzo[1,2-b:4,5-b']dithiophene))-alt-(5,5-(1',3'-di-2-thienyl-5',7'-bis(2-ethylhexyl)benzo[1',2'-c:4',5'-c']dithiophene-4,8-dione)] (PBDB-T). We show improved efficiency of P3HT/$(3BS)_2$-SiPc devices using an inverted structure, achieving an average power conversion efficiency (PCE) of 3.6 %, the highest reported for SiPc-based NFA devices. PBDB-T/$(3BS)_2$-SiPc devices show an average PCE of 3.4 % with an impressive open circuit voltage as high as 1.10 V arising from a minimal donor/acceptor energetic offset. Under reduced light intensity the $(3BS)_2$-SiPc devices show higher relative PCE compared to reference phenyl-C61-butyric acid methyl ester ($PC_{61}BM$) devices, suggesting the materials could perform well in indoor or diffuse light applications. These results show great promise for SiPc derivatives as electron acceptors, with the potential for further improvement with optimization of active layer morphology and device architecture.

4.4. Introduction

Organic photovoltaic (OPV) devices have seen extensive research interest as a solar technology with the potential for inexpensive fabrication onto flexible substrates and low energy payback time.[1] Recently single junction OPV devices have been demonstrated with impressive power conversion efficiencies (PCEs) up to 18 %.[2–5] The recent rapid improvement in PCE has largely been achieved through the development of novel polymer donors as well as non-fullerene acceptors (NFAs). High PCE polymer donors commonly employ carefully selected alternating donor and acceptor units which can provide broader absorption and improved hole mobility.[6,7] High PCE NFAs are similarly designed with acceptor-donor-acceptor structures allowing for highly tuneable energy levels as well as improved stability and light absorption compared to fullerene derivatives.[8,9] The increased PCEs produced from these novel active materials however has often come at the cost of increased synthetic complexity, which can severely limit the commercial viability of the resulting devices.[10] It is therefore important to investigate materials that can be obtained through scalable chemistry and purification techniques to realize commercially relevant devices.

Derivatives of perylene diimide (PDI) have emerged as high-performance NFA materials which can be accessed through widely available starting materials and a relatively low number of synthetic steps.[11] Current potentially scalable PDI derivatives have achieved PCEs surpassing 9 % in solution-processed bulk heterojunction (BHJ) devices.[12,13] Other candidates for scalable, solution-processable NFAs include derivatives of other organic dyes such as indigo,[14] porphyrins,[15,16], and for our interest, phthalocyanines (Pcs). Pcs share similar traits with PDIs as solution processed NFA materials, namely general stability and strong absorption from use as organic dyes, relatively high-lying lowest unoccupied molecular orbital (LUMO) levels, chemical versatility, and straightforward chemical functionalization.[17] In OPV devices, derivatives of silicon Pc (SiPc) have seen some recent interest due to their ability to form bonds above and below the Pc chromophore, unlike the more common copper Pc and zinc Pc. These substituents facilitate increased solubility for use in solution-processed devices as well as a degree of control over the solid-state behavior of the material. The tendency of the Pc chromophores to aggregate in the solid state is also reduced in SiPc, unlike planar molecules such as CuPc, ZnPc, or PDI. The SiPc axial group can be functionalized through straightforward 1 or 2 step chemistry from a SiPc dichloride starting material to substitute silanes,[18] phenols,[19] and carboxylic acids[20–22]. Despite their effects

on physical properties, axial substituents leave the energetics of the SiPc relatively unchanged with typical highest occupied molecular orbital (HOMO) and LUMO energy levels ranging from 5.2-5.4 eV and 3.5-3.7 eV, respectively.[21,23–25] The optoelectrical properties of SiPc can more significantly be tuned though modification of the phthalocyanine chromophore, for example silicon napthalocyanine which has a reduced band gap and extended absorption beyond 800 nm.[26–28] However the ease and extent to which the optoelectrical properties of SiPc can be controlled through peripheral functionalization has not been widely investigated in the current literature.

SiPc derivatives have been commonly studied for use as ternary additives in OPV devices, where the material is added in low weight percentages to a conventional donor/acceptor blend. In poly(3-hexylthiophene)/phenyl-C_{61}-butyric acid methyl ester (P3HT/$PC_{61}BM$) devices, SiPc derivatives have been shown to increase photocurrent generation by providing additional light absorption between 650 – 750 nm from the strongly absorbing SiPc chromophore,[29] and are able to achieve external quantum efficiency (EQE) contributions of up to 40 % from the addition of as little as 3 wt % of SiPc into the active layer blend.[25] Despite their success as ternary additives there have been only two reports in the literature investigating SiPc derivatives as a NFA in solution processed devices, achieving a PCE up to 1.07 % when paired with P3HT[24] and 2.67 % when paired with PTB7[21]. Although these efficiencies are moderate, the devices exhibited relatively high open circuit voltage (V_{OC}) of 0.84 V and 1.03 V with P3HT and PTB7, respectively, due to the favorable energetics of SiPc in relation to the donor polymers providing relatively high overlap between the HOMO of the donor polymers and the LUMO the SiPc derivatives.

In this study, we match SiPc with a donor polymer having very similar HOMO and LUMO energy levels, namely the well know polymer poly[(2,6-(4,8-bis(5-(2-ethylhexyl)thiophen-2-yl)-benzo[1,2-b:4,5-b']dithiophene))-alt-(5,5-(1',3'-di-2-thienyl-5',7'-bis(2-ethylhexyl)benzo[1',2'-c:4',5'-c']dithiophene-4,8-dione)] (PBDB-T) in an attempt to maximize the device V_{OC}. Additionally, we continue to investigate SiPc materials for use as a NFA paired with P3HT. Given the synthetic simplicity of SiPc derivatives, their use as NFAs may be most appropriate when paired with P3HT which remains the most commercially relevant polymer donor in terms of synthetic scalability and compatibility with roll-to-roll processes despite its declining interest in the literature in lieu of low-bandgap polymers.[30] Through this work we demonstrate for the first time efficiencies above 3 % and approaching 4 % for a SiPc derivative as an NFA, providing evidence that these materials show potential for use as NFA materials.

4.5. Results and Discussion

In the literature, tri-n-alkylsilyl oxides are commonly used as a functional group for solution-processed SiPcs, providing high solubility while also reducing the tendency for the SiPc chromophores to aggregate in the solid-state.[29] For this study, we chose to use the previously reported bis(tri-n-butylsilyl oxide) SiPc ($(3BS)_2$-SiPc). This derivative has previously been marginally outperformed by bis(tri-n-isopropylsilyl oxide) SiPc in binary P3HT/SiPc devices,[24] however the isopropyl alkyl chains provided insufficient solubility for film forming at our optimized processing conditions therefore the more soluble butyl derivative was selected. $PC_{61}BM$ was used as a baseline to compare the performance of $(3BS)_2$-SiPc as an acceptor paired with both P3HT and PBDB-T. The molecular structures of the materials used in the study**,** along with their HOMO/LUMO energy levels and thin film absorption are shown in **Figure 4.1.**

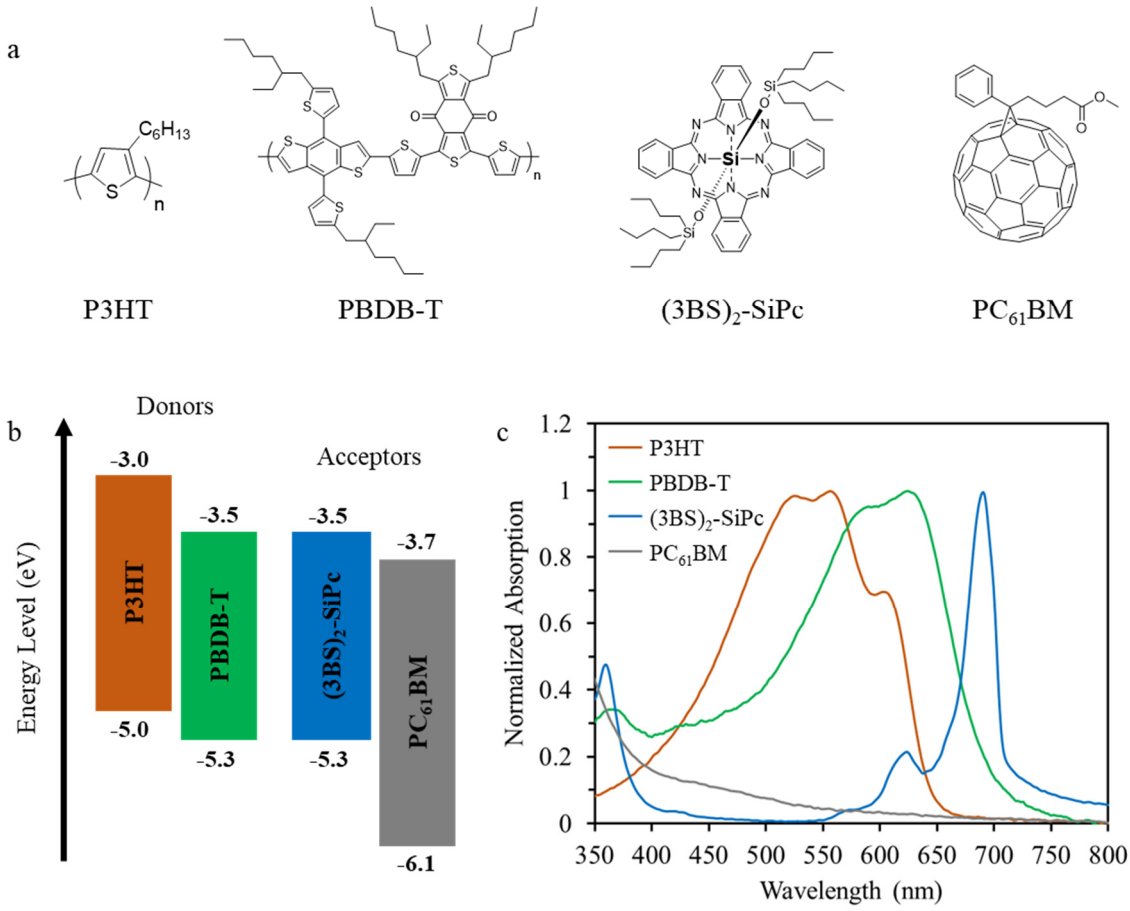

Figure 4.1: (a) Molecular structures, (b) electronic energy levels, and (c) thin film absorption spectra of PBDB-T, P3HT, $(3BS)_2$-SiPc and $PC_{61}BM$.

Bulk heterojunction (BHJ) devices were fabricated with an inverted structure (glass/ITO/ZnO/active layer/MoO_x/Ag), with an active layer thickness of 150 ± 10 nm for P3HT devices and 80 ± 5 nm for PBDB-T devices. Current density-voltage (*J-V*) characteristics for devices at 1 sun AM 1.5G are shown in **Figure 4.2** and device characteristics summarized in **Table 4.1**. Baseline P3HT/$PC_{61}BM$ and PBDB-T/$PC_{61}BM$ devices had average PCE of 3.0% and 6.4%, respectively, comparable to reports in the literature.[31,32]

Previously reported binary P3HT/$(3BS)_2$-SiPc devices achieved a PCE of 0.78% using a direct structure and donor/acceptor mass ratio of 1:0.55.[24] It was reported that at higher acceptor concentrations, inhomogeneous films were formed leading to non-functioning devices. Here, using an inverted structure and an optimized donor/acceptor ratio of 1:1 we achieve a four-fold improved average PCE of 3.6%, with a V_{OC} of 0.76 V, short circuit current density (J_{SC}) of 9.0 mA/cm^2, and a fill factor (*FF*) of 0.53. These significant results surpass the previously reported PCE as well as our $PC_{61}BM$ baseline. We found the drying time greatly affected the quality of P3HT/$(3BS)_2$-SiPc active layer films and the resulting device performance. Spinning films for 60 or more seconds, which allowed them to dry on the spin coater, was crucial for achieving homogeneous film formation. Films spun for 30 s, which dried after being removed from the spin coater, resulted in the formation of visible crystalline SiPc features and non-homogeneous films (**Figure S4.1**). We suspect that increasing spin time to speed the drying of the films allows for homogenous films at a higher acceptor concentration. In this manner, we were able to increase the donor/acceptor mass ratio above 1:0.55.

Table 4.1: *J-V* Characteristics for $(3BS)_2$-SiPc containing bulk hetero junction organic photovoltaic devices

Donor	Acceptor	PCE[a] (%)	V_{OC}[1](V)	J_{SC}[1](mA/cm^2)	*FF*[1]
P3HT	$PC_{61}BM$	3.00 ± 0.06	0.53 ± 0.01	9.4 ± 0.4	0.61 ± 0.02
P3HT	$(3BS)_2$-SiPc	3.6 ± 0.2	0.76 ± 0.01	9.0 ± 0.3	0.53 ± 0.02
PBDB-T	$PC_{61}BM$	6.4 ± 0.2	0.78 ± 0.01	12.1 ± 0.4	0.68 ± 0.01
PBDB-T	$(3BS)_2$-SiPc	3.43 ± 0.09	1.09 ± 0.01	7.0 ± 0.3	0.45 ± 0.02

[a] open circuit voltage (V_{OC}), power conversion efficiency (PCE), short circuit current (J_{SC}), and fill factor (*FF*) obtained under 1000 W/m^2 AM1.5G; average and standard deviation for at least 8 devices is given. Ambient test temperature of 23°C.

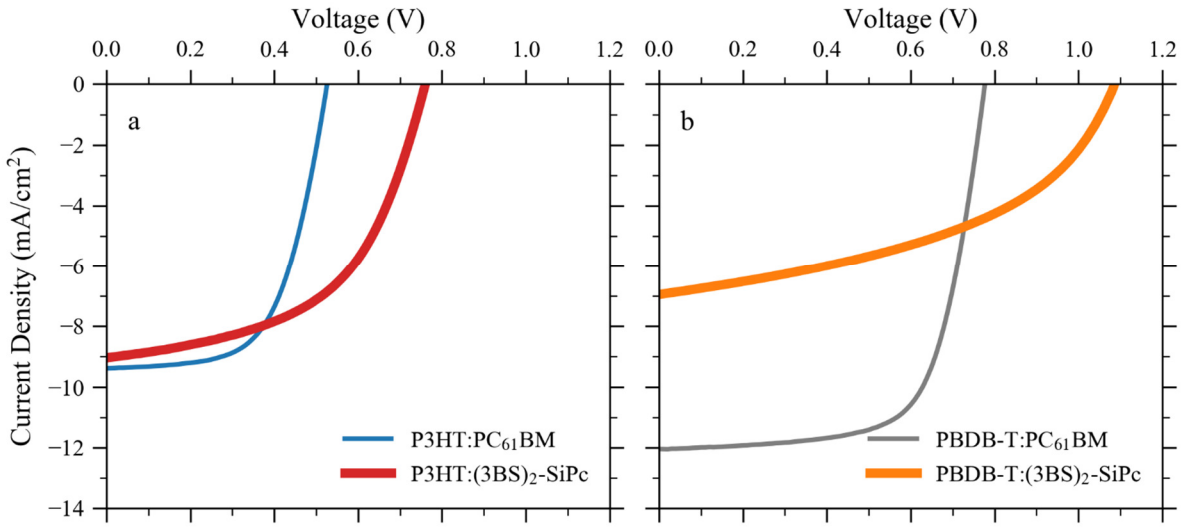

Figure 4.2: *J-V* curves for the (a) P3HT:$PC_{61}BM$ and P3HT:$(3BS)_2$-SiPc, and (b) PBDB-T:$PC_{61}BM$ and PBDB-T:$(3BS)_2$-SiPc devices, under 1000 W/m^2 AM1.5G.

The favorable energetics between $(3BS)_2$-SiPc and P3HT partially explain the increase in performance compared to P3HT/$PC_{61}BM$ devices. The shallower LUMO energy level of $(3BS)_2$-SiPc compared to $PC_{61}BM$ provides a larger energy gap between the acceptor LUMO and donor HOMO leading to an increased V_{OC}. This compensates for the slightly lower *FF* and $J_{SC,}$ likely due in part to the lower electron mobility of $(3BS)_2$-SiPc compared to $PC_{61}BM$.[33]

For PBDB-T/$(3BS)_2$-SiPc devices, peak performance was also found at a donor/acceptor ratio of 1:1, achieving an average PCE of 3.43 %, V_{OC} of 1.09 V, J_{SC} of 7.0 mA/cm^2, and *FF* of 0.45. The addition of the solvent additive diiodooctane (DIO) resulted in the formation of large SiPc domains that produced non-functioning devices (**Figure S4.2**). The V_{OC} of champion PBDB-T/$(3BS)_2$-SiPc devices reached 1.10 V, amongst the highest values achieved for devices using any derivative of PBDB-T.[34] The V_{OC} of 1.10 V equates to a voltage loss (E_g/q - V_{OC}) of approximately 0.7 V. The efficiency of these devices is limited by a low J_{SC} and *FF*, likely arising from inefficient charge extraction from the device. The HOMO/LUMO energy levels of PBDB-T and $(3BS)_2$-SiPc were measured to be -5.33/-3.54 eV and -5.29/-3.54 eV, respectively. HOMO levels were obtained from cyclic voltammetry (**Figure S4.4**) and LUMO levels from the solid-state optical band gap of the materials. Interestingly the moderate PCE of 3.4 % for PBDB-T/$(3BS)_2$-SiPc devices is achieved despite a negligible energetic driving force for charge dissociation. Photoluminescence

(PL) was measured on PBDB-T/$(3BS)_2$-SiPc blended films relative to neat $(3BS)_2$-SiPc films to investigate the effect of the extremely similar energy levels on charge transfer. The PL quenching efficiency of the PBDB-T/$(3BS)_2$-SiPc blended film was found to be approximately 65 % (**Figure S4.5**). While the quenching efficiency is low, sufficient exciton dissociation is inspired despite the lack of an energetic offset between PBDB-T and $(3BS)_2$-SiPc. The concept of a minimum 0.3 eV energetic driving force for charge dissociation in OPV devices has been shown to be unfounded, with a number polymer/NFA pairs with < 0.3 eV offset between their respective HOMO or LUMO energy levels yielding high efficiency devices in the literature.[13,35,36] Furthermore, polymer/NFA pairs having virtually identical HOMO and LUMO energy levels have also yielded OPV devices with moderate efficiency.[37] It stands that charge dissociation at the donor/acceptor interface is not limited by HOMO/LUMO energetic offset, and that entropic gain is sufficient to inspire exciton dissociation.[38,39] The kinetics and mechanisms for the charge transfer in PBDB-T/SiPc devices remains to be further investigated in more detail.

Atomic force microscopy (AFM) was used to characterize the active layer films for both P3HT and PBDB-T devices. The AFM height images are shown in **Figure 4.3**. The BHJ films of P3HT/$PC_{61}BM$ and P3HT/$(3BS)_2$-SiPc had similar surface features with root-mean-square (RMS) roughness of 23.2 nm and 26.0 nm, respectively, consistent with the relatively similar *FF* and J_{SC} values of the devices. The BHJ films of PBDB-T/$PC_{61}BM$ showed low an RMS roughness of 1.8 nm and small domain features. In contrast the PBDB-T/$(3BS)_2$-SiPc films showed much rougher surfaces, with an RMS roughness of 25.0 nm and large island features across the film. This morphological difference can partially explain the significantly lower *FF* and J_{SC} of PBDB-T/$(3BS)_2$-SiPc devices.

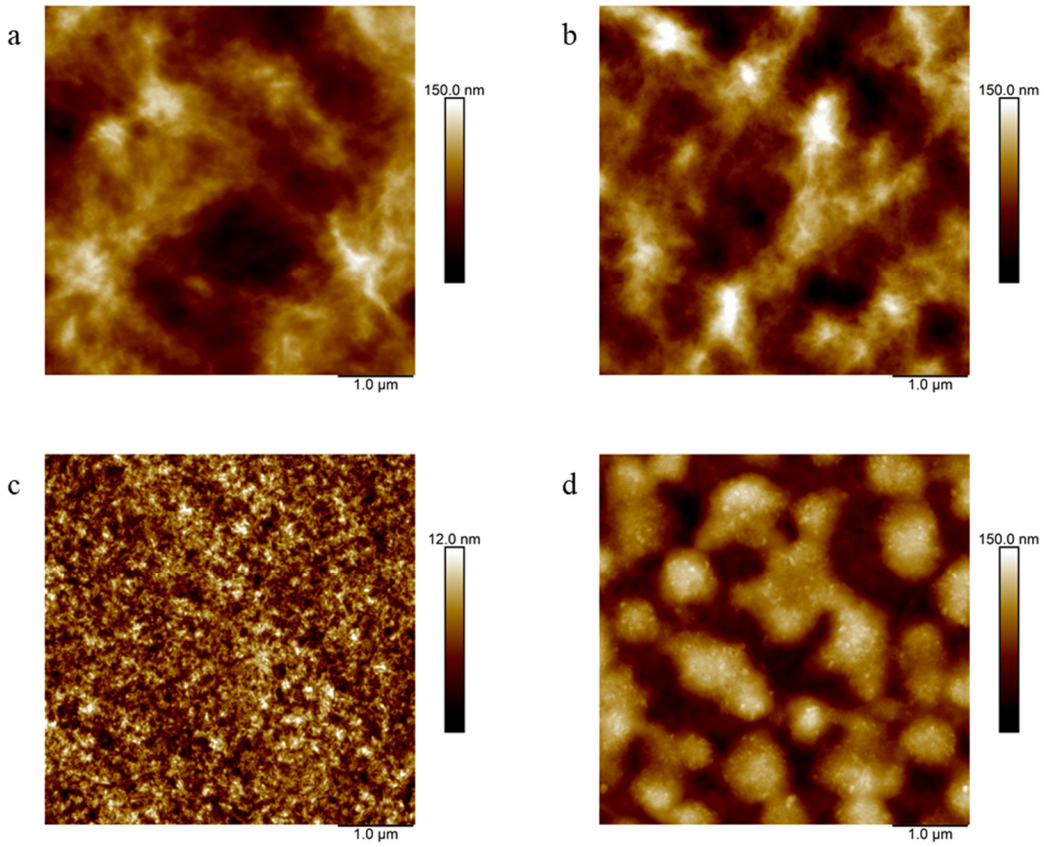

Figure 4.3. AFM height images of photoactive layers for (a) P3HT:$PC_{61}BM$, (b) P3HT:$(3BS)_2$-SiPc, (c) PBDB-T:$PC_{61}BM$, and (d) PBDB-T:$(3BS)_2$-SiPc devices

External quantum efficiency (EQE) of the BHJ devices was measured to assess the relative contribution of $(3BS)_2$-SiPc absorption to photocurrent generation. Ellipsometry measurements were also carried out on active layer films cast onto glass substrates under the same processing conditions as the devices (**Figure S4.3**). **Figure 4.4** shows both the EQE spectra and the film absorption coefficient calculated from *k* values modeled from ellipsometry. The peak in absorption coefficient in the 650-750 nm range typical of Pcs is seen in the $(3BS)_2$-SiPc devices paired with both P3HT and PBDB-T. In P3HT/$(3BS)_2$-SiPc devices, the SiPc absorption extends the absorption range of the device by approximately 70 nm, reaching a maximum EQE of 60 % at 680 nm. This is a 20 % improvement from previously reported devices.[24] In PBDB-T/$(3BS)_2$-SiPc devices the additional EQE contribution from the SiPc chromophore is less significant due to the similar band gaps of the materials, but is still observed as a shoulder at 700 nm.

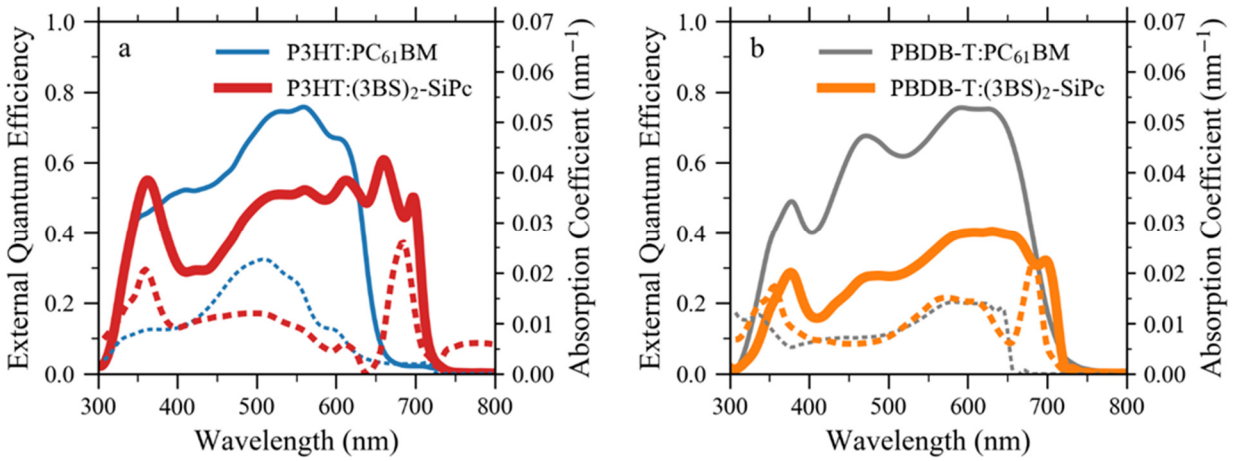

Figure 4.4: Absorption coefficient (dashed) and EQE (solid) of the (a) P3HT:$PC_{61}BM$ and P3HT:$(3BS)_2$-SiPc, and (b) PBDB-T:$PC_{61}BM$ and PBDB-T:$(3BS)_2$-SiPc blends and devices.

This further confirms that $(3BS)_2$-SiPc participates in charge transfer with PBDB-T despite the similar energetics of the two materials. The EQE reaches a maximum of 40 %, significantly lower than the 75 % achieved by the PBDB-T/$PC_{61}BM$ devices. This compromise between J_{SC} and V_{OC} is common in the literature of OPV devices with a $V_{OC} \geq 1.1$ V, which often exhibit a maximum EQE below 50 %,[40–44] and up to a maximum of approximately 60 % in top performing devices.[13,35,36,45–51]

To gain more insight into the recombination effects, we investigated the devices under the AM1.5G spectrum at 1000 W/m^2 down to a reduced intensity of 5 W/m^2. The intensity dependence of J_{SC}, V_{OC}, *FF*, and PCE are shown in **Figure 4.5.** Devices showed a linear dependence of J_{SC} as a function of intensity, which can be described by the power law $J_{SC} \propto I^{\alpha}$. For all devices, $\alpha \cong 1$, a value typical for OPV devices. A logarithmic dependence of V_{OC} as a function of intensity is most often observed for OPV devices, described by the relationship $V_{OC} \propto kT/q \ln(I)$, where k is the Boltzmann constant, T is the absolute temperature, and q is the elementary charge.[52] Systems where bimolecular recombination dominates will have a slope approximately equal to kT/q, while systems with trap-assisted recombination will have a slope > kT/q.[53] All devices show a logarithmic dependence of V_{OC} as a function of intensity. For PBDB-T devices with $PC_{61}BM$ and $(3BS)_2$-SiPc, slopes of 1.06 kT/q and 1.05 kT/q are observed, respectively, suggesting that bimolecular recombination is the dominant mechanism for these devices. Moderately higher slopes of 1.13 kT/q and 1.46 kT/q were observed for P3HT/$PC_{61}BM$ and P3HT/$(3BS)_2$-SiPc

devices, respectively, suggesting trap-assisted recombination is present under open circuit conditions.

A trend for *FF* as a function of intensity is less consistent in literature and can vary for different donor/acceptor systems. For $PC_{61}BM$ devices with both P3HT and PBDB-T, the *FF* initially increases with increasing intensity to approximately 100 W/m^2, after which it begins to decline. Interestingly for $(3BS)_2$-SiPc containing devices the *FF* has a maximum at 5 W/m^2 and decreases thereafter, resulting in higher relative efficiencies under low light compared to devices using $PC_{61}BM$. **Figure 4.6** shows the shunt resistance (R_{sh}) for each of the devices under 1000 and 5 W/m^2 illumination intensities.

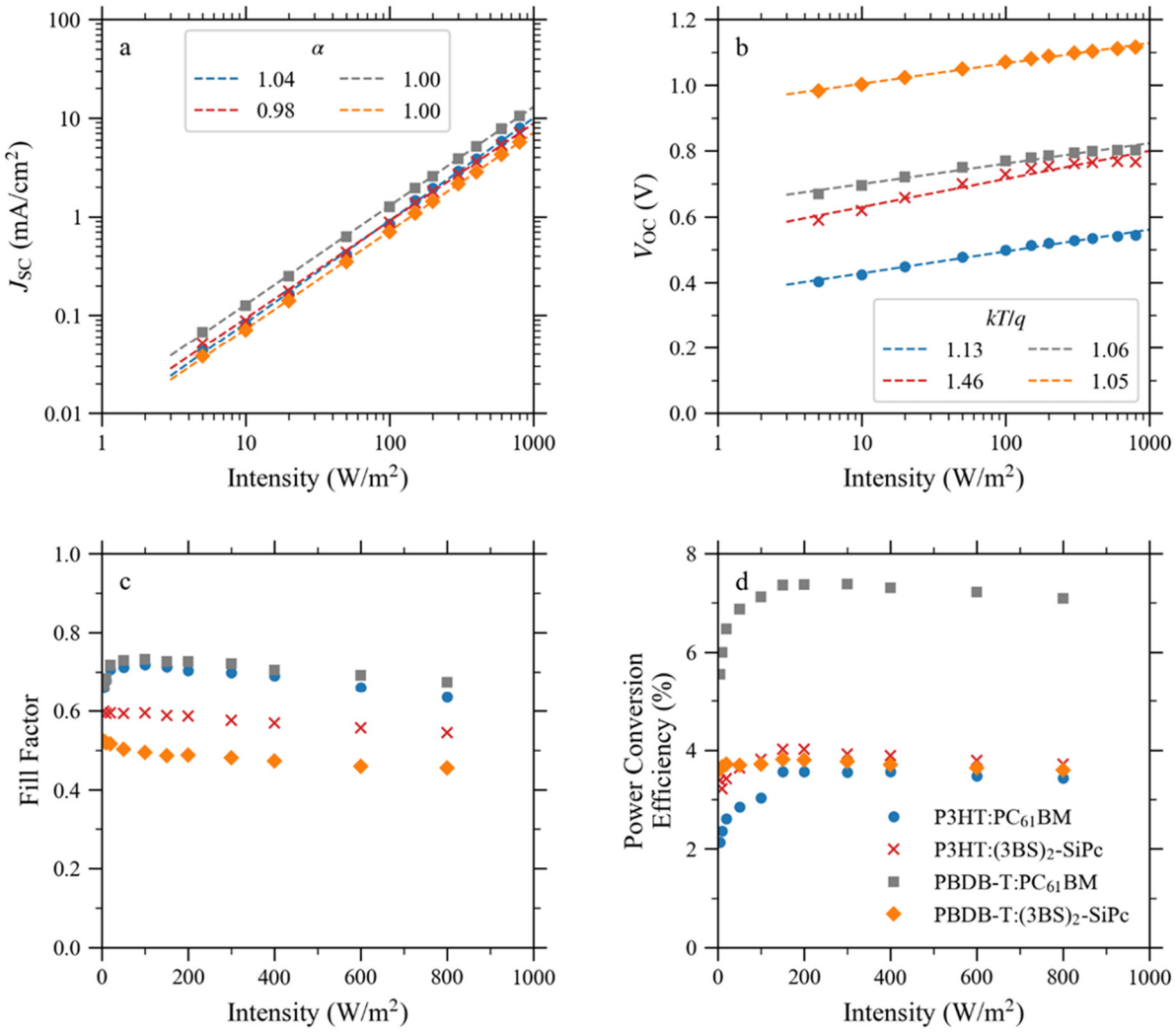

Figure 4.5. Variation of (a) short current density, (b) open circuit voltage, (c) fill factor, and (d) power conversion efficiency as a function of light intensity of devices under AM1.5G spectra at 23 °C. The legend in (d) applies for all figures.

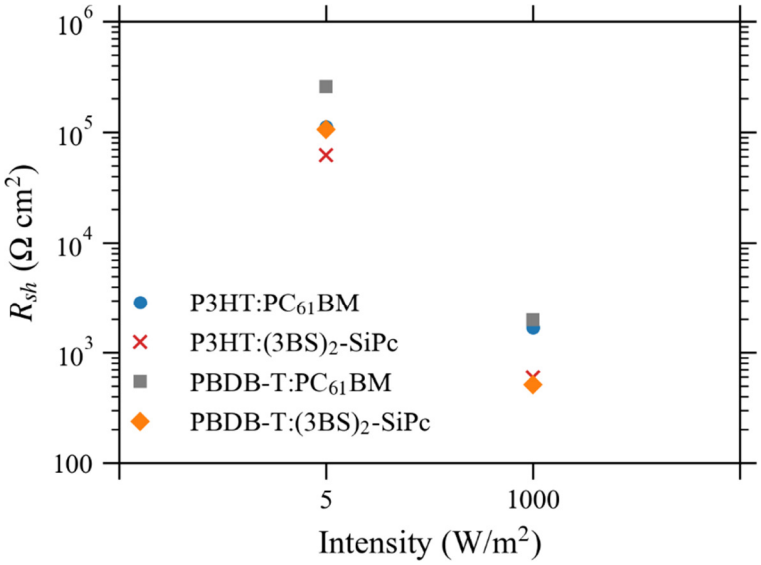

Figure 4.6. Shunt Resistance of devices tested at 5 and 1000 W/m^2

R_{sh} was estimated from the inverse slope of the illuminated *J-V* curve at short-circuit conditions. The relative change in *FF* can be partially attributed to the change in R_{sh} at decreased intensities. In general, under reduced illumination conditions, R_{sh} becomes more significant than series resistance (R_s), while at 1000 W/m^2 illumination, R_s has a greater impact than R_{sh} on the *FF*.[54] At 5 W/m^2 illumination, the R_{sh}, calculated as 6 x 10^4 Ω cm^2 for P3HT/(3BS)$_2$-SiPc devices and 1 x 10^5 Ω cm^2 for PBDB-T/(3BS)$_2$-SiPc devices, suppresses leakage current and provides *FF* values of 0.66 and 0.52, respectively. In contrast, at 1000 W/m^2 illumination, (3BS)$_2$-SiPc devices with both P3HT and PBDB-T suffer from low R_{sh} around 5 x 10^2 Ω cm^2, resulting in reduced *FF* values of 0.53 and 0.45, respectively. It is possible that the reduced number of charge carriers under lower light intensities decreases recombination effects in these devices to improve R_{sh} and *FF*. These results suggest that SiPc based NFAs may perform better under reduced illumination compared to PC$_{61}$BM.

The PCE at several incident angles was measured for further comparison. **Figure 4.7**shows that the PCE increases with incident angle for all devices. The PCE dependence on incident angle has been discussed in the literature to be thickness dependant, with device thicknesses in the range of 150 nm demonstrating a peak efficiency at higher angles of incidence.[55] This relative trend was observed, with the PCE of PBDB-T devices (80 nm thickness) reaching a peak efficiency at 50° incidence angle, and P3HT devices (150 nm thickness) reaching a maximum efficiency at 80°. Previous reports in literature have observed a decrease in absorption past 60° due to significant reflection losses at the air/glass interface above this incidence angle.[55,56] This drop in PCE was observed for PBDB-T based devices but was surprisingly missing from the P3HT based devices. Regardless, in both cases the reduction in PCE with increasing angle was more significant for $PC_{61}BM$ based devices compared to $(3BS)_2$-SiPc based devices. These results further suggest that SiPc based NFAs show promise under diffuse light conditions compared to $PC_{61}BM$.

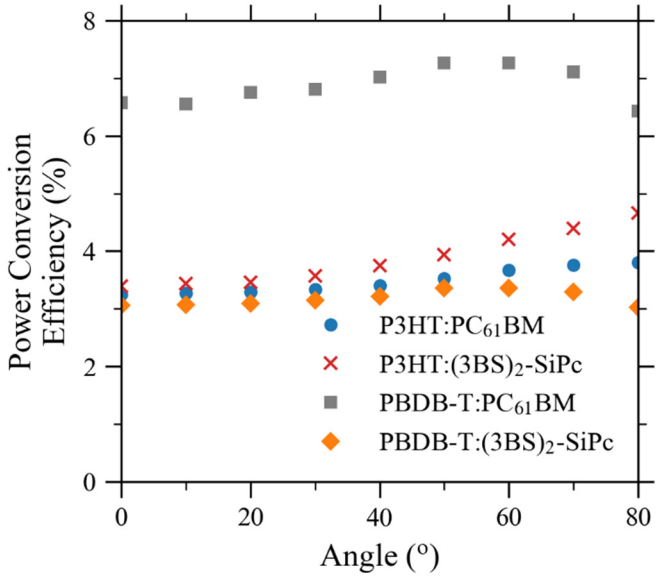

Figure 4.7. Device PCE as a function of AM1.5G spectra incident angle.

To understand diffuse light performance further, we performed angular EQE measurements on the devices, shown in **Figure 4.8**. In agreement with literature, the results from 0-40° incident angle demonstrated blue-shifted EQE peaks with increasing angle, which stems from an increased optical path length in the device leading to an increased modified thin-film interference pattern.[56] This shift was verified through an absorbance model of the devices, where the absorbance in the active layer was simulated over a range of incident angles (**Figure S4.7**). Simulated shifts in the EQE are similar when using $PC_{61}BM$ or $(3BS)_2$-SiPc as the acceptor. With both polymers, the shoulder from SiPc absorption remains unchanged with increasing angle.

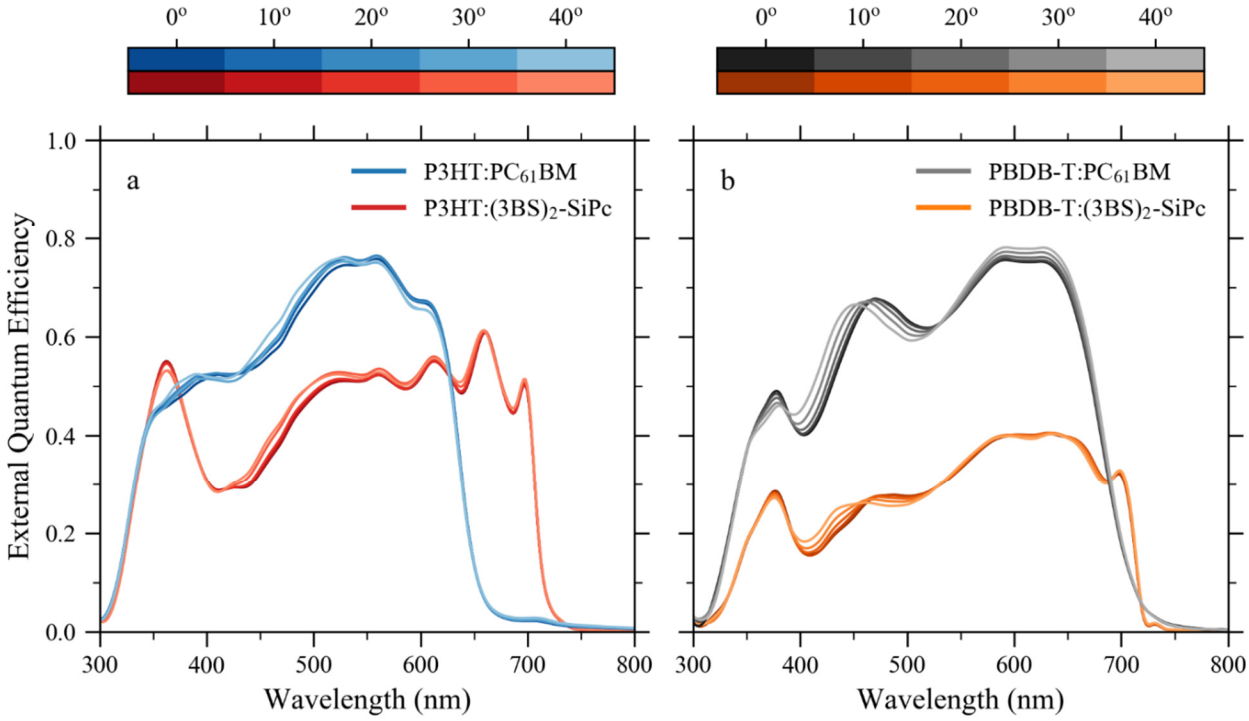

Figure 4.8. EQE measured at various angles for (a) P3HT:$PC_{61}BM$ and P3HT:$(3BS)_2$-SiPc, and (b) PBDB-T:$PC_{61}BM$ and PBDB-T:$(3BS)_2$-SiPc devices.

4.6. Experimental

Materials

P3HT was purchased from Rieke, PBDB-T was purchased from Brilliant Matters, and $PC_{61}BM$ was purchased from Nano-C. $(3BS)_2$-SiPc was prepared according to the literature[57] and purified by vacuum distillation prior to use in devices.

Organic Photovoltaic Devices

Inverted bulk heterojunction OPV devices were fabricated with the structure glass/ITO/ZnO/active layer/MoO_x/Ag. Prepatterned ITO coated slides were cleaned successively in a bath sonicator for 5 minutes with washes of soap-water, water, acetone, then methanol, before being exposed to air plasma for 15 minutes. A ZnO precursor solution was prepared mixing zinc acetate dihydrate (0.1956 g) ethanol (6 mL), and ethanolamine (0.054 mL), stirred at 50 °C for 1 h then stored at room temperature prior to use. The ZnO solution was spin cast at 2000 rpm for 1 minute on the plasma treated substrates for a thickness of 30 nm and baked at 180 °C for 1 h before the slides were moved into a nitrogen glove box for the remainder of fabrication.

Active layer solutions were prepared in 1,2-dichlorobenzene with a donor/acceptor mass ratio of 1:1 for all devices. For P3HT devices, solutions were prepared with a polymer concentration of 20 mg/mL, and stirred at 50 °C for 4 h before spin coating. P3HT/$PC_{61}BM$ devices were spun at 1200 rpm for 35s, while P3HT/$(3BS)_2$-SiPc devices were spun at 1500 rpm for 90 s to give a consistent thickness of approximately 150 nm. For PBDB-T devices, solutions were prepared with a polymer concentration of 10 mg/mL, stirred at 35 °C for 4 h before spin coating. 3 vol % 1,8-diiodooctane (DIO) was added to PBDB-T/$PC_{61}BM$ solutions 1 h before spin coating. All PBDB-T devices were spun at 1000 rpm for 60 s to achieve a thickness of approximately 80 nm. MoO_x (7 nm) and silver (70 nm) were deposited under high vacuum (< 2 x 10^{-6} torr) with a device area of 0.325 cm^2 as defined by a shadow mask. 1 sun measurements were conducted inside a glove box, then devices were encapsulated using a glass slide and optical adhesive (Norland NOA61) before testing outside of the glove box for EQE, reduced intensity, and angle variance measurements.

Current-Voltage and External Quantum Efficiency

Current density-voltage (*J-V*) characteristics were measured with two different solar simulators. Measurements under an intensity of 1000 W/m^2, corresponding to standard 1-sun illumination, were done under a nitrogen atmosphere with an Abet Technologies Sunlite 11002 solar simulator. Variable intensity and incident angle testing was performed using a Newport Oriel Sol3A-CPV solar simulator equipped with an AM1.5G filter. A continuously-variable aperture provided access to intensities from 100-1000 W/m^2, while an OD1.0 filter was used for lower intensities. External quantum efficiency (EQE) was measured using a modified Newport Oriel IQE 200 over 300-800 nm. The tilt angles of the *J-V* and EQE measurements were adjusted using custom setups that allowed for 0-80° and 0-40° rotations, respectively. Cosine losses were accounted for in *J-V* measurements at non-zero incident angles, but not required for the EQE measurements due to the small size of the beam.

Optical Parameters

The refractive index (*n*) and extinction coefficient (*k*) of the BHJ blends were determined using a Horiba UVISEL spectroscopic phase modulated ellipsometer with DeltaPsi2 software. Measurements were taken from 300-900 nm in 10 nm increments on each material at an angle of 70°. The organic films were deposited on soda-lime glass slides via spin coating with identical processing as the OPV devices. The thicknesses of the films were determined optically over 800-900 nm using the Cauchy Absorbent model and verified with a DektakXT profilometer. Optical data was fit for each organic compound using the New Amorphous Dispersion Formula for all materials except P3HT, PBDB-T, and $(3BS)_2$-SiPc, for which point-by-point extraction of optical parameters was done.

Device Modelling

BHJ devices were modelled as an optical stack of materials in Solcore, an open source modeling software for photovoltaics in Python.[58] Each stack (*Optistack* object) was constructed by creating uniform layers of materials (*Layer* objects), using the same architecture as the fabricated devices. Optical parameters for the simulation were determined experimentally for all materials except for MoO_3 and Ag, for which values were taken from literature.[59,60] The reflection, absorbance, and transmission through the optical stack was calculated using the *calculate_rat* method in the *transfer_matrix* module, which is based on the transfer matrix method (TMM) with the "tmm" software package.[61]

4.7. Conclusion

In this study we investigated the use of the phthalocyanine derivative $(3BS)_2$-SiPc as a NFA in BHJ OPV devices. Inverted devices fabricated with P3HT as the donor polymer achieved a PCE of 3.6 %, which is >300 % increase from the previously reports and currently the greatest reported PCE for SiPc-based NFA devices. Devices with PBDB-T as the donor polymer exhibited a PCE of 3.4 % and V_{OC} up to 1.10 V, which is among the highest achieved for PBDB-T based devices. Under reduced light, both P3HT/$(3BS)_2$-SiPc and PBDB-T/$(3BS)_2$-SiPc devices showed an improved *FF* as a result of reduced recombination, indicating these systems could be effective for diffuse light/indoor lighting applications. The relatively high V_{OC} arose from the inherent energetics of SiPc, suggesting that further functional group optimization could provide an improved J_{SC} and *FF* while maintaining a high V_{OC}. It is important to emphasize that the $(3BS)_2$-SiPc used in this study can be obtained through a straightforward 2 step synthesis and purified using sublimation techniques in contrast to many top performing NFA materials in the current literature. These results show the application of inexpensive dye-based materials such as SiPc demonstrate potential for low cost and scalable NFA materials.

4.8. References

(1) Brabec, C. J. Organic Photovoltaics: Technology and Market. *Sol. Energy Mater. Sol. Cells* **2004**, *83*, 273–292.

(2) Liu, Q.; Jiang, Y.; Jin, K.; Qin, J.; Xu, J.; Li, W.; Xiong, J.; Liu, J.; Xiao, Z.; Sun, K.; Yang, S.; Zhang, X.; Ding, L. 18% Efficiency Organic Solar Cells. *Sci. Bull.* **2020**, *65* (4), 272–275.

(3) Cui, Y.; Yao, H.; Zhang, J.; Zhang, T.; Wang, Y.; Hong, L.; Xian, K.; Xu, B.; Zhang, S.; Peng, J.; Wei, Z.; Gao, F.; Hou, J. Over 16% Efficiency Organic Photovoltaic Cells Enabled by a Chlorinated Acceptor with Increased Open-Circuit Voltages. *Nat. Commun.* **2019**, *10* (1), 2515.

(4) Lin, Y.; Adilbekova, B.; Firdaus, Y.; Yengel, E.; Faber, H.; Sajjad, M.; Zheng, X.; Yarali, E.; Seitkhan, A.; Bakr, O. M.; El-Labban, A.; Schwingenschlögl, U.; Tung, V.; McCulloch, I.; Laquai, F.; Anthopoulos, T. D. 17% Efficient Organic Solar Cells Based on Liquid Exfoliated WS2 as a Replacement for PEDOT:PSS. *Adv. Mater.* **2019**, *31*, 1902965.

(5) Lin, Y.; Firdaus, Y.; Nugraha, M. I.; Liu, F.; Karuthedath, S.; Emwas, A. H.; Zhang, W.; Seitkhan, A.; Neophytou, M.; Faber, H.; Yengel, E.; McCulloch, I.; Tsetseris, L.; Laquai, F.; Anthopoulos, T. D. 17.1% Efficient Single-Junction Organic Solar Cells Enabled by n-Type Doping of the Bulk-Heterojunction. *Adv. Sci.* **2020**, 1903419.

(6) Dou, L.; Liu, Y.; Hong, Z.; Li, G.; Yang, Y. Low-Bandgap Near-IR Conjugated Polymers/Molecules for Organic Electronics. *Chem. Rev.* **2015**, *115* (23), 12633–12665.

(7) Liu, C.; Wang, K.; Gong, X.; Heeger, A. J. Low Bandgap Semiconducting Polymers for Polymeric Photovoltaics. *Chemical Society Reviews*. **2016**, *45*, 4825–4846.

(8) Yan, C.; Barlow, S.; Wang, Z.; Yan, H.; Jen, A. K. Y.; Marder, S. R.; Zhan, X. Non-Fullerene Acceptors for Organic Solar Cells. *Nat. Rev. Mater.* **2018**, *3*, 18003.

(9) Hou, J.; Inganas, O.; Friend, R. H.; Gao, F. Organic Solar Cells Based on Non-Fullerene Acceptors. *Nat. Mater.* **2018**, *17* (2), 119–128.

(10) Wadsworth, A.; Moser, M.; Marks, A.; Little, M. S.; Gasparini, N.; Brabec, C. J.; Baran, D.; McCulloch, I. Critical Review of the Molecular Design Progress in Non-Fullerene Electron Acceptors towards Commercially Viable Organic Solar Cells. *Chem. Soc. Rev.* **2019**, *48* (6), 1596–1625.

(11) Wang, J.; Zhan, X. Rylene Diimide Electron Acceptors for Organic Solar Cells. *Trends Chem.* **2019**, *1* (9), 869–881.

(12) Duan, Y.; Xu, X.; Yan, H.; Wu, W.; Li, Z.; Peng, Q. Pronounced Effects of a Triazine Core on Photovoltaic Performance–Efficient Organic Solar Cells Enabled by a PDI Trimer-Based Small Molecular Acceptor. *Adv. Mater.* **2017**, *29* (7), 1605115.

(13) Liu, J.; Chen, S.; Qian, D.; Gautam, B.; Yang, G.; Zhao, J.; Bergqvist, J.; Zhang, F.; Ma, W.; Ade, H.; Inganäs, O.; Gundogdu, K.; Gao, F.; Yan, H. Fast Charge Separation in a Non-Fullerene Organic Solar Cell with a Small Driving Force. *Nat. Energy* **2016**, *1*, 16089.

(14) Brebels, J.; Klider, K. C. C. W. S.; Kelchtermans, M.; Verstappen, P.; Van Landeghem, M.; Van Doorslaer, S.; Goovaerts, E.; Garcia, J. R.; Manca, J.; Lutsen, L.; Vanderzande, D.; Maes, W. Low Bandgap Polymers Based on Bay-Annulated Indigo for Organic Photovoltaics: Enhanced Sustainability in Material Design and Solar Cell Fabrication. *Org. Electron.* **2017**, *50*, 264–272.

(15) Li, L.; Kang, S.; Harden, J.; Sun, Q.; Zhou, X.; Dai, L.; Jakli, A.; Kumar, S.; Li, Q. Nature-inspired Light-harvesting Liquid Crystalline Porphyrins for Organic Photovoltaics. *Liq. Cryst.* **2008**, *35* (3), 233–239.

(16) Yin, H.; Chen, S.; Cheung, S. H.; Li, H. W.; Xie, Y.; Tsang, S. W.; Zhu, X.; So, S. K. Porphyrin-Based Thick-Film Bulk-Heterojunction Solar Cells for Indoor Light Harvesting. *J. Mater. Chem. C* **2018**, *6* (34), 9111–9118.

(17) De La Torre, G.; Claessens, C. G.; Torres, T. Phthalocyanines: Old Dyes, New Materials. Putting Color in Nanotechnology. *Chem. Commun.* **2007**, No. 20, 2000–2015.

(18) Sasa, N.; Okada, K.; Nakamura, K.; Okada, S. Synthesis, Structural and Conformational Analysis and Chemical Properties of Phthalocyaninatometal Complexes. *J. Mol. Struct.* **1998**, *446*, 163–178.

(19) Lessard, H.; White, R. T.; Al-amar, M.; Plint, T.; Castrucci, S.; Josey, D. S.; Lu, Z.; Bender, T. P.; Lessard, B. H.; White, R. T.; Al-amar, M.; Plint, T.; Castrucci, S.; Josey, D. S.; Lu, Z.; Bender, T. P. Assessing the Potential Roles of Silicon and Germanium Phthalocyanines in Planar Heterojunction Organic Photovoltaic Devices and How Pentafluoro Phenoxylation Can Enhance $\pi - \pi$ Interactions and Device Performance. *ACS Appl. Mater. Interfaces* **2015**, *7*, 5076–5068.

(20) Barker, C. a.; Findlay, K. S.; Bettington, S.; Batsanov, A. S.; Perepichka, I. F.; Bryce, M. R.; Beeby, A. Synthesis of New Axially-Disubstituted Silicon-Phthalocyanine Derivatives: Optical and Structural Characterisation. *Tetrahedron* **2006**, *62* (40), 9433–9439.

(21) Zysman-colman, E.; Ghosh, S. S.; Xie, G.; Varghese, S.; Chowdhury, M.; Sharma, N.; Cordes, D. B.; Slawin, A. M. Z.; Samuel, I. D. W. Solution-Processable Silicon Phthalocyanines in Electroluminescent and Photovoltaic Devices. *Appl. Mater. Interfaces* **2016**, *8*, 9247–9253.

(22) Melville, O. A.; Grant, T. M.; Lessard, B. H. Silicon Phthalocyanines as N-Type Semiconductors in Organic Thin Film Transistors. *J. Mater. Chem. C* **2018**, *6* (20), 5482–5488.

(23) Ke, L.; Min, J.; Adam, M.; Gasparini, N.; Hou, Y.; Perea, J. D.; Chen, W.; Zhang, H.; Fladischer, S.; Sale, A.; Spiecker, E.; Tykwinski, R. R.; Brabec, C. J.; Ameri, T. A Series of Pyrene-Substituted Silicon Phthalocyanines as Near-IR Sensitizers in Organic Ternary Solar Cells. *Adv. Energy Mater.* **2016**, *6*, 1502355.

(24) Dang, M. T.; Grant, T. M.; Yan, H.; Seferos, D. S.; Bender, T. P. Bis(Tri-n-Alkylsilyl Oxide) Silicon Phthalocyanines: A Start to Establishing a Structure Property Relationship as Both Ternary Additives and Non-Fullerene Electron Acceptors in Bulk Heterojunction

Organic Photovoltaic Devices. *J. Mater. Chem. A* **2017**, *5* (24), 12168–12182.

(25) Vebber, M. C.; Grant, T. M.; Brusso, J. L.; Lessard, B. H. Bis(Trialkylsilyl Oxide) Silicon Phthalocyanines: Understanding the Role of Solubility in Device Performance as Ternary Additives in Organic Photovoltaics. *Langmuir* **2020**, *36* (10), 2612–2621.

(26) Honda, S.; Ohkita, H.; Benten, H.; Ito, S. Multi-Colored Dye Sensitization of Polymer/Fullerene Bulk Heterojunction Solar Cells. *Chem. Commun.* **2010**, *46* (35), 6596–6598.

(27) Lim, B.; Bloking, J. T.; Ponec, A.; Mcgehee, M. D.; Sellinger, A. Ternary Bulk Heterojunction Solar Cells: Addition of Soluble NIR Dyes for Photocurrent Generation beyond 800 Nm. *ACS Appl. Mater. Interfaces* **2014**, *6*, 6905–6913.

(28) Ke, L.; Gasparini, N.; Min, J.; Zhang, H.; Adam, M.; Rechberger, S.; Forberich, K.; Zhang, C.; Spiecker, E.; Tykwinski, R. R.; Brabec, C. J.; Ameri, T. Panchromatic Ternary/Quaternary Polymer/Fullerene BHJ Solar Cells Based on Novel Silicon Naphthalocyanine and Silicon Phthalocyanine Dye Sensitizers. *J. Mater. Chem. A* **2017**, *5* (6), 2550–2562.

(29) Honda, S.; Nogami, T.; Ohkita, H.; Benten, H.; Ito, S. Improvement of the Light-Harvesting Efficiency in Polymer/Fullerene Bulk Heterojunction Solar Cells by Interfacial Dye Modification. *ACS Appl. Mater. Interfaces* **2009**, *1* (4), 804–810.

(30) Po, R.; Bernardi, A.; Calabrese, A.; Carbonera, C.; Corso, G.; Pellegrino, A. From Lab to Fab: How Must the Polymer Solar Cell Materials Design Change?-An Industrial Perspective. *Energy Environ. Sci.* **2014**, *7* (3), 925–943.

(31) Dang, M. T.; Hirsch, L.; Wantz, G. P3HT:PCBM, Best Seller in Polymer Photovoltaic Research. *Adv. Mater.* **2011**, *23* (31), 3597–3602.

(32) Qian, D.; Ye, L.; Zhang, M.; Liang, Y.; Li, L.; Huang, Y.; Guo, X.; Zhang, S.; Tan, Z.; Hou, J. Design, Application, and Morphology Study of a New Photovoltaic Polymer with Strong Aggregation in Solution State. *Macromolecules* **2012**, *45* (24), 9611–9617.

(33) Grant, T. M.; Rice, N. A.; Muccioli, L.; Castet, F.; Lessard, B. H. Solution-Processable n-Type Tin Phthalocyanines in Organic Thin Film Transistors and as Ternary Additives in Organic Photovoltaics. *ACS Appl. Electron. Mater.* **2019**, *1* (4), 494–504.

(34) Zheng, Z.; Yao, H.; Ye, L.; Xu, Y.; Zhang, S.; Hou, J. PBDB-T and Its Derivatives: A Family of Polymer Donors Enables over 17% Efficiency in Organic Photovoltaics. *Mater. Today* **2020**, *35*, 115–130.

(35) Baran, D.; Kirchartz, T.; Wheeler, S.; Dimitrov, S.; Abdelsamie, M.; Gorman, J.; Ashraf, R. S.; Holliday, S.; Wadsworth, A.; Gasparini, N.; Kaienburg, P.; Yan, H.; Amassian, A.; Brabec, C. J.; Durrant, J. R.; McCulloch, I. Reduced Voltage Losses Yield 10% Efficient Fullerene Free Organic Solar Cells with >1 V Open Circuit Voltages. *Energy Environ. Sci.* **2016**, *9* (12), 3783–3793.

(36) Zhang, H.; Li, S.; Xu, B.; Yao, H.; Yang, B.; Hou, J. Fullerene-Free Polymer Solar Cell Based on a Polythiophene Derivative with an Unprecedented Energy Loss of Less than 0.5

EV. *J. Mater. Chem. A* **2016**, *4* (46), 18043–18049.

(37) Yi, X.; Peng, Z.; Xu, B.; Seyitliyev, D.; Ho, C. H. Y.; Danilov, E. O.; Kim, T.; Reynolds, J. R.; Amassian, A.; Gundogdu, K.; Ade, H.; So, F. Critical Role of Polymer Aggregation and Miscibility in Nonfullerene-Based Organic Photovoltaics. *Adv. Energy Mater.* **2020**, *10* (8), 1902430.

(38) Hood, S. N.; Kassal, I. Entropy and Disorder Enable Charge Separation in Organic Solar Cells. *J. Phys. Chem. Lett.* **2016**, *7* (22), 4495–4500.

(39) Gluchowski, A.; Gray, K. L. G.; Hood, S. N.; Kassal, I. Increases in the Charge Separation Barrier in Organic Solar Cells Due to Delocalization. *J. Phys. Chem. Lett.* **2018**, *9* (6), 1359–1364.

(40) Li, S.; Liu, W.; Shi, M.; Mai, J.; Lau, T. K.; Wan, J.; Lu, X.; Li, C. Z.; Chen, H. A Spirobifluorene and Diketopyrrolopyrrole Moieties Based Non-Fullerene Acceptor for Efficient and Thermally Stable Polymer Solar Cells with High Open-Circuit Voltage. *Energy Environ. Sci.* **2016**, *9* (2), 604–610.

(41) Gupta, A.; Rananaware, A.; Srinivasa Rao, P.; Duc La, D.; Bilic, A.; Xiang, W.; Li, J.; Evans, R. A.; Bhosale, S. V.; Bhosale, S. V. An H-Shaped, Small Molecular Non-Fullerene Acceptor for Efficient Organic Solar Cells with an Impressive Open-Circuit Voltage of 1.17 V. *Mater. Chem. Front.* **2017**, *1* (8), 1600–1606.

(42) Wang, Y.; Kan, B.; Ke, X.; Liu, F.; Wan, X.; Zhang, H.; Li, C.; Chen, Y. Two Thieno[3,2-b]Thiophene-Based Small Molecules as Bifunctional Photoactive Materials for Organic Solar Cells. *Sol. RRL* **2018**, *2* (2), 1700179.

(43) Xiao, B.; Tang, A.; Yang, J.; Wei, Z.; Zhou, E. P3HT-Based Photovoltaic Cells with a High Voc of 1.22 V by Using a Benzotriazole-Containing Nonfullerene Acceptor End-Capped with Thiazolidine-2,4-Dione. *ACS Macro Lett.* **2017**, *6* (4), 410–414.

(44) Liu, X.; Du, X.; Wang, J. J.; Duan, C.; Tang, X.; Heumueller, T.; Liu, G.; Li, Y.; Wang, Z.; Wang, J. J.; Liu, F.; Li, N.; Brabec, C. J.; Huang, F.; Cao, Y. Efficient Organic Solar Cells with Extremely High Open-Circuit Voltages and Low Voltage Losses by Suppressing Nonradiative Recombination Losses. *Adv. Energy Mater.* **2018**, *8* (26), 1801699.

(45) Zhang, Y.; Guo, X.; Guo, B.; Su, W.; Zhang, M.; Li, Y. Nonfullerene Polymer Solar Cells Based on a Perylene Monoimide Acceptor with a High Open-Circuit Voltage of 1.3 V. *Adv. Funct. Mater.* **2017**, *27* (10), 1603892.

(46) Tang, A.; Xiao, B.; Wang, Y.; Gao, F.; Tajima, K.; Bin, H.; Zhang, Z. G.; Li, Y.; Wei, Z.; Zhou, E. Simultaneously Achieved High Open-Circuit Voltage and Efficient Charge Generation by Fine-Tuning Charge-Transfer Driving Force in Nonfullerene Polymer Solar Cells. *Adv. Funct. Mater.* **2018**, *28* (6), 1704507.

(47) Gao, B.; Yao, H.; Hong, L.; Hou, J. Efficient Organic Solar Cells with a High Open-Circuit Voltage of 1.34 V. *Chinese J. Chem.* **2019**, *37* (11), 1153–1157.

(48) Tang, A.; Song, W.; Xiao, B.; Guo, J.; Min, J.; Ge, Z.; Zhang, J.; Wei, Z.; Zhou, E. Benzotriazole-Based Acceptor and Donors, Coupled with Chlorination, Achieve a High

VOC of 1.24 v and an Efficiency of 10.5% in Fullerene-Free Organic Solar Cells. *Chem. Mater.* **2019**, *31* (11), 3941–3947.

(49) Chen, Y.; Zhang, Q.; Du, M.; Li, G.; Li, Z.; Huang, H.; Geng, Y.; Zhang, X.; Zhou, E. Benzotriazole-Based p-Type Polymers with Thieno[3,2- b]Thiophene π-Bridges and Fluorine Substituents To Realize High Voc. *ACS Appl. Polym. Mater.* **2019**, *1* (4), 906–913.

(50) Hendsbee, A. D.; Sun, J. P.; Law, W. K.; Yan, H.; Hill, I. G.; Spasyuk, D. M.; Welch, G. C. Synthesis, Self-Assembly, and Solar Cell Performance of N-Annulated Perylene Diimide Non-Fullerene Acceptors. *Chem. Mater.* **2016**, *28* (19), 7098–7109.

(51) Zhang, J.; Li, Y.; Huang, J.; Hu, H.; Zhang, G.; Ma, T.; Chow, P. C. Y.; Ade, H.; Pan, D.; Yan, H. Ring-Fusion of Perylene Diimide Acceptor Enabling Efficient Nonfullerene Organic Solar Cells with a Small Voltage Loss. *J. Am. Chem. Soc.* **2017**, *139* (45), 16092–16095.

(52) Koster, L. J. A.; Mihailetchi, V. D.; Ramaker, R.; Blom, P. W. M. Light Intensity Dependence of Open-Circuit Voltage of Polymer:Fullerene Solar Cells. *Appl. Phys. Lett.* **2005**, *86* (12), 123509.

(53) Mandoc, M. M.; Kooistra, F. B.; Hummelen, J. C.; De Boer, B.; Blom, P. W. M. Effect of Traps on the Performance of Bulk Heterojunction Organic Solar Cells. *Appl. Phys. Lett.* **2007**, *91* (26), 263505.

(54) Steim, R.; Ameri, T.; Schilinsky, P.; Waldauf, C.; Dennler, G.; Scharber, M.; Brabec, C. J. Organic Photovoltaics for Low Light Applications. *Sol. Energy Mater. Sol. Cells* **2011**, *95* (12), 3256–3261.

(55) Rahman, M. S. S.; Alam, M. K. Effect of Angle of Incidence on the Performance of Bulk Heterojunction Organic Solar Cells: A Unified Optoelectronic Analytical Framework. *AIP Adv.* **2017**, *7* (6), 65101.

(56) Dennler, G.; Forberich, K.; Scharber, M. C.; Brabec, C. J.; Tomiš, I.; Hingerl, K.; Fromherz, T. Angle Dependence of External and Internal Quantum Efficiencies in Bulk-Heterojunction Organic Solar Cells. *J. Appl. Phys.* **2007**, *102* (5), 54516.

(57) Gessner, T.; Sens, R.; Ahlers, W.; Vamvakaris, C. Preparation of Silicon Phthalocyanines and Germanium Phthalocyanines and Related Substances. *US 2010/0113767* **2010**.

(58) Alonso-Álvarez, D.; Wilson, T.; Pearce, P.; Führer, M.; Farrell, D.; Ekins-Daukes, N. Solcore: A Multi-Scale, Python-Based Library for Modelling Solar Cells and Semiconductor Materials. *J. Comput. Electron.* **2018**, *17* (3), 1099–1123.

(59) Stelling, C.; Singh, C. R.; Karg, M.; König, T. A. F.; Thelakkat, M.; Retsch, M. Plasmonic Nanomeshes: Their Ambivalent Role as Transparent Electrodes in Organic Solar Cells. *Sci. Rep.* **2017**, *7* (1), 1–13.

(60) Software Spectra Inc. Optical Data from Sopra SA http://www.sspectra.com/sopra.html.

(61) Byrnes, S. J. Multilayer Optical Calculations. *arXiv:1603.02720* **2016**, 1–20.

Chapter 5: SiPc as a Synthetically Facile NFA in P3HT-based Devices

This chapter contains work published in *Materials Advances:*

T. M. Grant, C. Dindault, N.A Rice, S. Swaraj, and B.H. Lessard. *Materials Advances*, 2021

5.1. Context

Through a series of synthetic work in our group exploring the effect of alkyl chain length in the solubility of alkylsiloxy-functionalized SiPc derivatives, we identified bis(tri-n-propylsiloxide) silicon phthalocyanine as a unique material having an interesting combination of high solubility and thermal stability. This is a relatively rare combination, and allows a solution-processable material to be purified by sublimation. As a follow-up addition to our previous work in **Chapter 4** using SiPc as an NFA, I investigated the use the new SiPc variant as an NFA in P3HT devices.

5.2. Contribution of Authors

I performed all the chemical synthesis and characterization of the reported phthalocyanine compounds, as well as the fabrication and characterization of all OPV devices. NAR performed the AFM measurements. SS performed XTSM measurements, which were analyzed and compiled by CD. I solely wrote the first draft of the manuscript and received editing contributions from all other authors.

5.3. Abstract

We demonstrate organic photovoltaic devices with extremely low synthetic complexity by paring poly(3-hexithiophene) (P3HT) with a novel non-fullerene acceptor (NFA) bis(tri-*n*-propylsilyl oxide) silicon phthalocyanine ($(3PS)_2$-SiPc). $(3PS)_2$-SiPc possesses a relatively unique combination of high solubility as well as excellent thermal stability, facilitating its ease of processing by both solution and sublimation techniques. Binary P3HT/$(3PS)_2$-SiPc devices achieved an average power conversion efficiency of 4.3 %, a new record for SiPc NFAs. AFM and synchrotron STXM measurements reveal a unique morphology of P3HT/$(3PS)_2$-SiPc, with significant phase separation due to the strong crystallization of $(3PS)_2$-SiPc.

5.4. Introduction

Rapid progress in solution-processed organic photovoltaic (OPV) devices over the last five years has come largely from the development of novel non-fullerene acceptors (NFAs). In combination with low bandgap polymer donors, record power conversion efficiencies (PCEs) above 18 % have been achieved.[1] However, in the pursuit of maximizing PCE, the scale-up feasibility of many novel NFAs has not been considered in their design leading to increasingly complex molecules. It has become apparent that the synthetic complexity of NFAs and polymer donors must be reduced for the realization of commercial OPV devices.[2] This understanding has prompted increased research interest in the design of less complex NFAs to pair with poly(3-hexithiophene) (P3HT), which continues to be the most scalable and cost effective polymer donor. PCEs as high as 9 % have been achieved in P3HT/NFA devices, however the synthetic complexity of the incorporated NFAs remains prohibitively high.[3,4]

Derivatives of phthalocyanine are appealing materials for synthetically simple active materials in OPV devices given their established scale-up chemistry for use as dyes and pigments and known efficacy in organic electronic devices.[5] Silicon phthalocyanine (SiPc) derivatives prepared from straightforward synthetic routes have been established as effective ternary additives in solution-processed OPV devices,[6–8] and have shown potential for use as NFAs.[9,10] In recent work, we demonstrated that using alkylsiloxy-functionalized SiPc as an NFA with P3HT can yield devices with a promising PCE of 3.6 %, slightly higher than a PCE of 3.4 % achieved when combined with the state-of-the-art polymer poly[(2,6-(4,8-bis(5-(2-ethylhexyl)thiophen-2-yl)-benzo[1,2-b:4,5-b']dithiophene))-alt-(5,5-(1',3'-di-2-thienyl-5',7'-bis(2-ethylhexyl)benzo[1',2'-c:4',5'-c']dithiophene-4,8-dione)] (PBDB-T).[11] The synthetic simplicity of SiPc derivatives compels continuing investigations into its use as an NFA, specifically paired with P3HT to minimize the overall synthetic complexity of the active layer materials. In this work, we show that the SiPc derivative bis(tri-*n*-propylsilyl oxide) silicon phthalocyanine ($(3PS)_2$-SiPc), which possesses a unique combination of excellent solubility and thermal properties, can achieve an impressive PCE of 4.3 % as an NFA in a P3HT-based device.

5.5. Results and Discussion

The chemical synthesis of $(3PS)_2$-SiPc is outlined in the supporting information (Scheme S5.1). The conjugated macrocycle of SiPc is formed in a 1-step reaction of diiminoisoindoline with silicon tetrachloride to form silicon phthalocyanine dichloride. The substitution of tripropylsiloxy ligands can then be performed in a 1-step reaction with tripropylchlorosilane in the presence of sodium hydroxide and a phase transfer catalyst.[12] This straightforward synthetic pathway is in contrast to many high-performance NFAs in the literature, such as Y6 which requires 15 steps to synthesize from commercial reagents.[13]

The chemical structure, energy levels, and optical absorption of $(3PS)_2$-SiPc in relation to P3HT and $PC_{61}BM$ are shown in **Figure 5.1**. A maximum absorption of 672 nm was measured in toluene solution, with a corresponding molar extinction coefficient of 4.2 x 10^5 $M^{-1}cm^{-1}$. HOMO and LUMO energy levels of 5.3 eV and 3.5 eV, respectively, were estimated from cyclic voltammetry measurements (Figure S5.2) and the optical band gap. $(3PS)_2$-SiPc also exhibited a strong tendency to crystalize from solution, easily producing large crystals grown from chloroform solvent evaporation. The observed optoelectrical properties and high crystallinity are typical for SiPc derivatives with alkylsiloxy functional groups.[14]

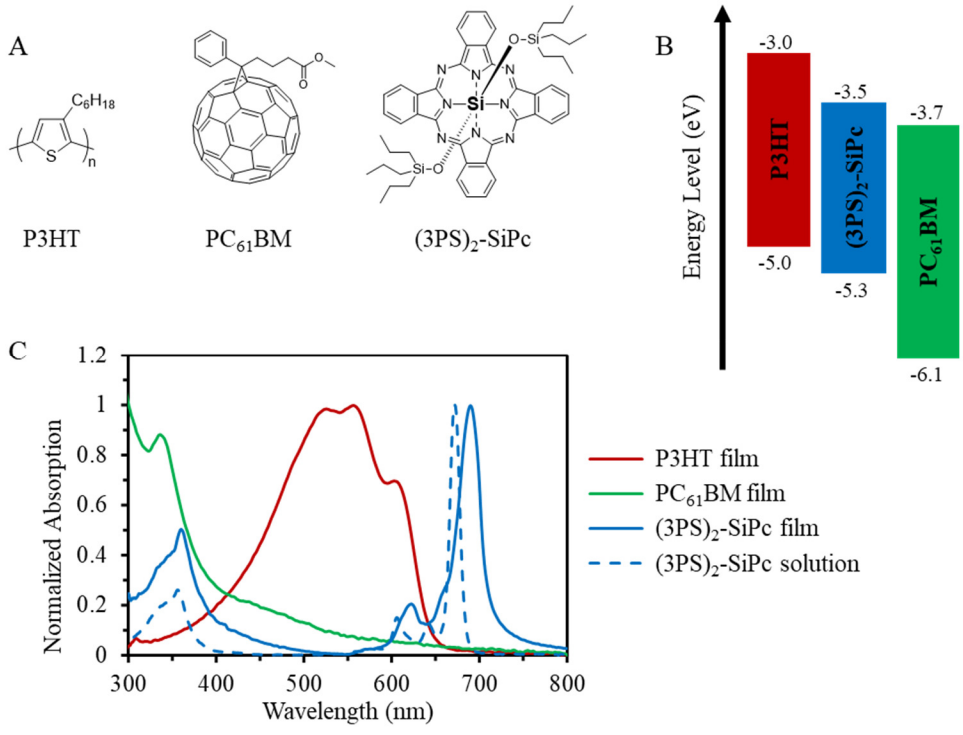

Figure 5.1: (A) Chemical structures, (B) energy levels, and (C) UV-Vis absorption of thin films of P3HT, $PC_{61}BM$ and $(3PS)_2$-SiPc, as well as $(3PS)_2$-SiPc in toluene.

Our group has recently reported the synthesis and characterization of a series of soluble alkylsiloxy-functionalized SiPcs with a range of chain lengths.[15] Naturally, ligands with shorter alkyl chains provide lower solubility to the planar conjugated phthalocyanine macrocycle. In this work, we have found that tri-*n*-propylsilpxy ligands are the shortest chain length that can be incorporated while still providing sufficient solubility (> 15 mg/mL) for effective processing as an NFA from chlorinated solvents. SiPc derivatives functionalized with bulkier triisopropylsiloxy or shorter triethylsiloxy ligands yield maximum concentrations below 10 mg/mL in 1,2-dichlorobenzene, rendering them impractical for use as NFAs.

Interestingly, in addition to strong solubility, $(3PS)_2$-SiPc readily sublimes at 200 °C under 100 mTorr pressure, significantly lower than its decomposition temperature at approximately 340°C measured by thermogravimetric analysis (Figure S5.3). Differential scanning calorimetry measurements also show that $(3PS)_2$-SiPc has no phase transitions between 25 °C and 240 °C, allowing it to directly sublime upon heating (Figure S5.4). This is in contrast to previously reported SiPc derivatives with longer tributylsiloxy or trihexylsiloxy ligands which have a melting transition below their sublimation temperature and therefore undergo distillation instead of sublimation.[10] The ability for a soluble organic compound to sublime is highly advantageous, given sublimation purification is relatively simple to perform on larger kilogram scales. This obviates the need to employ resource intensive solution-based purification techniques such as column chromatography, reducing time and materials costs during synthesis. To highlight the processability of $(3PS)_2$-SiPc, we fabricated planar heterojunction (PHJ) devices processed by physical vapor deposition (PVD) paired with alpha-sexithiophene (α-6T) as a small molecule donor. The PHJ α-6T/$(3PS)_2$-SiPc devices show relatively low performance with an average PCE of 0.73 ± 0.06 %, short circuit current density (J_{SC}) of 2.2 ± 0.1 mA/cm^2, open circuit voltage (V_{OC}) of 0.62 ± 0.01 V, and fill factor (*FF*) of 0.53 ± 0.03 (Figure S5). These device metrics are comparable to previously reported PHJ devices utilizing fluorophenoxy-functionalized SiPcs paired with α-6T.[16] The α-6T/$(3PS)_2$-SiPc devices were not characterized further due to their relatively poor performance, however they readily demonstrate the ability of $(3PS)_2$-SiPc to be processed by sublimation.

The performance of $(3PS)_2$-SiPc as an NFA with P3HT was evaluated in inverted bulk heterojunction (BHJ) OPV devices (glass/ITO/ZnO/active layer/MoO_x/Ag) with an active area of 0.325 cm^2. Current density-voltage (*J-V*) characteristics for optimized devices at 1 sun AM 1.5G are shown in **Figure 5.2A,** and tabulated device metrics in **Table 5.1**. Baseline P3HT/$PC_{61}BM$ devices fabricated for comparison yielded an average PCE of 3.0 ± 0.1 %, consistent with average performance reported in the literature.[17] P3HT/$(3PS)_2$-SiPc devices were optimized to a thickness of approximately 100 nm, with performance found to be dependant on the molecular weight of P3HT. Maximum PCE was achieved using a moderately low P3HT molecular weight of 35 kDa, consistent with results reported for other NFAs in the literature.[18] Interestingly, annealing did not increase the PCE for devices prepared using this low molecular weight P3HT, with maximum efficiency observed for as cast devices. Optimized devices achieved an average PCE of 4.3 ± 0.2 %, with a J_{SC} of 8.9 ± 0.5 mA/cm^2, V_{OC} of 0.79 ± 0.01 V, and *FF* of 0.61 ± 0.01. These values are the highest reported for an OPV device employing a SiPc derivative. The device metrics are similar to the $PC_{61}BM$ baseline devices, except for a greater V_{OC} of approximately 0.8 V due to the more favorable shallow LUMO level of $(3PS)_2$-SiPc (**Figure 5.1 B**). External quantum efficiency (EQE) is shown in **Figure 5.2 B**. P3HT/$(3PS)_2$-SiPc devices show a weaker contribution from P3HT absorption below 600 nm compared to the baseline P3HT/$PC_{61}BM$ devices, however the increased spectral coverage from the strong phthalocyanine contribution between 680 nm and 700 nm affords a comparable J_{SC}.

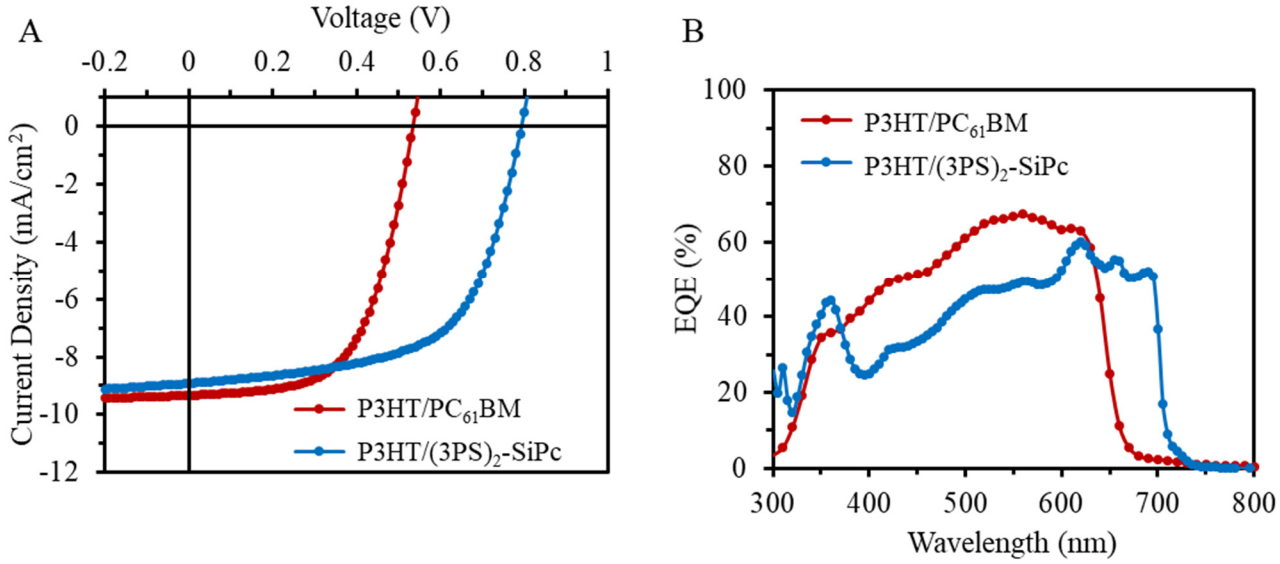

Figure 5.2. (A) Characteristic current density-voltage (*J-V)* curves measured under 1000 W/m^2 AM1.5G irradiation and (B) their respective EQE spectra.

Table 5.1. Current density – voltage characteristics of BHJ OPV devices measured at AM1.5G 1000 W/m^2

Active Layer	PCE [a] [%]	J_{SC} (J-V)[a] [mA/cm^2]	J_{SC} (EQE) [mA/cm^2]	V_{OC} [a] [V]	FF [a]
P3HT/PC$_{61}$BM	3.0 ± 0.1	9.3 ± 0.1	9.7	0.53 ± 0.01	0.60 ± 0.01
P3HT/(3PS)$_2$-SiPc	4.3 ± 0.2	8.9 ± 0.5	9.6	0.79 ± 0.01	0.61 ± 0.01

[a.] Average and standard deviation for at least 10 devices

It is important to note that while SiPc derivatives have conventionally been used as an additive in ternary devices, the average PCE of 4.3% herein reported for binary P3HT/SiPc devices surpasses the PCE achieved in ternary P3HT/PC$_{61}$BM/SiPc devices. For comparison, ternary P3HT/PC$_{61}$BM/(3PS)$_2$-SiPc devices show an average PCE of 3.4 ± 0.1 %, J_{SC} of 10.4 ± 0.2 mA/cm^2, V_{OC} of 0.55 ± 0.02 V, and *FF* of 0.59 ± 0.02 (Figure S6), consistent with similar alkylsiloxy SiPc derivatives.[15] The addition of (3PS)$_2$-SiPc as a ternary additive effectively provides a J_{SC} increase of 12 % compared to P3HT/PC$_{61}$BM devices, while its use as an NFA in place of PC$_{61}$BM results in a V_{OC} increase of approximately 50 % affording a significantly higher PCE. This demonstrates that appropriately designed SiPc derivatives may be more suitable for use as NFAs when paired with P3HT, eliminating the requirement to include PC$_{61}$BM to achieve a competitive PCE and dramatically reducing the combined synthetic complexity active materials.

The morphology of P3HT/(3PS)$_2$-SiPc and P3HT/PC$_{61}$BM films were compared using atomic force microscopy (AFM) shown in **Figure 5.3**. The P3HT/PC$_{61}$BM film was relatively smooth with an RMS roughness of 9.5 nm. The film surface consists of fine-grained features on the nanoscale, indicating a well mixed donor/acceptor network. The P3HT/(3PS)$_2$-SiPc film was significantly rougher with a film surface dominated by larger crystalline features, yielding an RMS roughness of 15.7 nm. These large domains are generally unfavorable for achieving efficient exciton dissociation, with optimal P3HT/NFA systems characterized by domain sizes on the order of 10-20 nm.[3,4] The highly crystalline nature of (3PS)$_2$-SiPc is likely the cause of the relatively large domain sizes.

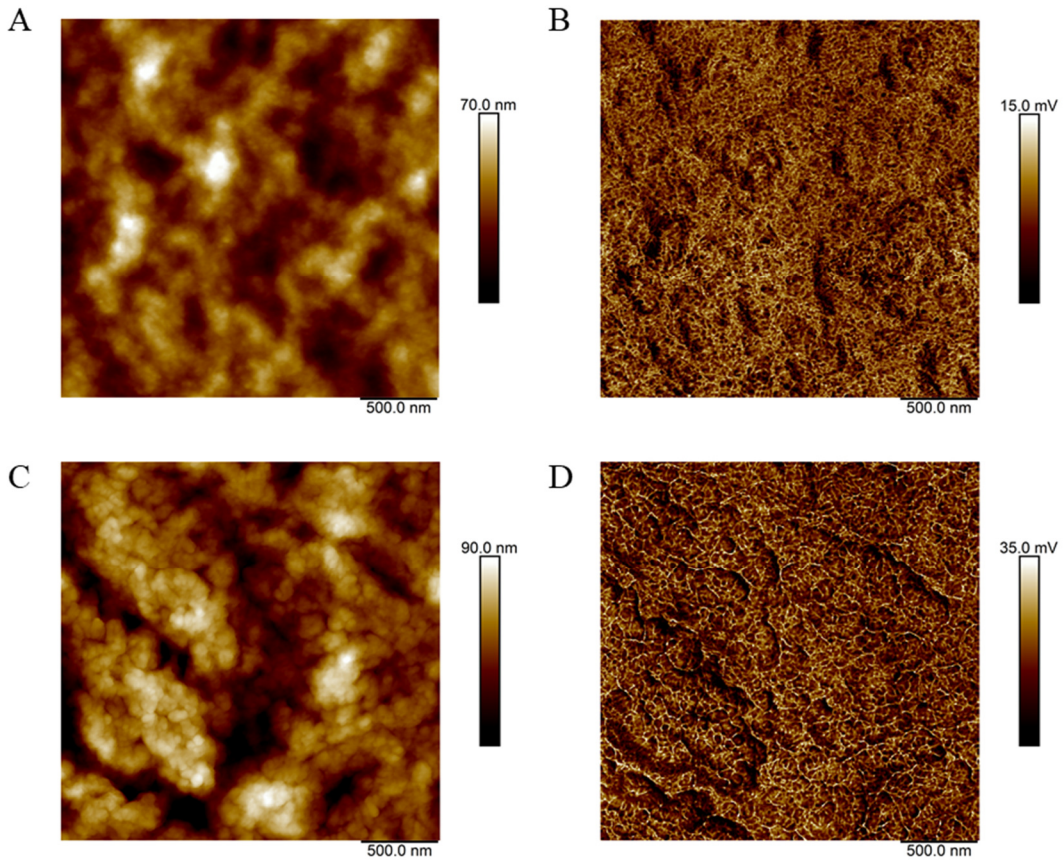

Figure 5.3. AFM (A) height and (B) inphase images for P3HT/$PC_{61}BM$ films, as well as (C) height and (D) inphase images for P3HT/$(3PS)_2$-SiPc.

The blend film morphologies were further characterized by scanning transmission X-ray microscopy (STXM), with the resulting through-plane composition maps shown in **Figure 5.4**. The composition maps of P3HT/$PC_{61}BM$ and P3HT/$(3PS)_2$-SiPc blended films were drawn from thickness values obtained from singular value decomposition (SVD) of energy stacks at the carbon K-edge using absorption spectra of reference films for each of the active materials (P3HT, $PC_{61}BM$, and $(3PS)_2$-SiPc) (Figure S5.7).[19–21] Experimental optical density (OD) spectra of reference films were scaled down to an elemental thickness of 1 nm using simulated OD spectra. These 1 nm experimental OD spectra were used to fit energy stacks of the different blends following the SVD linear regression. For P3HT/acceptor blended films, the 1 nm experimental spectra of the pure reference films were used for the SVD fitting to yield thickness maps of both components of the blend. The composition maps shown in **Figure 5.4** are obtained from the thickness maps as follows: % of P3HT = thickness of P3HT / (thickness of P3HT + thickness of acceptor).

For both blended films, the composition maps show similar characteristics to the surface topographies obtained from AFM. The P3HT/$PC_{61}BM$ film shows a relatively small variance in composition with no distinct features, indicative of a homogeneous morphology. The measured compositions are consistent with a 1:1 weight ratio P3HT/$PC_{61}BM$ blended film having a molar ratio of approximately 0.84:0.16 (P3HT:$PC_{61}BM$). The P3HT/$(3PS)_2$-SiPc composition maps indicate large domains rich with $(3PS)_2$-SiPc on the same scale as the topographic features observed in AFM images. This further suggests that the large topographic features are comprised of mainly $(3PS)_2$-SiPc arising from crystallization during film formation. It is possible through suppression of SiPc crystallization and reduced domain sizes that the exciton dissociation efficiency could be improved to afford increased J_{SC} and FF values, further justifying the continued interest into these promising NFAs. The long term thermal and morphological stability of binary P3HT/SiPc devices also remains to be investigated.

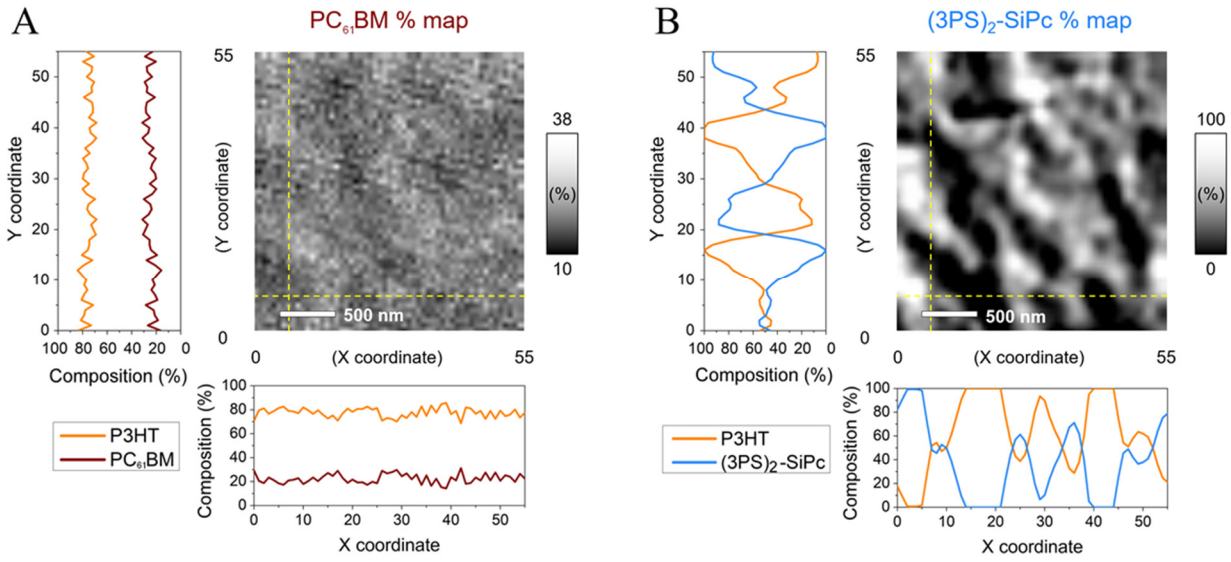

Figure 5.4. Composition maps of (A) $PC_{61}BM$ in P3HT/$PC_{61}BM$ blend and (B) $(3PS)_2$-SiPc in P3HT/$(3PS)_2$-SiPc blend obtained from singular value decomposition of STXM energy stacks. Profile lines Y = 7 and X = 7 are plotted for each blend.

To highlight the chemical simplicity and scale-up potential of $(3PS)_2$-SiPc we evaluated its relative synthetic complexity index (SC) in relation to $PC_{61}BM$ and several NFAs commonly employed for achieving high PCE devices in the literature, shown in **Table 5.2**. The SC was defined using the model introduced by Po et. al. (Equation 1), which has become a standard for comparing the relative scalability and cost of active materials in OPV devices.[22] The model uses five weighted parameters to define the SC: the number of synthetic steps (NSS), the reciprocal of the cumulative synthetic yield (RY), the number of unit operations (NUO), the number of column chromatography purification steps (NCC), and the number of highly hazardous chemicals involved in the synthesis (NHC). Each parameter is normalized to the maximum value within the group of materials being compared.

$$SC = 35\frac{NSS}{NSS_{max}} + 25\frac{\log(RY)}{\log(RY_{max})} + 15\frac{NUO}{NUO_{max}} + 15\frac{NCC}{NCC_{max}} + 10\frac{NHC}{NHC_{max}} \quad (1)$$

A relative SC index of 12 was calculated for $(3PS)_2$-SiPc, lower than any of the other NFAs surveyed by a factor of three. The extremely low SC index of $(3PS)_2$-SiPc results from a combined effect of a two-step synthesis from commercially available starting materials, circumvention of the use of highly hazardous chemicals such as *n*-butyllithium or organotin compounds, and the ability to be purified exclusively by sublimation thus eliminating column chromatography steps. Notably, the SC for $(3PS)_2$-SiPc is approximately 4.5 times lower than that of O-IDTBR, which is currently the leading candidate NFA for the upscaling of P3HT-based devices.[23–25] The SC is also approximately three times lower than A1, a recently shown simplified analogue of O-IDTBR.[26] The extremely low SC of $(3PS)_2$-SiPc, combined with a competitive PCE above 4 % in P3HT-based devices, demonstrates excellent promise for phthalocyanines as low cost NFAs.

Table 5.2. Synthetic complexity (SC) for $(3PS)_2$-SiPc in relation to $PC_{61}BM$ and commonly used high performance NFAs.

Acceptor	NSS	RY	NUO	NCC	NHC	SC[a]	Ref
$(3PS)_2$-SiPc	2	3.9	1	0	4	12	This work
$PC_{61}BM$	5	23.2	6	2	6	32	[26]
O-IDTBR	11	23.1	24	6	16	55	[26]
A1	7	3.5	16	5	29	37	[26]
ITIC-2F	13	44.5	22	8	30	66	[27]
ITIC	10	142	19	8	28	67	[27]
Y6	15	8.9	28	6	25	59	[28]

[a] To maintain consistency with the literature, the values used for normalization are: NSS_{max} = 22, RY_{max} = 86.9, NUO_{max} = 39, NCC_{max} = 13, NHC_{max} = 44

5.6. Conclusion

In summary, we have shown a novel silicon phthalocyanine derivative $(3PS)_2$-SiPc with the rare ability to be processed by both PVD and solution techniques. Solution processed P3HT/$(3PS)_2$-SiPc BHJ OPV devices achieved a high average PCE of 4.3 %, the highest reported value for binary or ternary blends of P3HT with SiPcs. AFM and STXM measurements reveal the $(3PS)_2$-SiPc forms relatively large domains due to its highly crystalline nature. Future work suppressing the crystallization of $(3PS)_2$-SiPc may yield a more optimal morphology to increase J_{SC} and *FF*. These promising results pave the way for inexpensive solar energy generation using a polymer donor and NFA that are synthetically facile to synthesize on a commercial scale.

5.7. References

(1) Liu, Q.; Jiang, Y.; Jin, K.; Qin, J.; Xu, J.; Li, W.; Xiong, J.; Liu, J.; Xiao, Z.; Sun, K.; Yang, S.; Zhang, X.; Ding, L. 18% Efficiency Organic Solar Cells. *Sci. Bull.* **2020**, *65* (4), 272–275.

(2) Wadsworth, A.; Moser, M.; Marks, A.; Little, M. S.; Gasparini, N.; Brabec, C. J.; Baran, D.; McCulloch, I. Critical Review of the Molecular Design Progress in Non-Fullerene Electron Acceptors towards Commercially Viable Organic Solar Cells. *Chem. Soc. Rev.* **2019**, *48* (6), 1596–1625.

(3) Xu, X.; Zhang, G.; Yu, L.; Li, R.; Peng, Q. P3HT-Based Polymer Solar Cells with 8.25% Efficiency Enabled by a Matched Molecular Acceptor and Smart Green-Solvent Processing Technology. *Adv. Mater.* **2019**, *31*, 1906045.

(4) Yang, C.; Zhang, S.; Ren, J.; Gao, M.; Bi, P.; Ye, L.; Hou, J.; Zhang, S.; Ye, L.; Hou, J. Molecular Design of a Non-Fullerene Acceptor Enables a P3HT -Based Organic Solar Cell with 9.46% Efficiency. *Energy Environ. Sci.* **2020**, *13* (9), 2864–2869.

(5) Claessens, C. G.; Hahn, U.; Torres, T. Phthalocyanines: From Outstanding Electronic Properties to Emerging Applications. *Chem. Rec.* **2008**, *8* (2), 75–97.

(6) Honda, S.; Nogami, T.; Ohkita, H.; Benten, H.; Ito, S. Improvement of the Light-Harvesting Efficiency in Polymer/Fullerene Bulk Heterojunction Solar Cells by Interfacial Dye Modification. *ACS Appl. Mater. Interfaces* **2009**, *1* (4), 804–810.

(7) Grant, T. M.; Gorisse, T.; Dautel, O.; Wantz, G.; Lessard, B. H. Multifunctional Ternary Additive in Bulk Heterojunction OPV: Increased Device Performance and Stability. *J. Mater. Chem. A* **2017**, *5* (4), 1581–1587.

(8) Ke, L.; Min, J.; Adam, M.; Gasparini, N.; Hou, Y.; Perea, J. D.; Chen, W.; Zhang, H.; Fladischer, S.; Sale, A. C.; Spiecker, E.; Tykwinski, R. R.; Brabec, C. J.; Ameri, T. A Series of Pyrene-Substituted Silicon Phthalocyanines as Near-IR Sensitizers in Organic Ternary Solar Cells. *Adv. Energy Mater.* **2016**, *6* (7), 1502355.

(9) Zysman-Colman, E.; Ghosh, S. S.; Xie, G.; Varghese, S.; Chowdhury, M.; Sharma, N.; Cordes, D. B.; Slawin, A. M. Z.; Samuel, I. D. W. Solution-Processable Silicon Phthalocyanines in Electroluminescent and Photovoltaic Devices. *ACS Appl. Mater. Interfaces* **2016**, *8* (14), 9247–9253.

(10) Dang, M. T.; Grant, T. M.; Yan, H.; Seferos, D. S.; Lessard, B. H.; Bender, T. P. Bis(Tri-n-Alkylsilyl Oxide) Silicon Phthalocyanines: A Start to Establishing a Structure Property Relationship as Both Ternary Additives and Non-Fullerene Electron Acceptors in Bulk Heterojunction Organic Photovoltaic Devices. *J. Mater. Chem. A* **2017**, *5* (24), 12168–12182.

(11) Grant, T. M.; Kaller, K. L. C.; Coathup, T. J.; Rice, N. A.; Hinzer, K.; Lessard, B. H. High Voc Solution-Processed Organic Solar Cells Containing Silicon Phthalocyanine as a Non-Fullerene Electron Acceptor. *Org. Electron.* **2020**, *87*, 105976.

(12) Gessner, T.; Sens, R.; Ahlers, W.; Vamvakaris, C. Preparation of Silicon Phthalocyanines and Germanium Phthalocyanines and Related Substances. US 2010/0113767 A1, 2010.

(13) Yuan, J.; Zhang, Y.; Zhou, L.; Zhang, G.; Yip, H. L.; Lau, T. K.; Lu, X.; Zhu, C.; Peng, H.; Johnson, P. A.; Leclerc, M.; Cao, Y.; Ulanski, J.; Li, Y.; Zou, Y. Single-Junction Organic Solar Cell with over 15% Efficiency Using Fused-Ring Acceptor with Electron-Deficient Core. *Joule* **2019**, *3* (4), 1140–1151.

(14) Lessard, B. H.; Dang, J. D.; Grant, T. M.; Gao, D.; Seferos, D. S.; Bender, T. P. Bis(Tri-n-Hexylsilyl Oxide) Silicon Phthalocyanine: A Unique Additive in Ternary Bulk Heterojunction Organic Photovoltaic Devices. *ACS Appl. Mater. Interfaces* **2014**, *6*, 15040–15051.

(15) Vebber, M. C.; Grant, T. M.; Brusso, J. L.; Lessard, B. H. Bis(Trialkylsilyl Oxide) Silicon Phthalocyanines: Understanding the Role of Solubility in Device Performance as Ternary Additives in Organic Photovoltaics. *Langmuir* **2020**, *36* (10), 2612–2621.

(16) Lessard, B. H. B. H.; Grant, T. M.; White, R.; Thibau, E.; Lu, Z.-H.; Bender, T. P. The Position and Frequency of Fluorine Atoms Changes the Electron Donor/Acceptor Properties of Fluorophenoxy Silicon Phthalocyanines within Organic Photovoltaic Devices. *J. Mater. Chem. A* **2015**, *3*, 24512–24524.

(17) Dang, M. T.; Hirsch, L.; Wantz, G. P3HT:PCBM, Best Seller in Polymer Photovoltaic Research. *Adv. Mater.* **2011**, *23* (31), 3597–3602.

(18) Wadsworth, A.; Hamid, Z.; Bidwell, M.; Ashraf, R. S.; Khan, J. I.; Anjum, D. H.; Cendra, C.; Yan, J.; Rezasoltani, E.; Guilbert, A. A. Y.; Azzouzi, M.; Gasparini, N.; Bannock, J. H.; Baran, D.; Wu, H.; de Mello, J. C.; Brabec, C. J.; Salleo, A.; Nelson, J.; Laquai, F.; McCulloch, I. Progress in Poly (3-Hexylthiophene) Organic Solar Cells and the Influence of Its Molecular Weight on Device Performance. *Adv. Energy Mater.* **2018**, *8* (28), 1801001.

(19) Koprinarov, I. N.; Hitchcock, A. P.; McCrory, C. T.; Childs, R. F. Quantitative Mapping of Structured Polymeric Systems Using Singular Value Decomposition Analysis of Soft X-Ray Images. *J. Phys. Chem. B* **2002**, *106* (21), 5358–5364.

(20) Kinyangi, J.; Solomon, D.; Liang, B.; Lerotic, M.; Wirick, S.; Lehmann, J. Nanoscale Biogeocomplexity of the Organomineral Assemblage in Soil. *Soil Sci. Soc. Am. J.* **2006**, *70* (5), 1708–1718.

(21) Michelin, A.; Drouet, E.; Foy, E.; Dynes, J. J.; Neff, D.; Dillmann, P. Investigation at the Nanometre Scale on the Corrosion Mechanisms of Archaeological Ferrous Artefacts by STXM. *J. Anal. At. Spectrom.* **2013**, *28* (1), 59–66.

(22) Po, R.; Bianchi, G.; Carbonera, C.; Pellegrino, A. "All That Glisters Is Not Gold": An Analysis of the Synthetic Complexity of Efficient Polymer Donors for Polymer Solar Cells. *Macromolecules* **2015**, *48* (3), 453–461.

(23) Holliday, S.; Ashraf, R. S.; Wadsworth, A.; Baran, D.; Yousaf, S. A.; Nielsen, C. B.; Tan, C. H.; Dimitrov, S. D.; Shang, Z.; Gasparini, N.; Alamoudi, M.; Laquai, F.; Brabec, C. J.; Salleo, A.; Durrant, J. R.; Mcculloch, I.; Alamoudi, M. High-Efficiency and Air-Stable P3HT-Based Polymer Solar Cells with a New Non-Fullerene Acceptor. *Nat. Commun.* **2016**, *7*, 11585.

(24) Corzo, D.; Almasabi, K.; Bihar, E.; Macphee, S.; Rosas-Villalva, D.; Gasparini, N.; Inal, S.; Baran, D. Digital Inkjet Printing of High-Efficiency Large-Area Nonfullerene Organic Solar Cells. *Adv. Mater. Technol.* **2019**, *4* (7), 1900040.

(25) Fernández Castro, M.; Mazzolini, E.; Sondergaard, R. R.; Espindola-Rodriguez, M.; Andreasen, J. W. Flexible ITO-Free Roll-Processed Large-Area Nonfullerene Organic Solar Cells Based on P3HT:O-IDTBR. *Phys. Rev. Appl.* **2020**, *14* (3), 034067.

(26) Andersen, T. R.; Weyhe, A. T.; Tao, Q.; Zhao, F.; Qin, R.; Zhang, S.; Chen, H.; Yu, D. Novel Cost-Effective Acceptor:P3HT Based Organic Solar Cells Exhibiting the Highest Ever Reported Industrial Readiness Factor. *Mater. Adv.* **2020**, *1* (4), 658–665.

(27) Du, X.; Heumueller, T.; Gruber, W.; Classen, A.; Unruh, T.; Li, N.; Brabec, C. J. Efficient Polymer Solar Cells Based on Non-Fullerene Acceptors with Potential Device Lifetime Approaching 10 Years. *Joule* **2019**, *3* (1), 215–226.

(28) Brabec, C. J.; Distler, A.; Du, X.; Egelhaaf, H. J.; Hauch, J.; Heumueller, T.; Li, N. Material Strategies to Accelerate OPV Technology Toward a GW Technology. *Adv. Energy Mater.* **2020**, *10* (43), 2001864.

Chapter 6: Conclusions and Future Work

6.1. Summary and Main Findings

The development of low-cost, scalable active materials for OPV devices has been identified as a critical area of research for commercially relevant devices to be realized. Group 14 phthalocyanines represent a promising candidate for this application. To recall, the goal of this thesis was to address the following questions:

1) How will the chemical and physical properties of structurally analogous soluble SnPcs compare to SiPcs, and is SnPc a viable option to access more complex peripheral chemistry in OPV applications?
2) Can the chemical versatility of MPcs be utilized to incorporate crosslinking functionality to address active layer stability as a ternary additive?
3) Can the PCE of SiPc derivatives as NFAs be improved, or are they more suited for use as additives in ternary devices?

In Chapter 2, soluble SnPc derivatives were synthesized for the first time and compared to structurally analogous SiPc derivatives. The solid-state packing of the SnPc derivatives was altered, counterintuitively allowing for more significant overlap of neighbouring phthalocyanine chromophores. This led to an increase in charge transport capabilities as calculated from DFT and confirmed with OTFT devices. The SnPc derivatives showed relatively poor performance as ternary additives in P3HT/$PC_{61}BM$ OPV devices, decreasing overall PCE despite significantly contributing to photocurrent generation. Poor photostability suggest that soluble SnPc derivatives may only be suited for OTFT applications and at present are not a viable alternative for SiPc in OPV devices.

In Chapter 3, a soluble azide-functionalized SiPc was synthesized for the first time. As an additive at 10 wt% with respect to $PC_{61}BM$, $(HxN_3)_2$-SiPc increased the short circuit current density (Jsc) by 9 % due to increased photocurrent generation in the near IR region. Additionally, a PCE retention of 97 % was achieved after thermal ageing at 150 C for 23 h (compared to 47 % retention for baseline $PC_{61}BM$ devices) due to effective crosslinking of the active layer. This showed the first example of a multifunctional dye additive in an OPV device that simultaneously broadens the spectral coverage and stabilizes the active layer morphology.

In Chapter 4 SiPc was proven to be a promising NFA material, achieving a PCE of 3.6 % with P3HT and 3.4 % with PBDB-T. Energy level matching also produced a high V_{OC} up to 1.10 V which is among the highest achieved for PBDB-T based devices. Under reduced light, both P3HT/SiPc and PBDB-T/SiPc devices showed an improved *FF* from reduced recombination, indicating these systems could be effective for diffuse light/indoor lighting applications. The proficiency of SiPc as an NFA was further demonstrated in Chapter 5, with the unique compound $(3PS)_2$-SiPc. The material achieved the highest reported PCE of 4.3 % for binary or ternary blends of P3HT-based devices employing a SiPc derivative, while also holding great potential for scalable chemistry.

Ultimately, this thesis has laid the groundwork for many exciting applications of SiPc derivatives in OPV devices. The studies presented herein have shown the use of SiPc derivatives is not exclusively limited to dye additives in polymer-fullerene devices, and demonstrated how straightforward chemistry can be applied to functionalize the axial position of SiPc to work as an NFA or perform additional roles such as crosslinking. In a broader sense, this work shows a compelling example of how older, less complex, and well-known dye molecules with minimal chemical modification may be utilized to produce OPV devices with respectable PCE. The validity of these types of synthetically simple active materials will ultimately depend on the target commercial application for an OPV module in which they are employed, and whether its market success will be more significantly determined by the device PCE or manufacturing cost. Applications where a compromise between PCE and device cost can be made, such as portable electronics or indoor light recovery, may serve as fitting applications for synthetically simple materials as demonstrated in this thesis. Further functional group and device optimization may also yield further improved performance for these SiPc materials to strike a more optimal cost-PCE balance for other applications.

6.2. Recommendations for Future Work

The following sections describe research pathways that I believe to be the logical next steps for continuation of the work shown in this thesis.

6.2.1. Indoor testing

Given the extreme synthetic simplicity of the SiPc NFA materials explored in this study along with their promising performance with P3HT, a rational target application for P3HT/SiPc devices could be found in low-cost indoor OPV devices for light recovery. Indoor OPV applications have given life to donor/acceptor systems that have previously been disregarded due to relatively poor performance under 1 sun illumination, and devices with relatively poor PCE under 1 sun have shown drastically improved performance under indoor lighting conditions.[1]

As discussed previously, one of the main disadvantages of P3HT for outdoor applications is its low maximum absorption around 650 nm which fails to cover a large portion of the solar spectrum. However, the low max absorption of P3HT is less relevant in indoor applications due to the condensed visible-range spectrum of most indoor lighting sources, for example between 400-700 nm for LED lights, which allows P3HT-based devices to absorb a significantly higher percentage of incoming photons.[2] The combined absorption of P3HT and SiPc would therefore be able to cover the entire emission spectrum of an LED light. Furthermore, lower incoming light intensity (< 100 $\mu W/cm^2$) reduces the quantity of charge carriers and recombination events within the device to significantly increase the device *FF* under indoor conditions, which was observed for P3HT/SiPc devices in preliminary reduced intensity studies in **Chapter 4**. A complete *JV* characterization study under LED lighting of ranging colour temperature would determine if P3HT/SiPc devices may be considered for indoor OPV applications.

6.2.2. Fabrication by Scalable Processing

The processing scalability of emerging OPV materials plays a critical role in determining their commercial viability. Therefore, the optimization of P3HT/SiPc devices using non-halogenated and scalable processing techniques is an important study to understand their true potential. A blade coating system suitable for such a study was acquired at the University of Ottawa during the completion of the work presented in this thesis.

The performance of OPV devices is generally reduced when transitioning from spin coating techniques to a printing technique such as blade coating due to a combination of increasing

device size, changes in film morphology, and increased thickness requirements.[3] Device optimization in **Chapter 4 & 5** showed the morphology of P3HT/SiPc devices was highly dependant on the film drying time, thus balancing solubility and solvent volatility will be particularly important in maximizing the performance in alternative solvent systems. Non-halogenated solvents for this study could include toluene, *o*-xylene, trimethylbenzene, and *o*-methylanisole, all of which have been commonly used for printed OPV devices.[4] Previous work in our group has already studied the effect of alkyl chain length on SiPc solubility in chlorinated solvents to serve as a baseline for optimizing the relative solubilities of P3HT and SiPc to aid in controlling domain sizes during film formation.[5,6]

6.2.3. Stability studies

Finally, the long-term stability of P3HT/SiPc devices should be studied and addressed if necessary. Stability studies should be conducted under baseline dark, inert conditions, as well as under an ambient environment, prolonged light-soaking, and thermal stress. The poor miscibility of donor and acceptor materials has been attributed to the poor stability of many fullerene-based devices.[7] It would be predicted that SiPc derivatives having similar surface energies and Flory-Huggins interaction parameters to those of P3HT would show improved stability.[8]

The possible demixing of P3HT/SiPc devices could be addressed in several ways. The literature has also shown that utilizing a mixture of two structurally similar donors may improve morphological stability over time by suppressing crystalization.[9] In this way, devices could be fabricated using, for example, a 1:0.5:0.5 ratio of P3HT:$(3BS)_2$-SiPc:$(3PS)_2$-SiPc. Furthermore, crosslinking functional groups similar to those demonstrated in **Chapter 3** could be utilized to improve the device stability. Alternative crosslinking groups to azide, such as akenyl or bromide, could be investigated for a self-crosslinking material that may be achieved using more straightforward chemistry.[10] For example, an alkenylsilane-functionalized SiPc could be employed either as an additive or as an acceptor material to actively stabilize the active layer morphology.

6.3. References

(1) Arai, R.; Furukawa, S.; Sato, N.; Yasuda, T. Organic Energy-Harvesting Devices Achieving Power Conversion Efficiencies over 20% under Ambient Indoor Lighting. *J. Mater. Chem. A* **2019**, *7* (35), 20187–20192.

(2) Cutting, C. L.; Bag, M.; Venkataraman, D. Indoor Light Recycling: A New Home for Organic Photovoltaics. *J. Mater. Chem. C* **2016**, *4* (43), 10367–10370.

(3) Ro, H. W.; Downing, J. M.; Engmann, S.; Herzing, A. A.; Delongchamp, D. M.; Richter, L. J.; Mukherjee, S.; Ade, H.; Abdelsamie, M.; Jagadamma, L. K.; Amassian, A.; Liu, Y.; Yan, H. Morphology Changes upon Scaling a High-Efficiency, Solution-Processed Solar Cell. *Energy Environ. Sci.* **2016**, *9* (9), 2835–2846.

(4) McDowell, C.; Bazan, G. C. Organic Solar Cells Processed from Green Solvents. *Curr. Opin. Green Sustain. Chem.* **2017**, *5*, 49–54.

(5) Vebber, M. C.; Grant, T. M.; Brusso, J. L.; Lessard, B. H. Bis(Trialkylsilyl Oxide) Silicon Phthalocyanines: Understanding the Role of Solubility in Device Performance as Ternary Additives in Organic Photovoltaics. *Langmuir* **2020**, *36* (10), 2612–2621.

(6) Strohm, S.; Machui, F.; Langner, S.; Kubis, P.; Gasparini, N.; Salvador, M.; McCulloch, I.; Egelhaaf, H. J.; Brabec, C. J. P3HT: Non-Fullerene Acceptor Based Large Area, Semi-Transparent PV Modules with Power Conversion Efficiencies of 5%, Processed by Industrially Scalable Methods. *Energy Environ. Sci.* **2018**, *11* (8), 2225–2234.

(7) Li, N.; Perea, J. D.; Kassar, T.; Richter, M.; Heumueller, T.; Matt, G. J.; Hou, Y.; Güldal, N. S.; Chen, H.; Chen, S.; Langner, S.; Berlinghof, M.; Unruh, T.; Brabec, C. J. Abnormal Strong Burn-in Degradation of Highly Efficient Polymer Solar Cells Caused by Spinodal Donor-Acceptor Demixing. *Nat. Commun.* **2017**, *8*, 14541.

(8) Xiao, J.; Ren, M.; Zhang, G.; Wang, J.; Zhang, D.; Liu, L.; Li, N.; Brabec, C. J.; Yip, H. L.; Cao, Y. An Operando Study on the Photostability of Nonfullerene Organic Solar Cells. *Sol. RRL* **2019**, *3* (7), 1900077.

(9) Hultmark, S.; Paleti, S. H. K.; Harillo, A.; Marina, S.; Nugroho, F. A. A.; Liu, Y.; Ericsson, L. K. E.; Li, R.; Martín, J.; Bergqvist, J.; Langhammer, C.; Zhang, F.; Yu, L.; Campoy-Quiles, M.; Moons, E.; Baran, D.; Müller, C. Suppressing Co-Crystallization of Halogenated Non-Fullerene Acceptors for Thermally Stable Ternary Solar Cells. *Adv. Funct. Mater.* **2020**, *30* (48), 2005462.

(10) Wantz, G.; Derue, L.; Dautel, O.; Rivaton, A.; Hudhomme, P.; Dagron-Lartigau, C. Stabilizing Polymer-Based Bulk Heterojunction Solar Cells via Crosslinking. *Polym. Int.* **2014**, *63* (8), 1346–1361.

Chapter 7: Additional Contributions

Throughout my thesis, I was involved in several additional projects providing material synthesis and/or fabrication of devices. Following is a list of all non-first author publications for which I contributed.

7.1. Silicon phthalocyanines as N-type semiconductors in organic thin film transistors

O.A. Melville, T.M. Grant, B.H. Lessard

Journal of Materials Chemistry C, 2018, 6 (20), 5482-5488

Abstract

Silicon phthalocyanines (SiPcs) represent a large class of molecules that have been studied as donors, acceptors and ternary additives in organic photovoltaics but not in organic thin-film transistors (OTFTs). We synthesized three novel SiPcs using axial substitution and examined their performance as the active layer in bottom-gate bottom-contact (BGBC) OTFTs. All three molecules exhibit N-type behaviour, with the dibenzoate substituted SiPc showing the greatest field-effect mobility of roughly 6×10^{-4} cm^2 V^{-1} s^{-1} in vacuum. This performance improved to >0.01 cm^2 $V^{-1}s^{-1}$ when using a combination of dielectric modification with octadecyltrichlorosilane (ODTS) and a substrate temperature during deposition of 200 °C. These promising results point towards the possibility of high-performance N-type SiPcs by exploring the wealth of available options in axial and peripheral substitution and careful process control during fabrication.

Contributions

I synthesized and characterized the novel phthalocyanine compounds used in this study, which were initially intended for use as electron acceptors in planar heterojunction OPV devices but upon characterization were more suited for OTFTs. I then co-fabricated and tested the OTFT devices and assisted in drafting the manuscript.

7.2. High performance near-infrared (NIR) photoinitiating systems operating under low light intensity and in the presence of oxygen.

A.H. Bonardi, F. Dumur, T.M. Grant, G. Noirbent, D. Gigmes, B.H. Lessard, J.-P. Fouassier, J. Lalevée

Macromolecules, **2018**, 51 (4), 1314-1324

Abstract

Photopolymerization under near-infrared (NIR) light is challenging due to the low energy of the absorbed photon but, if successful, presents significant advantages. For example, this lower energy wavelength is safer than UV light that is currently the standard photocuring light source. Also, NIR allows for a deeper light penetration within the material and therefore resulting in a more complete curing of thicker materials containing fillers for access to composites. In this study, we report the use of three-component systems for the NIR photopolymerization of methacrylates: (1) a dye used as a photosensitizer in the NIR range, (2) an iodonium salt as a photoinitiator for the free radical polymerization of the (meth)acrylates, and (3) a phosphine to prevent polymerization inhibition due to the oxygen and to regenerate the dye upon irradiation. Several NIR-absorbing dyes such as a cyanine borate and a silicon–phthalocyanine are presented and studied. Systems using borate dyes resulted in methacrylate monomer conversion over 80% in air. We report three types of irradiation system: low-power LED at 660 and 780 nm as well as a higher power laser diode at 785 nm. The excellent performance reported in this work is due to the crucial role of the added phosphine.

Contributions

I synthesized and characterized a novel silicon phthalocyanine derivative that was investigated as apart of this study as a NIR photo-initiator for polymerization.

7.3. Photoinduced thermal polymerization reactions

A.-H. Bonardi, F. Bonardi, F. Morlet-Savary, C. Dietlin, G. Noirbent, T.M. Grant, J.-P. Fouassier, F. Dumur, B.H. Lessard, D. Gigmes, J. Lalevée

Macromolecules, **2018**, 51 (21), 8808-8820

Abstract

The combination of thermally induced and photoinduced free radical polymerization of (meth)acrylic monomers has only been scarcely presented in the literature. In this study, a two-component system with a near-infrared (NIR) dye combined with a thermal initiator is presented. The dye acts as a very efficient heat generator (heater) upon irradiation with NIR light. Several thermal initiators are presented such as an alkoxyamine (e.g., BlocBuilder-MA), azo derivatives, and (hydro)peroxides. The heat delivered by the dye dissociates the thermal initiator, which initiates the free radical polymerization of (meth)acrylates. Several types of heat generators are presented such as borate-based dyes and a silicon phthalocyanine derivative. For the first time, the effects of the NIR heater concentration, light intensity, and monomer structure on the heat released are studied using thermal imaging studies. NIR light curing is challenging but offers significant advantages: it is safer than shorter wavelength, and it allows a deeper penetration of the light and therefore a better curing of filled samples for a unique access to composites. Systems using a cyanine borate as a dye give high conversion rate of C═C for methacrylate monomer under air. Two wavelengths of irradiation are studied: 785 and 850 nm. The presence of additives (phosphines or iodonium salts) can also improve the polymerization profiles.

Contributions

Similar to section **7.3**, I synthesized and characterized a second novel silicon phthalocyanine derivative that was investigated in this study as a NIR photo-initiator for polymerization.

7.4. Old Molecule, New Chemistry: Exploring Silicon Phthalocyanines as Emerging N-Type Materials in Organic Electronics.

N.J. Yutronkie, T.M. Grant, O.A. Melville, B.H. Lessard, J.L. Brusso

Materials, **2019**, 12 (8), 1334

Abstract

Efficient synthesis of silicon phthalocyanines (SiPc) eliminating the strenuous reaction conditions and hazardous reagents required by classical methods is described. Implementation into organic thin-film transistors (OTFTs) affords average electron field-effect mobility of 3.1×10^{-3} $cm^2V^{-1}s^{-1}$ and threshold voltage of 25.6 V for all synthetic routes. These results demonstrate that our novel chemistry can lead to high performing SiPc-based n-type OTFTs

Contributions

This study investigated alternative synthetic routes for Cl_2-SiPc. I performed the chemistry and purification for the additional axial functionalization of the various Cl_2-SiPc samples to allow for testing in OTFT devices.

7.5. Silicon phthalocyanines as acceptor candidates in mixed solution/evaporation processed planar heterojunction organic photovoltaic devices.

M.D.M. Faure, T.M. Grant, B.H. Lessard.

Coatings, **2019**, 9 (3), 203

Abstract

Silicon phthalocyanines (SiPc) are showing promise as both ternary additives and non-fullerene acceptors in organic photovoltaics (OPVs) as a result of their ease of synthesis, chemical stability and strong absorption. In this study, bis(3,4,5-trifluorophenoxy) silicon phthalocyanine ($(345F)_2$-SiPc)) and bis(2,4,6-trifluorophenoxy) silicon phthalocyanine ($(246F)_2$-SiPc)) are employed as acceptors in mixed solution/evaporation planar heterojunction (PHJ) devices. The donor layer, either poly(3-hexylthiophene) (P3HT) or poly[N-9′-heptadecanyl-2,7-carbazole-alt-5,5-(4′,7′-di-2-thienyl-2′,1′,3′-benzothiadiazole)] (PCDTBT), was spin coated followed by the evaporation of the SiPc acceptor thin film. Several different donor/acceptor combinations were investigated in addition to investigations to determine the effect of film thickness on device performance. Finally, the effects of annealing, prior to SiPc deposition, after SiPc deposition, and during SiPc deposition were also investigated. The devices which performed the best were obtained using PCDTBT as the donor, with a 90 nm film of $(345F)_2$-SiPc as the acceptor, followed by thermal annealing at 150 °C for 30 min of the entire mixed solution/evaporation device. An open-circuit voltage (V_{OC}) of 0.88 V and a fill factor (FF) of 0.52 were achieved leading to devices that outperformed corresponding fullerene-based PHJ devices.

Contributions

I synthesized and purified the phthalocyanine derivatives used in this study. I also trained and assisted the first author in fabricating and characterizing the OPV devices.

7.6. Straightforward and Relatively Safe Process for the Fluoride Exchange of Trivalent and Tetravalent Group 13 and 14 Phthalocyanines.

T.M. Grant, V. McIntyre, J. Vestfrid, H. Raboui, R.T. White, Z.H. Lu, B.H. Lessard, T.P. Bender

ACS Omega, **2019**, 4 (3), 5317-5326

Abstract

To avoid the use of hydrofluoric acid, a series of fluorinated trivalent and tetravalent metal-containing phthalocyanines (MPcs) were synthesized using a straightforward one-step halide substitution process using cesium fluoride (CsF) as the fluoride source and by reflux in N,N-dimethylformamide for less than an hour. The resulting fluoro MPcs were characterized and compared to the parent chloro MPcs. In some cases, very little change in properties was observed between the fluoro MPcs and the chloro MPcs. In other cases, such as fluoro aluminum phthalocyanine, a blue shift in the absorbance characteristics and an increase in oxidation and reduction potential of as much as 0.22 V was observed compared to the chloro derivative. Thermo gravimetric analysis was performed on all halo-MPcs, indicating that the choice of halo substitution on the axial position can have an effect on the decomposition or sublimation temperature of the final compound. After initial establishment and characterization of the fluoro MPcs, the halide substitution reaction of difluoro silicon phthalocyanine (F_2-SiPc) was further explored by scaling the reaction up to a gram scale as well as considering tetrabutylammonium fluoride (TBAF) as an additional safe fluoride source. The scaled-up reactions producing F_2-SiPc using CsF and TBAF as fluoride exchange sources were successfully reproducible, resulting in reaction yields of 100 and 73%, respectively. Both processes led to pure final products but results indicate that CsF, as the fluoride exchange reagent, appears to be the superior reaction process as it has a much higher yield.

Contributions

I performed the preliminary chemistry for the fluorination of the MPcs examined in this study using CsF. I then supervised V.M. for the remainder of the synthetic work investigating alternative fluoride sources.

7.7. Ambipolarity and Air Stability of Silicon Phthalocyanine Organic Thin-Film Transistors.

O.A. Melville, T.M. Grant, B. Mirka, N.T. Boileau, J. Park, B.H. Lessard.

Advanced Electronic Materials, **2019**, 5 (8), 1900087

Abstract

Silicon phthalocyanines (SiPcs) are a class of conjugated, planar molecule that have recently been investigated for use in organic photovoltaics (OPVs), organic light-emitting diodes (OLEDs), and organic thin-film transistors (OTFTs) due to their variable structure and ease of synthesis. Bottom-gate, bottom-contact OTFTs with four SiPc derivatives used as the semiconducting layers are prepared using physical vapor deposition. Devices using bis(pentafluorophenoxy) silicon phthalocyanine (F10-SiPc) deposited on 140 °C substrates demonstrate electron field-effect mobilities (μ) of up to 0.54 $cm^2\ V^{-1}s^{-1}$, among the best currently reported for N-type phthalocyanine-based transistors. All materials show dramatic changes in charge transport when characterized under vacuum (P < 0.1 Pa) compared to in air at atmospheric pressure, typically switching from electron majority charge carriers to holes, with the change dependent on material structure and energetics. F10-SiPc is close to balanced ambipolar in air, with μ around 5×10^{-3} $cm^2\ V^{-1}\ s^{-1}$ for both holes and electrons. These results demonstrate SiPcs' potential as N-type semiconductors in OTFTs as well as their adjustable charge transport as affected by operation environment.

Contributions

I preformed the synthesis and purification of the SiPc materials used in this study.

7.8. Functionalization of commercial pigment Hostasol Red GG for incorporation into organic thin-film transistors.

O.A. Melville, T.M. Grant, N.A. Rice, B. Wang, P. Josse, B.H. Lessard.

New Journal of Chemistry, 44 (3), **2020**, 845-851

Abstract

In the development of organic electronic devices, it is important to consider the overall cost of the carbon-based semiconductors. Many of the state-of-the-art semiconductors available today are prohibitively expensive, limiting their commercial functionality. The dye and pigment industries offer a wealth of cheap conjugated starting materials. In this study, we explored functionalizing the dye 14*H*-anthra[2,1,9-*m,n,a*]thioxanthen-14-one (Hostasol Red GG) through a simple one-pot Grignard reaction. Phenyl, primary and secondary alkyl substituents were introduced onto the parent thioxanthene benzanthrone, with 1,4-addition occurring preferentially to addition at the carbonyl for all products. The substituted Red GG derivatives were incorporated into organic thin film transistors. While the alkyl derivatives resulted in decreased device performance compared to native Red GG, transistor performance improved for the phenyl derivative. A combination of inexpensive starting materials and simple chemistry offers an abundance of possible new semiconductor targets for organic electronic devices with commercial potential.

Contributions

I performed the preliminary novel chemistry for the materials presented in this study. I also co-trained and co-supervised B.W. for a portion of the remaining synthetic work.

7.9. Bis (trialkylsilyl oxide) Silicon Phthalocyanines: Understanding the Role of Solubility in Device Performance as Ternary Additives in Organic Photovoltaics.

M.C. Vebber, T.M. Grant, J.L. Brusso, B.H. Lessard.

Langmuir, **2020**, 36 (10), 2612-2621

Abstract

The use of ternary additives in organic photovoltaics is a promising route for improving overall device performance. Silicon phthalocyanines (SiPcs) are ideal candidates due to their absorption profile, low cost, and ease of synthesis and chemical tunability. However, to date, only a few examples have been reported and specific strategies for aiding in the design of improved ternary additives have not been established. In this study, we report a relationship between ternary additive solubility and device performance, demonstrating that device performance is maximized when the SiPc additive solubility is similar to that of the donor polymer (P3HT, in this case). This improved performance can be attributed to the favored interfacial precipitation of the SiPc when its solubility matches that of the other components of the thin film. The power conversion efficiency (PCE) varied from 2.4% to 3.4% by using axially substituted SiPcs with different solubilities, where the best ternary additive led to a 25% increase in PCE compared to that of the baseline device.

Contributions

I trained the first author on both the synthesis of the phthalocyanine compounds presented in the study, as well as the fabrication and characterization of OPV devices.

7.10. Contact Engineering Using Manganese, Chromium, and Bathocuproine in Group 14 Phthalocyanine Organic Thin-Film Transistors.

O.A. Melville, T.M. Grant, K. Lochhead, B. King, R. Ambrose, N.A. Rice, N.T. Boileau, A.J. Peltekoff, M. Tousignant, I.G. Hill, B.H. Lessard.

ACS Applied Electronic Materials, **2020**, 2 (5), 1313-1322

Abstract

Silicon and tin(IV) phthalocyanines, which have been demonstrated as simple-to-synthesize materials for n-type organic thin-film transistors (OTFTs), have relatively shallow lowest unoccupied molecular orbital (LUMO) levels that create a Schottky barrier with the gold source–drain contacts typically used in device fabrication. To reduce the contact resistance (RC) associated with this barrier and improve the OTFT performance, we fabricated bottom-gate top-contact (BGTC) devices using low-work-function metals (Mn/Cr) and an electron dopant material (bathocuproine, BCP) as contact interlayers. We characterized two tin phthalocyanines (SnPcs), tin bis(pentafluorophenoxy)phthalocyanine (F10-SnPc) and tin bis(2,4,6-trifluorophenoxy)phthalocyanine (246F-SnPc), as organic semiconductors (OSCs) and compared them to their silicon phthalocyanine (SiPc) analogues. We found that using Mn and Cr interlayers with SiPc OTFTs reduces RC to as low as 11.8 kΩ cm and reduces the threshold voltage (V_T) to as low as 7.8 V while improving linear region characteristics compared to devices using silver or gold electrodes only. BCP interlayers appear to reduce V_T in all SiPc and SnPc devices and increase the off-state conductivity of SnPc devices if covering the entire OSC. Overall, this work demonstrates the potential for metal interlayers and solid-state organic interlayers for improving electron transport in low-cost, n-type OTFTs using group 14 phthalocyanines.

Contributions

I performed the preliminary chemistry for the materials used in this study, then trained and supervised K.L for the remainder of the synthetic work.

7.11. Silicon Phthalocyanines for n-Type Organic Thin-Film Transistors: Development of Structure–Property Relationships.

B. King, O.A. Melville, N.A. Rice, S. Kashani, C. Tonnelé, H. Raboui, S. Swaraj, T.M. Grant, T. McAfee, T.P. Bender, H. Ade, F. Castet, L. Muccioli, B.H. Lessard

ACS Applied Electronic Materials, **2021**, 3 (1), 325-336

Abstract

Silicon phthalocyanines (SiPcs) have shown great potential as n-type or ambipolar organic semiconductors in organic thin-film transistors (OTFTs) and organic photovoltaics. Although properly designed SiPcs rival current state-of-the-art n-type organic semiconducting materials, relatively few structure–property relationships have been established to determine the impact of axial substituents on OTFT performance, hindering the intelligent design of the next generation of SiPcs. To address this omission, we have developed structure–property relationships for vapor-deposited SiPcs with phenoxy axial substituents. In addition to thorough electrical characterization of bottom-gate top-contact OTFTs, we extensively investigated SiPc thin films using X-ray diffraction, atomic force microscopy (AFM), grazing-incidence wide-angle X-ray scattering (GIWAXS), and density functional theory (DFT) modeling. OTFT performance, including relative electron mobility (μ_e) of materials, was in general agreement with values obtained through DFT modeling including reorganization energy. Another significant trend observed from device performance was that increasing the electron-withdrawing character of the axial pendant groups led to a reduction in threshold voltage (V_T) from 47.9 to 21.1 V. This was corroborated by DFT modeling, which predicted that V_T decreases with the square of the dipole induced at the interface between the SiPc pendant and substrate. Discrepancies between modeling predictions and experimental results can be explained through analysis of thin-film morphology and orientation by AFM and GIWAXS. Our results demonstrate that a combination of DFT modeling to select prospective candidate materials, combined with appropriate processing conditions to deposit molecules with a favorable thin-film morphology in an "edge-on" orientation relative to the substrate, yields high-performance n-type SiPc-based OTFTs.

Contributions

I performed the synthesis and purification for a portion of the SiPc derivatives used in this study.

Appendix A: Supplementary Information for Chapter 2

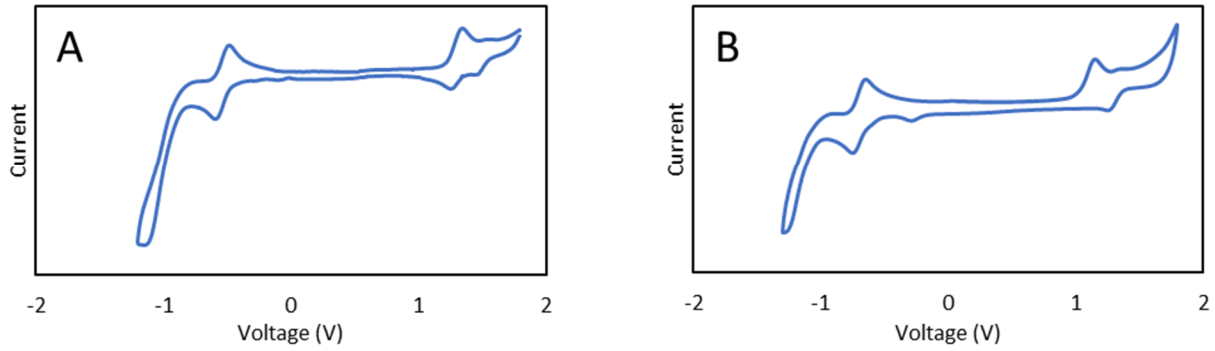

Figure S2.1: Characteristic cyclic voltammograms for (A) $(3HS)_2$-SnPc and (B) $(3BS)_2$-SnPc

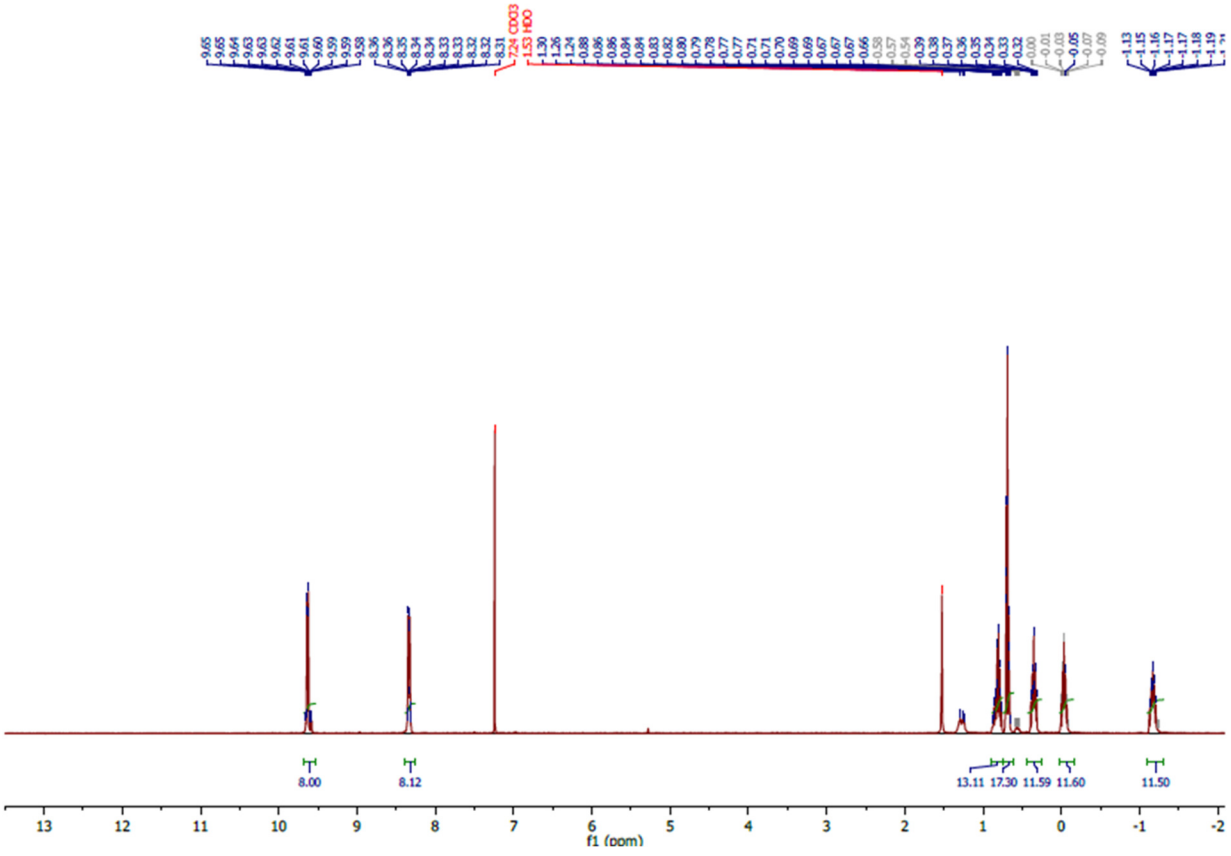

Figure S2.2: ^{1}H NMR (400 MHz, CDCl3) spectrum obtained for $(3HS)_2$-SnPc

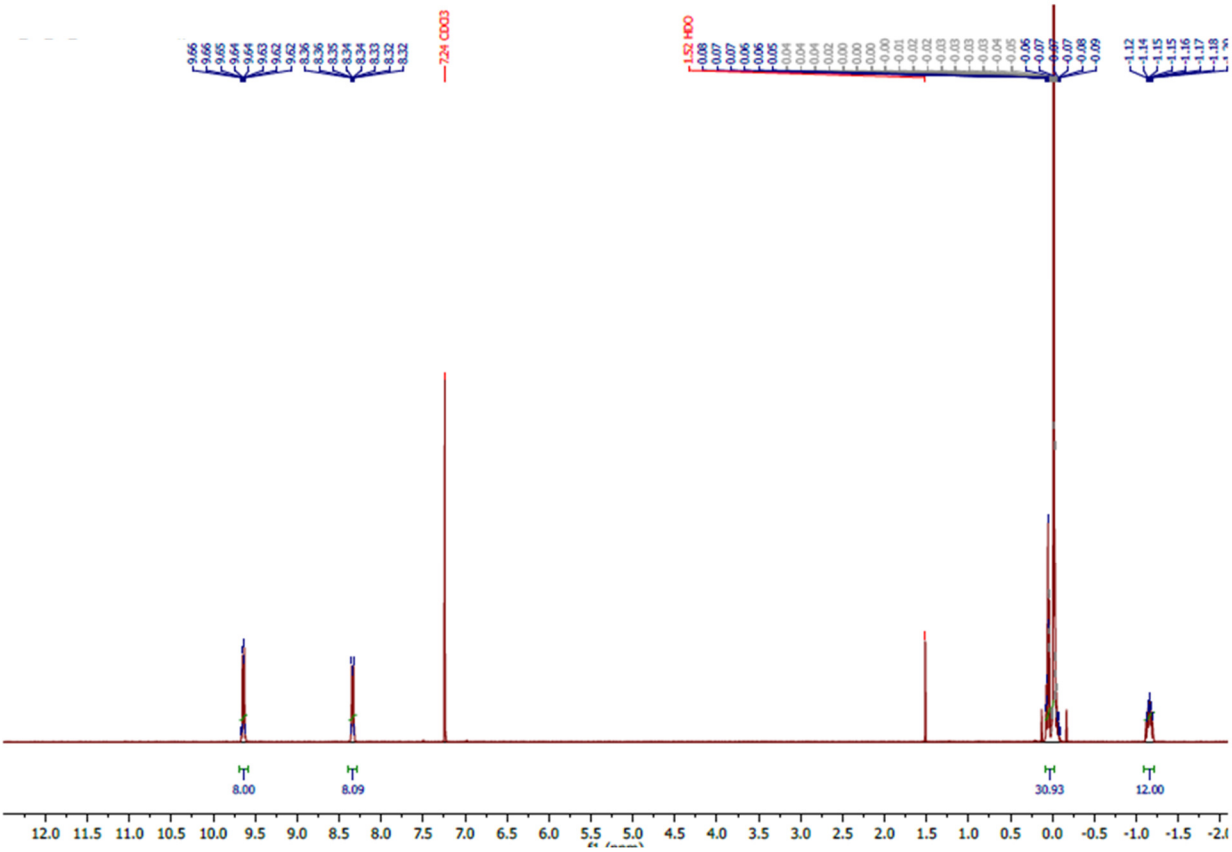

Figure S2.3: ^{1}H NMR (400 MHz, CDCl3) spectrum obtained for $(3BS)_2$-SnPc

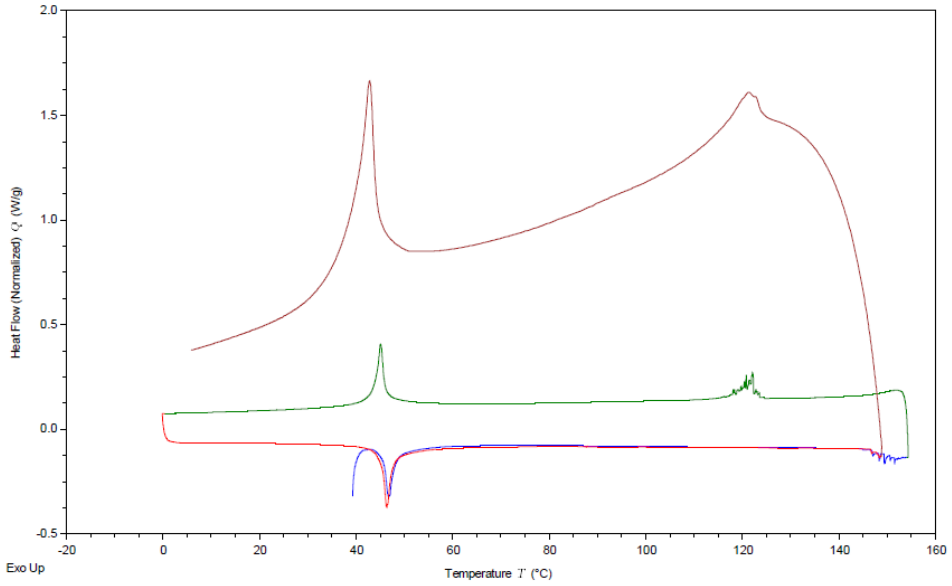

Figure S2.4: Differential scanning calorimetry (DSC) obtained from $(3HS)_2$-SnPc powder using the following heating profile: first heat at +5°C/min to 180 °C (blue), first cool at -5 °C/min to 0 °C (green), second heat at +5 °C/min to 150 °C (red), flash cool at -100 °C/min to 0 °C (brown)

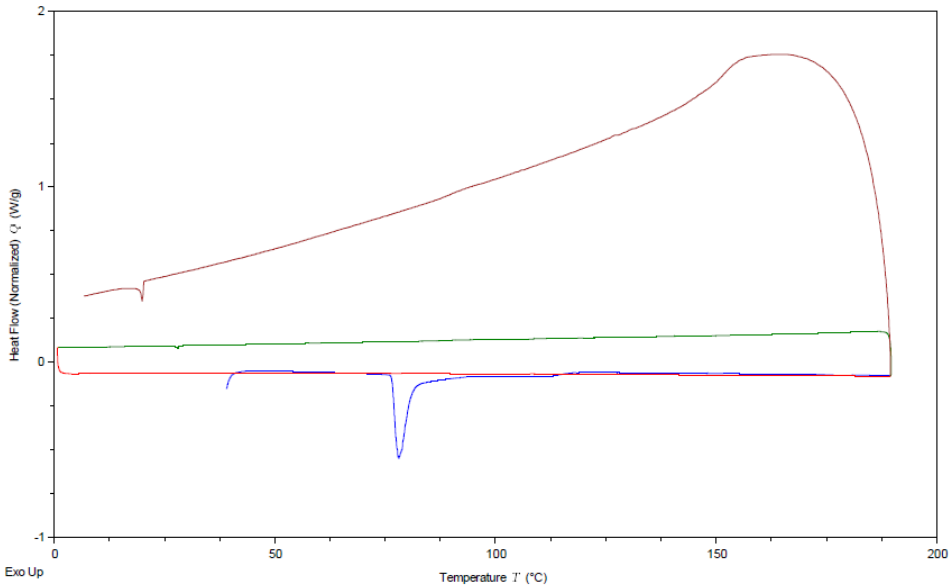

Figure S2.5: Differential scanning calorimetry (DSC) obtained from $(3BS)_2$-SnPc powder using the following heating profile: first heat at +5°C/min to 190 °C (blue), first cool at -5 °C/min to 0 °C (green), second heat at +5 °C/min to 190 °C (red), flash cool at -100 °C/min to 0 °C (brown)

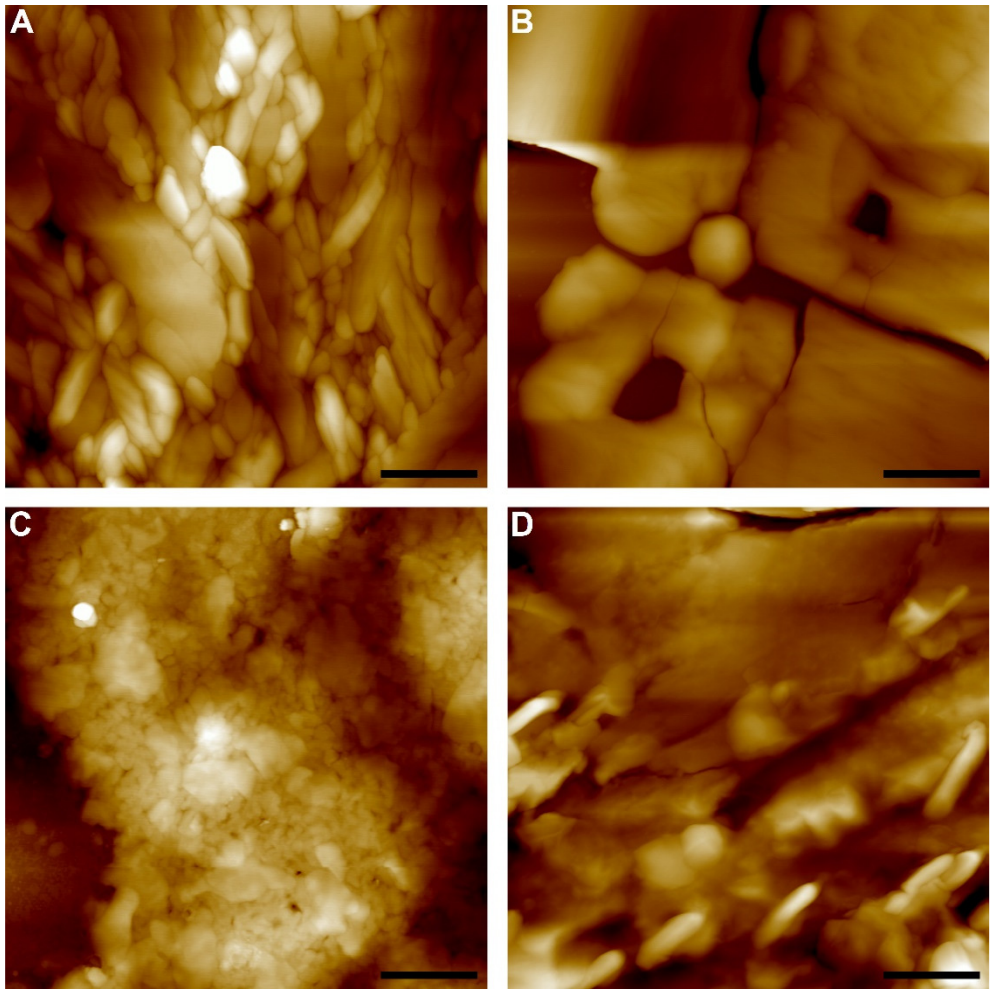

Figure S2.6: AFM images of drop cast films for $(3BS)_2$-SiPc (A) dried at 100 °C, (B) annealed at 150 °C, and $(3BS)_2$-SnPc (C) dried at 100 °C, (D) annealed at 150 °C. Sale bar represents 1 μm

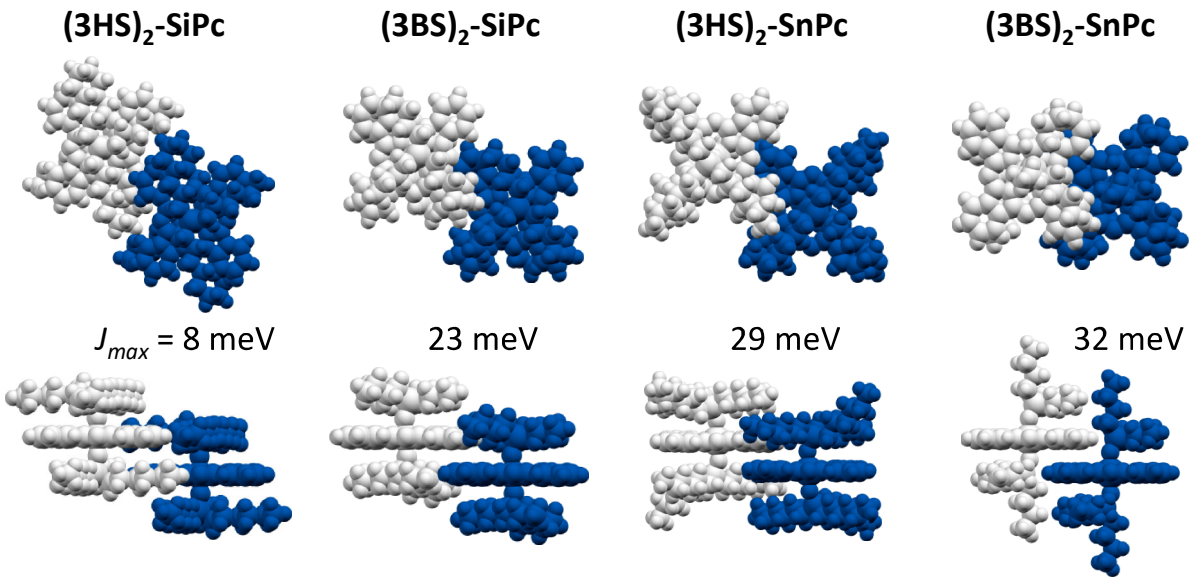

Figure S2.7: Top and side views of the molecular pairs giving rise to the largest electronic couplings (J_{max}) in $(3HS)_2$-SiPc, $(3BS)_2$-SiPc, $(3HS)_2$-SnPc and $(3BS)_2$-SnPc, as extracted from the experimental crystal structures. Transfer integrals are calculated at the B3LYP/6-31G(d) level.

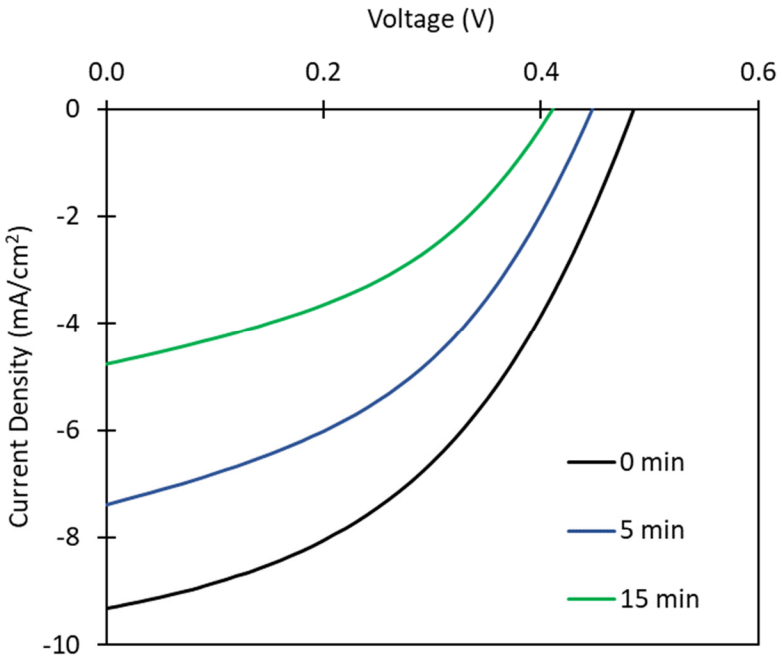

Figure S2.8: Characteristic current density-voltage (J-V) curves for a P3HT/$PC_{61}BM$/$(3BS)_2$-SnPc (1:0.8:0.09) device after exposure to simulated solar light for 0 min (black), 5 min (blue) and 15 min (green)

Table S2.1. Non-negligible transfer integrals ($J_k \geq 1$, in units of meV), calculated between a reference molecule and its first neighbours in the four phthalocyanine crystal structures discussed in the main text. The crystallographic directions corresponding to intermolecular vectors joining the reference molecule with its neighbours are given in the basis of direct lattice vectors.

Crystal	Direction	J_κ
(3HS)2-SiPc	±(1, 0, 0)	3
	±(0, 1, 0)	8
	±(0, 0, 1)	5
(3BS)$_2$-SiPc	±(1, 0, 0)	1
	±(0, 1, 0)	23
	±(0, 0, 1)	7
(3HS)$_2$-SnPc	(-1/2, 0, -1/2)	3
	(-1/2, 0, 1/2)	8
	(-1/2, 1, 1/2)	8
	(1/2, 0,-1/2)	29
	(1/2, -1, 1/2)	1
(3BS)$_2$-SnPc	±(1, 0, 0)	32
	±(0, 1, 0)	9
	±(1, -1, 0)	3

Appendix B: Supplementary Information for Chapter 3

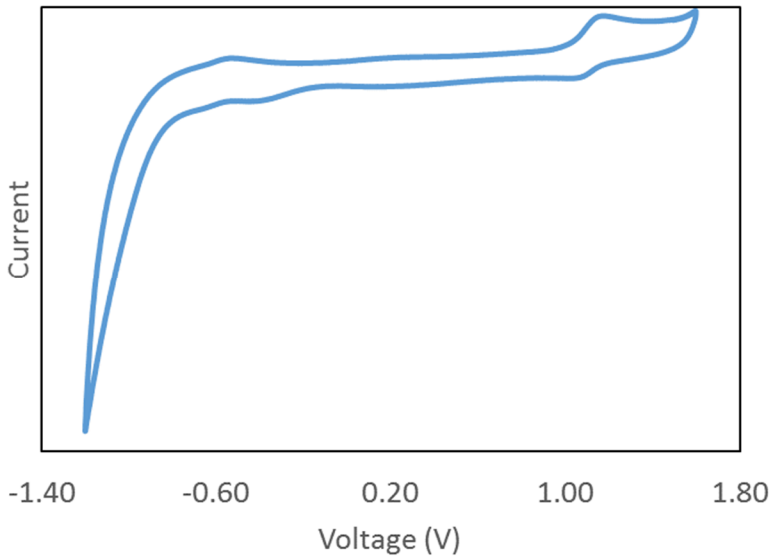

Figure S3.1. Characteristic cyclic voltammogram for $(HxN_3)_2$-SiPc.

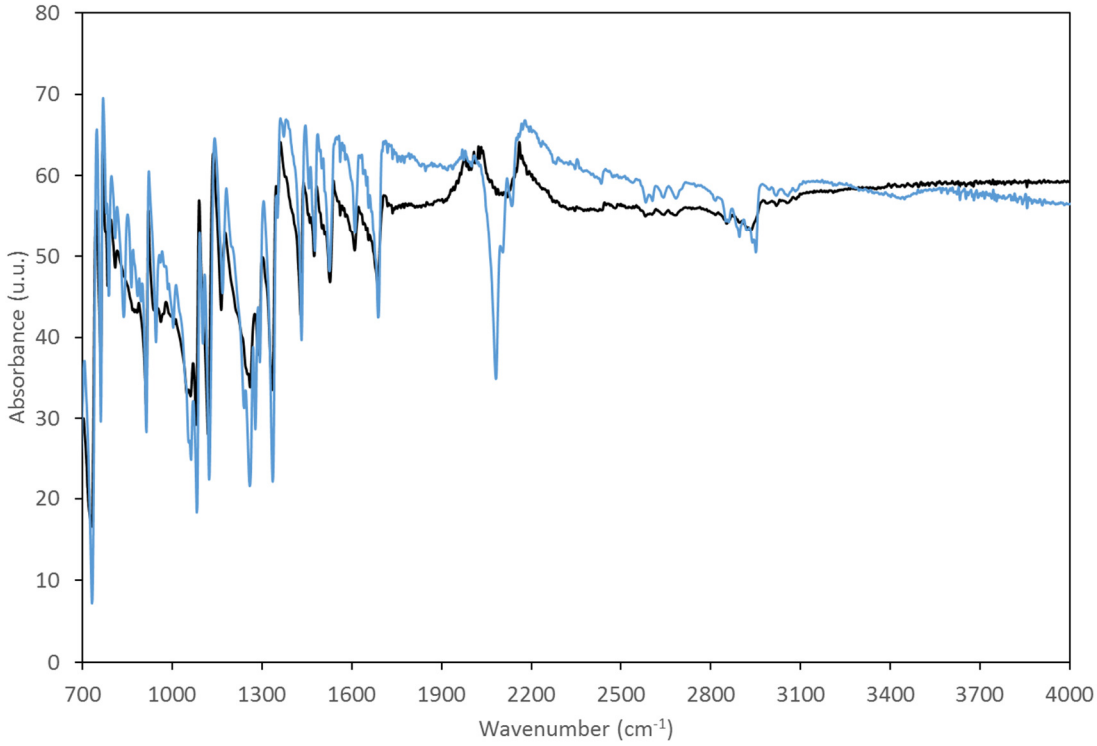

Figure S3.2. FTIR spectrum obtained for $(HxCl)_2$-SiPc (black) and $(HxN_3)_2$-SiPc (blue)

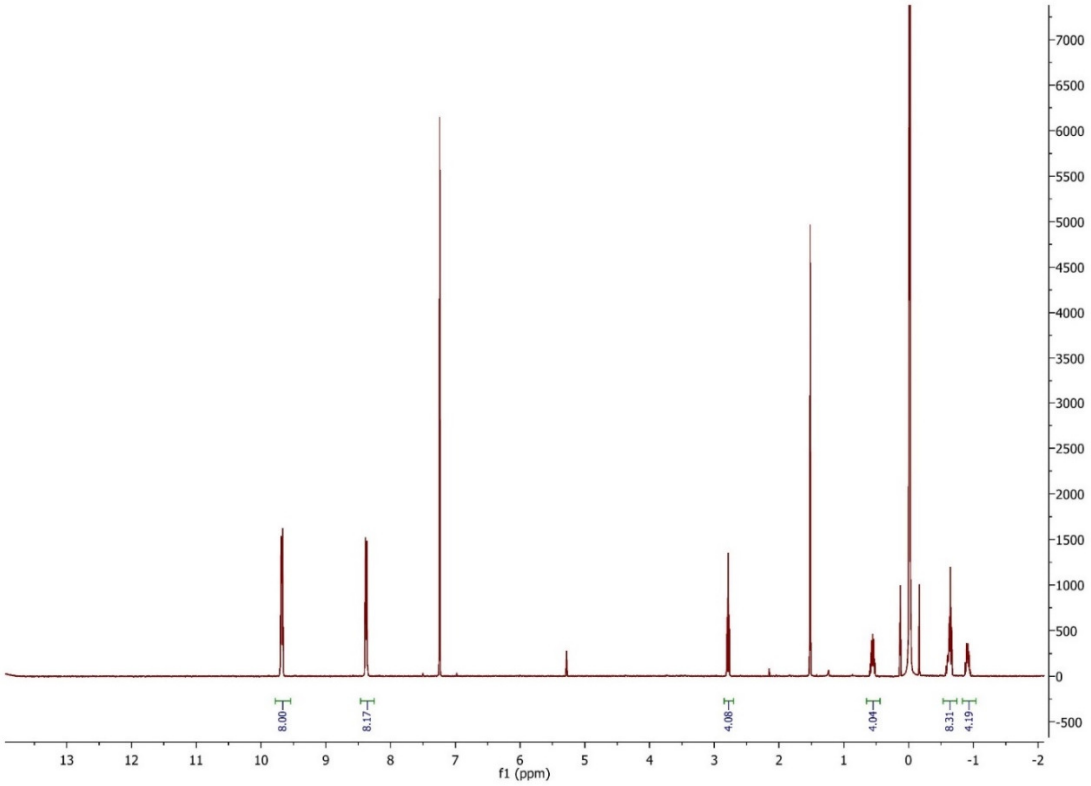

Figure S3.3. ^{1}H NMR (400 MHz, $CDCl_3$) spectrum obtained at 296 K for $(HxCl)_2$-SiPc

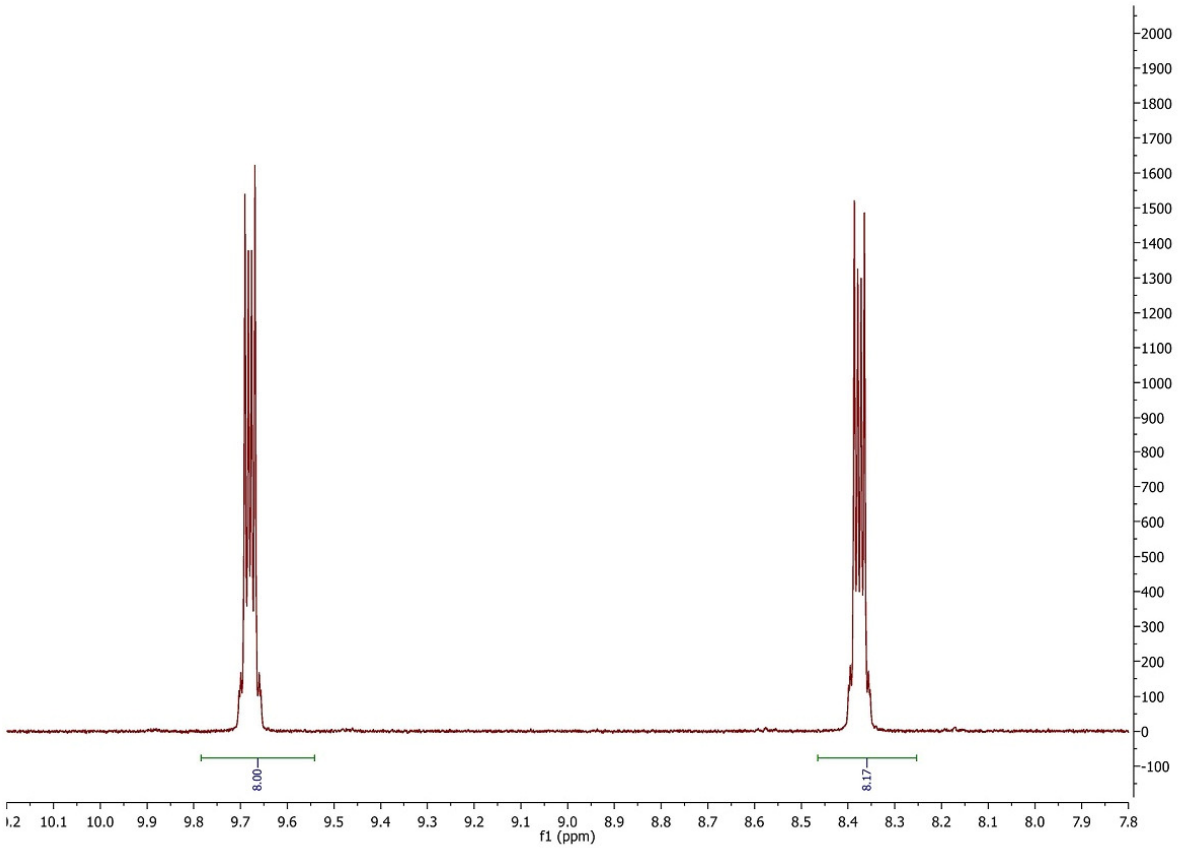

Figure S3.3. ^{1}H NMR (400 MHz, $CDCl_{3,}$) spectrum obtained at 296 K for $(HxCl)_2$-SiPc displaying the aromatic region.

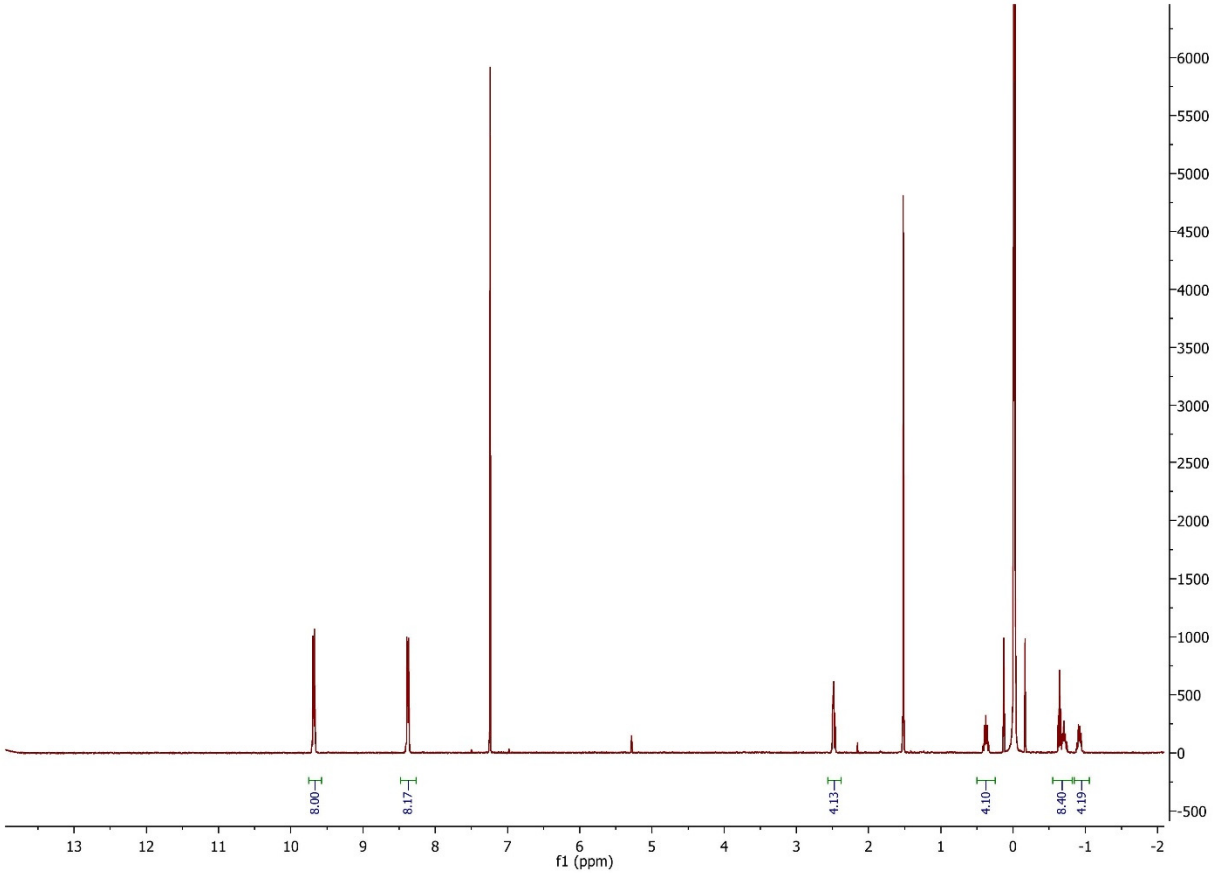

Figure S3.4. ^{1}H NMR (400 MHz, $CDCl_3$) spectrum obtained at 296 K for $(HxN_3)_2$-SiPc

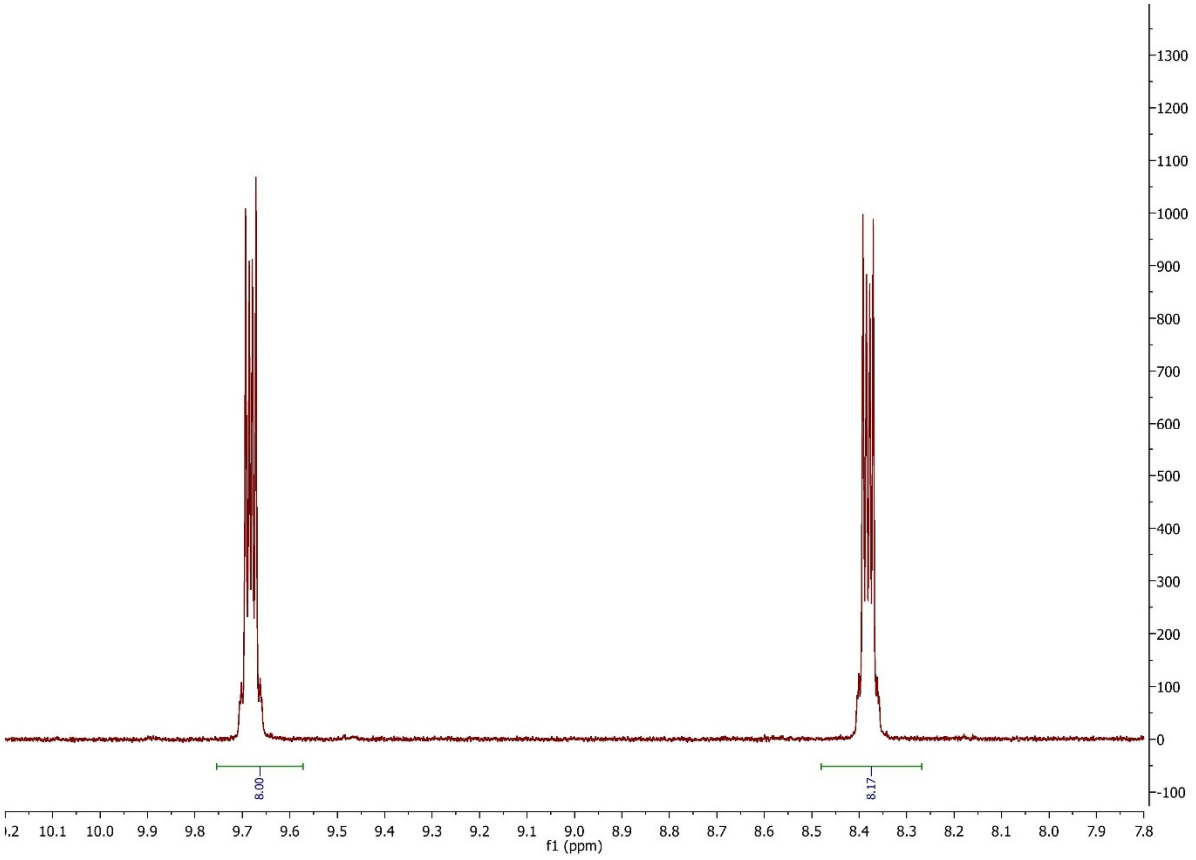

Figure S3.5. ^{1}H NMR (400 MHz, $CDCl_3$) spectrum obtained at 296 K for $(HxN_3)_2$-SiPc displaying the aromatic region.

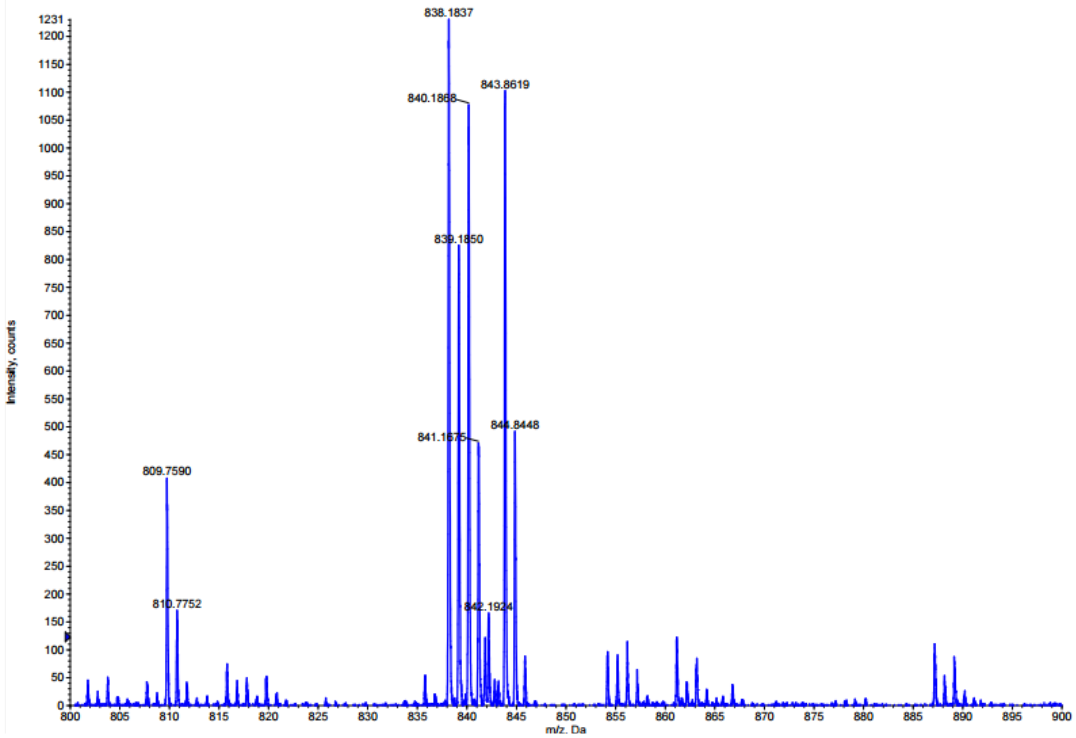

Figure S3.5. MS spectrum for $(HxCl)_2$-SiPc (Ion Spray)

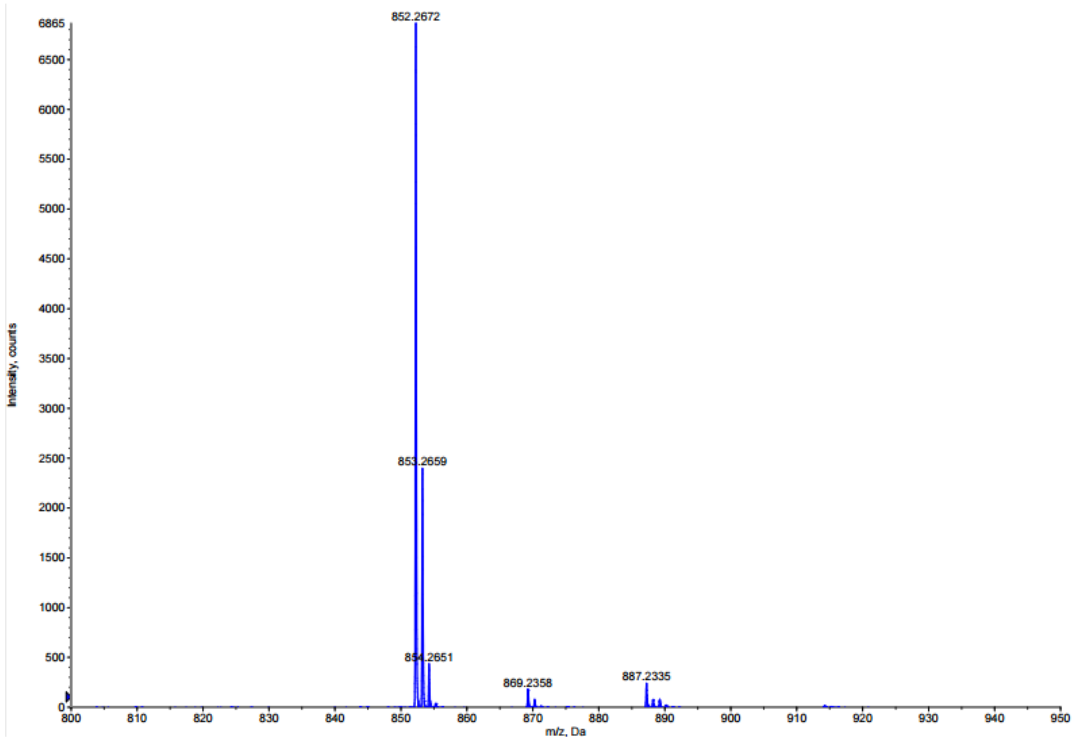

Figure S3.6. MS spectrum for $(HxN_3)_2$-SiPc (Ion Spray)

Appendix C: Supplementary Information for Chapter 4

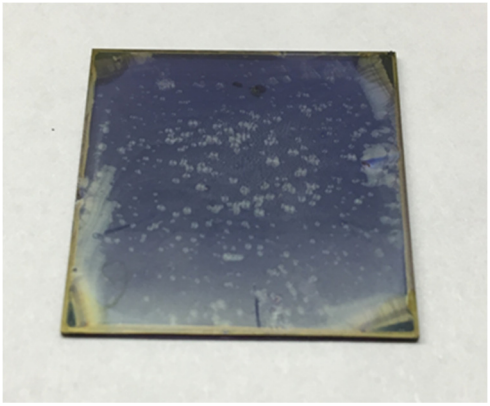

Figure S4.1: Film of P3HT/$(3BS)_2$-SiPc (DCB, 20 mg/mL polymer concentration, 1:1 ratio) cast at 1500 rpm for 30s.

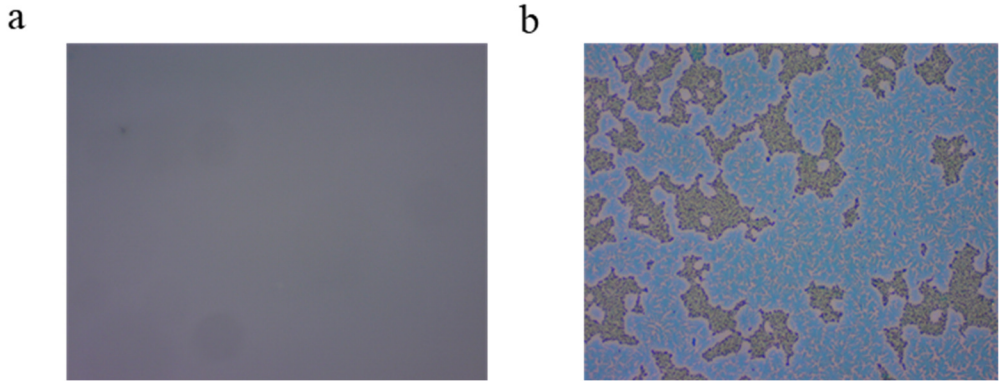

Figure S4.2: Films of PBDB-T/$(3BS)_2$-SiPc (DCB, 10 mg/mL polymer concentration, 1:1 ratio, 1000rpm) at 100x magnification with (a) no additive, and (b) containing 1 vol% DIO.

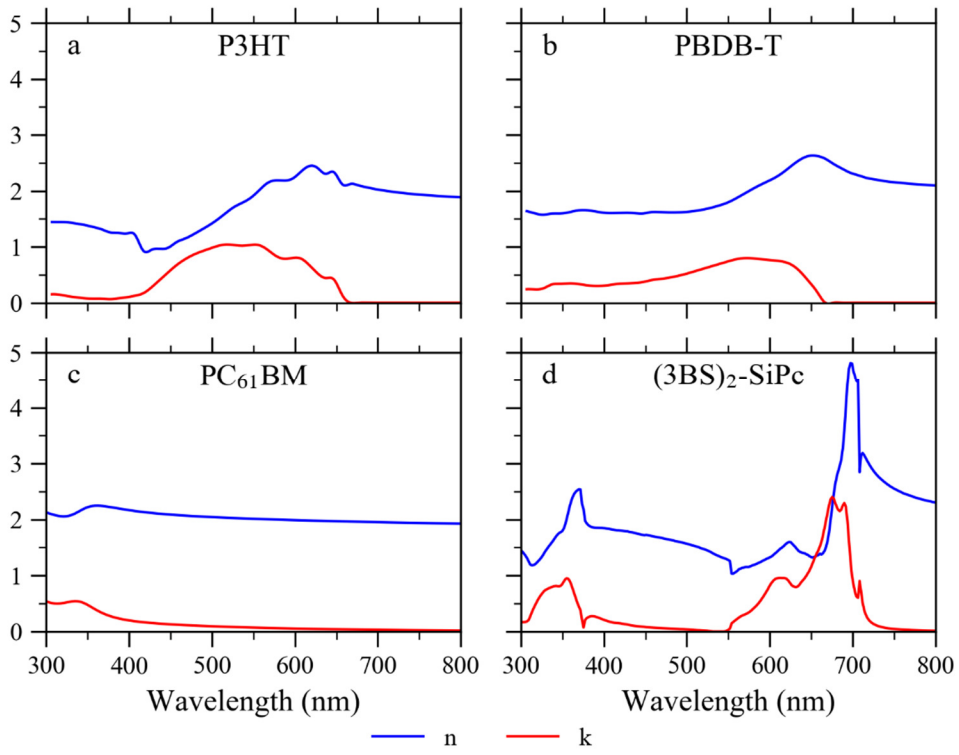

Figure S4.3: Optical parameters of donors (a) P3HT and (b) PBDB-T, and acceptors (c) $PC_{61}BM$ and (d) $(3BS)_2$-SiPc obtained from ellipsometry measurements

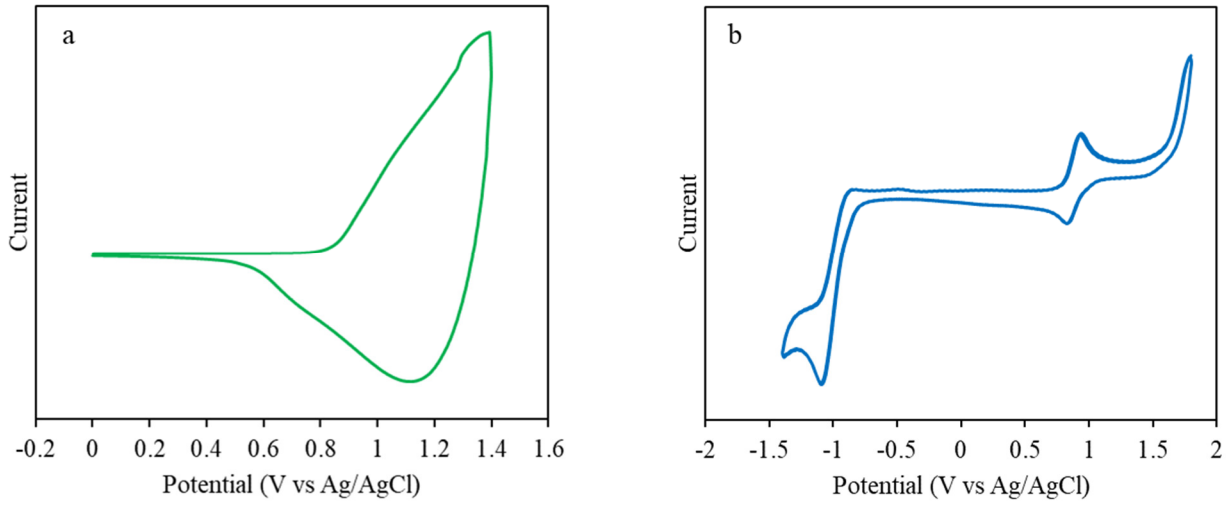

Figure S4.4: Cyclic voltammograms of (a) PBDB-T film in ACN and (b) $(3BS)_2$-SiPc in DCM solution. Tetrabutylammonium perchlorate was used as the supporting electrolyte and a scan rate of 0.1 Vs^{-1} was used. HOMO energy levels were estimated from the correlation: E_{HOMO} (eV) = -($E_{ox,onset}$ – $E_{ox\ Fc/Fc+,\ onset}$) – 4.80 eV, where $E_{ox,onset}$ and $E_{ox\ Fc/Fc+,\ onset}$ are the onset oxidation potentials vs Ag/AgCl for the sample and ferrocene reference, respectively.

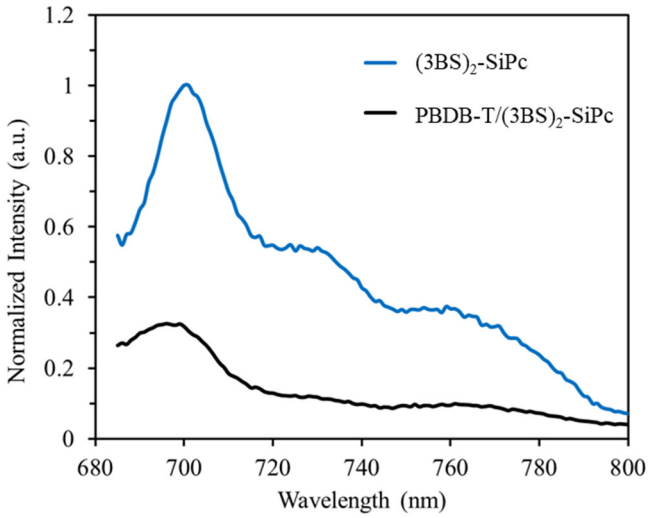

Figure S4.5: Normalized photoluminescence (PL) spectra of nest $(3BS)_2$-SiPc (blue) and 1:1 blended PBDB-T/$(3BS)_2$-SiPc films (black), excited at 670 nm. The spectra were corrected for the relative absorption of the films at the excitation wavelength.

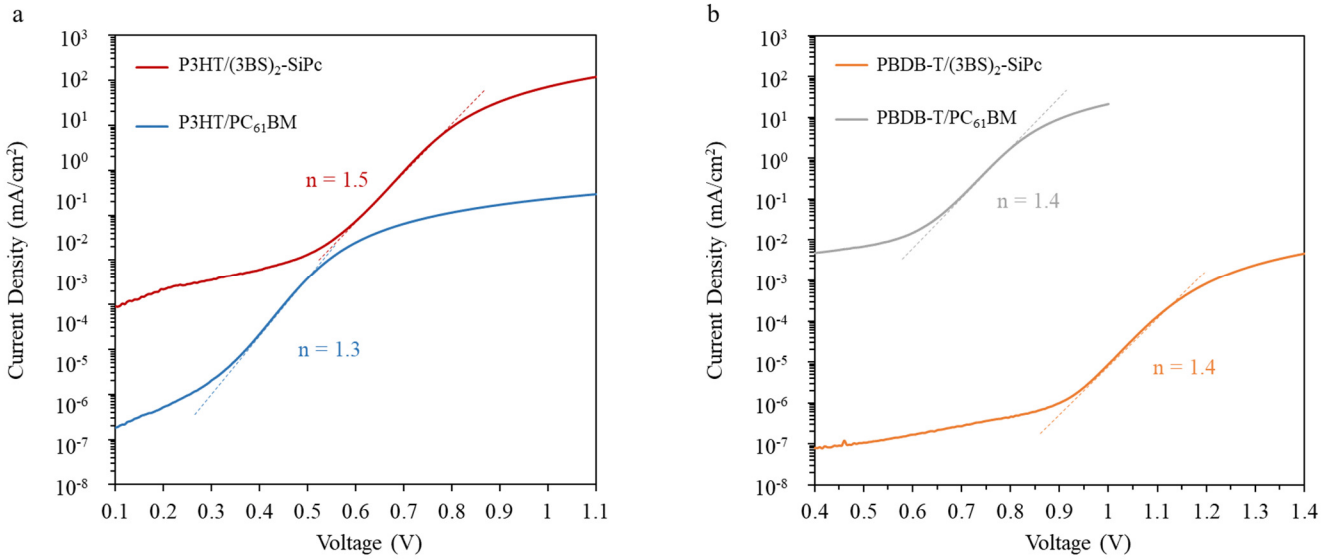

Figure S4.6: Dark *J-V* curves and extracted dark ideality factors for (a) P3HT/$(3BS)_2$-SiPc (red) and P3HT/$PC_{61}BM$ (blue), and (b) PBDB-T/$(3BS)_2$-SiPc (orange) and PBDB-T/$PC_{61}BM$ (grey) devices.

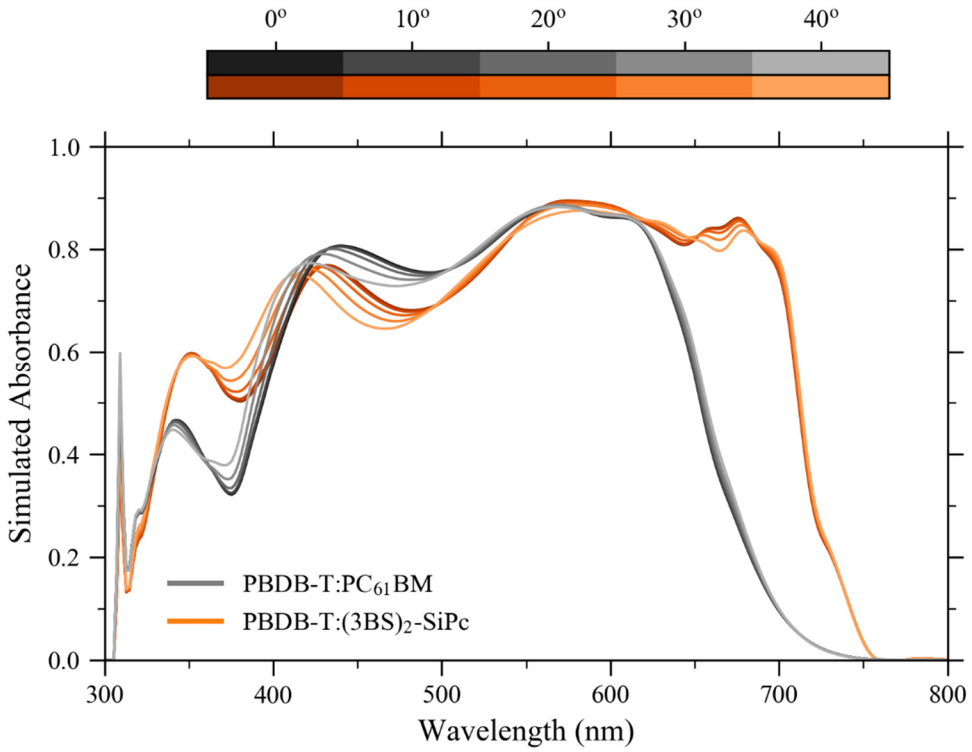

Figure S4.7: Simulated active layer film absorbance at various angles for PBDB-T:$PC_{61}BM$ and PBDB-T:$(3BS)_2$-SiPc devices.

Table S4.1: D/A ratio optimization for $(3BS)_2$-SiPc devices, obtained at 1000 W/m^2 AM1.5G

Active Layer	Ratio	PCE (%)	V_{OC} (V)	J_{SC} (mA/cm^2)	*FF*
P3HT/$(3BS)_2$-SiPc	1:0.6	2.7	0.74	7.1	0.52
	1:0.8	2.8	0.77	7.4	0.50
	1:1	3.6	0.76	9.0	0.53
	1:1.2	2.6	0.79	6.7	0.50
PBDB-T/$(3BS)_2$-SiPc	1:0.8	3.1	1.09	6.9	0.42
	1:1	3.4	1.09	7.0	0.45
	1:1.2	2.1	1.08	5.6	0.36
	1:1.4	2.0	1.08	5.4	0.35

Appendix D: Supplementary Information for Chapter 5

Materials

P3HT was purchased from Rieke. Alphasexithiophene (α-6T, purified by sublimation) was purchased from TCI and used as received. $PC_{61}BM$ was purchased from Nano-c. Triisopropyl silane was purchased from Gelest. Silicon phthalocyanine dichloride (Cl_2-SiPc) was synthesized according to the literature procedure.[1]

Synthesis of $(3PS)_2$-SiPc

$(3PS)_2$-SiPc was synthesized following the general procedure described by Gessner et al.[2] A 100 mL reaction flask was charged with Cl_2-SnPc (1.50 g, 2.45 mmol), sodium hydroxide (0.52 g, 13.05 mmol), tripropylchlorosilane (1.51 g, 7.83 mmol), Aliquat HTA-1 (0.053 g) and chlorobenzene (30 mL). The reaction mixture was stirred under reflux (132 °C) for 1 hour before adding additional tripropylchlorosilane (0.50 g, 2.61 mmol). After a further hour of reflux, sodium hydroxide (0.21 g, 5.25 mmol) and tripropylchlorosilane (0.50 g, 2.61 mmol) were added. The reaction mixture was refluxed for a further 4 hours before being allowed to cool to room temperature. The reaction mixture was filtered, and the filtrate was evaporated to dryness via rotary evaporation. The remaining solids were suspended in methanol, filtered under vacuum, washed with methanol and water, then dried in a vacuum oven (0.79 g, yield = 36 %). The product was purified by train sublimation (200 °C, 100 mtorr, CO_2 carrier gas) before use in devices (sublimation yield = 91 %, final yield = 33 %). ^{1}H NMR (400 MHz, $CDCl_3$) δ: 9.60–9.65 (m, 8 H), 8.28–8.32 (m, 8 H), 0.31-0.34 (m, 18 H), −1.13 to −1.23 (m, 12 H). MS [EI] calculated mass: 886.40; obtained mass: 886.4.

Fabrication of Photovoltaic Devices

Inverted BHJ OPV devices were fabricated with the structure glass/ITO/ZnO/P3HT:acceptor/MoO_x/Ag. Prepatterned ITO coated slides were cleaned with successive 5 minute washes of soap-water, water, acetone, then methanol in a bath sonicator. before being exposed to air plasma for 15 minutes. A ZnO precursor solution containing zinc acetate dihydrate (0.196 g) ethanol (6 mL), and ethanolamine (0.054 mL) was spin cast at 2000 rpm for 60 seconds onto the plasma treated substrates, then baked in air for 1 h at 180 °C. The active layers were deposited in a nitrogen atmosphere from solutions in 1,2-dichlorobenzene with a P3HT:acceptor mass ratio of 1:1. The P3HT concentration was 20 mg/mL for devices with

$PC_{61}BM$ and 15 mg/mL for devices with $(3PS)_2$-SiPc. P3HT/$PC_{61}BM$ devices were spun at 1000 rpm for 35s, and P3HT/$(3PS)_2$-SiPc devices were spun at 2000 rpm for 90 s. Finally, MoO_x (7 nm) and silver (70 nm) were deposited through a shadow mask to define an area of 0.325 cm^2 per device.

Inverted PHJ OPV devices were fabricated with the structure glass/ITO/ZnO/$(3PS)_2$-SiPc/α-6T/MoO_x/Ag. ITO substrates were cleaned and cast with ZnO in the same method as the BHJ devices. $(3PS)_2$-SiPc (30 nm) and α-6T (40 nm) were deposited sequentially onto the ZnO films at a rate of 1 A/s. Thickness of the layers was monitored with a quartz crystal microbalance and were confirmed using stylus profilometry. MoO_x (7 nm) and silver (70 nm) were deposited similarly to the BHJ devices.

XTSM Measurements

Scanning Transmission X-ray Microscopy (STXM) measurements were performed on HERMES beamline at SOLEIL synchrotron facility. Composition maps of blends were drawn from thickness values obtained from Singular Value Decomposition of energy stacks at the Carbon K-edge using absorption spectra of reference films (P3HT, $PC_{61}BM$ and $(3PS)_2$-SiPc). These simulations are based on the following parameters: thickness = 1 nm for all 3 reference materials, formula: P3HT = $C_{10}H_{14}S$, $PC_{61}BM$ = $C_{72}H_{14}O_2$, $(3PS)_2$-SiPc = $C_{50}H_{58}N_8O_2Si_3$, and densities: P3HT = 1.1 g/cc, $PC_{61}BM$ = 1.5 g/cc, $(3PS)_2$-SiPc = 1.25 g/cc. All processing steps of STXM data are carried out using aXis2000 software (http://unicorn.chemistry.mcmaster.ca/aXis2000.html).

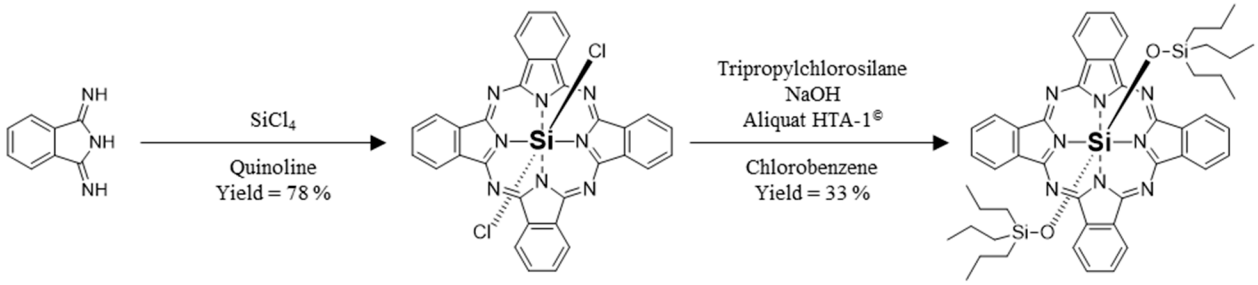

Scheme S5.1. Synthetic pathway of $(3PS)_2$-SiPc from diiminoisoindoline.

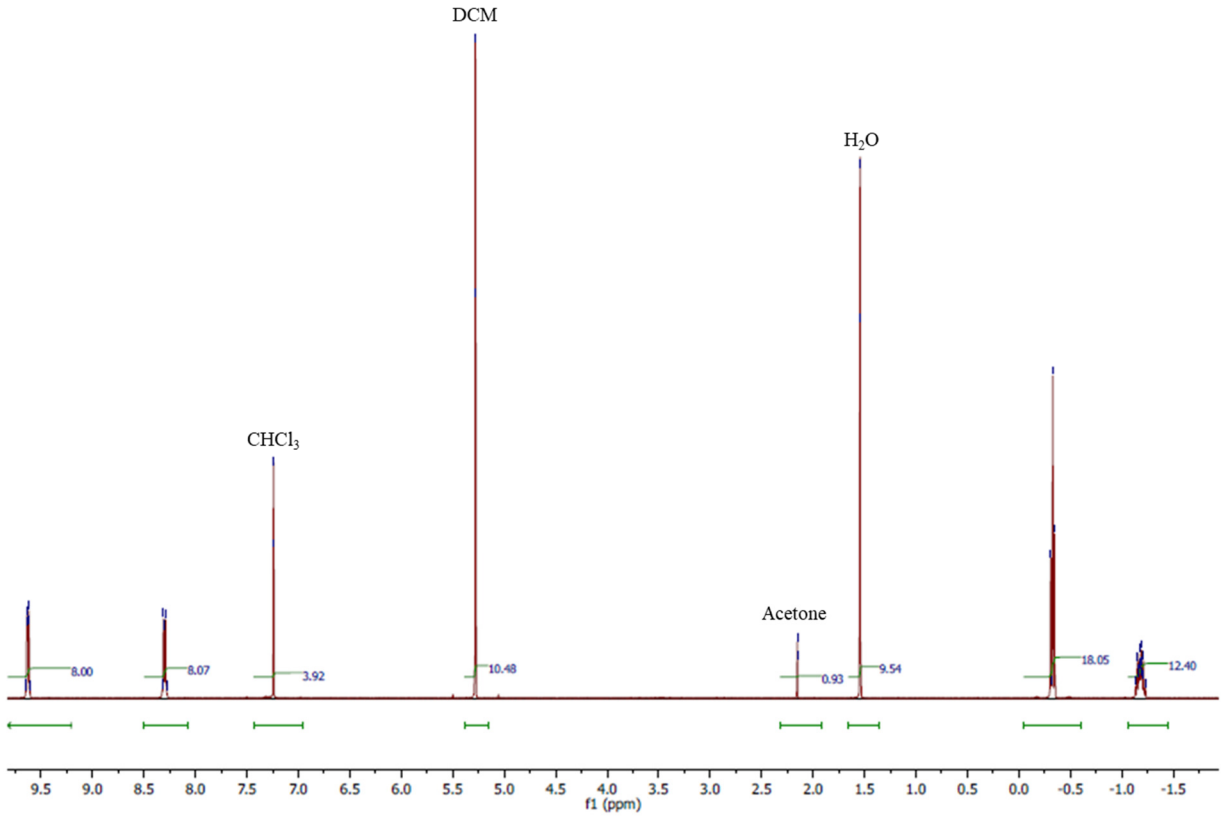

Figure S5.1. ^{1}H NMR spectrum of $(3PS)_2$-SiPc in $CDCl_3$

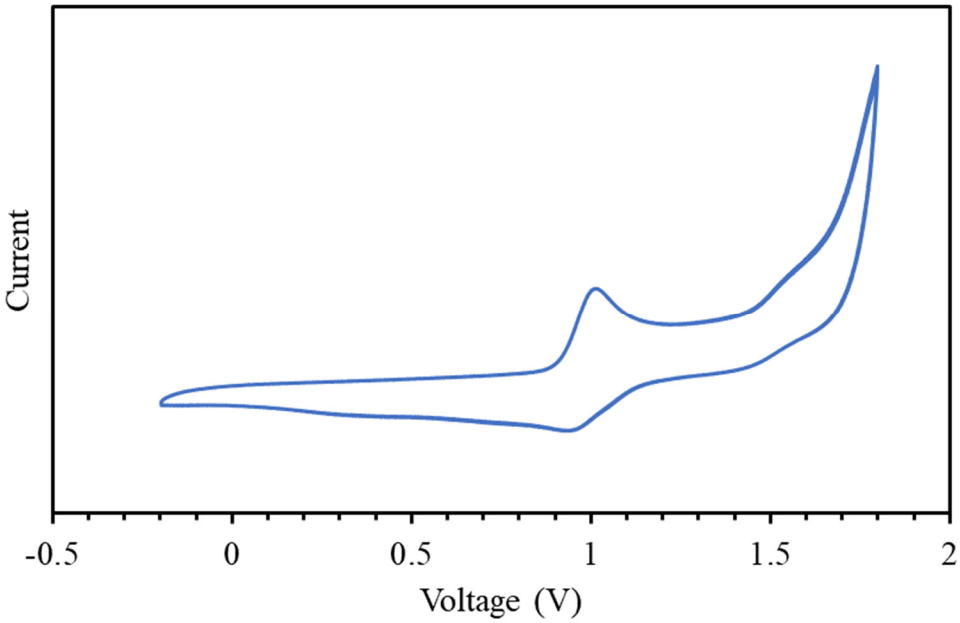

Figure S5.2. Cyclic voltammogram of $(3PS)_2$-SiPc in dichloromethane with tetrabutylammonium perchlorate supporting electrolyte and a scan rate of 0.1 V/s.

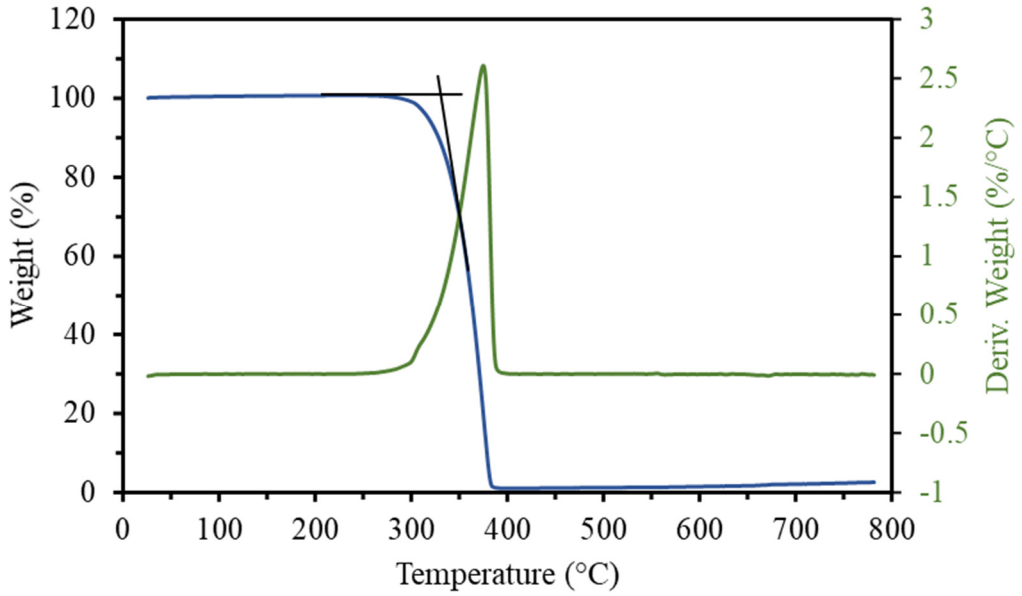

Figure S5.3. Thermogravimetric analysis (TGA) of $(3PS)_2$-SiPc measured at a ramp rate of 10 °C min^{-1}.

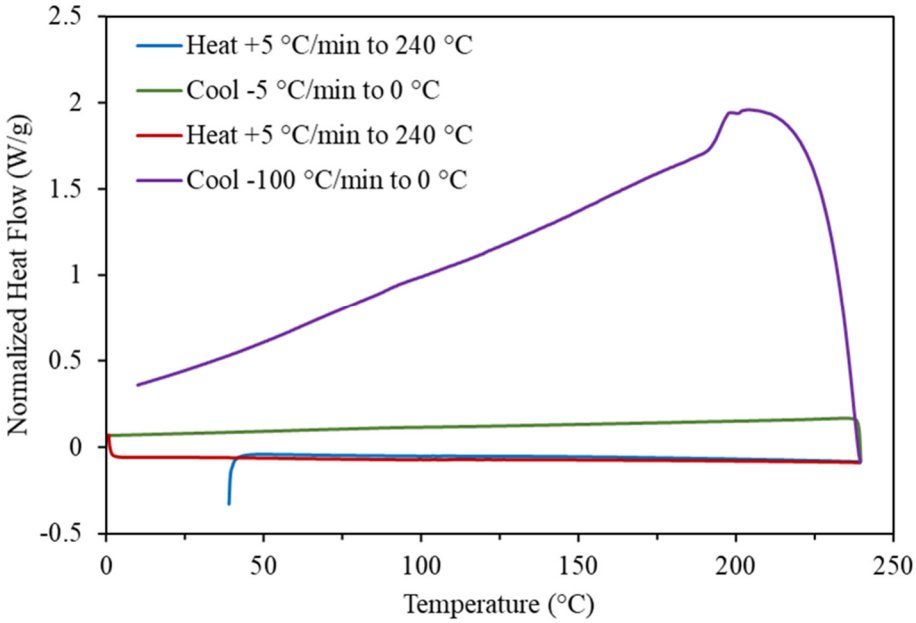

Figure S5.4: Differential scanning calorimetry (DSC) obtained from $(3PS)_2$-SiPc powder.

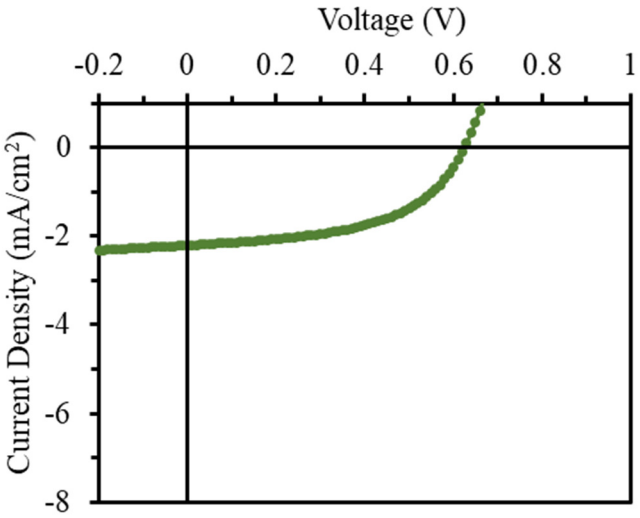

Figure S5.5: Characteristic current density-voltage (J-V) curve measured under 1000 W/m^2 AM1.5G irradiation for inverted α-6T (60 nm) / $(3PS)_2$-SiPc (30 nm) PHJ devices.

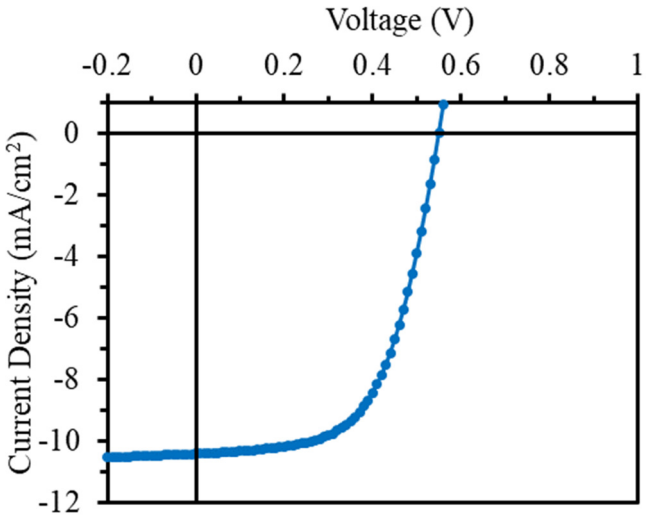

Figure S5.6: Characteristic current density-voltage (*J-V*) curve measured under 1000 W/m^2 AM1.5G irradiation for inverted P3HT/$PC_{61}BM$/$(3PS)_2$-SiPc (1:0.8:0.07) BHJ devices.

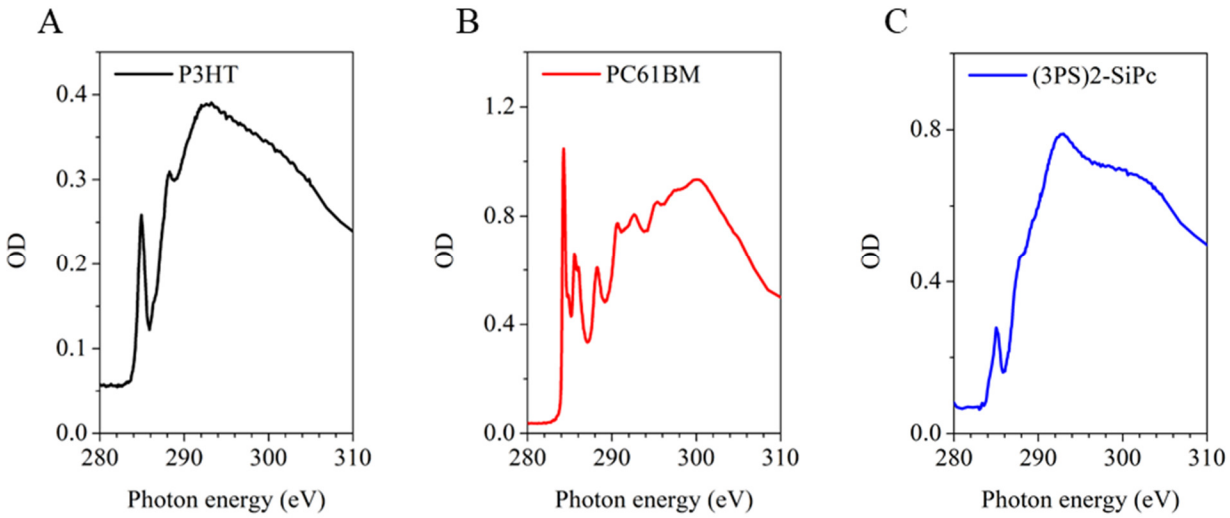

Figure S5.7: NEXAFS spectra at C K-edge of reference films of (A) P3HT, (B) $PC_{61}BM$ and (C) $(3PS)_2$-SiPc.

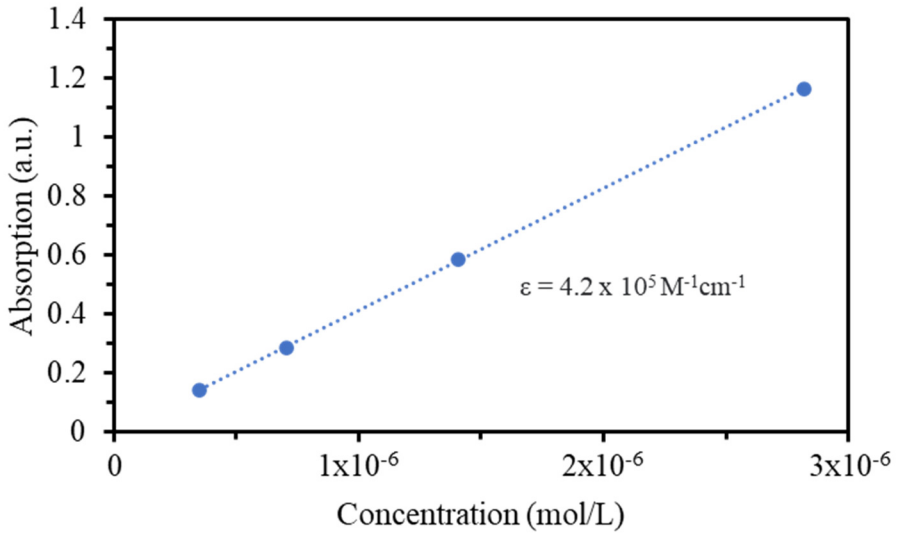

Figure S5.8. Determination of the molar extinction coefficient of $(3PS)_2$-SiPc in toluene solution according to the Beer-Lambert law.

(1) Lowery, M. K.; Starshak, A. J.; Esposito, J. N.; Krueger, P. C.; Kenney, M. E. Dichloro(Phthalocyanino)Silicon. *Inorg. Chem* **1965**, 128.

(2) Gessner, T.; Sens, R.; Ahlers, W.; Vamvakaris, C. Preparation of Silicon Phthalocyanines and Germanium Phthalocyanines and Related Substances. US 2010/0113767 A1, 2010.